Evaluation of inorganic scaling and scaling inhibition by antiscalants in high-pressure membrane filtration for drinking water treatment

Dissertation (monograph)

approved by the Doctoral Degree Committee of
Hamburg University of Technology

in pursuit of the academic degree of

Doktor-Ingenieurin (Dr.-Ing.)

written by

Shambhavi Arvind Kaushik

from

Bangalore, India

2026

Reviewers

1. Reviewer: Prof. Dr. Mathias Ernst

2. Reviewer: Prof. Dr. Jens Muff

Chairman of the Examination Committee

Prof. Dr. Bastian Oesterle

Date of the oral examination

November 28, 2025

DOI

https://doi.org/10.15480/882.17621

ORCID ID

https://orcid.org/0009-0009-7171-1794

Acknowledgements

This dissertation is not solely the product of my efforts, but of the generosity, wisdom and unwavering support of many individuals. It is a privilege to acknowledge their contributions here.

Foremost, I am sincerely grateful to Mathias Ernst for giving me the opportunity to work on this topic, for his trust in my work and his supervision. His guidance, patience and continuous encouragement have been invaluable in shaping both this dissertation and my development as a researcher.

My sincere gratitude also goes to Prof. Jens Muff for undertaking the role of second reviewer of this dissertation, and to Prof. Bastian Oesterle for serving as the chair of my examination committee. I greatly appreciate their willingness to dedicate their time and expertise to the evaluation of this work.

My heartfelt thanks go to all the colleagues at the Institute of Water Resources and Water Supply, as well as the DVGW Research Centre TUHH. I am especially grateful for the unwavering support of Dorota and Thorsten in the laboratory, their joyful conversations, participation in my impromptu scientific exchanges and for holding me accountable to high standards of good lab practice! I'm also deeply thankful to Barbara for several discussions and exchanges on project planning. Big thanks also to Daniel Steinbarth for patiently dealing with all my setup modification demands and stepping in during crucial troubleshooting moments. To my fellow PhD colleagues - Saskia Dillmann, Margarethe Langer, Tomi Mantel, Muhammad Usman, Jakob Kämmler (for also helping with my presentation!), Jakob Stumme, Jonas Schuster, Charlotte Kast, Muhammad Ismahil, Natalie Lüdemann and Jon Wullenweber - thank you for sharing the unique experience of doctoral life with me. Through the challenges, uncertainties and achievements, your support, mutual understanding, conversations and friendship made this journey much more enjoyable and I am deeply grateful for those moments.

To every colleague at TUHH-WWV & DVGW-TUHH: thank you for the exchange of ideas, the help and encouragement along the way, and for creating a workplace where I felt welcomed and valued. As someone who came to Germany from another country, I especially appreciate the openness, kindness and friendships that made this place feel like a second home – a feeling particularly meaningful in the midst of a pandemic!

A special thank you goes to all the students I had the privilege of working with and supervising during my doctoral studies. It was truly rewarding to share this journey with Pranav Sharma, Steven Fogang, Andres Acevedo, Rafael Prien, Aditya Mulay, Justin Dittmer, Saulab Bangia and Vikramsheel Singh. I greatly appreciate your dedication, enthusiasm and contributions to this research. I learned a great deal from each of you.

I would like to extend my gratitude to all collaborators and partners of KonTriSol project funded by BMBF (02WAV1530) & DVGW (W201807-A) who contributed to this research. Your expertise, cooperation and willingness to share your knowledge were invaluable to the success of this work. Special thanks to DVGW-TZW, especially Dominic Armbruster, for the excellent collaboration and enriching scientific exchanges.

Finally, I would like to express my deepest gratitude to my parents, my siblings, family and friends in India, Germany and across the world, for their unconditional love, endless support and constant belief in me, even from afar. I am forever grateful to my parents for giving me the freedom to pursue my choice of path and their unwavering support to realize my potential - this achievement is a reflection of your love and support as much as it is of my own efforts.

Abstract

Reverse osmosis (RO) and nanofiltration (NF) are established processes for removing hardness, sulfates, nitrates, trace organics, and other anthropogenic contaminants. However, membrane scaling remains a major operational challenge and is commonly overcome by adding antiscalants. Key issues with antiscalant use include varying effectiveness of different active ingredients, their dosage considerations and environmental concerns over the disposal of concentrate streams containing these chemicals.

This study evaluates the effectiveness of various commercial antiscalants, focusing on appropriate evaluation methods, dosage behaviour and potential side-effects. Key objectives include (i) comparing methods for detecting scaling and inhibition potential and (ii) investigating scale inhibition performance against gypsum and calcite salts. A detailed evaluation of the molecular weight fractions and biological growth potential of PAA-based antiscalant was also examined. Additionally, the performance of a novel phosphorus (P)-free, plant-based CMI antiscalant was experimentally assessed.

Evaluation of various methods for assessing scaling and antiscalant performance revealed significant differences based on scalant applicability, setup complexity, material requirements, and level of precision. Both the stirred-beaker test and membrane crossflow filtration were suitable for testing with gypsum and calcite, capturing differences in scaling behaviour and antiscalant performance. The stirred-beaker test, while simple to set up, effectively assessed threshold inhibition using induction time derived from rate of change of turbidity of the solution. The crossflow filtration test offered deeper insight into antiscalant performance under practical filtration conditions by monitoring rate of flux decline and followed by SEM characterization, but was more resource and time -intensive.

Among the antiscalants tested, P-based ATMP, DTPMP, PAA+DTPMP showed better gypsum scale inhibition at 1 mg/L TS than at 0.5 mg/L TS, whereas PBTC performed poorly at both doses. In contrast, P-free PAA and CMI exhibited strong gypsum inhibition even at low dosages. In the case of calcite, ATMP and PBTC showed strong threshold inhibition at low dosage, whereas DTPMP performed comparatively poorly. Interestingly, the PAA+DTPMP and PAA antiscalant showed poor threshold inhibition, but good calcite dispersion property. CMI demonstrated strong threshold inhibition for calcite at all tested dosages. In nearly all cases, antiscalants modified the crystal structure and original morphology of the scaling salts.

In-depth examination of the commercial PAA antiscalant and its molecular weight fractions (≤500 Da and ≥500 Da), revealed that the low molecular weight PAA fraction showed poor inhibition against both gypsum and calcite, while the high molecular weight PAA fraction demonstrated excellent inhibition potential. Bioavailability testing indicated that the low molecular weight fraction had higher biological growth potential, given by increased total cell count (TCC). Since the fractions ≤ 500 Da may potentially pass through less dense NF/RO membranes, it highlights additional challenges associated with antiscalant application in drinking water treatment.

Overall, this study defined suitable test conditions and parameters for evaluating scaling inhibition in NF/RO, thereby supporting informed decision-making for the safe use of antiscalants in drinking water treatment.

Zusammenfassung

Umkehrosmose (UO) und Nanofiltration (NF) sind etablierte Verfahren zur Entfernung von Härtebildnern, Sulfaten, Nitraten und anderen anthropogenen organischen Spurenstoffen. Membran-Scaling stellt jedoch weiterhin eine große betriebliche Herausforderung dar und wird üblicherweise durch den Einsatz von Antiscalants bewältigt. Zentrale Fragestellungen hierbei sind die unterschiedliche Wirksamkeit verschiedener Wirkstoffe, Dosierungsaspekte sowie Umweltbedenken hinsichtlich der Entsorgung von Konzentratströmen mit diesen Chemikalien.

Diese Studie untersucht die Wirksamkeit verschiedener kommerzieller Antiscalants mit Fokus auf geeignete Bewertungsmethoden, Dosierverhalten und mögliche Nebenwirkungen. Die Hauptziele umfassen (i) den Vergleich von Methoden zur Erfassung des Scaling- und Hemmungspotenzials sowie (ii) die Untersuchung der Wirksamkeit gegenüber Gips- und Calcit-Ablagerungen. Zusätzlich wurden Molekulargewichtsfraktionen und biologisches Wachstumspotenzial eines Polyacrylsäure (PAS)-basierten Antiscalants analysiert sowie die Wirksamkeit eines neuartigen Phosphor (P)-freien CMI-Antiscalants experimentell bewertet.

Die Bewertung verschiedener Methoden zur Untersuchung von Scaling und Antiscalant-Wirksamkeit zeigte erhebliche Unterschiede hinsichtlich Anwendbarkeit, experimentellem Aufwand, Materialbedarf und Messgenauigkeit. Sowohl der Rührbecher-Test als auch die Membran-Crossflow-Filtration erwiesen sich als geeignet für Gips- und Calcit-Versuche, da sie die Erfassung von Unterschieden im Scaling-Verhalten und in der Antiscalant-Wirksamkeit ermöglichten. Der Rührbecher-Test ermöglichte mit einem vergleichsweise einfachen Aufbau die Bestimmung der Threshold-Hemmung (Hemmung der Kristallkeimbildung) anhand der aus der Trübungsänderungsrate abgeleiteten Induktionszeit. Der Crossflow-Filtrationsversuch lieferte durch die Überwachung der Permeatflux-Abnahmerate und anschließende REM-Charakterisierung tiefere Einblicke unter praxisnahen Filtrationsbedingungen, war jedoch mit höherem Zeit- und Ressourcenaufwand verbunden.

Unter den getesteten Antiscalants zeigten die P-basierten ATMP, DTPMP und PAS+DTPMP bei 1 mg/L TS eine bessere Gips-Scaling-Hemmung als bei 0,5 mg/L TS, während PBTC bei beiden Dosierungen eine geringe Wirksamkeit aufwies. Die P-freien Antiscalants PAS und CMI zeigten hingegen bereits bei niedrigen Dosierungen eine starke Hemmwirkung gegenüber Gips. Bei Calcit zeigten ATMP und PBTC bereits bei niedriger Dosierung eine starke Threshold-Hemmung, während DTPMP vergleichsweise schlecht abschnitt. PAS+DTPMP und PAS zeigten trotz geringer Threshold-Hemmung gute Dispergiereigenschaften gegenüber Calcit. CMI zeigte bei allen getesteten Dosierungen eine starke Threshold-Hemmung gegenüber Calcit. In nahezu allen Fällen veränderten Antiscalants die Kristallstruktur und die ursprüngliche Morphologie der Scaling-Salze. Die Untersuchung des kommerziellen PAS-basierten Antiscalants und seiner Molekulargewichtsfraktionen (≤500 Da und ≥500 Da) zeigte, dass die niedermolekulare Fraktion gegenüber Gips und Calcit eine geringe Hemmwirkung aufwies, während die hochmolekulare Fraktion ein ausgezeichnetes Hemmpotenzial zeigte. Die niedermolekulare Fraktion wies zudem ein höheres biologisches Wachstumspotenzial auf, erkennbar an einer erhöhten Gesamtzellzahl (GZZ). Da Fraktionen ≤500 Da potenziell weniger dichte NF-/UO-Membranen passieren können, ergeben sich zusätzliche Herausforderungen für den Einsatz von Antiscalants in der Trinkwasseraufbereitung.

Zusammenfassend wurden in dieser Studie geeignete Testbedingungen und Parameter zur Bewertung der Scaling-Hemmung in NF-/UO-Verfahren definiert und damit eine fundierte Entscheidungsgrundlage für den sicheren Einsatz von Antiscalants in der Trinkwasseraufbereitung geschaffen.

Table of Contents

List of Figures

List of Tables

List of Abbreviations

AFM	Atomic force microscopy
AMPA	Aminomethylphosphonic acid
AOC	Assimilable organic carbon
ATMP	Aminotris methylenephosphonic acid
CAS	Chemical Abstracts Service
CMI	Carboxymethyl inulin
CNT	Classical nucleation theory
CP	Concentration polarization
CP_{factor}	Concentration polarization factor
DOC	Dissolved organic carbon
DTPMP	Diethylenetriamine penta(methylene phosphonic acid)
EINECS	European Inventory of Existing Commercial Chemical Substances
HEDP	1-hydroxyethane-1,1- bis phosphonic acid
HMP	Hexametaphosphate
HPMA	Poly maleic anhydride
LC-OCD	Liquid chromatography organic carbon detection
LPRO	Low-pressure reverse osmosis
MF	Microfiltration
MW	Molecular weight
NACE	National Association of Corrosion Engineers

NF	Nanofiltration
NTU	Nephelometric turbidity unit
PAA	Polyacrylic acid
PALAM	Polyallylamine hydrochloride
PAMALAM	Poly(acrylamide-co-diallyldimethylammonium chloride)
PAMAM	Polyaminoamide
PBTC	2-phosphonobutane 1,2,4-tricarboxylic acid
PEI	Polyethyleneimine
RO	Reverse osmosis
SDGs	Sustainable development goals
SEM	Scanning electron microscopy
SHMP	Sodium hexametaphosphate
SI	Saturation index
TFC	Thin-film composites
TMP	Transmembrane pressure
TOC	Total organic carbon
TPP	Tripolyphosphate
TrinkwV	German Drinking Water Ordinance
TS	Total solids
UF	Ultrafiltration
WGM	Whispering gallery mode
XRD	X-ray diffraction

1 Introduction

1.1 Background

Freshwater is one of the most crucial resources that sustains and nurtures our life on earth, with agriculture (70%), industrial (19%) and domestic use (11%) constituting the major applications for human consumption (Du Plessis 2022). However, since the last few decades, factors such as overuse and misuse of water, pollution of water resources, improper management of water, climate change and growing population with increased water demand have led to a water scarcity crisis. Degradation of freshwater resources has been regarded as one of the foremost challenges of the 21st century, seriously threatening the achievement of the sustainable development goals (SDGs) (Baggio et al. 2021). Alterations to hydroclimatic patterns induced by climate change, combined with exacerbated pollution of dwindling freshwater resources jeopardize economic growth while heightening risks to public health, food security, and ecological functions (Du Plessis 2022). Ensuring water security and resilience requires immediate action to protect existing freshwater sources, along with a betterment of drinking water treatment technologies and equitable access to them. In response to these growing water challenges in a changing world, water treatment solutions—such as water reuse and recycling, desalination, and the upgrading of existing treatment plants—have gained increasing importance in recent years (Zhai et al. 2022).

Membrane processes are widely used in water and wastewater industries for the removal of hardness, color, organic compounds, disinfection by-products and their precursors to achieve desired water quality (Shirazi et al. 2010). Membrane separation processes like reverse osmosis (RO) and nanofiltration (NF) are increasingly applied for drinking water treatment in Germany primarily targeting hardness reduction, removal of inorganic water constituents such as nitrate, sulphate or selenium, trace natural organic substances (humic substances) and anthropogenic trace substances (Bergdolt et al. 2019). Despite higher energy and cost considerations, NF and RO are established technologies to reliably separate dissolved substances compared to alternative processes such as activated carbon filtration or ion exchange, particularly if the process objectives are hardness reduction and removal of trace substances. Although membrane treatment is not remarkably widespread in drinking water treatment in Germany, a survey conducted by (Müller 2010) estimated that there were approximately thirty NF/RO plants in operation for the treatment of drinking water until 2010 and projected to increase due to changes in raw water quality, the necessity to extract groundwater from deeper wells driven by shifting demographics and climate change, as well as the growing issue of nitrate contamination. As per the KonTriSol 2023 report, approximately ninety waterworks in Germany utilize nanofiltration or low-pressure reverse osmosis (LPRO) for the production of drinking water. Internationally, membrane technologies for drinking water treatment offer high potential for use, especially in regions where water availability is limited or raw water resources are heavily polluted. “Zero liquid discharge” (ZLD) systems play a significant role in arid regions that necessitate maximizing water yield.

1.2 Objective and structure of thesis

With the increasing need to resort to low-pressure and high-pressure reverse osmosis treatment technologies to meet the rising water demand and ensure sufficient drinking water quality, the focus on inhibiting scaling within the membrane systems has significantly increased. Process optimizations such as ion exchange, Donnan dialysis and electrodialysis integrated with reverse osmosis have shown potential to enable chemical-free operation of reverse osmosis, but require complex technical modifications and are yet to prove reliability and cost-effectiveness, especially when implemented in full-scale drinking water systems (McGovern et al. 2014, Vanoppen et al. 2015). The addition of antiscalants is common practice to ensure smooth operation of the reverse osmosis plant with minimal process modifications. However, antiscalant application is associated with several limitations based on lack of transparency of their ingredients and their effectiveness against different salts. This work, therefore, aims to fill some of these knowledge gaps in terms of effectiveness of different antiscalants, dosage considerations, potential side-effects and selection of a method to evaluate antiscalant effectiveness. More specifically, it is categorized into the following broad themes:

- Comparison of antiscalant effectiveness against gypsum scaling at different dosages of different active ingredients through experimental investigations in a jar test and a lab-scale cross-flow filtration plant

- Comparison of effectiveness of different antiscalants ingredients at different dosages to inhibit calcite scaling, using the jar test and lab-scale cross-flow filtration plant

- Experimental evaluation of the suitability of other alternative methods tested to determine antiscalant efficacy

- An in-depth evaluation of the effectiveness of phosphorus-free (P-free) antiscalants is presented, including experimental evidence on the behaviour of different molecular weight fractions and initial insights into novel “green” scale inhibitors.

2 Theoretical Background

2.1 Pressure-driven membranes

Membrane is a semi-permeable barrier between two phases that allows selective transport based on the differences in the physical and/or chemical properties of permeating components across the membrane (Howe et al. 2012, Shirazi et al. 2010). Broadly, membranes used in water and wastewater industry can be classified as porous and non-porous membranes. Porous membranes like microfiltration, ultrafiltration and loose-end nanofiltration separate particles based on sieving, straining, or size exclusion, whereas non-porous membrane (tight-knit nanofiltration, reverse osmosis) separation is based on the differences in solubility or diffusivity between the solvent and the solute in the membranes (Crittenden et al. 2012). Additionally, membranes also differ in their pore sizes, operating pressures, and applications (Shirazi et al. 2010). Figure 1 depicts the impurities that are eliminated by different pressure-driven membrane systems as well as their corresponding pore size ranges.

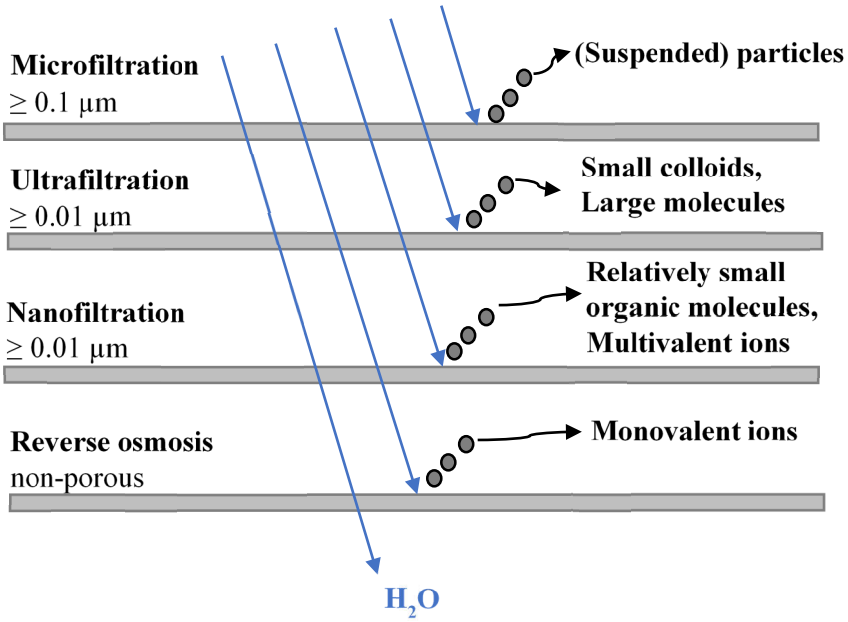

Figure 1: Selectivity of pressure-driven membranes according to solute size and type (adapted from Crittenden et al. 2012

During low-pressure membrane filtration, porous membranes reject particles, germs, viruses, and bacteria through a size exclusion separation process (Aptel and Buckley 1996). In contrast, non-porous and dense membranes can reject dissolved salts, sugars, and divalent and monovalent ions during filtration via the solution-diffusion mechanism (Howe et al. 2012). Microfiltration (MF) and ultrafiltration (UF) employ porous membranes, whereas nanofiltration (NF) and reverse osmosis (RO) use dense and non-porous membranes. As the membrane structure becomes more open, the required hydrostatic pressure decreases; thus, low pressures are sufficient for microfiltration, while reverse osmosis requires relatively high pressures (Crittenden et al. 2012). During solution diffusion transport in RO membrane systems, the

substance of interest dissolves in the membrane and then diffuses through the membrane, with the movement of solvent and solute being independent of each other. The driving force in this case is the difference between the pressure across the membrane, between the feed and the permeate, also called transmembrane pressure (TMP) (Aptel and Buckley 1996). Pressure-driven membrane processes can be divided into low- and high-pressure filtration processes. Low-pressure membrane filtration consists of microfiltration (MF) and ultrafiltration (UF) in which the transmembrane pressure (TMP) lies in the range of 0.2-5 bars. High pressure includes nanofiltration and reverses osmosis with TMP between 5 to 100 bars (Howe et al. 2012).

Pressure-driven membrane filtration can be carried out using two different modes, namely dead-end filtration and crossflow filtration as shown in Figure 2.

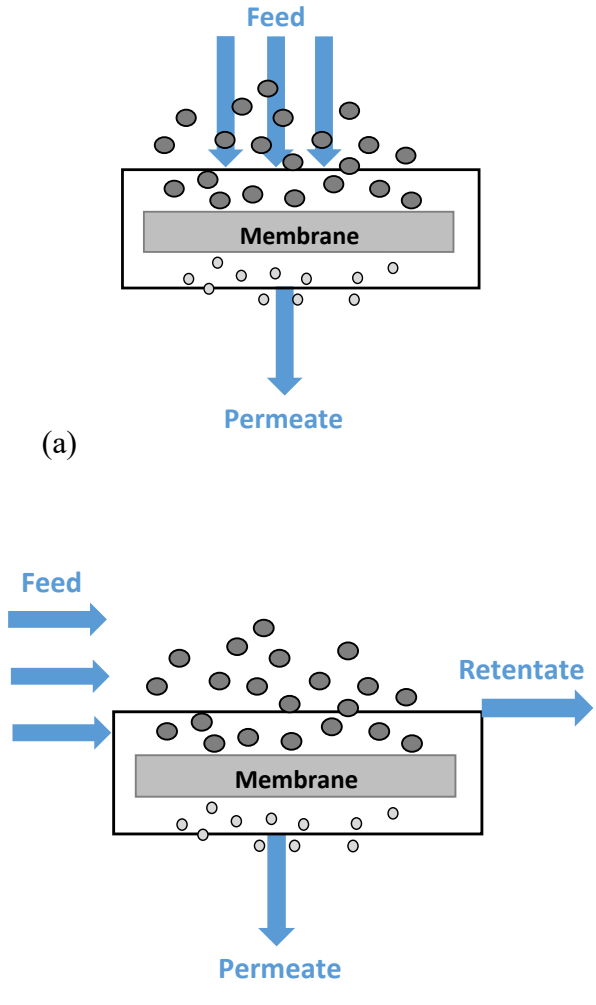

Figure 2: Schematic representation of (a) dead-end filtration and (b) crossflow filtration mechanism in pressure-driven membrane treatment

During dead-end filtration (Figure 2(a)), the feed solution flows perpendicular to the membrane surface, wherein, the permeate is forced through the membrane and the feed solution decreases

in volume. In this mode, pressure is constant over the whole membrane area. Conversely, in crossflow filtration, the feed solution flows tangentially or parallel to the membrane surface as shown in Figure 2(b), and subsequently the influent stream yields two effluent streams – permeate and retentate. Although a flux will be induced due to high pressure on the feed side, due to tangential flow through the membrane, pressure is not distributed uniformly across the membrane area. According to Kucera 2023, tangential flow during crossflow operation of high-pressure membranes aids in keeping the surface clean by scouring the surface, which helps to avoid fouling or scaling on the membrane. Minimum flow rates across the membrane surface are necessary to successfully scour the surface. Theoretically, crossflow is a continuous process since the scouring action constantly removes any contaminants from the membrane surface. However, in practice, the scouring effect of crossflow by itself is insufficient to avoid complete fouling and scaling. The membranes must periodically be removed from operation and cleaned to remove any debris that has gathered at the surface or additional mitigation measures must be put into place (Kucera 2023).
As the experimental part of this thesis was conducted in a crossflow RO system, the following sections focus on RO filtration concepts.

2.2 High-pressure membrane processes: Reverse osmosis

As the world's population and the consequent demand for water supply increase, local water scarcity and contamination of available freshwater sources poses a serious threat to the present and future generations. In order to combat the negative consequences of this threat, solutions such as water recycling, water reuse, desalination and improvement of currently water treatment plants are heavily pursued (Alzahrani et al. 2013, Ang et al. 2015, Benecke 2018). Desalination plants constructed based on reverse osmosis technology using semi-permeable membranes that let pressurized water pass through but retain salts, have proved to be revolutionary to the water treatment sector (Fritzmann et al. 2007).

Principles and transport mechanisms in reverse osmosis

Osmosis is a natural process in which water flows across a semipermeable membrane from the region of lowest concentration of dissolved particles to the region with higher dissolved substance concentration, usually with no change of phase (Kucera 2023, Rozova 2014). Figure 3(a) shows a cell divided by a semipermeable membrane that allows water and certain ions to pass through it, but withholds most dissolved particles on one side. In case of osmosis, water will continue to flow through the membrane until the concentration on both sides of the membrane are in equilibrium. At equilibrium, both compartments have the same concentration of dissolved solids and no more net water flow takes place. However, the compartment that originally held the higher concentration of dissolved solids has a greater water level than the other compartment. The osmotic pressure of the solution at equilibrium is given by the difference in height between the two compartments (Figure 3 (b)).

The osmotic pressure is calculated as follows ((Howe et al. 2012)):

$$\pi = i \cdot C \cdot R \cdot T \qquad \text{[Equation 1]}$$

where, π = osmotic pressure [bar]; i = osmotic coefficient [-] defined for non-ideal conditions in van't Hoff's law which describes the relation of molecules dissociated in solution compared to pure structure depending on the electrolyte involved; C = concentration of all solutes [mol·L^{-1}]; R = universal gas constant, 0.08315 [(L·bar)/(mol·K)]; T = absolute temperature [K]

If an external pressure greater than the osmotic pressure is applied to the compartment with a higher solute concentration, water is forced to flow in the opposite direction of natural osmosis, from the concentrated solution toward the dilute solution. This process is known as reverse osmosis (RO). In this way, dissolved particles are withheld while relatively pure water travels through a membrane into the other (Kucera 2023). Separation of solutes from water during RO filtration is governed by the solution-diffusion mechanism.

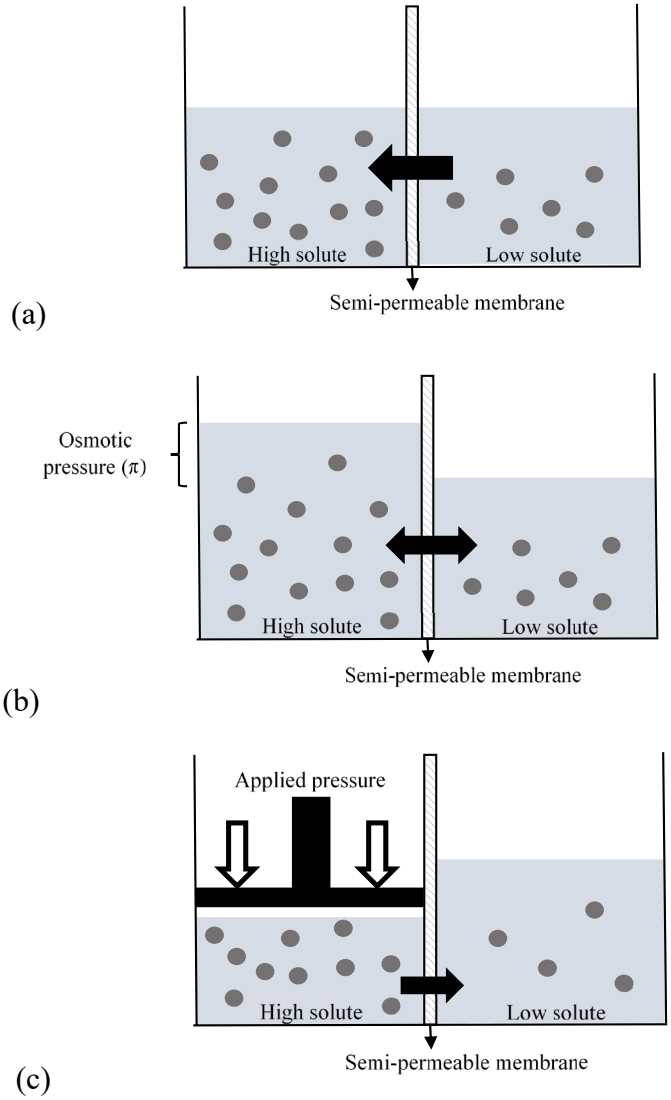

Figure 3: Schematic representation of (a) osmosis, (b) osmotic pressure at equilibrium and (c) reverse osmosis

Water flux and solute flux is given by Equation 2 and Equation 3 (Howe et al. 2012), respectively:

$$J_w = K_w \cdot (\Delta P - \Delta \pi) \qquad \text{[Equation 2]}$$

where, J_w = permeate flux [L·m^{-2}·h^{-1}]; K_w = water permeability coefficient [L·m^{-2}·h^{-1}·bar^{-1}]; ΔP = transmembrane pressure [bar]; $\Delta \pi$ = osmotic pressure difference across the membrane wall [bar]

$$J_s = K_s \cdot (C_f - C_p) \qquad \text{[Equation 3]}$$

where, J_s = solute flux [L·m^{-2}·h^{-1}]; K_s = solute permeability coefficient [L·m^{-2}·h^{-1}·bar^{-1}]; C_f = feed concentration [mol·L^{-1}]; C_p = solute concentration [mol·L^{-1}]

According to the solution-diffusion model, water and solute molecules diffuse through the active layer and finally into the permeate stream and are intrinsic to the type of membrane material. Water and solute permeability coefficients (K_w and K_s) vary with active layer thickness and temperature, and are responsible for the selectivity of the active layer of non-porous membranes. The permeability-selectivity trade-off of these membranes implies that an increase in the permeability of water is associated with an even greater increase in the solute permeability, thereby presenting enormous challenges to have a membrane with high water permeability and high selectivity (Benecke 2018).

Concentration polarization

Concentration polarization (CP) refers to the phenomenon of build-up of solute molecules at the membrane surface compared to the bulk solution (Figure 4). The concentration gradient adjacent to the membrane surface drives the diffusion of rejected solutes back into the bulk solution. A steady-state concentration profile is established when the convective transport of rejected solutes towards the membrane surface is balanced by their back diffusion into the bulk solution (Chen et al. 2004).

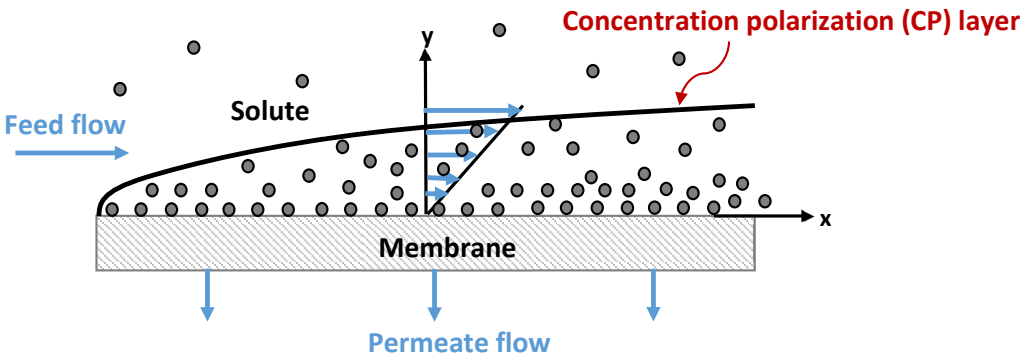

Figure 4: Schematic of representation of concentration polarization adapted according to (Chen et al. 2004)

For solutions containing solutes <100 nm that have high rejection of about 100%, Brownian diffusion dominates, the concentration polarization factor (CP_{factor}) is given by:

$$CP_{factor} = {}^{Cm} / {}_{Cb} = \exp ({}^{Jw}/_{k}) \qquad \text{[Equation 4]}$$

where C_m refers to concentration of rejected solutes at the membrane surface, C_b refers to concentration of the solutes in the bulk solution, J_w permeate water flux and k is the mass transfer coefficient given by:

$$k = {}^{D} / {}_{\delta} \qquad \text{[Equation 5]}$$

where, D is the solute diffusion coefficient and δ is the boundary layer thickness.
A higher water flux (J_w) or lower mass transfer coefficient (k) increases concentration polarization. Since D decreases with molecule size and δ decreases with higher flow velocity or turbulence, CP_{factor} is influenced by solute size and hydrodynamics. It is generally accepted that concentration polarization at the membrane surface can lead to solute adsorption and solute precipitation, resulting in a decrease in the water flux through the membrane This, in turn, increases operating costs due to possibly reduced membrane lifetime (Sablani et al. 2001).
In more porous membranes, membrane fouling forms an immobile solid phase forms at the liquid-membrane interface unlike concentration polarization, although the latter can accelerate fouling by supplying the membrane with a higher effective foulant concentration (Benecke 2018; Chen et al. 2004).

Concentrate from high pressure-driven membrane treatment

Nanofiltration and reverse osmosis treatment is associated with a concentrate or retentate stream generated as a by-product of the filtration process and contains higher concentrations of the removed substances. The composition of raw water, operating parameters of the membrane process and extent of pre-treatment can influence characteristics and volume of the concentrate generated (Joo and Tansel 2015). In order to minimize the volume of the concentrate and increase the permeate volume, it is usually desired to operate the NF/RO system at higher recovery, although this is associated with higher operational costs. Concentrates from NF and RO systems contain higher concentrations of ions, smaller organic molecules as well as chemicals added during the treatment step including antiscalants. Untreated or improperly managed concentrate can result in adverse environmental effects due to high salinity, nutrients (phosphorus, nitrogen) and organic contaminants including emerging contaminants (van der Bruggen et al. 2003), and must therefore be monitored regularly and managed responsibly.
The additional challenges of concentrate stream with respect to antiscalants are discussed under Sections 2.4.3 and 2.5.

2.3 Membrane scaling

Although reverse osmosis is considered as one of the most efficient and reliable seawater desalination technologies for potable water production, it is severely limited by fouling and scaling issues. The prominent types of fouling in desalination can be classified into organic fouling, inorganic scaling, and biofouling (Spinthaki and Demadis 2020). Inorganic salt precipitation, also known as scaling, refers to the accumulation of carbonate, sulfate salts of

calcium, magnesium, barium and silicates on the surface of the membrane and within membrane filtration system. Scale precipitation is triggered by supersaturated solutions of sparingly soluble salts, resulting in solute phase transformation from liquid to solid. Scaling drastically interferes with the performance of membrane-based desalination processes by blocking the active membrane layer where the water-salts separation occurs, leading to higher hydraulic resistance, reducing the separation performance of the membrane by decreasing the permeability and rejection and subsequently damaging the active membrane layer. According to Mullin 2001, unlike amorphous solids, crystalline solids are characterized by the highly ordered arrangement of the constituent molecules into some fixed rigid pattern known as a lattice which extends into all directions and smooth crystal faces develop during crystal growth. Benecke 2018 hypothesizes the scale formation to occur under fast reaction kinetics where solid phase formation may not be limited to the formation of crystalline solids but may include the occurrence of amorphous phases too. Some of the most common scale-forming salts in natural waters are calcium sulfate dihydrate (gypsum, $CaSO_4 \cdot 2H_2O$), calcium carbonate (calcite, $CaCO_3$), silicon dioxide (silica, SiO_2) and barium sulfate (barite, $BaSO_4$) (Shirazi et al. 2010). Broadly, scaling in RO membranes is classified as alkaline (e.g., calcium carbonate), non-alkaline (e.g., calcium sulfate) or silica-based.

The following sub-sections delve into the theoretical aspects of sulfate and carbonate scales of calcium, which are of experimental relevance in the present work.

Calcium Sulfate

Calcium sulfate ($CaSO_4$) is a common inorganic foulant usually occurring in the form of calcium sulfate dihydrate ($CaSO_4 \cdot 2H_2O$), widely known as gypsum, calcium sulfate anhydrous ($CaSO_4$), and calcium sulfate hemihydrate ($CaSO_4 \cdot 0.5H_2O$), with gypsum being the most common variant in natural deposits. Figure 5 shows views of the crystal structures of the three common forms of calcium sulfate as gypsum, hemihydrate and anhydrite.

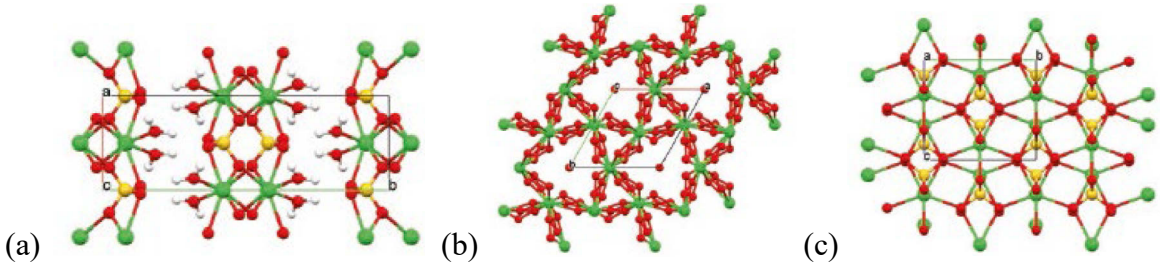

Figure 5: Crystal structures of calcium sulfate salts in the form of (a) gypsum viewed along c-axis (b) hemihydrate viewed along c-axis and (c) anhydrite viewed along a-axis, where Ca=green, O=red, S=yellow, H=white (Source: (Spinthaki and Demadis 2020))

The crystal structure of gypsum consists of CaO_8 and SO_4 polyhedra stacked along the b-axis to form layers. Water molecules are located between the layers. The water molecule shares an oxygen atom with the Ca-polyhedron and hydrogen atoms form (at ambient pressure) weak hydrogen bonds with the oxygen atoms belonging to SO_4 and CaO_8 polyhedra. The structure of calcium sulfate hemihydrate ($CaSO_4 \cdot 0.5H_2O$) is very different. In case of calcium sulfate hemihydrate, the Ca atoms are coordinated by six O atoms, all originating from different sulfate anions. The Ca-sulfate coordination creates triangles within which the water molecule is

situated, thus creating a "channel" running parallel to the a-axis. In contrast to gypsym, the water is not coordinated to a Ca center, but can be better described as lattice water. The anhydrite form of calcium sulfate contains no water (either bound, or in the lattice). The coordination of Ca by the oxygens of the sufate anion creates a dense, three-dimensional structure. The Ca atoms are coordinated by seven oxygens, originating from different sulfate anions (Spinthaki and Demadis 2020).

Calcium Carbonate

Calcium carbonate ($CaCO_3$) is another mineral commonly responsible for scaling via calcium and bicarbonate ions in industrial water, seawater, or groundwater sources. It crystallizes in three different crystal forms: calcite, aragonite, and vaterite (Saji et al. 2020). While Ca^{2+} is abundant in surface or ground waters, bicarbonate (HCO^{3-}) is one of the most common anions found in potable water due to the dissolution of atmospheric CO_2, and thereby leading to abundance in $CaCO_3$ presence. Figure 6 shows the crystal polymorphs of calcite, aragonite and vaterite.

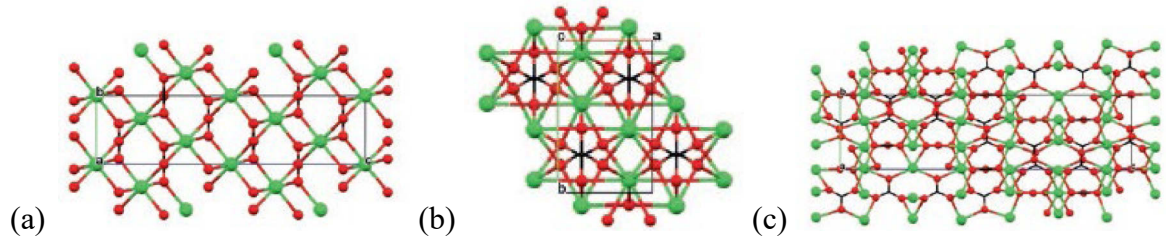

Figure 6: Crystal structures of calcium carbonate salts in the form of (a) calcite viewed along a-axis (b) aragonite viewed along c-axis and (c) vaterite viewed along a-axis, where Ca=green, O=red, C=black (Source: (Spinthaki and Demadis 2020))

The three main polymorphs of calcium carbonate occur as calcite, aragonite, and vaterite, each characterized by distinct crystal structures. In calcite, planar carbonate ions (CO_3^{2-}) are coordinated with Ca^{2+} ions, which are surrounded by oxygen atoms in distorted octahedral arrangements. The carbonate groups are organized in layered structures, with neighbouring layers exhibiting a 60° rotation relative to each other along the c-axis. Aragonite has a denser orthorhombic structure and is generally considered stable at higher pressures; however, it can also crystallize under ambient conditions and persist in a metastable state for extended periods. Its pseudo-hexagonal arrangement contributes to its characteristic twinning behaviour associated with a 60° rotation around the c-axis. Vaterite possesses a more complex and less stable structure, in which Ca^{2+} ions form a hexagonal framework and carbonate groups occupy interstitial positions in an ordered arrangement. The overall structure of vaterite exhibits an approximately hexagonal close-packed organization of carbonate groups (Spinthaki and Demadis 2020).While the calcite is categorised as a hard scale, aragonite and vaterite are generally considered softer types of scale that are more easily removed (Saji et al. 2020).

Silica-based scaling

Unlike typical mineral scales, silica-based scaling is a complex phenomenon involving multiple types of mechanisms (Milne et al. 2014). Silica in the form of SiO_2 is commonly found in groundwater originating from weathering of rocks. The main dissolution reaction is the hydrolysis of Si-O-Si bonds, resulting in production of silicic acid (H_4SiO_4). When silicic acid concentration reaches a certain level, it begins to polymerize, forming polymeric, colloidal, and particulate silica. The small clusters are collectively known as polysilicic acid or polymeric silica. The polymerization of amorphous silica occurs through a process where soluble silica units break down and silicate anions combine to form larger macromolecules. This polymerization rate is highly pH dependent, proceeding quickly in neutral to slightly alkaline conditions, but dropping to a minimum at pH values above 9.5 and below 6.5 (Park et al. 2020). Additionally, it has been described that between pH 7-8, negatively charged silicate ions are predominant leading to further particle growth of stable crystals, but below pH 7, low charge leads to poor aggregation of molecules resulting in scaling in the form of gel (Spinthaki and Demadis 2020).

Besides SiO_2, the presence of multivalent cations can also impact the solubility of silica due to their ability to interact with the silicate anion. Ca and Mg silicates are known to cause severe scaling industrial cooling towers. Additionally, aluminium, iron and some trace metals are also known to affect the solubility of silicates, leading to the formation of metal silicates with varying scaling intensity and pH behaviour (Milne et al. 2014, Yu et al. 2020).

2.3.1 Scaling mechanisms

In order to increase the efficiency and lifetime of a NF/RO system, it is important to understand the underlying mechanisms of scaling. Understanding the different interactions between membrane surfaces and scalants can help guide the scaling mitigation process and make more specific scaling predictions.

The following sections present the general mechanisms of scale formation, factors influencing it and its mitigation by antiscalants.

Supersaturation

The fundamental pre-requisite for scaling to take place from dissolved minerals in solution is the condition of supersaturation. A supersaturated solution contains more dissolved solids than that given by the solubility limit of the salt. Spontaneous crystallization is impossible in the unsaturated ‘stable’ zone, improbable in the supersaturated ‘metastable’ zone and probable in the supersaturated ‘labile’ zone (Mullin 2001, Benecke 2018) as shown by the regions A-B-C in Figure 7.

The supersaturation ratio (S) and saturation index (SI) of sparingly soluble salts in aqueous solution are widely used to express the degree of supersaturation in aqueous solution, given in Equation 4:

$$SI = \log_{10}(S) = \log_{10}(IAP \cdot K_{sp}^{-1}) \qquad \text{[Equation 4]}$$

where IAP is the ion activity product of the salt ions in solution and K_{sp} is the solubility product, i.e., the equilibrium value of IAP. As a result, at SI < 0, a solution is unsaturated, saturated at SI = 0, and supersaturated at SI > 0 (Benecke 2018, Mullin 2001).

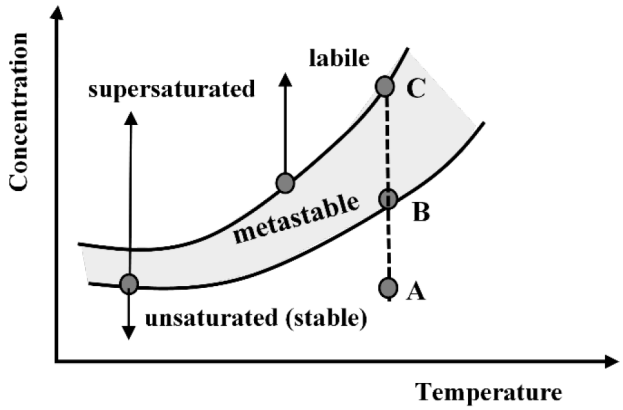

Figure 7: Schematic of supersaturation achieved from an unsaturated solution during pure water filtration represented by lines A-B-C (Benecke 2018)

Nucleation and Crystallization

Any supersaturated solution will eventually, if not spontaneously, overcome its saturation limit, resulting in the appearance of new structures - nucleation refers to this process where free or dissolved ions or molecules gather and organize to form new structures. According to classical nucleation theory (CNT), critical nuclei arise in small areas of extremely high supersaturation from solution via assembly of ions (Karthika et al. 2016). CNT assumes that the nucleus formed may be of any size, but has the same structural, compositional, and thermodynamic features as the stable crystalline phase, including the same structure, composition, and density (Benecke 2018, Karthika et al. 2016, Prien 2021). Newer research has revealed that the nucleation process goes through intermediate stages before reaching a thermodynamically stable phase, such as the formation of prenucleation clusters, which aggregate into amorphous nanoparticles and polycrystals and eventually form crystalline domains (Beckmann 2013, Karthika et al. 2016). Many subcritical nuclei fail to achieve a critical size before redissolving during nucleation (Mullin 2001). However, once a critical size is reached, the change in free enthalpy caused by adding another building block (ion or atom) becomes negative, making growth more advantageous than the dissolution of the resulting stable or critical nucleus (Beckmann 2013).

The nucleation process is normally characterized as primary and secondary nucleation – while primary nucleation describes the mechanisms underlying the creation or appearance of the first

crystal germ, secondary nucleation relates to the crystals pre-existing within the system. Therefore, primary nucleation is commonly correlated to the "induction time" while secondary crystallization describes further crystal growth and is attributed to the "crystallization time". Primary nucleation can further be divided into homogeneous and heterogeneous nucleation (Benecke 2018, Prien 2021, Saji et al. 2020).

The process of forming such a crystal involves specific energy called the free energy of activation of nucleation. For a given crystalline phase and temperature, the rate of nucleation (J_N) is strongly governed by the supersaturation ratio (S), the temperature (T) and the solution-mineral interfacial energy, σ ($J \cdot m^{-2}$) as indicated by Equation 5 (Benecke 2018):

$$J_N \propto \exp [- \Delta G^* \cdot R^{-1} \cdot T^{-1}], \text{ where } \Delta G^* \propto \sigma^3 \cdot T^{-2} \cdot \ln^{-2} S \quad \text{[Equation 5]}$$

where ΔG* is the Gibbs free energy of homogeneous nucleation in $J \cdot mol^{-1}$ and R the ideal gas constant in $J \cdot mol^{-1} \cdot K^{-1}$. Below a certain critical supersaturation ratio, J_N is practically zero, however, at higher supersaturation ratios, J_N increases exponentially.

Homogeneous nucleation takes place in the liquid phase, mostly due to turbulence in the system as represented in Figure 8(a). It has been hypothesized that the actual formation of such a nucleus result from the simultaneous collision of the number of necessary salt molecules (Saji et al. 2020), though this is difficult to quantify in practice. Nucleation is said to be heterogeneous when the nucleus forms on a surface, which in the case of NF/RO operation is most likely on the surface of the membrane (Figure 8(b)).

It is generally accepted that heterogeneous nucleation can be initiated at a lower degree of super-saturation than homogeneous nucleation. The variation in free enthalpy associated with heterogeneous nucleation is lower than that associated with homogeneous nucleation. The secondary nucleation in a weakly supersaturated solution is induced and supported by seed crystals of the same nature as the precipitate (Saji et al. 2020).

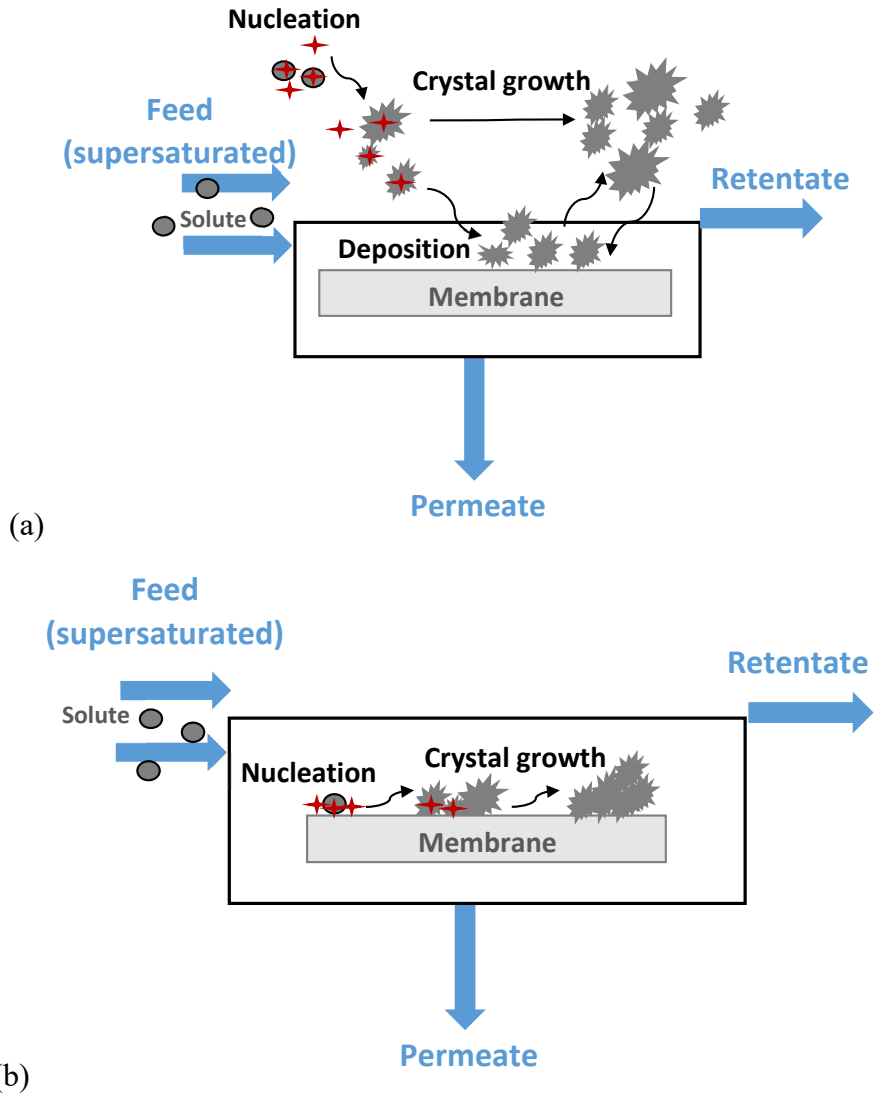

Figure 8: (a) Homogeneous scale formation mechanism in liquid phase of the solution, and (b) heterogeneous scale formation mechanism between liquid solution-solid surface phase

Heterogeneous nucleation on foreign surfaces is energetically favourable and reduces the required supersaturation for spontaneous nucleation (Beckmann 2013). However, for high nucleation rates, the surface available for heterogeneous nucleation can become limiting. The overall free energy change associated with nuclei formation must be less in the case of heterogeneous nucleation than in the case of homogeneous nucleation. This is explained by the lower surface free excess energy GS required in the case of heterogeneous nucleation to generate a critical-sized crystal nucleus (Mullin 2001). As a result, heterogeneous nucleation can occur at lower supersaturation ratios than homogeneous nucleation. Because it is hard to generate a solution fully devoid of foreign materials, some theories dismiss the possibility of perfect homogeneous nucleation as a common event (Beckmann 2013, Oshchepkov et al. 2021). Nonetheless, bulk crystals generated by homogeneous scaling affect membrane performance differently than surface-triggered heterogeneous crystals. The probability of scale formation is enhanced by concentration polarization, a phenomenon that results in elevated

solute concentration at the membrane surface compared to the bulk solution. Most immediate consequences of concentration gradient from bulk solution to membrane surface are higher risk of scaling, deterioration of permeate water quality and permeate flux decline due to increased osmotic pressure (Wang and Tarabara 2007). The degree of concentration polarization is considered to trigger heterogeneous nucleation compared to homogeneous crystallization (Matin et al. 2019).

Induction time

Nucleation and crystallization theories describe that prior to the appearance of the solid phase in a homogeneous liquid system, critical nuclei must first be formed, which must then grow to a detectable size (Söhnel and Mullin 1988). Following this, crystals begin to grow and elementary building blocks are added to the existing crystal surfaces. Crystal growth is broadly hypothesized to comprise of convective and diffusive transport of the elementary building blocks to the crystal surface and the subsequent incorporation of the building blocks into the crystal. Depending on the material system and the fluid dynamic boundary conditions, either the initial transport or the incorporation can determine the speed of the overall mass transfer. A variety of aspects influence the pace of crystal formation in a complicated way. Supersaturation, temperature, particle size, morphology, contaminants, flow conditions, and the surface orientation of the growth front are some important factors. Induction time is a general expression encompassing these different nucleation and crystal growth mechanisms. It is the inherent property of a supersaturated solution to eventually, if not spontaneously, release its supersaturation. At constant metastable supersaturation, a specific amount of time, known as induction time, elapses between supersaturation and the formation and subsequent identification of a new crystalline phase. The nucleation time necessary for the production of stable nuclei and the time required for the nuclei to develop to detectable size define the induction time (Karthika et al. 2016, Mullin 2001). Therefore, induction time can be considered as being made up of several periods such as intermediate time, stable nucleus formation time and growth time. Intermediate time is the time required for a supersaturated system to achieve a quasi-steady-state distribution of molecular clusters, following which time is also required for the formation of a stable nucleus and finally crystal growth time can be defined as the time for the nucleus to grow to a detectable size. Thus, induction time can be the sum of all these periods, although distinguishing and separately measuring these individual times is extremely challenging (Mullin 2001). Alternatively, in practice, induction time may be defined as the time taken for first observable change in solution properties (Benecke 2018). It is a critical parameter of nucleation kinetics that is essential for optimizing operational modes in membrane systems for brine treatment (Rolf et al. 2022). Induction time is affected by the level of supersaturation, presence of contaminants, the state of agitation, viscosity and the temperature of the solution. Higher supersaturation levels, for example, may cause shorter induction times due to enhanced rate of nucleation, while increase in flow rate may decrease the induction time due to enhanced secondary nucleation. Impurities can either lengthen or shorten the induction time depending on their chemical characteristics. For instance, some metal ion impurities may delay the onset of crystal formation while crystal seeds reduce the induction time (Hasson and Semiat 2006).

Several authors have previously used different experimental methods to determine induction time, owing to the fact that no standard procedure exists due to several parameters and complicated measurement techniques (Zeino et al. 2018). Some studies defined induction time as a change in pH value by 0.03 units from the original value (Waly et al. 2012), while some studies monitored the electrical conductivity of a solution (Saji et al. 2020). Other techniques such as light scattering or turbidity were also commonly utilized for induction time determination (Zeino et al. 2018). Khormali et al. 2016 measured the concentration of calcium ions a stirred tank containing scaling solution and induction time was defined at first instance where the Ca^{2+} concentration in solution started to decrease due to precipitation of mineral scale.

Induction period is not a fundamental property of a system, since the objective is to identify the initiation of crystalline growth or to detect crystal growth after its inception and is variable when applied in practice. In this study, induction time in the stirred-beaker tests is determined via turbidity measurement.

2.3.2 Factors influencing scaling

The following factors are known to influence the likeliness and extent of scaling in high-pressure membrane filtration systems:

Saturation index (SI): Solute supersaturation is the fundamental requirement for scaling to take place and is described in detail under Section 2.3.1. Increasing supersaturation accelerates the nucleation rate. If supersaturation occurs at the membrane–liquid interface, heterogeneous scaling on the membrane surface is likely. However, if the supersaturation region is away from the membrane surface, homogeneous crystals form in the bulk solution and deposit on the surface scales. The period of time which elapses between the achievement of supersaturation and the appearance of the first crystals, is referred to as the induction time and is governed by the degree of supersaturation (saturation index), temperature and turbulence (Rozova 2014; Shirazi et al. 2010).

Temperature: The temperature of the feed is one of the underlying reasons for scale formation as it impacts the separation performance of the membrane. Temperature affects the viscosity of water, the solubility and the mass transfer coefficient of inorganic salts or particles. The viscosity of water decreases with temperature. As a result, the permeate flux increases in higher temperature and convective transportation of scalants to the membrane is more significant. Consequently, membrane scaling is expected to be severe. However, the mass transfer coefficient also increases with temperature. Therefore, back diffusion of solutes to the bulk solution is faster at high temperature (Hu et al. 2025). Additionally, temperature affects the solubility of salts and their degree of supersaturation as well (Shirazi et al. 2010).

pH: The pH of NF/RO feed is an important parameter to determine whether scale-precursor ions remain dissolved in solution or could subsequently precipitate. The scaling species

occurring at a given pH can be determined using the acid dissociation constant (pK_a) given in literature (Rolf et al. 2022). In the case of calcite scaling, carbonic acid has two pKa values of 6.37 and 10.32, where CO_3^{2-} becomes the dominant form in solutions at pH over 10.32 inducing more precipitation of calcium carbonate. Reducing the pH of the solution to below 6.37 can prevent calcium carbonate scaling as carbonic acid predominates (MacAdam and Parsons 2004). The solution pH also additionally controls the $Ca–CO_3$ binding strength which decides the type of calcium carbonate polymorph being formed (Rolf et al. 2022). In contrast to calcium carbonate, pH adjustment is not effective for the control of gypsum ($CaSO_4 \cdot 2H_2O$) scaling because speciation of the sulfate ion barely changes with respect to solution pH. However, pH of the supersaturated sulfate solution is responsible for the structure of resulting gypsum scale especially the length to width aspect ratio (van Driessche et al. 2019). $MgSO_4$ is known to precipitate a solution with pH between 9 and 10.5, while barium sulfate is the least of the three sulfate species and also undergoes structural change with respect to pH (Rolf et al. 2022).

Ionic strength: The ionic strength of the feedwater may alter precipitation kinetics, such that polymorphs that are dominant at low and high ionic strengths are different and additionally vary in their size and surface charge due to intramolecular forces between the scalants and background electrolyte ions (Rolf et al. 2022). As per the Debye–Hückel law, as the ionic strength estimated from background NaCl concentration increases, the ionic activity of other scaling ion species may decrease. Reduced ionic activity leads to a higher ion solubility, and, correspondingly, a lower degree of supersaturation (Reznik et al. 2011).

Membrane properties: Surface roughness of membranes influence extent of scaling, whereby rough membranes provide more contact sites for scaling ions and reduce shear forces, while additionally increasing surface free energy increasing likeliness for crystal deposition and growth on the membrane surface. Hydrophilic membranes are more likely to form hydrogen bonds with water molecules, which increases energy barrier for nucleation and leads to lesser likelihood for scaling to take place on the membrane (Hu et al. 2025). While silica scaling is considered to be dependent on surface charge of membrane material, dependence of gypsum and calcite scaling on membrane surface charge has yet been derived with certainty (Rolf et al. 2022).

Membrane filtration operational parameters: The extent of scaling within a membrane system may be attributed to the operational conditions, more specifically the crossflow velocity and transmembrane pressure (TMP). Dense membrane like NF and RO when operated at high pressure are more likely to experience enhanced scaling due to higher potential for concentration polarization even at low concentration of scaling ions in the feed. Drinking water systems are operated at high TMP to increase water recovery and subsequently may experience higher scaling within the system, due to lowering of impact of crossflow shear stress. Lower permeate flux may be able to control level of heterogeneous scaling at membrane surface (Rolf et al. 2022).

2.3.3 Scaling detection methods

Scale deposition occurs when mineral salts have low solubility in water and deposit on any surface that is contact with water. According to Amjad 2014, Mullin 2001 and Zhang et al. 2018, most scaling processes and their corresponding detection with or without scale inhibitors, must take into consideration at least one of the five steps given below, although sometimes there is no absolute boundary between each step:

i. Initiation period: Refers to the induction period between the establishment of a supersaturation condition and the onset of scale nucleation. During this period, no visible deposition occurs, but the solution is thermodynamically primed for crystal formation.
ii. Scale crystal formation and growth: Describes the growth of the scale nuclei to become crystalline structures.
iii. Transport and deposition: Involves the migration of formed crystals to solid surfaces, where they adhere and contribute to the growth of scale layers, including deposition onto pre-existing crystalline structures.
iv. Scale removal: Involves the partial or complete detachment of deposited scale from surfaces either via chemical dissolution or mechanical forces such as fluid shear stress, depending on the adhesion strength of the deposit.
v. Deposit aging: Process of recrystallization, where phase transformation and Ostwald ripening of large crystals from smaller crystals to preserve surface energy occur, subsequently increasing the mechanical and chemical resilience of the scale layer, making it more stable.

Amjad 2014 broadly categorises scale inhibition test methods as static methods, dynamic methods, electrochemical methods, membrane tests and analytical methods which deal with scale identification during one of the above-mentioned stages. The different experimental apparatuses differ in terms of surface area, ionic strength, solution pH, SI and hydraulic conditions and reflects different characteristics of antiscalants (Zhang et al. 2018).

Static tests commonly involve “beaker” or “jar” tests, which monitor the precipitation of scale-forming species from supersaturated solutions over time. Scaling is evaluated based on the rate and extent of precipitation within a specified period. Although standardized by National Association of Corrosion Engineers (NACE), test conditions such as salt concentration, pH, temperature and duration are often varied to reflect different operational scenarios (Amjad 2014). Other static tests include heat exchanger tests, monitoring of pH change, Ca concentration change and conductivity change over time to detect scale formation and progress.

Dynamic scale detection methods involve hydrodynamic conditions generating turbulent conditions that mimic fluid flow conditions based on shear stress, Reynold’s number or mass transfer coefficient. Examples including rotating disc apparatus, dynamic capillary flow tests and modifications to membrane tests (Amjad 2014). In most cases, dynamic tests result in much

longer induction times compared to static tests – this most likely due to the tendency of the test to interact with the nucleation stage compared to the crystal growth stage.

Additionally, analytical methods have also been used exclusively or potentially integrated with some static or dynamic methods to improve scaling detection. Microscopy and spectroscopy techniques like scanning electron microscopy (SEM), atomic force microscopy (AFM), XRD spectroscopy, infrared (IR) spectroscopy and particle size distributions methods have also been used to evaluate the scaling potential of a solution (Amjad 2014, Yu et al. 2020, Zhang et al. 2018). Since each method targets specific features of scale formation, so far, no single method has been prescribed to detect scaling. Therefore, multiple complementary methods are generally used to determine the scaling potential of a solution and resulting scale inhibition performance of an inhibitor (Ansari and Pandit 2020).

2.4 Scale inhibition

Scaling control is necessary during drinking water treatment to sustain smooth and long-term operation of the NF/RO system. Techniques for scale inhibition include measures which tackle the factors causing scaling that were described previously in Section 2.3.2. Novel membrane materials and surface modification may have a considerable impact on scaling propensities. Polyamide thin-film composites (TFC) have been used to develop NF/RO membranes and surface material modifications such as with nanoporous graphene or metal oxides are further introduced to improve anti-scaling performance by altering properties such as surface charge, morphology, chemical groups, as well as hydrophilicity (Saji et al. 2020). Physical and chemical cleaning involving removal and soaking the membrane in a suitable cleaning solution for a few minutes or even a few hours, constitutes a more conventional form of scale control in NF and RO. However, this method is not always practical and is ineffective to prevent scaling triggered by concentration polarization during NF/RO filtration especially at high recoveries (Saji et al. 2020). Feed pre-treatment is another physico-chemical scale inhibition method adopted depending on the characteristics of the water to improve reliability and lifespan of the membrane. Some of the widely used RO pre-treatment processes include coagulation, ion-exchange and some instances of electrolytic $CaCO_3$ scale removal via high pH environment around the cathode (Antony et al. 2011). Changes in system design and operational settings such as filtration with a rotating membrane module, limited product recovery, intermediate chemical mineralization, etc. can reduce the likelihood of scale formation by lowering scaling kinetics and maintaining scaling ion concentrations below the solubility levels (Antony et al. 2011). Although dense membranes cannot be backwashed, innovations such as osmotic backwashing of spiral-wound RO membrane systems by varying the pressure-concentration conditions across the membrane for periodic permeate-flow direction reversal could transform scale inhibition in NF/RO systems (Sagiv et al. 2008). Acidification of the feed water to pH 5–7 may increase solubility of alkaline scales such as calcite and preserves calcium carbonate in the dissolved form. Hydrochloric acid is preferred over sulfuric acid due to the potential for the latter to form sulphate scales such as $CaSO_4$, $BaSO_4$ and $SrSO_4$. While acidification may be

effective against calcium phosphate scale, it is unsuccessful against certain scales like barium sulfate and may not be cost-effective for high flow rates and additionally poses the danger of corrosion in pipe systems due to the strong acids (Antony et al. 2011, Ismail et al. 2019).

A widely used technique for controlling scale deposition is by dosage of an antiscalant (AS) at sub-stoichiometric amounts (typically 0.5–10 mg/L). Antiscalants are chemicals which are capable of delaying the precipitation of sparingly soluble salts and producing morphological changes that result in lower adherence of scale deposits on flow surfaces (Ismail et al. 2019). The addition of antiscalants is one of the most commonly applied methods for inhibiting scaling in the reverse osmosis (RO) process, particularly under high water recovery conditions, where reduced concentrate discharge increases the potential for scaling (Darton 2000, Rahardianto et al. 2007, Tong et al. 2019). Antiscalants are predominantly polyelectrolytes and their performance is dependent on the constituting functional groups, molecular weight and charge density. Their effectiveness may also be influenced by external parameters such as the temperature and pH. The choice of a specific antiscalant depends on the feed water quality. Generally commercial antiscalants are designed to target specific scalants. Where antiscalant performance is known to be limited, sometimes a combination of two or more antiscalants may be employed to improve scale inhibition performance. Maintaining the correct antiscalant dosage level is crucial and higher dosage does not necessarily minimize scaling as the presence of certain precipitates can alter the effectiveness of applied antiscalants (Kelle Zeiher et al. 2003). The optimal dosing and allowable maximum saturation levels of scale forming ions are generally determined by specific software programmed by suppliers or given by manufacturers themselves or determined from previous experience or trial and error (Antony et al. 2011).

The following sections offer detailed background and insights into different types of antiscalants, inhibition mechanisms and their limitations that are relevant in the context of this study.

2.4.1 Types of antiscalants and state-of-art of application

Antiscalants can be broadly categorized as phosphorus-containing antiscalants and phosphorus-free antiscalants, sometimes debatably referred to as “eco-friendly” antiscalants. They are essentially comprised of chemical additives capable of controlling either the formation of scales or its deposition on the membrane or both. Different antiscalant active ingredients are effective against a specific type of scalant(s). Besides the active ingredients, scale inhibition efficiency of antiscalants is also dependent on ion concentration, temperature, pressure, pH along with characteristics of antiscalants such as functional groups, molecular weight, polydispersity, molecular configuration, etc. (Saji et al. 2020). Conventionally used antiscalants include hexametaphosphate (HMP), tripolyphosphate (TPP), phosphonic acids like aminotris methylenephosphonic acid (ATMP), 1-hydroxyethane-1,1- bis phosphonic acid (HEDP), 2-phosphonobutane 1,2,4-tricarboxylic acid (PBTC), organic polymeric products like polyacrylic acid (PAA), polycarboxysulfonates, etc. (Yu et al. 2020). They interact with various functional groups such as phosphonic, carboxylic and sulfonic groups, and inhibit scale formation by

interacting with one or more aspects of the nucleation and crystal growth process (Al-Roomi and Hussain 2016, Amjad 2014, Darton 2000, Dobberschütz et al. 2018).
Phosphorus-based antiscalants typically include phosphates and phosphonates; the former is comprised of O-P-$(O)_3$ linkages derived from orthophosphoric acids in linear or cyclic form, while the latter refer to highly soluble salts and esters of phosphonic acid, $HPO(OH)_2$ (Antony et al. 2011). Sodium hexametaphosphate (SHMP) is a polyphosphate which was among the first antiscalants commercially available to the membrane industry due to its excellent sequestering property and ability to modify crystal structures (Antony et al. 2011). Phosphonates are considered to be more stable than phosphates due to C-P bonds. Both compounds are reported to have excellent complexing properties. Phosphates are considered to prevent scale formation or dissolve precipitates by forming relatively stable soluble complexes with metal ions, but may also easily hydrolyze into orthophosphate ions, which may increase risk of phosphate scaling within the membrane system (Yu et al. 2020). Phosphonates are known to produce more stable complexes with scaling ions, especially when they contain a greater number of phosphonic acid groups (Yu et al. 2020). Since NF/RO treatment was associated with generation of a concentrate stream containing large amounts of phosphorous from the antiscalants, the development of phosphorus-free scale inhibitors gained popularity. Polycarboxylates characterized by -COOH groups and comprising of homopolymers, copolymers of acrylic acid and maleic acid, as well as polymers like polymethacrylic acid and polyasparates were developed as antiscalants (Yang et al. 2017, Yu et al. 2020). Polycarboxylic acid based antiscalants have excellent chelating properties and lead to dispersion and lattice distortion of scaling crystals (Antony et al. 2011). Saji et al. 2020 also reported that polysuccinimide and citric acid were effective to inhibit gypsum scaling by interacting with the active sites and distorting the crystal morphologies. Ketrane et al. 2009 compared performance of three polyphosphates, one polyphosphonate and one polycarboxylic acid for CaCO3 scaling inhibition, and found phosphonates to have maximum inhibition potential for the longest time.

Apart from anionic polymeric antiscalants, Yu et al. 2020 reported studies which used cationic polymers such as polyaminoamide (PAMAM), polyethyleneimine (PEI), polyallylamine hydrochloride (PALAM), and poly(acrylamide-co-diallyldimethylammonium chloride) (PAMALAM) to inhibit silica scaling, since the former have no effect on silica growth which is a polymerization phenomenon instead of crystallization. Besides, typical phosphonates and polycarboxylic acid based antiscalants, a diverse combination of active ingredients have emerged in the antiscalant market for drinking water treatment. Shen et al. 2018 synthesized a product based on HEDP and PAA, and synthesized hydrolyzed poly maleic anhydride (HPMA) and found that it could inhibit calcite scaling by over 85%. Typically, HEDP is known to change calcite morphology, HPMA adsorbs to the carbonate ions and PAA is known to distort calcium crystal and inhibit its growth (Saji et al. 2020). In addition to polycarboxylic acid antiscalants, natural polymeric antiscalants are increasingly being applied as antiscalants. Starch, cellulose, lignin, inulin, tannin, collagen and vegetable extracts are being pursued as potential environment-friendly antiscalants due to their advantages of abundant source, low cost, and biodegradability (Guo et al. 2021, Melnik et al. 2020, Yu et al. 2020). Carboxymethyl inulin

(CMI) is one such ingredient gaining popularity as a commercial antiscalant due to environmental benefits (Boels and Witkamp 2011).

In Germany, it was reported that the majority of municipal drinking water systems which implement NF/RO filtration for removal of sulfate, nitrates, chlorides and hardness causing salts, use antiscalants based on phosphonates, especially DTPMP and ATMP, while a small number of suppliers resort to P-free antiscalants based on PAA (Bergdolt et al. 2019). CMI antiscalants, although popular in Europe, have not yet been approved for use in German municipal drinking water systems according to the German Drinking Water Ordinance. The number of commercially available antiscalants for NF/RO filtration is large and new formulations are continuously introduced into the market, sometimes with little transparency on the ingredients, resulting in a fluid status quo on antiscalant application.

2.4.2 Inhibition mechanisms

The inhibition mechanisms of antiscalants are generally complex and often involve ambiguous fundamental processes. At the fundamental level, antiscalants interact with a certain stage of scaling process, most likely nucleation, crystallization or polymerization (in case of silica). While they do not entirely eliminate the scaling constituents or the precipitation tendency, the consequences of antiscalant addition are manifested as changes in the crystal number, crystal size distribution and in the type of the precipitating polymorph. They are generally regarded to extend the nucleation phase (subsequently resulting in high induction period) or retard precipitation during the crystal growth phase, causing morphological changes and leading to decreased crystal deposition on surfaces. They may additionally affect the rates and/or mechanisms of some or all the growth processes including nucleation, crystal growth, aggregation, and phase transformation (Amjad 2014).
Scaling inhibitors are generally demonstrated and hypothesized to work based on the following major underling mechanisms:

- Threshold inhibition effect: The threshold inhibition potential of antiscalants refers to the interaction of the antiscalant with the scaling ions at sub-stoichiometric levels. It is hypothesized that the adsorption of the inhibitor onto the nucleation sites of the scaling ions takes place, thereby interfering with crystal growth and morphology (Amjad 2014). Once the solution reaches supersaturation for a certain scalant, certain types of antiscalants adsorb onto the embryo crystals of the scalant potentially due to similarities in the structure. This is then known to prevent crystal growth phase from taking over and can delay further crystal growth for significantly longer amount of time (Amjad 2014, Spinthaki and Demadis 2020). Melnik et al. 2020 reported that for an antiscalant to possess threshold inhibition potential, it must have strong adsorption capability even in the presence of thermodynamically unstable molecules in the solution. Additional branches in the antiscalant molecule adhere onto the entire surface of the scaling crystal and allowing no free sites for scaling ions to grow further. Over time, as the scaling nuclei are dissolved due to changes in solution saturation, the antiscalant molecules are desorbed into the solution and may interact with other nuclei which appear in the system. However, for maximum threshold inhibition effect,

scale inhibitors must be added in sufficient amount to be able to adsorb effectively with a certain level of scaling salts.

- Crystal distortion effect: Crystal distortion refers to a change in the normal crystal growth pattern of the scaling salt, subsequently leading to a change in configuration of the resulting crystal structure (Amjad 2014, Saji et al. 2020). Melnik et al. 2020 describes a Kossel model, according to which there exists three regions on the crystal where the antiscalant adsorb and result in changed crystal structure - growth step breaks referred to as kinks, growth steps, and facets as shown in Figure 9.

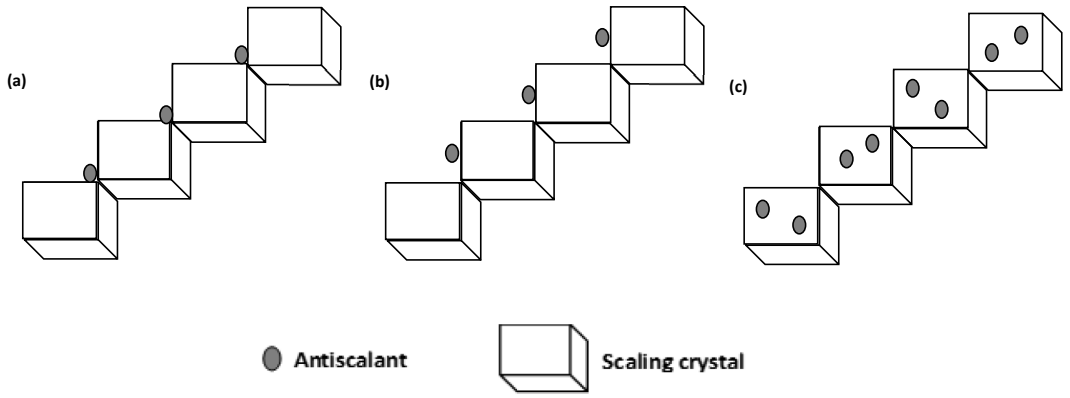

Figure 9: Schematic of scaling crystal distortion via antiscalant adsorption onto crystal growth sites along (a) kinks (b) steps and (c) facets of crystal (Melnik et al. 2020)

According to this hypothesis, for small antiscalant molecules, steps and kinks on the scaling crystal are sites of high activity and also the most preferable adsorption sites, while for antiscalants with large molecule sizes, sorption of the antiscalant takes place on more likely on the facets. In case of sorption along facets, the adsorbed antiscalant must cover a larger surface in order to prevent the growth of a step along the surface of a crystal, implying that it must be dosed sufficiently or include an ingredient with a large molecule. If antiscalant adsorption takes place along kinks and on steps, the growth of a crystal can be prevented even at low dosage. Crystal distortion property of antiscalants is unable to stop crystals to form in supersaturated conditions, but may affect the nature of the resulting crystal properties including adhesion, roughness, crystal size and even structure of the crystal.

- Dispersion: Certain antiscalant ingredients, although not being able to prevent nucleation and crystal growth, have the ability to prevent the scaling crystals from attaching to critical surface such as the membrane itself. Essentially, this keeps the crystals suspended in solution. It is generally regarded that antiscalants impart a certain surface charge on the crystal along with similar charges cause the crystals to repel one other. The high ionic charges prevent the crystals from agglomerating and settling. Examples of threshold scale inhibitors that mainly function in this mode are organic polymeric inhibitors (Zhang et al. 2016a).
- Chelation: Chelating agents function by sequestration or binding ions to form stable water-soluble complexes. The chelating antiscalant molecules are generally negatively charged and will bond with as many scaling cations as possible depending on the stoichiometric ratio, thereby preventing reaction with the scaling anion. The stronger the coordinate bond

between the scaling cation and the negative antiscalant species, the stronger the extent of inhibition. Chelation requires relatively high concentrations of the inhibitor. Antiscalant inhibition via chelation will prevent the scaling process only at certain supersaturation conditions and salt precipitation is triggered if the equilibrium conditions are disturbed (Mpelwa and Tang 2019).

2.4.3. Toxicity tests for antiscalants

Increasing demand for reverse osmosis technology across the world and subsequent application of antiscalants is garnering focus on the ecotoxicity and human toxicity potential of different scale inhibitors and their dosage considerations. Low biodegradability and eutrophication risks from P-based antiscalants are a persistent problem in NF/RO treatment with respect to handling and discharge of the resulting brine steams which endanger quality of receiving water bodies (Verma et al. 2021). While there are investigations on ecotoxic effects of concentrate streams from RO and other desalination systems, there is still a dearth of information regarding specific toxicity of antiscalant products and corresponding test batteries (Yu et al. 2020). For instance, in Norway, antiscalants such as PAA, ATMP and copolymers of maleic and acrylic acids face strict environmental regulations in terms of ecotoxicity, bioaccumulation, and biodegradability standards set by the Convention for the Protection of the Marine Environment of the North-East Atlantic according to the Oslo–Paris (OSPAR) commission (Ganguly et al. 2024). The EU-WFD describes requirements for concentrate discharge into water bodies, but insufficiently assesses the ecotoxicological effects of antiscalants occurring in NF/RO concentrates (Liwarska-Bizukojc 2022). Falkenberg and Styan 2015 carried out whole effluent toxicity (WET) assessments for different concentrate streams from RO plants in 3 regions in Australia. For instance, in the Cape Riche area, for six marine species (microalgae, macroalgae, annelid echinoderm, mollusc, crustacean, fish) considered and tested, they found that the concentrate containing Nalco Permatreat PC-1020 antiscalant needed to be diluted 53-fold in order to ensure resulting concentrations where 99% of the species are unaffected by long-term exposure. However, they also pointed out that changing the antiscalant would lead to imprecise toxicity assessments from their simulation due to varying influencing factors, thereby highlighting the complexity of evaluating toxicity of concentrations and antiscalants exclusively.

Liwarska-Bizukojc 2022 reviewed a range of species and methods used to evaluate toxicity of effluents from municipal wastewater treatment plants having complex water matrices including high concentration salt and treatment chemicals. These include 72 h growth inhibition tests with algae cell number end point, phytotoxic effects, etc. In KonTriSol 2023 project report, researchers from the Department Evolutionary Ecology & Environmental Toxicology at the Institute of Ecology, Evolution and Diversity, Goethe University Frankfurt assessed holistic bioassay batteries for antiscalants and active ingredients, concentrates and treated water, comprising both acute and mechanism-specific analysis methods, carried out in in-vivo (ecotoxicity) and in-vitro (human toxicity) approaches. The in-vivo test procedure evaluated ecotoxicological endpoints such as growth inhibition, mobility acute toxicity and

developmental acute toxicity via algae growth inhibition test (DIN EN ISO 8692:2012), daphnia immobilisation test (DIN EN ISO 6341 (2012)) and fish embryo toxicity test (DIN EN ISO 15088 (2009)), respectively. The in-vitro test procedures examined human toxicological endpoints like cytotoxicity (MTT test, DIN EN ISO 10993-5 (2009)), oestrogenic effect (ERα-CALUX®, ISO 19040-3 (2018)), anti-oestrogenic effect (anti-ERα-CALUX®), androgenic effect (AR-CALUX®), anti-androgenic effect (anti-AR-CALUX®), genotoxicity (*in-vitro* micronucleus test, OECD Guideline No. 487) and mutagenicity (Ames fluctuation test, ISO 11350 (2012)). Effects were observed for PAA and phosphonates in both the algae growth inhibition test and the Daphnia immobilisation test, but no effects were detected in the in vitro human toxicity assays at concentrations up to approximately 100 mg/L. The tested PBTC product showed lowest toxic effects to humans and the environment, whereas DTPMP antiscalant showed the relatively stronger effects, especially in the acute organismic tests and with higher algal growth effects even at low dosages similar to concentrate occurrence. Although algae were the most sensitive organism for most phosphonate antiscalants, daphnia were more sensitive to polyacrylic acid (KonTriSol 2023). However, they highlighted the necessity for integrating chemical analysis of antiscalants with bioanalytical investigations to verify toxicity behaviour of antiscalants at lower concentrations and enable more precise detailed comparison between polymeric and phosphonic acid antiscalants.

2.5 Regulatory framework

Reverse osmosis and nanofiltration processes generate different quantities of concentrate which contain a higher concentration of the separated substances. Antiscalants in the feed, predominantly phosphonates and carboxylates, are also concentrated in the concentrate stream along with the separated solutes. Disposal of concentrates directly into a surface water body or indirectly after treatment in wastewater treatment plant (which incurs additional costs), require approval of the competent water authorities. Untreated or improperly managed concentrate streams can result in adverse environmental effects, due to high salinity, nutrients (phosphorus, nitrogen) and organic contaminants including emerging contaminants. Roberts et al. 2010 review on the ecological impacts of desalination plants concluded that there is a widespread belief and recognition that brine discharge poses a potentially serious threat to marine ecosystems. Laboratory-based experiments, toxicological investigations and manipulative field experiments clearly demonstrate the potential for brines and their constituents to illicit adverse impacts on aquatic organisms when present at sufficient concentrations (Joo and Tansel 2015). Cost-effective treatment and management strategies for concentrate are still in their infancy. One option is to discharge concentrate directly into surface waters, which requires a governmental permission. The German Wastewater Directive specifies certain conditions for the chemical and biological parameters to be met, for the discharge of wastewater into natural water bodies. Additionally, drinking water treatment plants discharging concentrate must abide by the EU Water Framework Directive (WFD) to avoid degradation of water quality and ensure high environmental protection level (Feiner et al. 2015).

In recent years, discharge of concentrates into a water body is increasingly viewed critically by the authorities, especially when the concentrates contain trace anthropogenic substances that are untypical to the feed, including chemicals added during treatment, i.e., antiscalants containing including polyphosphonates and carboxylates or salts in high concentrations. Since the refusal the discharge permit for the concentrates is generally equivalent avoiding the NF/RO technology altogether, solutions are required that allow the use of this innovative and advantageous technology in drinking water treatment in the long term. Introduction of organophosphorous compounds through technical phosphonate antiscalants is known to form N-phosphonomethylglycine (glyphosate) and its major metabolite aminomethylphosphonic acid (AMPA) with ozonation (Engelbart et al. 2025). Both glyphosate and AMPA are associated with toxicological side-effects especially for aquatic ecosystems, although AMPA is still less researched compared to glyphosate. Tresnakova et al. 2021 reported that glyphosate is associated with genotoxicity, immunotoxicity, and cardiotoxicity in fish and AMPA may potentially lead to may cause genotoxicity and immunotoxicity in fish, adverse changes in haemolymph parameters, effects on mussels' antioxidant enzymes, and developmental delay and survival of tadpoles. AMPA is also known to have a much longer half-life compared to glyphosate, implying that it tends to remain the aquatic environment or soil for longer periods of time (Ojelade et al. 2022). Despite it being more persistent and resisting microbial degradation, limited information currently exists on the ecotoxicological effects of AMPA. Nevertheless, it remains concerning that prolonged accumulation of such compounds in humans, animals, and the environment may pose health risks, as glyphosate exerts subtle, long-term effects (Ojelade et al. 2022). Armbruster et al. 2019 reported that even slight traces of phosphonate antiscalant by-products in permeate may trigger AMPA formation in subsequent disinfection and therefore established the basis for a method for trace analysis of P-based antiscalant residues. The lack of long-term safe and approvable solutions represents a significant brake in technology and may lead to a decision dilemma and investment backlog for the water utilities.

Regulations on antiscalants within Europe are varied. Countries with limited application of NF/RO in their treatment chain have little to no regulation on antiscalant application, and if required, tend adopt the limitations or certifications employed by the neighbouring countries with similar situations. Four EU Member States at the time, France, Germany, the Netherlands and the United Kingdom (4MS) and Denmark joining as a full member in 2018, announced formalized arrangements in 2011 to work together on aspect of the regulatory frameworks they have in place to ensure the hygienic safety of drinking water. The primary goals of 4MS which also are relevant for antiscalant application in drinking water treatment include (www.uba.de):

- Adoption of common, or directly comparable, practices for the acceptance of the constituents used in materials in contact with drinking water,
- Testing of materials,
- Use of common test methods and setting acceptance levels, specification of tests to be applied to products,

- Reviewing factory production control and setting audit testing requirements, and
- Assessing the capabilities of certification and testing bodies

With increased application of membrane technologies in drinking water treatment and awareness on antiscalant use and their environmental implications, certain regulatory bodies have formulated limits on their applications. The EN 15039:2014 and EN 15040:2014 are European standardizations applicable to polycarboxylic acids/salts and phosphonic acids/salts, respectively, used as antiscalants for membranes for the treatment of water intended for human consumption. It outlines the corresponding analytical methods for polycarboxylic acids and salts, the raw material characteristics, technical formulations, residual monomers, contaminants and specifies requirements for area of application and dosage, including worst-case scenario estimate for antiscalant permeation through NF and RO membranes.

The §20 of the German Drinking Water Ordinance (TrinkwV) (2023) is part of the European Standardization series “Products for the treatment of Water intended for Human Consumption” ensures international harmonization of the quality of treatment substances for the production of drinking water. The regulation prescribes a limit of 2.5 mg/L based on dry mass, for phosphonates and polycarboxylates added in the feed stream of the treatment process as given in Table 1. The limits are also accompanied with Chemical Abstracts Service (CAS) registry number which correspond to the search results at "STN International" (http://www.cas.org/index) and European Inventory of Existing Commercial Chemical Substances (EINECS) which correspond to the search results at the "European Chemical Substances Information System".

The current regulation aims to control the amount of antiscalant active ingredients added into the feed, based on the increased concentration of the antiscalants occurring in the retentate stream. However, there is currently no value mentioned on the residual concentration of antiscalant active ingredient after the treatment step in the permeate. Although a variety of phosphonic acids are approved for use in drinking water treatment according to the list, polycarboxylic acids like PAA constitute the most common P-free antiscalants approved for NF/RO filtration (TrinkwV 2023, KonTriSol 2023). The novel scale inhibitors based on CMI are a recent advancement and have not yet been approved for use in drinking water treatment systems in Germany. It is expected that the TrinkwV in Germany will be improved more specifically for antiscalants application during drinking water treatment based on different active ingredients and their safe hygiene requirements.

Table 1: Regulation for antiscalant application in drinking water treatment in Germany according to the §20 TrinkwV (2023) - "List of permitted treatment substances used as solutions or as gases"

Substance name	**CAS-Number**	**EINECS-Number**	**Intended use**	**Purity requirements**	**Maximum permissible addition**	**Maximum concentration after completion of processing**	**Reaction products to be observed**	**Remarks**
Sodium tripolyphos-phate	7758-29-4	231-838-7	Inhibition of corrosion, Inhibition of stone deposition with decentralized application, Antiscalants for membranes	DIN EN 1210 Tab. 1 and 2	2.2 mg/L P	-	-	-
Phosphonic acids	6419-19-8 22042-96-2 32545-75-8 2809-21-4 15827-60-8 1429-50-1 5995-42-6 37971-36-1 23605-74-5	229-146-5 244-751-4 251-094-7 220-552-8 239-931-4 215-851-5 227-833-4 253-733-5 245-781-0	Antiscalants for Membranes	DIN EN 15040	2.5 mg/L Dry mass of the product	-	-	-
Polycarboxylic acids	9003-01-4 9003-06-9 29132-58-9	-	Antiscalants for Membranes	DIN EN 15039	2.5 mg/L Dry mass of the product	-	-	-

In the Netherlands, the Kiwa Watermark certification is applicable for producers and suppliers of drinking water products and indirectly aimed at drinking water companies, installers and owners of drinking water installations. Evaluation of the products is carried out based on Kiwa evaluation guidelines which contain requirements with respect to the functionality and durability of the product, as well as requirements with respect to the production process at the location of production. Evaluation guidelines for products that come into contact with drinking water also include the legal requirements for hygienic aspects and often based upon European standards. The Kiwa Watermark certifications and evaluation guidelines have been drafted for various applications, including antiscalant use for drinking water production (www.kiwa.com). More specifically, the BRL K15003 evaluation guideline certifies products used for treatment and / or production of drinking water intended for human consumption, including chemicals for scale control or antiscalants. Commercial antiscalants certified by Kiwa Watermark specify a certain for maximum dosage (mg/L) in feedwater for every product and a new certification must be obtained in there is a change in the composition of the antiscalant. For instance, at the time of writing this work, Kiwa certificate K107128/01 specifies maximum dosage of 3 mg/L for an antiscalant containing phosphonic acids/salts and certificate K1024/07 specifies maximum dosage of 5 mg/L for an antiscalant containing polycarboxylic acids/salts (https://www.kiwa.com/nl/en-nl/certificate-finder).

For most USA states and Canadian provinces and territories, certification according to NSF (National Sanitation Foundation), ANSI (American National Standards Institute) and CAN (Standards Council of Canada) is necessary for the operation of drinking water treatment systems. Particularly, certification according to the standardization NSF/ANSI/CAN 60 ("Drinking Water Treatment Chemicals - Health Effects") is a mandatory requirement for the application of corrosion and scale control chemicals. This certification ensures that chemicals used in the treatment of public drinking water are safe and suitable, protecting public health by preventing harmful contaminants from entering the water supply. An example of NSF/ANSI/CAN 60 certification listing for antiscalants from Kurita America Inc. for a facility in USA is given in Table 2 (accessed on 07.08.2025 via https://www.nsf.org/).

Table 2: Example of NSF/ANSI/CAN 60 certification for a certain antiscalant products in USA

Trade Designation	*Product function*	*Max Use*
AvistaVitec™ 8200	Reverse osmosis antiscalant	7 mg/L
VItec™ SI410	Reverse osmosis antiscalant	3 mg/L
VItec™1600	Reverse osmosis antiscalant	20 mg/L

In Norway, according to Oslo-Paris (OSPAR) commissions regulations for primarily petrochemical industry, chemicals listed as PLONOR (Pose Little Or NO Risk) are assessed to be extremely safe for use and discharge in marine waters with no threat to the aquatic ecosystems. To be classified as PLONOR, a chemical must demonstrate low bioaccumulation potential, low toxicity, and a high degree of biodegradability and face no restrictions on the concentrations that are dosed (Ganguly et al. 2024). Scale inhibitors with active ingredients like polyacrylates, organophosphonates, polyaspartates, polyvinyl sulfonates are not listed as PLONOR, whereas CMI inhibitors meet PLONOR requirements to be discharged safely into aquatic bodies (Ganguly et al. 2024; Ganie et al. 2025). Nonetheless, for drinking water applications, traditional and novel biodegradable scale inhibitors require a comprehensive hygienic assessment, including long-term impact studies (Ganie et al. 2025).

Increasingly, awareness on antiscalants has shed light on the enhanced difficulties of concentrate disposal. Appropriate concentrate pretreatment that can remove or degrade antiscalants is favorable by certain regulatory bodies (KonTriSol 2023). However, the eco-toxicity effects of antiscalants, especially when directly discharged into receiving water bodies, have not been fully studied and effective methods to mitigate their adverse effects are not yet established (Falkenberg and Styan 2015, Royo et al. 2023, Yu et al. 2020). While use of P-free antiscalants is increasingly considered for their non-eutrophication properties and easier concentrate disposal, there are general knowledge gaps on suitability of antiscalants and dosages, side-effects and behavior in in concentrate stream. It is expected that with more in-depth studies to improve the understanding of the role of antiscalants in concentrate disposal and the optimization of the entire RO system and its side-effects, the regulation on antiscalant application, types of antiscalants used and dosages used in drinking water treatment may become more concrete.

3 Materials and Methods

3.1 Solutions and chemical reagents

Ultrapure water

Ultrapure water used for solution preparation and cleaning was obtained from 'Millipore Direct-Q 5 UV System' (Merck, Darmstadt, Germany), with the water output having an electrical resistivity of 0.056 $\mu S \cdot cm^{-1}$ (at 25 °C) and total organic carbon (TOC) concentration < 5 $\mu g \cdot L^{-1}$. The water passes a built-in photo oxidation UV lamp before leaving the device. Purification cartridges were replaced as recommended by the manufacturer.

Scaling solutions

The effectiveness of the antiscalant was tested against $CaSO_4$ and $CaCO_3$ scalants in this work. To achieve supersaturated concentrations of the two salts, a mixture of different amounts of Na_2SO_4 with $CaCl_2$ (Carl Roth GmbH) and $NaHCO_3$ with $CaCl_2$ (Carl Roth GmbH) were respectively used. The concentration and SI of the scalants used in this study are given under Table 3. Based on the type of experimental method used, corresponding saturation indices were used – choosing supersaturated solutions enabled relatively quick measurement of changes in solution scaling conditions in absence of antiscalants and correspondingly reasonably extended the experimental time in the presence of antiscalants

Table 3: Scaling salts and concentrations used in different experimental test methods

Experimental method	Scalants tested	Concentration of salt solution	Saturation Index (determined using AQION)
Stirred beaker test	$CaSO_4$	68 mM Na_2SO_4 + $CaCl_2$	$SI_{gypsum} \approx 0.72$
	$CaCO_3$	33 mM $NaHCO_3$ + $CaCl_2$	$SI_{calcite} \approx 2.06$
Crossflow filtration test	$CaSO_4$	25 mM Na_2SO_4 + $CaCl_2$	$SI_{gypsum} \approx 0.2$
	$CaCO_3$	20 mM $NaHCO_3$ + $CaCl_2$	$SI_{calcite} \approx 1.09$
Dead-end filtration test	$CaSO_4$	25 mM Na_2SO_4 + $CaCl_2$	$SI_{gypsum} \approx 0.2$
	$CaCO_3$	20 mM $NaHCO_3$ + $CaCl_2$	$SI_{calcite} \approx 1.09$
Whispering gallery mode	$CaCO_3$	5 mM $NaHCO_3$ + $CaCl_2$ 11 mM $NaHCO_3$ + $CaCl_2$ 33 mM $NaHCO_3$ + $CaCl_2$	$SI_{calcite} \approx 0.2$ to 2.06

Different concentrations for different tests were chosen based on the parameter being evaluated and its sensitivity of detection. Level of saturation was adapted to practically optimize experimental times for scaling experiments with and without antiscalants. Gypsum experimental conditions were adapted from Benecke 2018 who used 68mM Na_2SO_4 + $CaCl_2$ in

the stirred-beaker tests which was retained in the given study; 17 mM Na_2SO_4 + $CaCl_2$ in the membrane test with permeate removal was altered to 25 mM Na_2SO_4 + $CaCl_2$ at complete recirculation to keep the saturation conditions constant so that any changes in flux behaviour could be attributed to scaling or effectiveness of antiscalants. Calcite concentrations were also chosen to be supersaturated and optimized based on rate of change of flux observed.

Stock solutions of the order of 50 $g \cdot L^{-1}$ of Na_2SO_4, 20 $g \cdot L^{-1}$ of $NaHCO_3$ and 50 $g \cdot L^{-}$ $CaCl_2$ were used for all experiments and stored in the refrigerator for a maximum of 3 days; $NaHCO_3$ was freshly prepared before each experiment. All salt stock solutions were filtered through a 0.1 µm cellulose nitrate filtrate to remove undissolved particles that may trigger crystal nuclei formation and negatively impact reproducibility of results. The pH of the stock solutions was adjusted to 7.5 using 0.1 $mol \cdot L^{-1}$ or 1 $mol \cdot L^{-1}$ HCl and 0.1 $mol \cdot L^{-1}$ NaOH, if required.

Antiscalants

A comparison of different kinds of antiscalants was carried out in this study, using commercially used antiscalants that are commonly employed in NF/RO filtration for drinking production in Germany. With regard to the active ingredients of the antiscalants, a distinction was made between P-containing products, often based on organic phosphonic acids, and P-free products, often based on polyacrylic acids or polymaleic acids. Additionally, low-P antiscalant containing both active ingredients were also used. An overview of the antiscalants investigated in this study, along with the corresponding active ingredients mentioned by the manufacturer and total solids (TS) content measured by monitoring change in weight after 24 h of drying at 105 °C, are given in Table 4.

Cleaning solutions

Experimental setups and electrodes used during scaling experiments were thoroughly cleaned after each trial to ensure removal of any remaining scaling crystal nuclei and avoid interference with subsequent experiments. Gypsum experiments in the pilot plant were followed by cleaning with 1 %(w) Na4EDTA (Carl Roth GmbH) and 0.1 % (w) NaOH (Carl Roth GmbH) as given by Benecke 2018. Carbonate experiments in the pilot plant were followed with thorough cleaning using 1 % citric acid monohydrate (Carl Roth GmbH). Cleaning after batch experiments and other filtration experiments was carried out using the same reagents along with gentle wiping of all surfaces and in certain cases, additionally immersing some components in 0.5 M HCl to remove stubborn crystals. Acid cleaning was followed immediately with thorough rinsing with pure water to ensure that the setup can reliably be used for the next set of scaling experiments.

Table 4: Active ingredients of commercial antiscalants used in this work

Active ingredient of antiscalant	Abbreviation	Total solids (TS)	Structure of active ingredient	Type of antiscalant
Polyacrylic acid	PAA	30.7 %	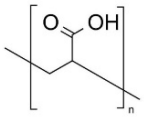	Phosphorous -free antiscalants
Carboxymethyl inulin (derived from chicory roots)	CMI	33.3 %	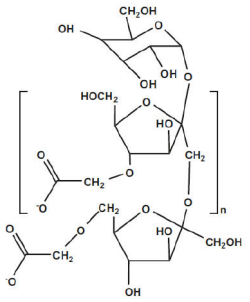	
Polyacrylic acid + Diethylenetriaminepentakis (methylphosphonic acid)	PAA + DTPMP	23.9 %		Phosphorous -based antiscalants
Diethylenetriaminepentakis (methylphosphonic acid)	DTPMP	25.4 %	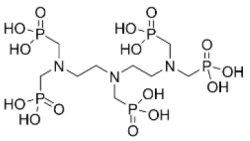	
2-Phosphonobutane-1,2,4-tricarboxylic acid	PBTC	47.2 %	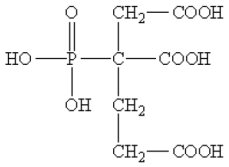	
Aminotris(methylenephosphonic acid)	ATMP	24.3 %	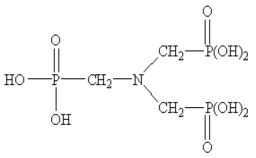	

3.2 Experimental setup and procedure

As part of this dissertation, four types of experimental test methods described below, were investigated for their suitability to serve as a scaling and antiscalant effectiveness determination method against CaSO4 and / or CaCO3 at different dosages of different antiscalants. Of these four methods, in-depth results using two test methods was obtained.

3.2.1 Stirred-beaker test

Static laboratory screening tests, also referred as "stirred-beaker test" in this study, have been previously reported to evaluate the performance of antiscalants and even standardized by the National Association of Corrosion Engineers (NACE). These tests evaluate the precipitation of mineral salts from its supersaturated solution as a function of time. The efficacy of inhibitors is given by the extent of retardation of the degree of precipitation in a given time. Although the method and test conditions are standardized, stirred-beaker tests are conducted under a variety of conditions including different salts concentrations, pH, temperature, test duration and antiscalant dosages (Amjad 2014).

Experimental setup: The stirred-beaker test set-up shown in Figure 10 consists of a 600 ml glass beaker surrounded with a darkened cooling jacket.

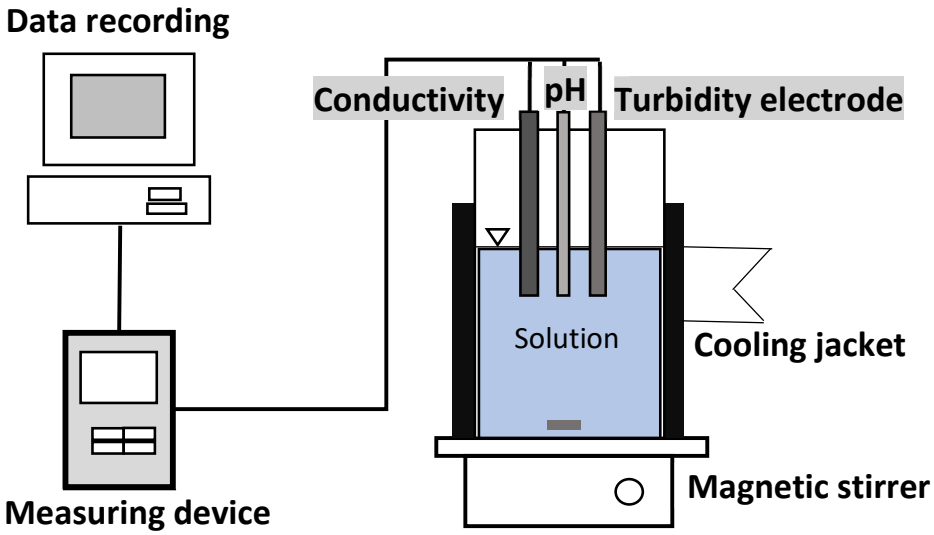

Figure 10: Schematic diagram of stirred-beaker setup used to experimentally evaluate effectiveness of antiscalants via determination of induction time

Scaling experiments were carried out using 500 ml of scaling solution with or without antiscalant, along with a magnetic stirrer (teflon-coated; 4 cm long). Measuring electrodes for turbidity, conductivity and pH, were suspended in the solution by a custom-made beaker cap to keep the set-up closed and avoid influence of atmospheric CO_2. Reliable turbidity measurement could be made due to the darkened shell outside the beaker. The temperature within the beaker was maintained at 11 ± 0.5 ºC throughout the experiment using the water-cooling jacket controlled by a cooler below the setup. The performance of the stirred-beaker test is dependent on hydrodynamic conditions and presence of additional contact surfaces (size of stirrer, electrodes, etc.). Therefore, clean beakers and magnetic stirrers of the same dimensions were used for all experiments, to ensure reliable reproducible results and each experiment was repeated two times.

Experimental procedure: To carry out the experiment, ultrapure water, predetermined volumes of the Na_2SO_4 or $NaHCO_3$ stock solution, and if applicable, antiscalant stock solutions were added to the beaker and combined using the magnetic stirrer. If required, pH was re-adjusted 7.5 using HCl or NaOH. It was ensured that the temperature of the solution within the beaker was 11 ºC. The start of the experiment was initiated by adding predetermined volume of $CaCl_2$ stock solution to the existing solution in the beaker while stirring continuously. Data recording using the Multimeter 3630 IDS device was started at this point until scaling in the solution was achieved.
After each experiment, electrodes were thoroughly cleaned to remove any remnants of scaling crystals by dipping in 0.5 M HCl. Prior to the next experiment, beaker and probes were thoroughly rinsed with ultrapure water.

Data evaluation: For data evaluation, turbidity was chosen as the most sensitive parameter compared to pH or conductivity. The induction time (t_{ind}) of the experiments was defined as the time in which the turbidity increases by 1 NTU since the beginning of the experiment (Benecke 2018). This is the time needed for the development of the first crystal nuclei after supersaturation. The experiments were carried up to a turbidity of 200 NTU, so that the crystallization time from 1 NTU to 200 NTU could also be estimated (Benecke 2018). This represents the further crystal growth after nucleation and is therefore also useful to evaluate the effectiveness of antiscalants.

3.2.2 Crossflow filtration test

In this study, a fully automated bench-scale crossflow RO filtration developed at the Institute of Water Resources and Water Supply (Hamburg University of Technology) by Benecke 2018 was used in this study. The crossflow filtration test could be operated with permeate extraction or in permeate recirculation mode as shown in Figure 11 .

The membrane test cell from Sterlitech SEPA CF II of rectangular configuration consisted of feed flow channel dimensions of 75 mil^2 x 14.6 cm x 9.5 cm without feed spacer. The membrane test cell was able to hold any flat sheet membrane resulting in 140 cm^2 active membrane area. The plant was equipped with a temperature-regulated feed tank having maximum capacity of 10 L and operated with a custom software (WWV_RO) developed at the university. It consisted of different user interfaces, including ‘mode selection’ interface which was used to adjust the type of filtration mode (permeate withdrawal or recirculation), thereby automatically controlling different valves at the feed, permeate and retentate streams.

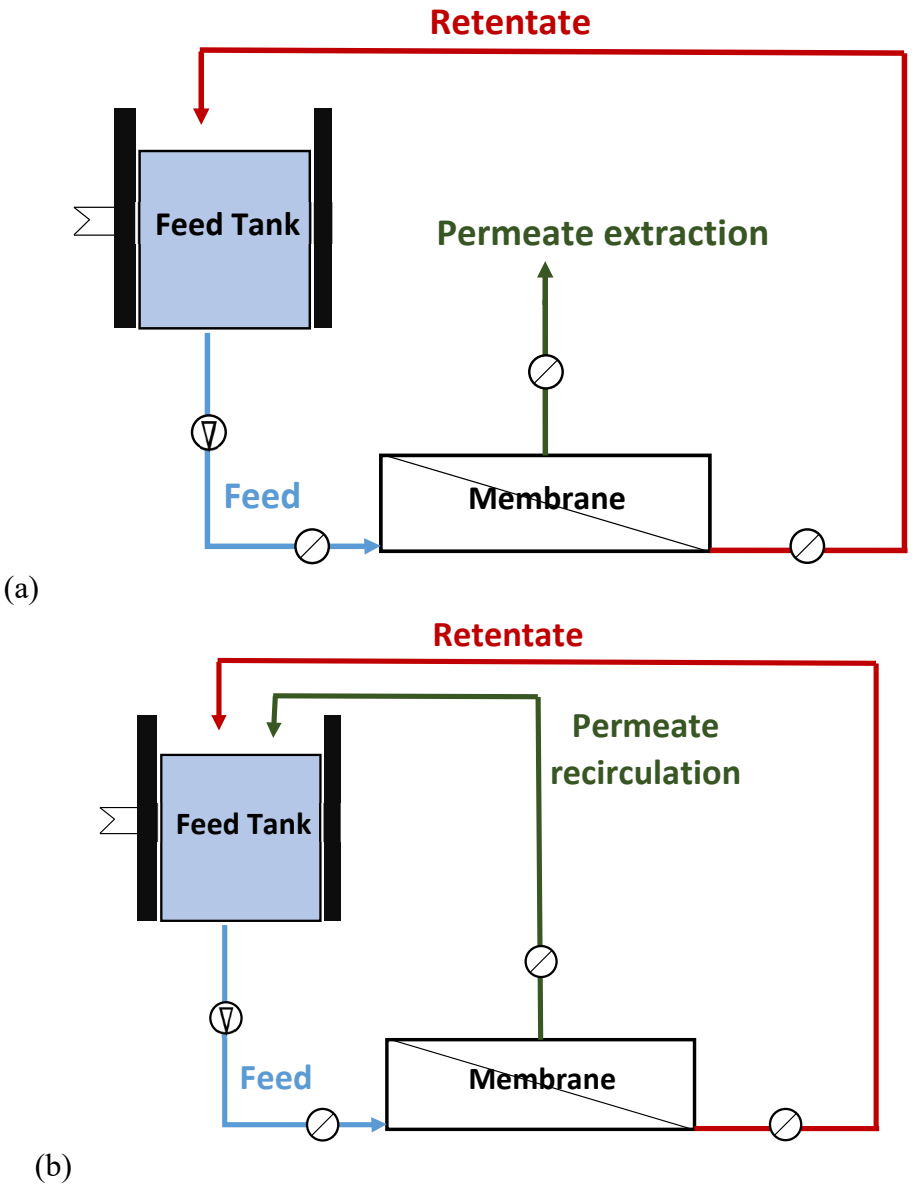

Figure 11: Schematic of crossflow filtration setup at WWV TUHH in (a) permeate extraction mode and (b) complete permeate recirculation mode

According to Saji et al. 2020, when the concentrate is recycled back to the feed tank and permeate is continuously extracted, there is a gradual increase of the concentration of the water in the feed tank which continuously increases in the scaling potential within the system. Since high recoveries may be achieved which allows for completion of experiment in shorter time, this mode of operation may be beneficial to estimate the maximum recovery possible with a certain antiscalant concentration. Alternatively, in recirculation mode, both the concentrate and permeate stream are recycled to the feed tank, thereby providing conditions to test scale formation at a certain saturation and determine the maximum efficacy of antiscalants at different dosages. Subsequently, irrespective of mode of operation of the filtration plant, antiscalant performance is governed by a gradual or rapid drop in membrane permeate flux, a substantial increase in feed water turbidity caused by bulk precipitation of the scaling species

and/or by images of the membrane surface obtained using SEM analysis or a high-resolution digital camera (Benecke 2018, Saji et al. 2020).
Experiments with the crossflow filtration cell was carried out in complete recirculation mode (permeate + retentate recirculation), at constant transmembrane pressure of 25 bar and temperature of 11 ºC.

Membrane details and membrane conditioning: Commercial flatsheet RO membranes, CR100 from DuPont were used for all crossflow filtration experiments, details of which are given in Annex I-2. The flatsheet membranes were cut and stored refrigerated in ultrapure water for at least 24 h before each experiment. At the beginning of each experiment, 6 L of ultrapure water was first filtered through the membrane at constant TMP 25 bar and temperature 11 ºC for 3 h, resulting in average flux of about 50 ± 10 $L \cdot m^{-2} \cdot h^{-1}$ for the CR100 membranes. Since scaling experiments involved saturated salt solutions as feed, the membranes needed to be pre-conditioned before each scaling experiment. As suggested by Benecke 2018, a solution with similar ionic strength as scaling feed, that is, 60 mM of NaCl was filtered through the membrane at similar operating conditions as the scaling experiment (TMP = 25 bar, T = 11 ºC, crossflow velocity = 0.1 $m \cdot s^{-1}$, complete recirculation mode), for 6 h (during the day) to 15 h (overnight). This ensured that any decrease in flux during the experiment with scaling salt could be attributed to scaling on the membrane surface rather that due to increase in osmotic pressure on introducing a salt.

Experimental procedure: Scaling experiments were conducted with slightly supersaturated solutions of the scaling salts. For this, 6 L of 25 mM Na_2SO_4 and $CaCl_2$ or 22 mM $NaHCO_3$ and $CaCl_2$ was used for gypsum and calcite experiments, respectively. The experiments were conducted in complete recirculation mode (retentate + permeate recycled into feed tank) at constant TMP of 25 bar, temperature 11ºC and constant crossflow velocity of 0.1 $m \cdot s^{-1}$ and/or 0.3 $m \cdot s^{-1}$, depending on the experiment. After membrane conditioning, the feed tank was emptied and filled with pre-determined amounts of cooled ultrapure water, sodium and calcium salt solution and antiscalant in sequential order and the plant recirculation was immediately started. Start of experiment was recorded once TMP and flow conditions were stabilized in the system and the experiments were carried out until flux dropped below 10 $L \cdot m^{-2} \cdot h^{-1}$ or for maximum of 1000 min, whichever preceded. Flux data was automatically recorded by the WWV_RO software every 30 s in the background. At the end of the scaling experiment, the filtration was stopped by gradually decreasing the TMP in small steps. The membrane was then carefully removed from the cell and dried for immediate SEM characterization of crystals on its surface or stored dry in the refrigerator until the next earliest possibility for SEM analysis.

Cleaning procedure: After each scaling experiment, the plant was then cleaned thoroughly to prepare it for the next set of scaling experiments. The scaled membrane was removed before cleaning and prepared for further characterization, while the membrane cell was reassembled without the membrane. Based on the type of scalant investigated, 1% (w) Na_4EDTA+ 0.1% NaOH (Carl Roth) solution was used to clean the system after sulfate scaling and 1 % Citric acid monohydrate (Carl Roth) solution was used after calcite experiments. Following

circulation with the cleaning solution, the feed tank was filled with tap water and recirculated for 20 min. This process was repeated about 2 - 3 times with fresh tap water in the feed tank to ensure no residual of the cleaning solution remains in the system, which was sometimes evident by the low pH value in the retentate stream. Finally, the plant was recirculated with ultrapure water a couple of times.

Data evaluation: The rate of flux change during the experiment was primarily used to evaluate the scaling and/or scale inhibition performance of antiscalants. Additional data like TMP, flow rate and temperature were also recorded for the given experimental time, but they remained mostly constant during all experiments. Although pH electrode was attached in the retentate stream, the measurement was not very sensitive due to practical problems, making it insignificant to the data interpretation. Stable flux behavior was attributed to good scale inhibition, while rapid flux decline was indicative of low scale inhibition potential. Interpretation of inhibition performance using flux data was further elaborated upon by SEM characterization of the scaled membranes.

3.2.3 Dead-end filtration test

Dynamic testing methods often give rise to a different ranking in antiscalant performance compared to tests performed under static conditions. The discrepancies are normally attributed to the generally longer times until scaling in observed in the presence or absence of antiscalants during membrane filtration. Moreover, depending on their chemistry, some scale inhibitors are effective in crystal growth prevention while others are more effective in delaying nucleation (threshold inhibition effect), implying that both mechanisms are time dependent. Since static methods occur under predominantly homogeneous scaling conditions and membrane tests sometimes require long experimental times, a dynamic method using dead-end membrane filtration was tested to investigate antiscalant effectiveness.

Experimental setup: Dead-end high-pressure filtration experiments were carried out using a stainless-steel membrane cell supplied by Sterlitech (HP 4750), having an active membrane area of 14.6 cm^{-2} and a feed volume of up to 300 ml feed when assembled. This particular Sterlitch cell could only be operated in dead-end filtration mode (without retentate stream), but could withstand high pressures upto 40 bar via pressurized nitrogen. To prevent concentration polarization and create “quasi” cross-flow conditions, stirring above the membrane surface was carried out by placing a magnetic stirrer within the cell and the entire setup was arranged on a magnetic stirring plate as shown in Figure 12. A container was placed on an analytical balance to collect the permeate and the amount of permeate collected was recorded automatically using Kern Balance software and resulting flux was calculated.

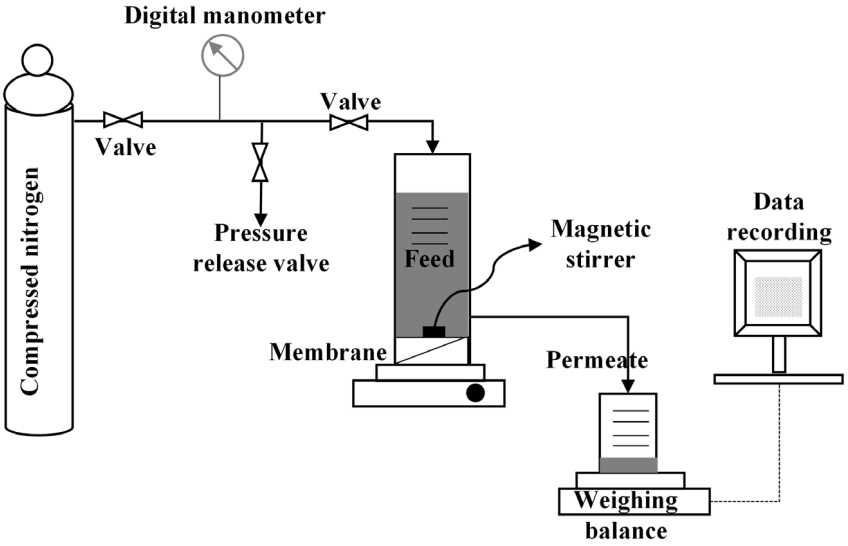

Figure 12: Schematic representation of Sterlitech cell dead-end filtration

Membrane fitting and assembly: Commercial RO membranes, CR100 from DuPont, were cut into 50 mm circles and soaked in DI water and stored in a refrigerator at least 12 hours before use. The membrane was placed in the filtration cell with the active side facing feed reservoir and assembled by carefully tightening the base screws. Pre-determined volumes of ultrapure water, followed by Na_2SO_4 (for $CaSO_4$ scaling) or $NaHCO_3$ (for $CaCO_3$ scaling) with antiscalant and finally $CaCl_2$ was filled in the feed tank. The magnetic stirrer was turned on immediately and the cell was closed quickly. The test cell was pressurized by opening the pressure source and gradually increasing the pressure with a regulator till desired (25 bar) pressure was achieved and was maintained constant throughout the experiment. Permeate weight was simultaneously recorded by the Kern balance software to determine flux.

Cleaning: Upon completion of the experiment, all membrane test cell parts were cleaned immediately. Similar to crossflow membrane filtration pilot plant, for sulfate scaling experiments, 1% (w) Na_4EDTA+ 0.1% NaOH solution was used, while 1 % citric acid monohydrate solution was used for cleaning after carbonate scaling experiments. Stubborn crystals were removed carefully with a cleaning brush. Finally, all membrane filtration cell components were washed thoroughly with ultrapure water and dried well before use in the next experiment.

3.2.4 Whispering gallery mode (WGM)

A feasibility study on the test possibility of WGM to detect scaling on surfaces was carried out in collaboration with Surflay Nanotec GmbH (Berlin, Germany). Whispering gallery mode (WGM) is a type of laser technique which generates coherent laser light through stimulated emission was a so-called whispering-gallery-mode resonator, where the light is confined via repeated total internal reflection at the boundary of the dielectric structure (Grossmann 2012).

Surflay's WhisperSense uses polymeric microparticles as WGM sensors. It works on the principle of temporarily trapping light within a particle and measuring the wavelengths of the escaping light before, during and after sample introduction. The escaping light creates peaks at certain wavelengths due to constructive waves, which are an outcome of the whispering gallery modes. Details on the sensing mechanism and concept are given in the Annex I-5.
The setup consisted of a sensor (microparticle) immobilized in a special open system microfluidic chip from IBIDI, a company which produces and supplies for functional cell-based assays and advanced products for cellular microscopy. It consisted of 18 reaction chambers with a diameter of 5 mm and a depth of about 2-3 mm, as well as a lid that prevents rapid evaporation of the aqueous solutions (Figure 13), a laser to activate the sensor and a spectrograph to detect the signal from the sensor. The sample was introduced into the microfluidic chip, optionally via an auto-sampler.

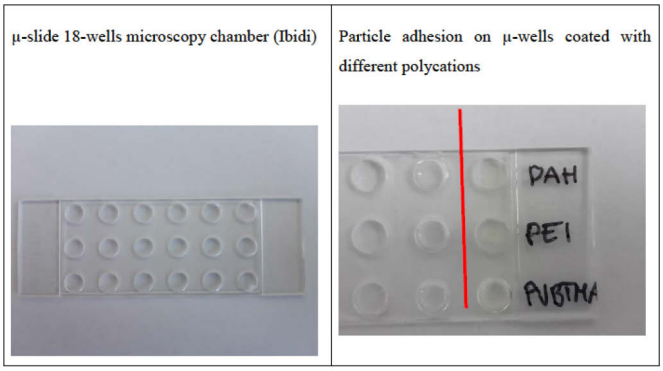

Figure 13: (Left)Selected chips from IBIDI for the WGM scaling tests and (Right) Adhesion tests of the WGM sensors by LbL coating of the chip carried out by Surflay GmbH

Each microparticle functions as a sensor in WhisperSense and require the sensors to be functionalized with specific ligands, which in this case constitutes the scaling cation or anion. Finally, as a crucial part of the setup, the computer hardware and software are embedded in WhisperSense in order to ensure a compact device and ease-of-use.
To apply a cationically charged polyelectrolyte layer, the hydrophobic chips were etched with ozone as well as with plasma at different times in the UV-Cleaner, resulting in a hydrophilic surface with negative zeta potential. The treated areas were coated with 4 different polycations according to the LbL method (PAH, PEI, PVBTMA and PDADMAC) and then equal amounts of the negatively charged sensor particles were immobilized on the surface. After drying, they were washed with a powerful water jet and the number of remaining particles in the wells was estimated. Optimum adhesion was obtained by treating them with ozone for 10 minutes and coating them with PAH or PEI, which showed approximately the same results. Finally, different solutions could be added to the particles successively without changing their position, which allowed continuous measurement.

Suitability of WGM for scaling detection was tested only with $CaCO_3$ scalant at different concentrations of $NaHCO_3$ and $CaCl_2$, due to easier cleaning of the system and to avoid damage to the expensive and highly sensitive WGM components due to the scaling crystals.

3.3 Membrane characterization using SEM

Recovered membranes after the crossflow membrane filtration experiments were prepared for surface characterization using SEM. For this, the preserved membranes were cut to approximately 10 mm squares, dried and sputtered with gold at current of 40 mA. SEM images were then taken using the Zeiss Supra 55 VP (Carl Zeiss AG, Oberkochen, Germany) at a voltage of 3.00 kV, aperture of 20.00 µm and with the working distance maintained between 5-10 mm

3.4 PAA antiscalant characterization using TOC and LC-OCD

Total organic carbon (TOC) and liquid chromatography organic carbon detection (LC-OCD) analysis were carried out only to characterize P-free antiscalants and supplement the experiments in Section 4.6.

The TOC/DOC of the commercial CMI and PAA antiscalant and its fractions were determined using the Shimadzu TOC-V CSM total organic carbon analyzer. Triplicate samples were used for the analysis, with the device performing 5 measurements per sample.

The P-free antiscalants were characterized by size-exclusion chromatography coupled to organic carbon detection (LC-OCD) and UV-detection (UVD; 254 nm) (DOC-Labor Dr. Huber). This setup was also used to identify qualitative changes in DOC within the samples. ChromeRES and ChromeCALC by DOC-Labor Dr. Huber were partly used for data analyses and correction measures.

3.5 Flow cytometry to determine biological stability of PAA antiscalant

Assimilable organic carbon detection (AOC) analysis was carried out only to supplement the experiments in Section 4.6.

The assimilable organic carbon (AOC) analysis was determined by total cell count (TCC) via flow cytometry (CyFlow™ Cube 6 V2m from Sysmex). The AOC reflects the concentration of organic nutrients that are converted during the growth of heterotrophic microorganisms in solution and is considered an important indicator for assessing the re-growth potential and thus the biostability of water. To determine the AOC content, a method was developed by Hammes and Egli 2005, whereby bacterial growth in water samples is observed using a combination of flow cytometry and fluorescence. Accordingly, TCC of a sample is tracked for 28 days using flow cytometry measurements carried out on day 0, 3, 7, 14, 21 and 28. On day 0, samples were divided into separate AOC vials for each measurement day (triplicate determination). The samples were then incubated in a shaker incubator at 30 °C and 120 rpm. With the flow cytometer used, all small particles/cells ranging in size from 0.1 µm to 100 µm could be detected and analyzed, with the maximum permitted particle rate being 15,000 events/second. For TCC determination, 1mL sample solution was prepared in a cuvette: each 100 µL sample was mixed together with 10 µL SYBR® Green I (SG) and 890 µL sterile evian® water. The mixed sample

solution was then incubated at 37 °C for 13 minutes. Both the AOC vials and the cuvettes were well homogenized before each measurement. The instrument was rinsed with the cleaning solution (provided by manufacturer Sysmex) between each sample. Subsequently the AOC content in µg C_{eq}/L was calculated using the equation $\Delta TCC_{flow\ cytometer} = TCC_{max} - TCC_{start}$ and conversion factor $1 \cdot 10^7$ Cells/µg C from AOC, as given by Hammes and Egli 2005 and Vital et al. 2007, respectively. In this study, the antiscalant samples (addition of 1 $mg \cdot L^{-1}$ TOC by PAA) were prepared in tap water (≈ 0.5 $mg \cdot L^{-1}$ TOC before PAA dosing) to provide the bacterial community for AOC analysis. In addition to the antiscalant samples, AOC measurements of the permeate arising from the NF membrane filtration were performed. For this, the lab-scale pilot plant was operated with the flatsheet commercial NF270 membrane, in crossflow mode (crossflow velocity = 0.12 $m \cdot s^{-1}$; flux = 62 ± 3 $L \cdot m^{-2} \cdot h^{-1}$) and at a constant TMP of 8 bar.

4 Results and Discussion

4.1 Evaluation of homogeneous and heterogeneous scaling in the crossflow filtration setup

In large-scale membrane filtration systems, besides differences in membrane module types, flow conditions and saturation levels, homogeneous and heterogeneous nucleation are difficult to distinguish since both mechanisms often occur simultaneously (Li et al. 2018, Rolf et al. 2022). Eventually, a decline in permeate flux results from the deposition of the scaling crystals on the membrane surface (Rolf et al. 2022). Several theoretical models have been used to investigate the effects of operating conditions, crystal particle size, crystal shape, and concentration of feed solution on the decline of flux. However, there is vast variability in the type of nucleation and/or crystal growth models and predictive capability employed in these studies.

In order to understand the implications of the different scaling mechanisms within the reverse osmosis system, the change in permeate flux and crystal morphologies were investigated in a lab-scale pilot plant setup. Separate experiments were performed for sulfate and carbonate scaling, with slightly supersaturated feed and under retentate and permeate recirculation mode to keep the saturation conditions approximately constant. High crossflow velocity of 0.31m·s^{-1} (high laminar range) and low crossflow velocity of 0.1 m·s^{-1} (low laminar range) operation was tested in the plant to induce predominantly homogeneous (bulk) crystallization in the former case and heterogeneous (surface) crystallization in the latter. As scaling proceeded, the rate of change of permeate flux in the pilot plant was monitored. Following the experiment, the membranes were characterized using SEM to derive the impact on the resulting scaling crystal size and morphology. Besides elucidating the scaling process itself, these set of experiments were also crucial to identify the plant operational conditions for further experiments involving antiscalants.

$CaSO_4$ scaling

Figure 14 shows the rate of change of permeate flux during crossflow filtration with sulfate feed ($SI_{gypsum} \approx 0.2$) using a flat-sheet RO membrane (without feed spacer) at constant TMP of 25 bar, temperature 11 ºC and at different cross flow velocities. At 0.1 m·s^{-1}, permeate flux through the membrane steadily decreases with time and reaches less than 50 % of the original value in about 900 min as a consequence of heterogeneous gypsum crystallization. In contrast, similar operation of the plant at 0.31 m·s^{-1} results in considerably steady flux through the membrane, decreasing by hardly 5 % even after about 2200 min. Based on Equation 4 and 5, the concentration polarization (CP_{factor}) at 0.1 m·s^{-1} was calculated to be higher at about 2.3, whereas CP_{factor} was calculated to be 1.69 at 0.3 m·s^{-1}. Scanning electron microscopy (SEM) images verified the abundance of gypsum scaling on both membranes, but revealed different crystal characteristics (Figure 15) in both cases. While the heterogeneously scaled membrane (heavily scaled) was covered by crystals that were short and dense, forming small gypsum rosettes, homogeneously scaled membranes had crystals that were longer and broader, forming wide-leaved gypsum rosettes. These results proved and verified that controlling heterogeneous

sulfate scaling, that is predominantly triggered by concentration polarization, was crucial to influence overall membrane performance in the filtration system in comparison to homogeneous crystallization.

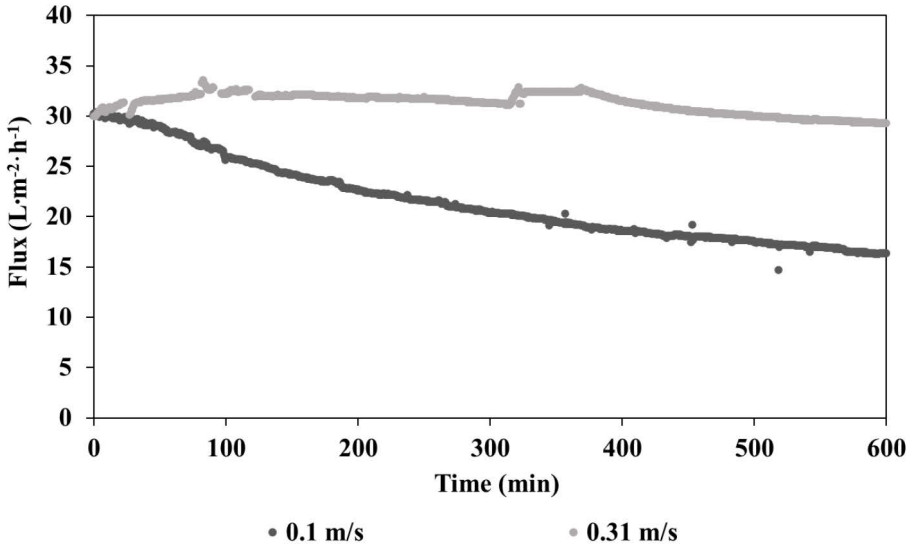

Figure 14: Flux behaviour in crossflow filtration setup using flat sheet RO membrane operated with 20 mM Na_2SO_4 and $CaCl_2$ feed and without antiscalant, in complete recirculation mode, at crossflow velocities 0.1 m·s^{-1} and 0.3 m·s^{-1} (TMP=25 bar, T=11 °C, $SI_{gypsum} \approx 0.2$)

(a) 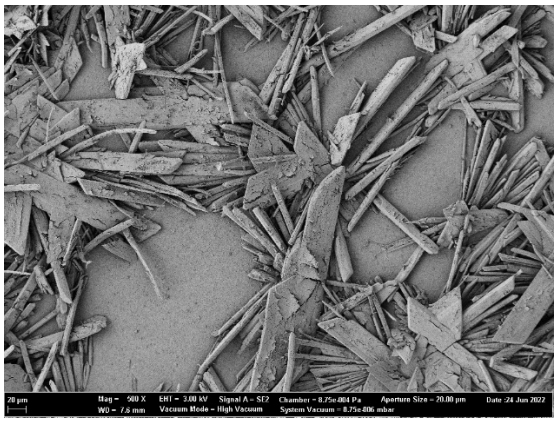 (b) 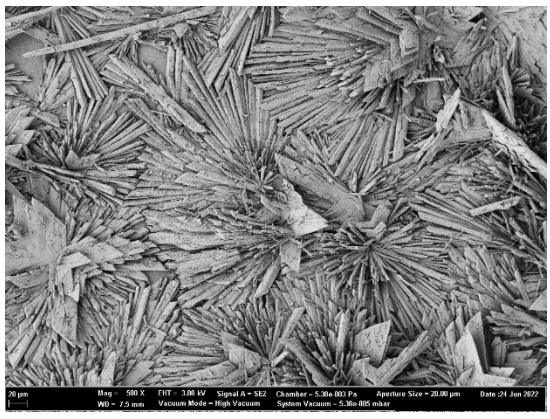

Figure 15: SEM pictures (Mag = 500 X, 20 µm) of RO membrane surface after crossflow filtration with 20 mM Na_2SO_4 and $CaCl_2$ and without antiscalant, in complete recirculation mode, at crossflow velocities (a) 0.3 m·s^{-1} and (b) 0.1 m·s^{-1}

There have been several studies which have elucidated the factors affecting bulk and surface gypsum scaling, although clearly distinctions in practice are rare due to complex physico-chemical reasons and limitations in the level and precision of detection. For instance, according to Benecke 2018, presence of organic macromolecules favors growth of heterogeneous gypsum crystals by adsorption and by increasing concentration polarization. Besides this, other parameters such as hydrodynamics, degree of supersaturation, temperature and pH affect the

type and extent of scaling mechanism. Matin et al. 2019 also pointed out that low velocity and high flux trigger surface crystallization, whereas bulk crystallization is more pronounced at moderate crossflow velocity and low pressure. Though the same flux was used for all trials in this study, the predominant reason for homogeneous crystallization to take place is higher fluid motion causing lesser concentration polarization. However, they also warn that though the nucleation is commenced, scaling can still be slow if there are insufficient number of nucleation sites for scaling to proceed. According to Matin et al. 2019, in presence of only heterogeneous crystallization, the flux decreases steadily, rapidly and continuously due to crystal growth at the membrane surface. Due to homogeneous scaling, flux decline is negligible up to a SI of 2, after which flux decline is rapid due to some surface crystallization and beyond SI 2.7, the flux decline due to bulk crystallization was sharp. Li et al. 2017 recommended using higher crossflow velocity to decrease concentration polarization and enhance mass transfer coefficient at the filtration boundary, through an innovative vibration-assisted desalination setup. Though Mi and Elimelech 2010 attributed higher scaling potential to polyamide membranes compared to cellulose acetate membranes, Shaffer et al. 2017 found that surface chemistry is not as crucial as the hydrodynamics of the filtration. In the critical review by Rolf et al. 2022, flux decline in RO was attributed to be mainly due to membrane surface coverage by lateral growth of gypsum scales induced from surface heterogeneous nucleation via model fitting. In another study, it was suggested that faster scale formation and flux decline at relatively low crossflow velocity are attributable to a thicker concentration polarization (CP) layer via modeling of membrane surface supersaturation.

Although the experiments using the crossflow filtration test were only carried out once, the effect of concentration polarization at different crossflow velocities on gypsum scaling potential was verified by stable permeate flux at high crossflow velocity followed by immediate continuous flux decline as the crossflow velocity was reduced and vice versa (Annex II-1).

$CaCO_3$ scaling

Similar to sulfate scaling, another set of experiments were carried out to monitor rate of permeate flux change during cross-flow filtration of carbonate solution ($SI_{calcite}$ = 1.09) at starting pH 7.5, using a flat-sheet RO membrane (without feed spacer) at constant TMP of 25 bar, temperature 11 ºC and at different cross flow velocities. As seen in Figure 16, at 0.1 ms^{-1}, permeate flux showed immediate decrease after experiment and in contrast to gypsum scaling, proceeded with a much more gradual rate of flux decline. Overall, even after 20 h of filtration (Annex II-2), heterogeneous carbonate scaling experiments did not show more than 10 % decrease in permeate flux. Operating the plant at 0.3 $m \cdot s^{-1}$ showed mostly stable flux throughout the experimental time Concentration polarization (CP_{factor}) for calcite scaling at 0.1 $m \cdot s^{-1}$ was calculated to be higher at about 2.5, whereas CP_{factor} was calculated to be 1.89 higher crossflow velocity. Measurement of feed pH at the beginning of the filtration and after 10 h resulted in change from pH 7.6 to about 7.0 during filtration under low crossflow conditions, in comparison to pH change from 7.6 to 7.3 during high crossflow filtration. According to Futterlieb and Panglisch 2025, as pH decreases the solubility of CaCO3 decreases, implying precipitation of carbonate crystals. Scanning electron microscopy (SEM) images verified the abundance of

round / rhomboidal calcite crystals on both membranes, but with homogeneous carbonate scales being bigger and more diverse shape forms, while heterogeneous carbonate crystals were small, round and denser (Figure 17).

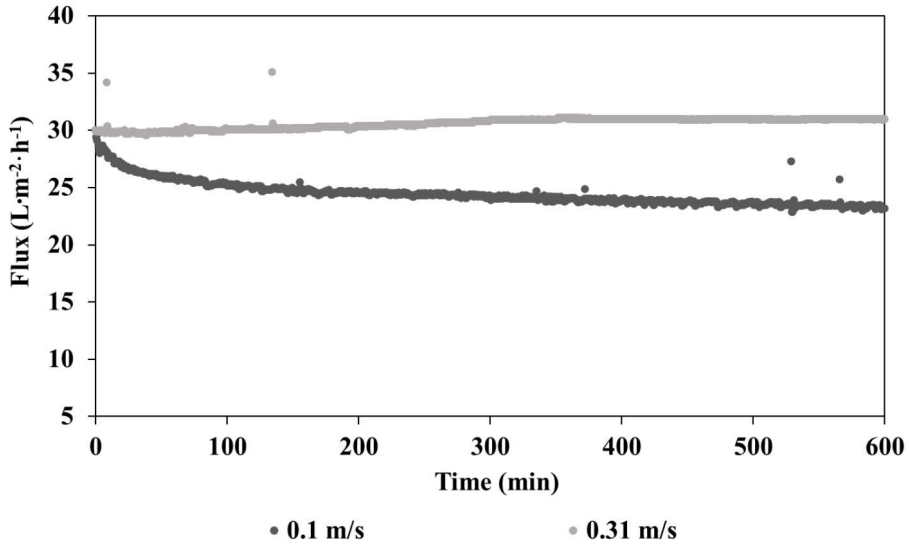

Figure 16: Flux behaviour in crossflow filtration setup using flat sheet RO membrane operated with 22 mM $NaHCO_3$ and $CaCl_2$ feed and without antiscalant, in complete recirculation mode, at crossflow velocities 0.1 $m \cdot s^{-1}$ and 0.3 $m \cdot s^{-1}$ (TMP=25 bar, T=11 °C, $SI_{calcite} \approx 1.09$)

(a) 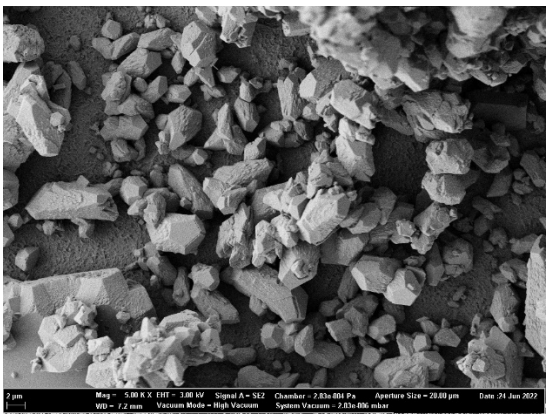 (b) 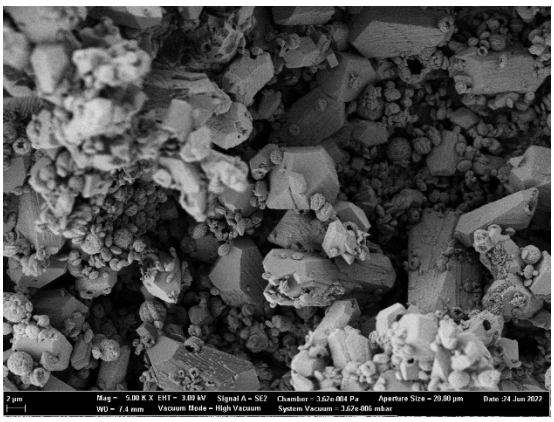

Figure 17: SEM pictures (Mag = 5.00K X, 2 µm) of RO membrane surface after crossflow filtration with 22 mM $NaHCO_3$ and $CaCl_2$ and without antiscalant, in complete recirculation mode, at crossflow velocities (a) 0.3 $m \cdot s^{-1}$and (b) 0.1 $m \cdot s^{-1}$

Unlike gypsum scaling, maximum of permeate flux decline of 10 % could be obtained for calcite scaling, despite long filtration times. While the reason for this could be partly attributed to the configuration of the membrane cell and lack of a feed spacer, the nature of calcite crystals to be smaller and more disintegrated unlike gypsum rosettes may also translate into different

permeate flux behavior. Time taken to observe first decrease of flux after start of filtration was then decisive to determine antiscalants effectiveness.

These results proved and verified that among the two scaling mechanisms reported, heterogeneous scaling which is accelerated by supersaturation on and near membrane surface due to enhanced concentration polarization (CP) was more detrimental to the membrane performance compared to homogeneous scaling. High crossflow hydrodynamics can minimize concentration polarization (CP) of scale-inducing ions adjacent to the membrane surface and thus, reduce surface-induced heterogeneous nucleation in membrane-based systems. Additionally, according to Rolf et al. 2022, it takes longer for surface crystallization to reach steady state because the high shear rate not only reduces the residence time but also induces better mixing of the solution near the membrane surface. They elucidated that homogeneous crystallization and subsequent crystal deposition on the membrane surface could be diminished via strong shear stress induced by high crossflow velocity. In contrast, heterogeneous nucleation on the membrane surface is accelerated at lower crossflow velocities. While the classical nucleation theory describes that the nucleus must overcome a single free energy barrier before continuing to form a stable crystalline scale particle, more recent nucleation theories describe a two-step energy barrier process for nucleation to crystallization as described in former Section 2.3.1. In the first step, amorphous clusters, or the dense liquid phase, are formed by overcoming the first free energy barrier. Because of the disordered interface with the solution, the surface energy of this amorphous cluster is lower than that of the crystalline nuclei. In the second step, an amorphous-to-crystalline transition occurs, wherein a crystalline cluster or nucleus is formed after overcoming a second free energy barrier, which is much lower than that in the direct crystallization process from solution (Rolf et al. 2022).

Due to the detrimental effects of low crossflow velocity and concentration polarization on scaling, further experiments to investigate scale inhibition using antiscalants in the pilot plant were carried out at low crossflow velocity (0.1 $m \cdot s^{-1}$) and similar saturation and operating conditions.

4.2 Antiscalant effectiveness using Stirred-Beaker Test

Gaining insight into the performance and mechanisms of various antiscalants is essential to guide their effective application in NF/RO applications. The overall scaling process includes both nucleation and crystal growth steps which are mechanistically different. A key parameter in nucleation is the induction time, defined as the interval between the onset of supersaturation and the first detectable signs of solid phase formation.

This section aims to experimentally compare the effectiveness of five different commercial antiscalants based on PAA, PAA+DTPMP, DTPMP, PBTC and ATMP as active ingredients, against gypsum and calcite scalants using a stirred-beaker setup described in detail in Section 3.2.1. Besides describing the effectiveness of different antiscalant active ingredients and dosages against two common scaling salts, these set of experiments also detailed upon suitability and limitations of this experimental method for scale inhibition detection. Supersaturated solutions of the order of $SI_{gypsum} \approx 0.72$ and $SI_{calcite} \approx 2.06$ were taken into

consideration for this method. Different gypsum and calcite concentrations were selected to achieve detectable turbidity changes within a reasonable timeframe without antiscalants (blank), while maintaining measurable changes during the slower crystallization process in the presence of antiscalants at identical supersaturation conditions.The effectiveness of commercial antiscalants was tested at two dosages – 0.5 mg·L^{-1} and 1 mg·L^{-1} based on total solids (TS), complying with the regulatory limit of maximum 2.5 mg·L^{-1} TS (TrinkWV), and mostly within manufacturer recommended dosages ranging from 1 to 8 mg·L^{-1} (about 0.3 mg·L^{-1} TS to 2.3 mg·L^{-1} TS depending on technical formulation) of the liquid product. Turbidity was used as the primary parameter to determine induction time, although pH and conductivity were also measured during initial experimental trials and disregarded to due to their delayed or lack sensitivity, respectively. The experiment started with initial turbidity of 0 NTU and increased continuously over the course of the experiment until 200 NTU was reached. Induction time based on turbidity increase of 1 NTU was considered for the data evaluation, while crystallization time (time for further turbidity increase until 200 NTU) was only considered in case it was exceptionally long. While sulfate scaling is said to be independent of pH, carbonate scaling is pH-dependent and expected to show decrease as calcite precipitates from the solution (Futterlieb and Panglisch 2025). To state an example shown in Figure 18, addition of 1.5 mg·L^{-1} of a DTPMP based antiscalant to 33 mM $NaHCO_3$ and $CaCl_2$ showed induction time of 38 min (average of 2 trials). The pH value decreases only 8-10 minutes after the increase in turbidity and is therefore not considered sufficiently sensitive for the definition of the induction time. The conductivity values showed no significant change and are therefore not shown. Further examples are given in the Annex II-6.

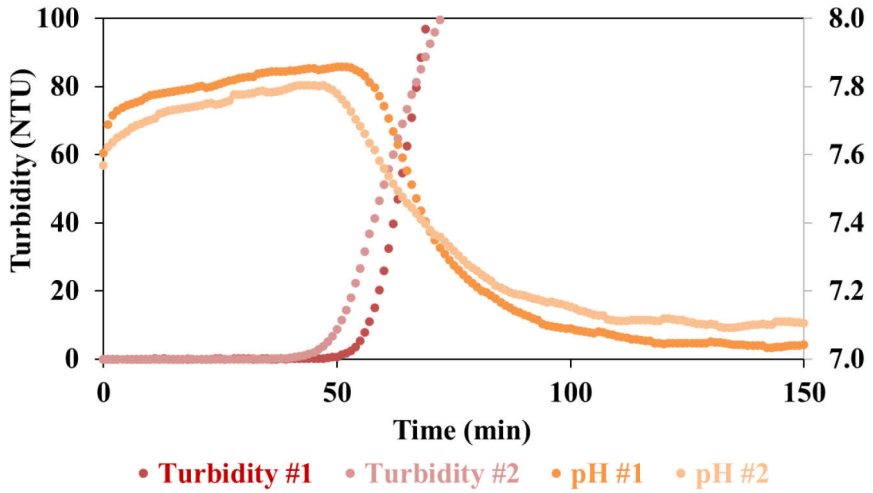

Figure 18: Turbidity and pH behavior of 33 mM NaHCO3 and CaCl2 + 1.5 mg·L^{-1} DTPMP antiscalants tested over two trials in the stirred-beaker test

4.2.1 Inhibition potential against gypsum scaling at different TS dosages

Controlling feed saturation, membrane hydrodynamics and membrane cleaning can help to mitigate scaling to a certain extent or restrict it to a specific mechanism, addition of antiscalants remains the most preferable option to ensure stable reliable operation of reverse osmosis,

especially at high recoveries during drinking water production which presents in higher scaling potential. In this section, the effect of commercial antiscalants was studied to understand their inhibition interaction with the scaling mechanisms. The first set of experiments involved comparison of effectiveness of five commercial antiscalants at a dosage of 0.5 mg·L^{-1} TS against gypsum scaling, with duplicate experimental trials to test reproducibility. As seen in Figure 19, without any antiscalant (blank), the superstaurated sulfate solution in the beaker shows an induction time of only about 10 min, indicating that formation of crystal nuclei is almost instantaneous and further crystal growth proceeds rapidly, resulting in an increase in turbidity of 1 NTU in 10 min. These measurements were considered as baseline in order to determine the effectiveness of antiscalants. Subsequently, on adding 0.5 mg·L^{-1} TS of antiscalants, we see in Figure 19 that different antiscalants extend the induction by different amounts - PAA and ATMP antiscalants show highest induction time at about 60 min indicating their enhanced ability to prevent gypsum scaling at the given dosage. While PAA+DTPMP antiscalant and DTPMP show average gypsum inhibition with about 35 min, PBTC shows the lowest induction time of 13 min, similar to the blank. All P-based antiscalants showed low crystallization times (Annex II-7) which indicated that at the given dosages there is limited ability of the antiscalants to prevent further crystal growth after primary or secondary nucleation.

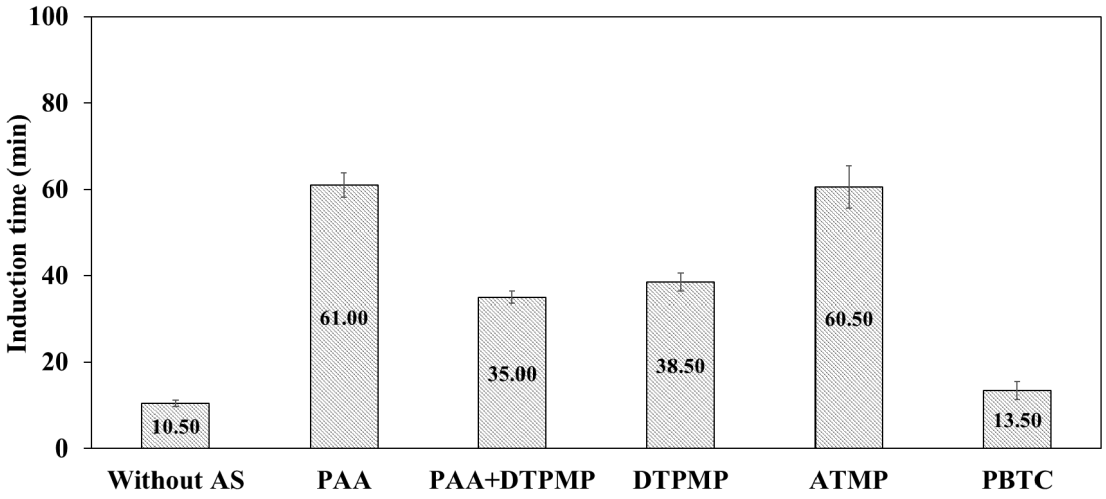

Figure 19: Induction time (based on 1 NTU turbidity increase) using the stirred beaker test with 68 mM Na_2SO_4 and $CaCl_2$ + 0.5 mg·L^{-1} TS of commercial antiscalants based on different active ingredients (T=11 °C, $SI_{CaSO4} \approx 0.72$, n=2)

Amjad 2012 showed that PAA based antiscalants are particularly effective gypsum inhibitors compared to phosphonate-based antiscalants. He hypothesized that PAA antiscalants are most likely to interact with the cations of the scalant in solution and interfere with the nature of crystal morphology, reducing their ability to agglomerate or attach to surfaces, although they did not generate specific experimental data to prove this. Zeino et al. 2018 used a similar batch setup to compare the effectiveness of ATMP, DTPMP and PAA to inhibit gypsum scaling. They maintained maximum experimental time of 40 min and carried out turbidity analysis every 5 min, along with measurement of Ca^{2+} concentration in solution using EDTA titration method.

They found that polyacrylic based inhibitors work much more effectively at preventing gypsum scaling compared to ATMP and DTPMP alone. Phosphonate based inhibitors were more likely to perform better when combined with another inhibiting agent, for instance, combining ATMP + DTPMP. They found that a combination of ATMP and DTPMP was capable of inhibiting sulfate scaling under even high "stress" environments of high SI. The authors however did not go into further details of the reasons and mechanisms underlying this phenomenon. El-Shall et al. 2002 found that ATMP is effectiveness gypsum inhibitor due to its ability to prevent crystal growth by decreasing surface energy, compared to the blank.

Since most manufacturer dosage recommendation for antiscalants is based on the degree of saturation of the scaling salt, an open-source software (Annex I-3) from the manufacturer suggested about 0.5 to 0.7 $mg \cdot L^{-1}$ TS for the P-based antiscalants while about 1.5 $mg \cdot L^{-1}$ TS was suggested for PAA based antiscalant. Subsequently, the stirred-beaker test was then used to determine the induction time of the five commercial antiscalants at a higher dosage of 1 $mg \cdot L^{-1}$ based on TS. As seen in Figure 20, increasing the dosage led to an increase in induction time of most antiscalants. More specifically, P-based antiscalants PAA+DTPMP, DTPMP and ATMP showed a considerable increase in the induction time, indicating that phosphonates tend to show enhanced scale inhibition potential at higher dosages. Interestingly, phosphonate-based PBTC antiscalant showed almost negligible improvement in its gypsum inhibition behaviour even at higher dosage, resulting in an induction time of only about 20 min. PAA antiscalant also showed increased induction time of 115 min at a higher dosage of 1 $mg \cdot L^{-1}$ TS.

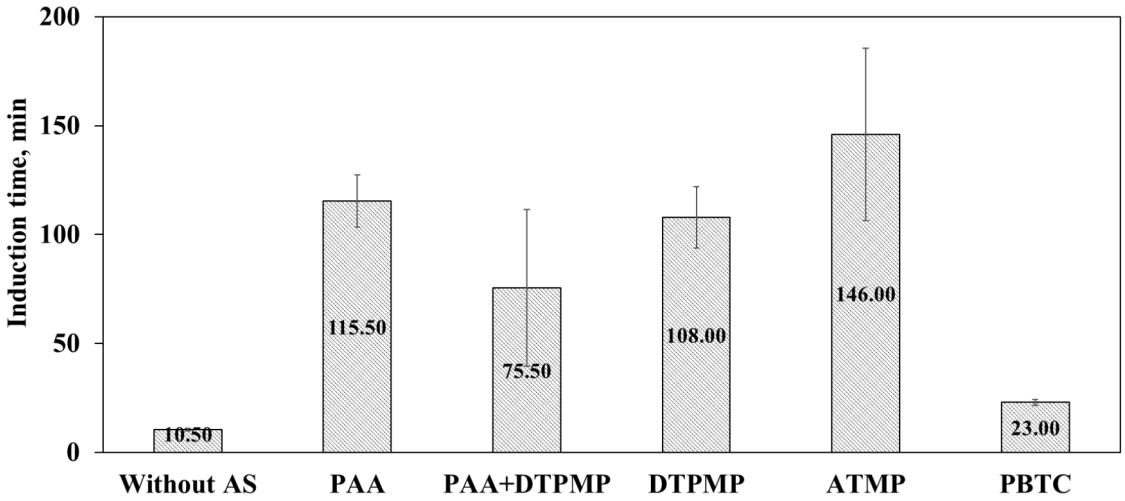

Figure 20: Induction time (based on 1 NTU turbidity increase) using the stirred beaker test with 68 mM Na_2SO_4 and $CaCl_2$ + 1 $mg \cdot L^{-1}$ TS of commercial antiscalants based on different active ingredients (T=11 °C, $SI_{CaSO4} \approx 0.72$, n=2)

Weijnen and Van Rosmalen 1986 studied the adsorption of phosphonates on gypsum crystals and found that for effective gypsum scale inhibition, a surface coverage of 4-5 % of phosphonates on gypsum crystals was necessary. They suggested that the adsorption of phosphonates on gypsum was a reversible process comprising of either complexation of the

Ca^{2+} ions with the phosphonate group or formation of hydrogen bridges between the hydroxyl groups and either the sulfate ions or the crystal water molecules at the gypsum crystal surface. Popov et al. 2019 compared the inhibition potential of ATMP and PBTC against gypsum scaling using a light scattering nanoparticle analyzer and zeta potential measurements. They investigated a novel dynamic measurement method along with comprehensive analytical and evaluation methods in a bulk supersaturated environment. Through their analyses, they concluded that certain phosphonates may alter the number of gypsum nuclei formed, but have no effect on the crystal growth kinetics. They proposed a non-classical hypothesis to gypsum inhibition where the Ca^{2+} and SO_4^{2-} ions mainly precipitate on the nano-impurities in solution, which exist despite any level of pre-filtration and that the antiscalants adsorb onto these heterogeneous impurities, indirectly affecting the number of gypsum nuclei being formed. Although this is a novel and bold interpretation of the scale inhibition mechanism, most parts of their hypothesis fit with the alteration of the kinetic behaviour described by the non-classical nucleation theory in Section 2.3.1. It is nonetheless important to mention that this reasoning involves complex measurement techniques and is difficult to directly corroborate with simple experimental data, and evidence of its validity is lacking in a membrane filtration system.

Induction time measurements conducted in the stirred-beaker test show that polyacrylic acid is quite stable in controlling gypsum scaling at 0.5 and 1 $mg \cdot L^{-1}$ TS. Phosphonate-based antiscalants, with the exception of PBTC, are effective gypsum inhibitors at higher dosages of 1 $mg \cdot L^{-1}$ TS. However, it must be considered that using P-based antiscalants has environmental implications in the context of handling and disposal of the resulting concentrate stream, which become more critical when higher feed dosages are used. While the stirred-beaker experiments were easy to set up and carry out and applicable to both gypsum and calcite scaling and wide variety of antiscalants, they were sometimes associated with high standard deviation. In order to improve the reliability of the antiscalant testing method and/or verify the effectiveness observed in the stirred-beaker, the effectiveness of the five commercial antiscalants were additionally investigated in a crossflow membrane filtration setup and discussed under Section 4.3.1.

4.2.2 Inhibition potential against calcite scaling at different dosages

Similar to gypsum salts, in this section, the effect of commercial antiscalants was investigated for their inhibition potential against calcite scaling at dosages 0.5 $mg \cdot L^{-1}$ and 1 $mg \cdot L^{-1}$ based on TS. Induction time based on turbidity increase of 1 NTU was used as the parameter to evaluate antiscalant effectiveness in the stirred-beaker test. While the pH dependency of carbonate scaling as previously been described, it was assumed that pH monitoring may provide earlier and better scaling detection compared to turbidity measurements. However, as described earlier in the introductory text of this section, pH decrease was less sensitive compared to the turbidity measurement by approximately + 10 min and associated with slower further change and therefore, disregarded as the evaluation parameter for further experiments. The induction time, based on 1 NTU turbidity increase, of different antiscalants were compared to the induction time of the scaling solution without antiscalant, referred to as the blank. As seen in Figure 21,

in the absence of any antiscalant, the supersaturated carbonate solution ($SI_{calcite} \approx 2.06$) at temperature of 11 °C and initial pH 7.5 showed an induction time of about 11 min in the stirred-beaker test. Addition of antiscalant dosage of 0.5 mg·L^{-1} TS resulted in an increase in the induction time by different amounts for the five commercial antiscalants with different active ingredients. Figure 21 shows that phosphonate-based antiscalants PBTC and ATMP showed highest induction times above 100 min even at the lower dosage of 0.5 mg·L^{-1} TS, implying excellent calcite inhibition potential. In contrast, at the same dosage, commercial antiscalant based on phosphonate DTPMP showed lowest induction time of 19 min, close to the blank solution, implying low threshold inhibition potential. In comparison, the PAA based antiscalant and PAA+DTPMP mixture showed slightly higher induction time of 35 min.

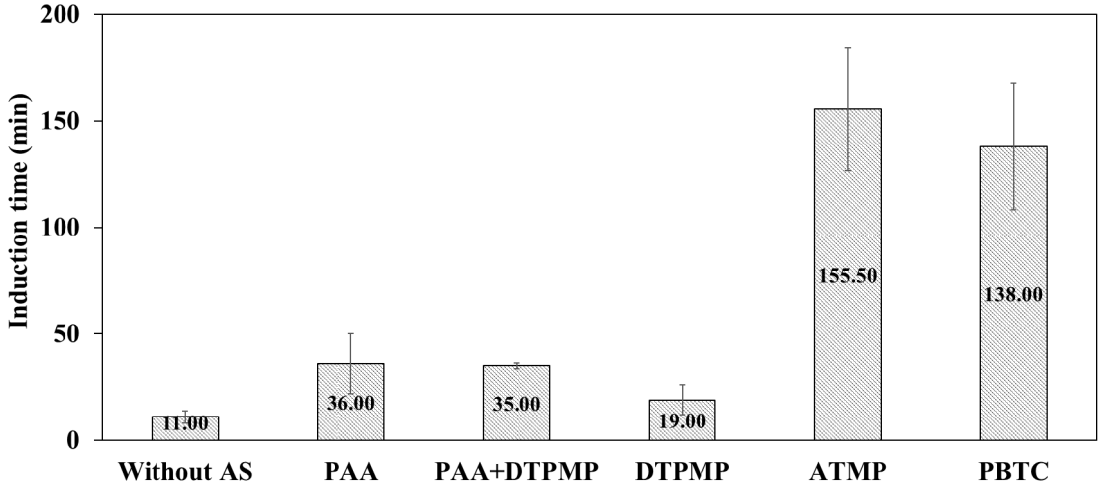

Figure 21: Induction time (based on 1 NTU turbidity increase) using the stirred beaker test with 33 mM $NaHCO_3$ and $CaCl_2$ + 0.5 mg·L^{-1} TS of commercial antiscalants based on different active ingredients (T=11 °C, $SI_{CaCO3} \approx 2.06$, n=2)

In the next step, the effectiveness of the commercial antiscalants with different active ingredients was tested against calcite scaling at higher dosage of 1 mg·L^{-1} TS. As seen in Figure 22, higher dosage of antiscalant translated to longer induction time for all antiscalants. As expected, phosphonates PBTC and ATMP consistently showed the best calcite inhibition potential with induction times over 200 min at 1 mg·L^{-1} TS dosage. While the induction time with DTPMP increased to 60 min, it remained lower compared to the other products. Surprisingly, at 1 mg·L^{-1} TS, the commercial antiscalant containing PAA+DTPMP mixture resulted in four times higher induction time of 184 min, while PAA antiscalant had optimal performance at 96 min.

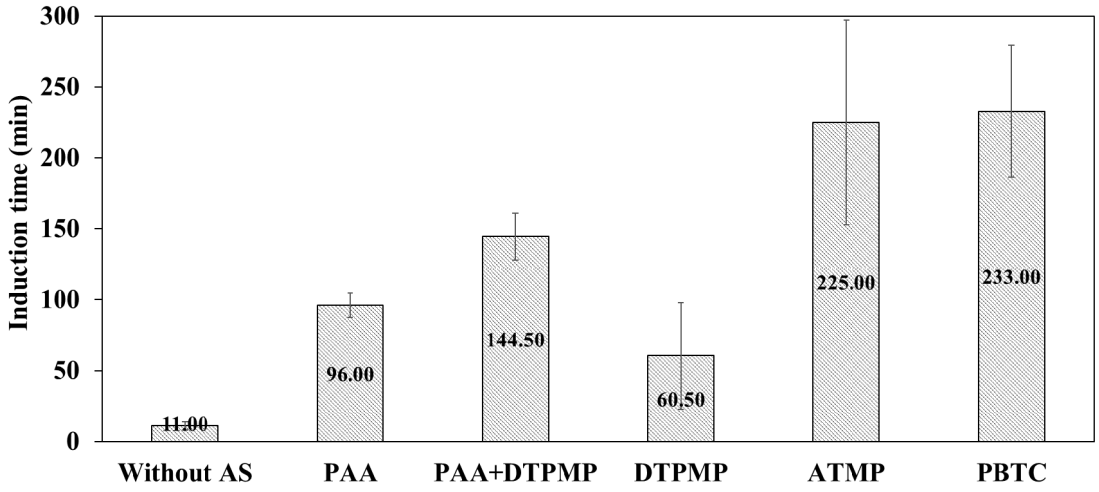

Figure 22: Induction time (based on 1 NTU turbidity increase) using the stirred beaker test with 33 mM $NaHCO_3$ and $CaCl_2$ + 1 mg·L^{-1} TS of commercial antiscalants based on different active ingredients (T=11 °C, $SI_{CaCO3} \approx 2.06$, n=2)

Corroborating results were reported by Tang et al. 2008 who compared calcite inhibition potential of PAA and ATMP; they found antiscalants containing phosphonic groups like ATMP and PBTC tend to show good threshold inhibition effect by adsorbing on carbonate crystals and preventing further growth, while PAA containing long polymer chains show negligible threshold effect and may likely interact with the mineral by enclosing the crystal grain and forming smooth or distorted scales. Liu and Zhang 2022 reviewed the effectiveness of different antiscalant active ingredients against scaling inhibition and concluded that DTPMP shows shorter induction in comparison to polycarboxylate-based or even phosphonate-polycarboxylate mixtures, which fits well to the induction time results obtained in this study for PAA, PAA+DTPMP and DTPMP. Basheer et al. 2021 investigated the effectiveness of ATMP antiscalant at different dosages through ultrasonification of a supersaturated calcium carbonate solution containing antiscalant. They determined the inhibition potential by comparing the change in calcium ion concentration within the system at the beginning of the experiment and after sonification time of 60 min, expressed as calcium carbonate inhibition percentage (CCI %). Similar to the results observed in this study, they found that addition of ATMP increases the scale inhibition potential of carbonate salt, with higher dosages leading to more effective inhibition. Interestingly, they found that at certain higher ATMP dosage, calcite inhibition percentage decreases and was attributed to potential fission of the C-P bond of the antiscalant and the formation of calcium orthophosphate which is also a precipitating salt in scaling systems. Thus, this indicated that certain scaling conditions and overdose of P-based antiscalants may produce additional risk of calcium orthophosphate precipitation besides calcium carbonate. Ji et al. 2017 determined binding energies via MD simulations and found it to be highest for ATMP, indicating strong interaction between antiscalant and mineral crystal surface.

While stirred-beaker experiments using turbidity measurements were relatively simple to carry out and were useful to obtain first impressions on the suitability of a certain antiscalant for scale inhibition based exclusively on nucleation and crystal growth behaviour, secondary set of experiments were carried out using a lab-scale crossflow filtration pilot plant to verify inhibition effectiveness and/or gain deeper insights on antiscalant mechanism during scale inhibition process.

4.3 Antiscalant effectiveness using crossflow filtration setup

While stirred-beaker test procedures reduce the laborious and costly efforts of field tests, they do not reflect membrane filtration conditions in which both crystallization and hydrodynamic transport mechanisms are involved and defined via heterogeneous crystallization and homogeneous crystallization (Amjad 2014). Experimental evaluation of the consequences of the two crystallization pathways in Section 4.1 in the present study showed that heterogeneous crystallization was more detrimental to membrane performance, with more dense crystals forming at the membrane surface at lower cross-flow velocity, i.e. at surface scaling conditions, owing to enhanced concentration polarization.

The following two sections evaluates the effectiveness of different commercial antiscalants in the laboratory scale cross-flow filtration pilot plant under low cross-flow velocity, or primarily heterogeneous scaling conditions. Antiscalants based on active ingredients PAA, PAA+DTPMP, DTPMP, PBTC and ATMP were tested at two dosages for their inhibition potential against $CaSO_4$ and $CaCO_3$ scaling. For this, 6 L of slightly supersaturated feed ($SI_{gypsum} \approx 0.2$; $SI_{calcite} \approx 1.09$) was taken in the feed tank at 11 °C and filtered through a pre-conditioned membrane at constant TMP of 25 bar, with complete retentate and permeate circulation back to feed. The relatively constant SI conditions ensured that any drop in permeate flux over time could be attributed to non-inhibitory effect of the antiscalant.

4.3.1 Inhibition potential against gypsum scaling at different dosages

This section describes the effectiveness of different commercial antiscalants via rate of change of flux in a lab-scale reverse osmosis plant in complete recirculation mode and at constant TMP of 25 bar at similar antiscalant dosages used in the batch setup. As seen in Figure 23, the flux with CaSO4 feed without antiscalant continuously decreases with time and reached less than 50 % of its original value in 600 min. At an antiscalant dosage of 0.5 $mg \cdot L^{-1}$ based on TS, antiscalants consisting of PAA+DTPMP mixture, DTPMP and ATMP showed some flux decline at the end of 600 min, while commercial PAA-based antiscalant showed almost no change in flux over entire 600 min, suggesting successful heterogeneous gypsum scale inhibition at the membrane surface. The PAA+DTPMP mixture showed 10 % flux decrease until about 400 min, after which the flux decline was more rapid. Commercial DTPMP-based antiscalant showed 10 % flux decline until approximately 300 min and proceeded further, similar to the PAA+DTPMP mixture. ATMP antiscalant showed 10 % flux decline slightly earlier than 300 min, indicating that nucleation and crystal deposition on the membrane had already taken place and following this, further flux decrease was slow, but steady until 600 min.

In contrast to the other antiscalants, commercial PBTC was unable to maintain stable flux and showed rapid flux decline from the beginning until 600 min, resembling the performance of the blank, with no antiscalant. Insufficient cooling during operation led to a slight increase in temperature temporarily, which corresponds to the slight increase in permeate flux for PBTC at the beginning and at 379 min. However, continuous decrease in flux despite the short-term higher temperatures is indicative of poor inhibition potential of PBTC.

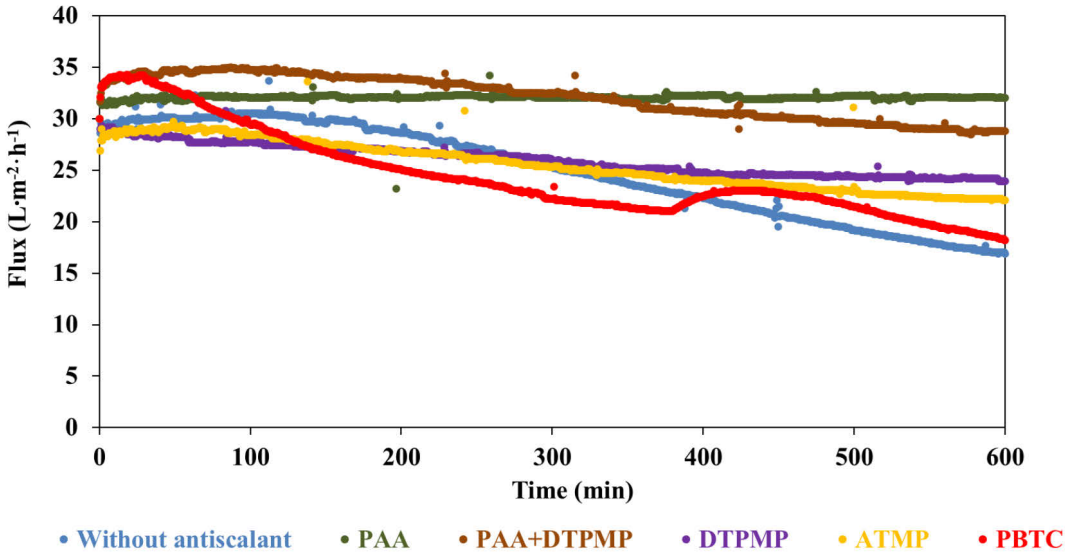

Figure 23: Flux behaviour in crossflow filtration setup using flat sheet RO membrane operated with 25 mM Na_2SO_4 and $CaCl_2$ feed + 0.5 mg·L^{-1} TS of different commercial antiscalants in complete recirculation mode, at crossflow velocity 0.1 m·s^{-1} (TMP=25 bar, T=11 °C, $SI_{gypsum} \approx 0.2$)

After the experiment, the membranes were carefully removed from the filtration cell, stored dry in the refrigerator and characterised via SEM at the next immediate possibility. Figure 24 shows the SEM images of the scaled membranes after the crossflow pilot plant experiments with 0.5mg·L^{-1} TS antiscalant in $CaSO_4$ solution under predominantly heterogeneous scaling conditions (low crossflow velocity, enhanced concentration polarization). The membrane operated without any antiscalant showed several gypsum crystals on its surface with dense, close-knit gypsum rosettes on its surface. Corroborating with the flux change results, SEM of the membrane operated with PAA antiscalant was the cleanest, with only some arbitrary crystals on its surface, suggesting that PAA was indeed suitable for gypsum scale inhibition even at 0.5mg·L^{-1} TS. Membranes operated with PAA+DTPMP mixture, DTPMP, PBTC and ATMP showed several crystals on their surface, indicating that they were not as effective inhibitors against gypsum at this dosage. Interestingly, SEM revealed that the morphology of the gypsum crystals had been altered by all the antiscalants. The typical gypsum rosettes observed in the absence of any antiscalant, was modified: while PAA caused smaller rosettes but predominantly decreased the overall number of crystals formed, thereby showing better CaSO4 inhibition potential, PAA+DTPMP disintegrated gypsum rosettes into much smaller components, which

may not immediately lead to membrane blocking but nonetheless lead to enhanced flux decline over time. DTPMP showed broader gypsum rods that were more widespread over the surface. PBTC showed dense layers of wide rods, while ATMP had altered the rosettes to form flat, larger gypsum crystals.

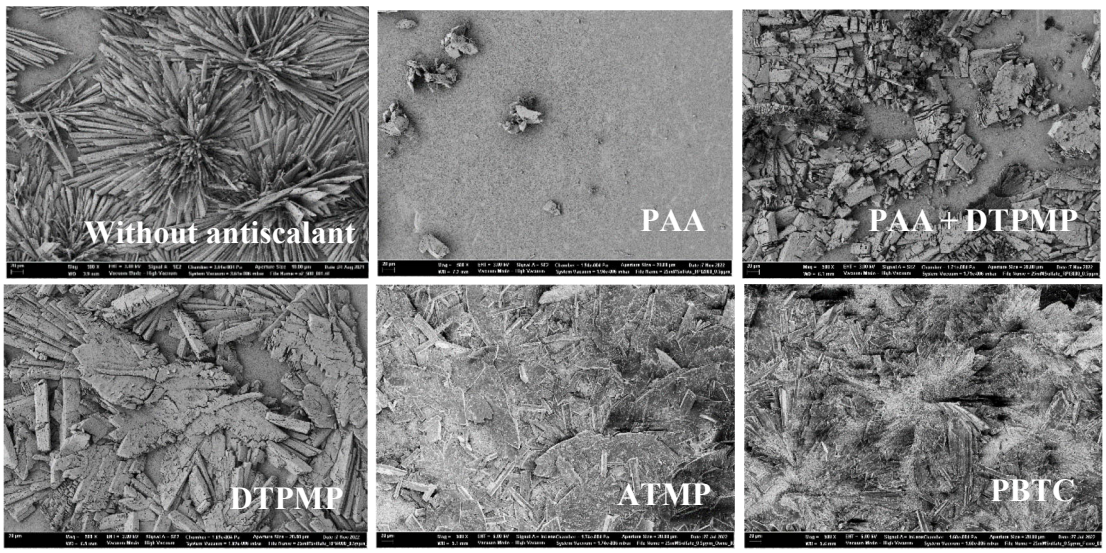

Figure 24: SEM pictures (Mag = 500 X, 20 µm) of RO membrane surface after crossflow filtration with 25 mM Na_2SO_4 and $CaCl_2$ + 0.5 mg·L^{-1} TS of different commercial antiscalants

The antiscalant performance observed in the crossflow pilot plant with 0.5 mg·L^{-1} TS antiscalant were mostly consistent with the results obtained in the stirred-beaker test. The blank showed lowest induction time in the stirred beaker test and most drastic flux decline in the pilot plant experiment. Similarly, at 0.5 mg·L^{-1} TS dosage, PBTC showed lowest induction and consequently caused rapid permeate flux decrease in the pilot plant, indicative of its negligible threshold inhibition potential. In contrast, at the same dosage, commercial PAA antiscalant showed highest induction time and most stable flux behaviour in the filtration experiment, suggesting its suitability to inhibit $CaSO_4$. SEM investigation showed few crystals on its surface, suggesting that the performance of PAA was mainly governed by its strong threshold inhibiting potential with some potential dispersion ability. PAA+DTPMP and DTPMP showed low induction time in the stirred-beaker test, which corroborated well with the slightly enhanced flux decline observed in the pilot plant and more gypsum crystals on membrane visible on SEM compared to PAA. Surprisingly, although ATMP showed good induction time in the stirred-beaker test, it was unable to maintain stable flux in the pilot plant with several gypsum crystals on the membrane surface, indicating that the threshold inhibition potential was satisfactory and its potential to prevent further crystal growth was poor. This could be verified to some extent in the stirred-beaker test through the crystallization time (Annex II-7) which was low for ATMP and higher for PAA at the same dosage.

Literature suggests that phosphonate antiscalants have a profound effect on the structure and morphology of gypsum crystals (Rosenberg et al. 2012). Akyol et al. 2009 demonstrated that

addition of phosphonate-based antiscalants to a supersaturated gypsum solution resulted in scaling with less elongated needle and plate-like crystals compared to a similar solution without additives. The arithmetic and geometric mean diameters of gypsum crystals were lowered in the presence of phosphonates compared to the absence of these products. On the molecular scale, Rosenberg et al. 2012 showed that the step morphology changes when exposed to a phosphonate additive with surface becoming more jagged and new parallel crystallographic directions being established.

Yin et al. 2022 studied the effect of PAA in inhibiting gypsum in RO and found that PAA was capable of interacting with the gypsum nuclei to prevent scaling or at low dosages, form a scale layer that is loose and permeable to water. More specifically, at low concentrations of PAA, morphological distortion of the gypsum scale layer was likely. Additionally, the authors also experimentally proved that addition of PAA was more effective at inhibiting gypsum scaling compared to membrane surface modifications for antiscaling properties. This finding fits well with the permeate flux behaviour and subsequent SEM membrane characterization observed in the present study at 0.5 $mg \cdot L^{-1}$ TS and 1 $mg \cdot L^{-1}$ TS for the commercial PAA antiscalant. Reiss et al. 2020 studied the effect of phosphonate antiscalant ATMP to control gypsum scaling in a desalination plant and found that it reduces the rate of nucleation of gypsum crystals, but does not affect the precipitation potential, subsequently leading to fewer, but larger crystals. This could explain the prevalence of gypsum crystal layer on the membrane surface despite longer induction time in the stirred-beaker test. Among phosphonates, several researchers have previously given detailed accounts of nitrilotris-methylene phosphonic acid (NTMP) being a good gypsum scale inhibitor. Prisciandaro et al. 2012 experimentally found that effectiveness of other phosphonates like PBTC control the formation of scale crystals by affecting the growth-controlled induction period instead of nucleation-controlled induction period, as usually hypothesized. However, they also reported that PBTC has no effect on the morphology of gypsum crystals which is contrary to the observations in this study, possibly due to differences in the nature of the experimental method and commercial PBTC formulation used in the current study, which contains other proprietary ingredients.

Similar to the stirred-beaker test, the effectiveness of the commercial antiscalants were tested for their flux behaviour in the lab-scale crossflow pilot plant at a higher dosage of 1 $mg \cdot L^{-1}$ based on TS. As seen in Figure 25, the blank experiment (without antiscalant addition) shows most rapid flux decline, followed by the membrane operated with PBTC, suggesting that the gypsum inhibition potential of PBTC is unimproved at higher dosages. PAA showed no change in permeate flux, similar to its behaviour at lower dosage. Interestingly, PAA+DTPMP, DTPMP and ATMP also showed stable flux over the entire experimental duration of 600 min, suggesting improved gypsum scale inhibition at higher antiscalant dosage of 1 $mg \cdot L^{-1}$ TS.

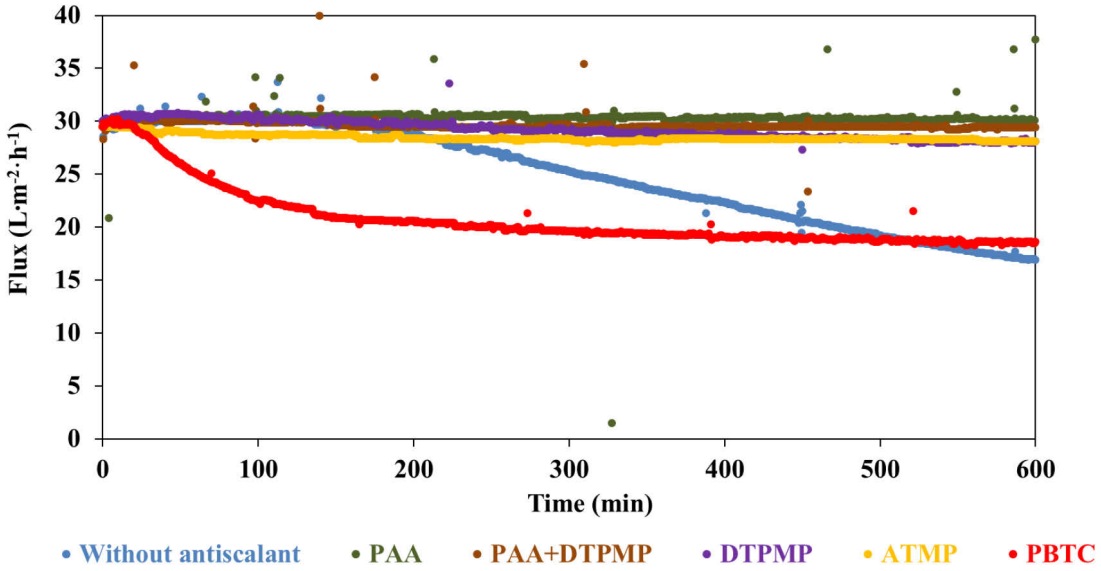

Figure 25: Flux behaviour in crossflow filtration setup using flat sheet RO membrane operated with 25 mM Na_2SO_4 and $CaCl_2$ feed + 1 mg·L^{-1} TS of different commercial antiscalants in complete recirculation mode, at crossflow velocity 0.1 m·s^{-1} (TMP=25 bar, T=11 °C, $SI_{gypsum} \approx 0.2$)

Experiments with crossflow filtration setup were conducted only once in this study due to the long and tedious nature of the experiments. However, corresponding augmentation with the SEM analysis and stirred-beaker test results were regarded to be sufficiently reliable. Nevertheless, initial experiments with the blank gypsum and 1 mg·L^{-1} TS were repeated a second time and successfully verified for their similar flux behaviour (Annex II-16 and II-17).

SEM characterization of the membranes after the experiment showed that the membrane operated with PBTC showed gypsum crystals on its surface that appeared more disintegrated than the rosettes observed in the absence of any antiscalants (Figure 26). Membranes operated with commercial PAA, PAA+DTPMP, DTPMP and ATMP were completely devoid of crystals, indicating successful gypsum scale inhibition at higher dosage of 1 mg·L^{-1} TS. Based on the stable flux in combination with crystal-free membrane surfaces given by SEM, it may be possible to conclude that the effectiveness of the four antiscalants are primarily governed by their increased threshold inhibition capability at higher dosages, i.e., the antiscalants are able to prevent formation of scale crystal nuclei for a sufficiently long amount of time.

Jain et al. 2019 investigated different phosphonate based antiscalants for scale inhibition mechanism – inherently, high-molecular-weight antiscalants with a larger number of amine groups like DTPMP have a bigger molecular structure compared to the low-molecular-weight antiscalants such as NTMP. Subsequently, when the antiscalant adsorbs on the incipient Ca^{2+} nuclei, the high-molecular-weight DTPMP molecules occupy a larger surface area of the nuclei structure, causing effective scale inhibition. This effect with DTPMP is especially pronounced at higher dosage concentrations. A similar hypothesis could be made of ATMP effectiveness against gypsum. Additionally, it was also suggested that the residual antiscalant concentration,

i.e., concentration of the antiscalant at the onset of scaling, enhances inhibition potential of phosphonate antiscalants. Thus, based on the results reported in this section, it is considered to be reasonable that most phosphonate antiscalants perform better at higher dosages.

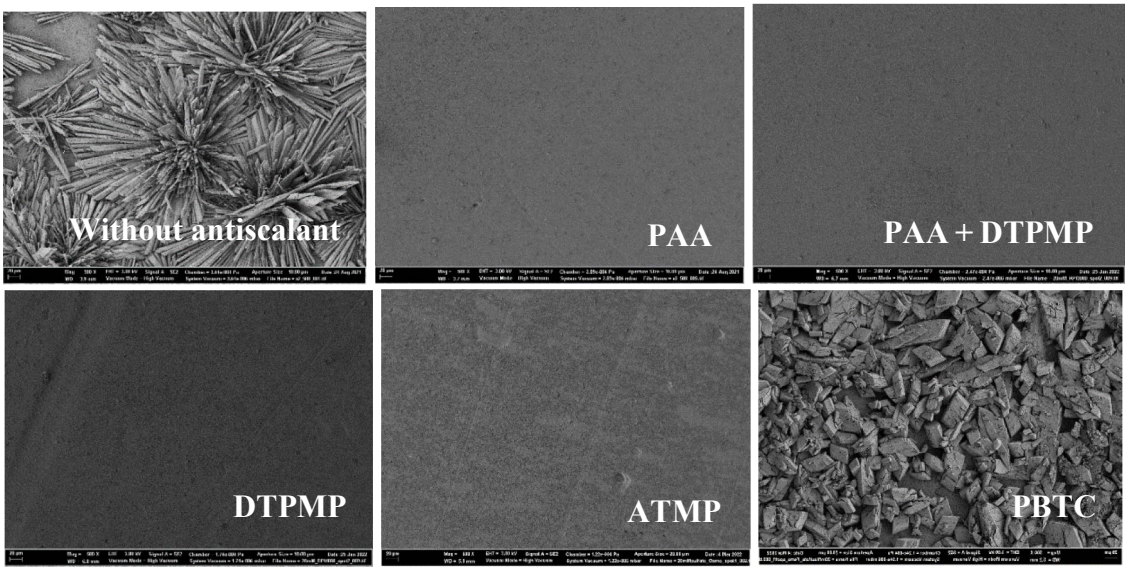

Figure 26: SEM pictures (Mag = 500 X, 20 µm) of RO membrane surface after crossflow filtration with 25 mM Na_2SO_4 and $CaCl_2$ + 1 mg·L^{-1} TS of different commercial antiscalants

Comparison of antiscalant performance against CaSO4 in the pilot plant at 1 mg·L^{-1} TS with the stirred-beaker tests shows consistent results – PBTC shows little improvement in induction time, which is reflected in rapid flux decline in the pilot plant. The remaining four antiscalants show higher induction times (Figure 20) at 1 mg·L^{-1} TS, which is validated by stable permeate flux in crossflow pilot plant experiments and absence of any scale crystals on the membrane surface after filtration.

4.3.2 Inhibition potential against calcite scaling at different dosages

The lab-scale crossflow pilot plant was used to evaluate the effectiveness of commercial antiscalants against carbonate scaling at different dosages. Antiscalants with PAA, PAA+DTPMP, DTPMP, PBTC and ATMP as active ingredients were tested at dosages 0.5 mg·L^{-1} TS and 1 mg·L^{-1} TS, with slightly supersaturated carbonate solution as feed ($SI_{calcite}$ ≈ 1.09), at constant temperature 11 ± 1 °C and initial pH 7.5. The feed was recirculated through the pre-conditioned membrane at constant TMP of 25 bar, with complete retentate and permeate circulation back to feed tank. The relatively constant SI conditions ensured that any drop in permeate flux over time was due to unsuccessful carbonate scale inhibition by the antiscalant. As seen in Figure 27, in the absence of any antiscalant the permeate flux in the pilot plant starts decreasing right from the beginning and declines by about 27 % in about 200 min and remains fairly unchanged thereafter, until the end of the experimental period of 600 min. This is unlike

sulfate scaling, which shows more than 50 % flux decrease in about 600 min. Addition of 0.5 mg·L^{-1} TS of different antiscalants to the carbonate solution causes different behavior in rate of change of flux for different active ingredients. As seen in Figure 27, 0.5 mg·L^{-1} TS of PAA causes the flux to gradually decrease in the beginning by about 25 % in around 210 min. Interestingly, after about 210 min, the flux increases again and reaches its original value by the end of 600 min. At the same dosage, PAA+DTPMP mixture, PBTC and ATMP maintain stable flux throughout the experimental time. In contrast, DTPMP maintains constant flux for about 200 min, after which it decreases rapidly by about 30 % of the initial flux by the end of 600 min.

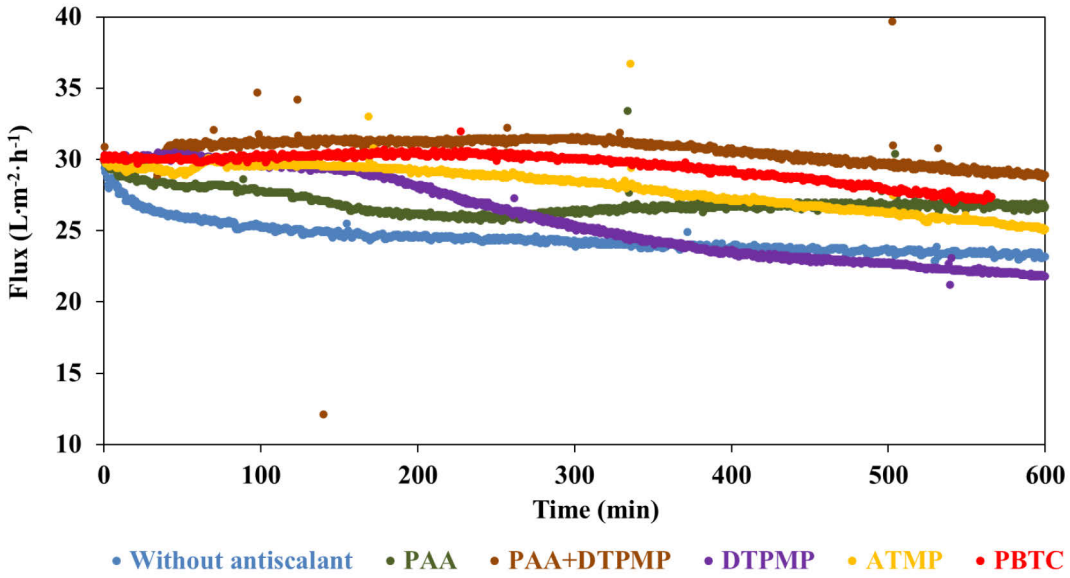

Figure 27: Flux behaviour in crossflow filtration setup using flat sheet RO membrane operated with 22 mM $NaHCO_3$ and $CaCl_2$ feed + 0.5 mg·L^{-1} TS of different commercial antiscalants in complete recirculation mode, at crossflow velocity 0.1 m·s^{-1} (TMP=25 bar, T=11 °C, $SI_{calcite} \approx 1.09$)

After the experiment in the reverse osmosis pilot plant, the membranes were carefully removed from the filtration cell, stored dry in the refrigerator and characterised through SEM at the next immediate possibility. Figure 28 shows the SEM images of the scaled membranes operated with carbonate scalant and 0.5 mg·L^{-1} TS antiscalant in the pilot plant under predominantly heterogeneous scaling conditions (low crossflow velocity; enhanced concentration polarization). The membrane operated without any antiscalant showed several calcite crystals on its surface that were dense and having small cube or rhomboid shapes. The membrane operated with 0.5 mg·L^{-1} TS PAA showed several calcite crystals on its surface that were slightly flattened from the typical cuboid shape. Surprisingly, despite stable flux in pilot plant, membrane operated with PAA+DTPMP mixture showed several slightly larger, deformed calcite crystals on its surface. Similarly, SEM characterization showed DTPMP membrane surface was also covered with calcium carbonate crystals. Contrarily, membranes operated with 0.5 mg·L^{-1} TS PBTC and ATMP showed almost no scales on its surface, suggesting superior

calcite inhibition potential of these antiscalants primarily via threshold inhibition and retardation of nucleation step of calcite molecules. Basheer et al. 2021 reported calcium carbonate crystals in the form of calcite to have rhomboidal structure, as seen in this study, and showed that phosphonates like ATMP do not affect morphological characteristics of calcite and have negligible interaction with the structure as part of its antiscaling mechanism.

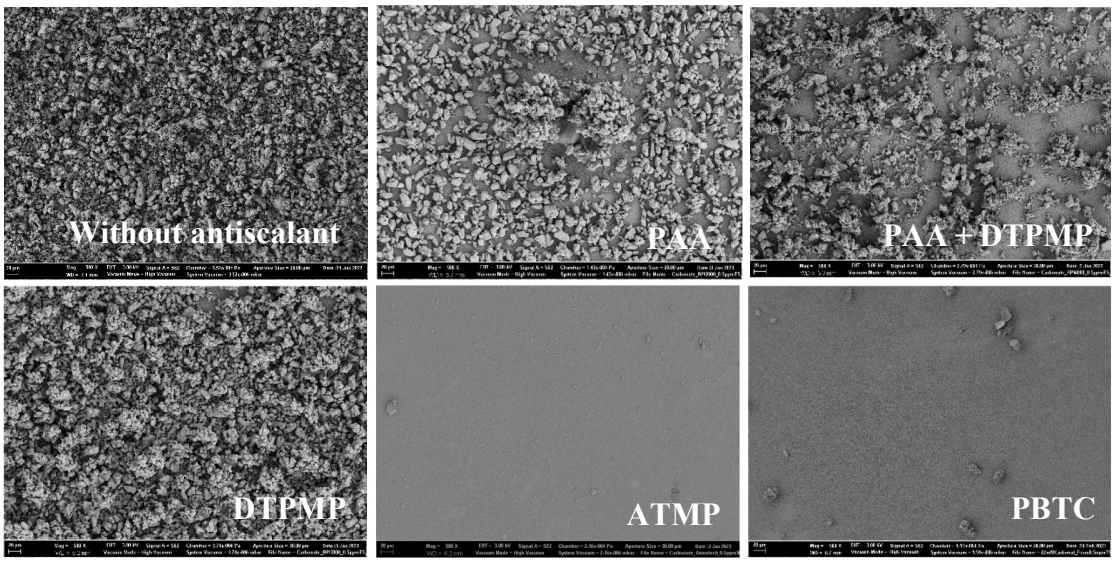

Figure 28: SEM pictures (Mag = 500 X, 20 µm) of RO membrane surface after crossflow filtration with 22 mM $NaHCO_3$ and $CaCl_2$ + 0.5 $mg \cdot L^{-1}$ TS of different commercial antiscalants

Comparison of the permeate flux behaviour of antiscalants against calcite scaling in the crossflow filtration pilot plant with the induction time in the stirred-beaker test revealed some similarities and certain irregularities. Absence of antiscalants in the calcite solution resulted in induction time of about 10 min in the former experiment and rapid permeate flux decline initially in the pilot plant, along with several calcite crystals observed on membrane surface. Interestingly, PAA had a very low induction time of only 36 min in the stirred-beaker test which corroborates with observed initial flux decline in the pilot plant. However, this is followed by an increase in flux to a stable value. Based on the prevalence of several calcite crystals on its surface, it could be derived that calcite inhibition potential of commercial PAA antiscalant is poorly governed by threshold inhibition effect and primarily controlled by dispersion property. Similarly, PAA+DTPMP only showed 35 min induction time against calcite but maintained stable flux throughout the pilot plant experiment, despite the SEM revealing formation and deposition of several carbonate crystals on the membrane surface. A similar hypothesis of strong dispersion ability of PAA+DTPMP could be derived from these observations. DTPMP showed lowest induction time of 19 min and continuous flux decline in pilot plant experiment, with several calcite crystals during SEM characterization, implying that it is incapable of effectively inhibiting calcite scaling. Commercial PBTC and ATMP showed stable flux in the pilot plant and no crystals on the membrane surface, corroborating well with the long induction

time data derived from the stirred-beaker test, suggesting strong calcite nucleation inhibition capability of these products.

Effectiveness of the five commercial antiscalants were evaluated at higher dosage of 1 mg TS/L in the crossflow-operated pilot plant. As seen in Figure 29, flux behaviour of PAA at higher dosage was quite similar to that observed at 0.5 mg·L^{-1} TS – permeate flux with PAA started to decrease continuously after about 100 min and after approximately 25 % decline, the flux increased again after 220 min and reached its original value by 400 min. PAA+DTPMP mixture was able to maintain a stable flux throughout experimental duration, while commercial DTPMP showed relatively stable flux in the beginning but decreased rapidly after about 400 min. As expected, with higher dosage of 1 mg·L^{-1} TS, phosphonate antiscalants PBTC and ATMP maintained stable initial flux throughout experimental duration, implying strong calcite inhibition potential.

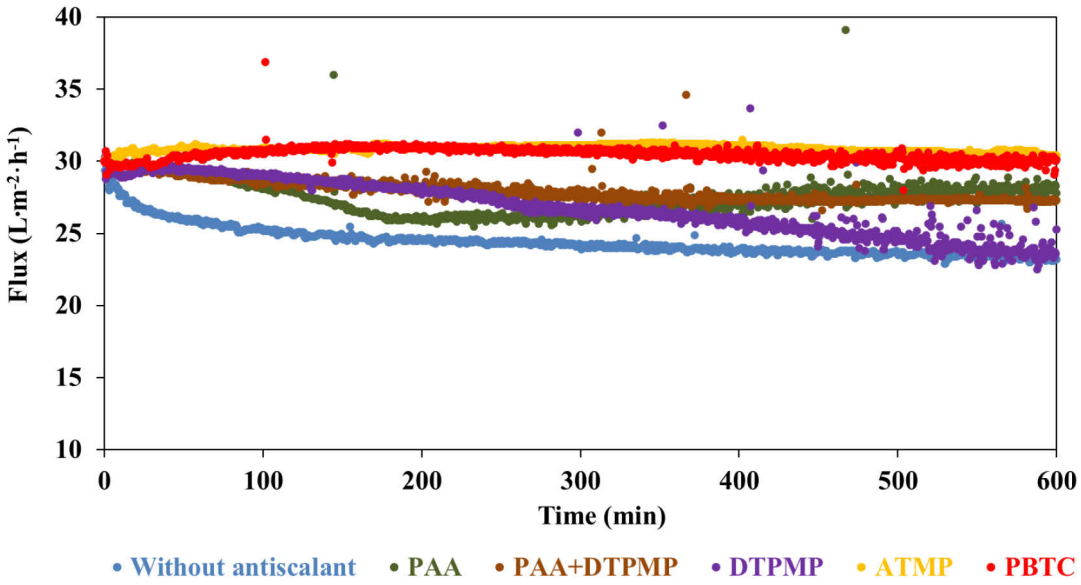

Figure 29: Flux behaviour in crossflow filtration setup using flat sheet RO membrane operated with 22 mM $NaHCO_3$ and $CaCl_2$ feed + 1 mg·L^{-1} TS of different commercial antiscalants in complete recirculation mode, at crossflow velocity 0.1 m·s^{-1} (TMP=25 bar, T=11 °C, $SI_{calcite} \approx 1.09$)

Similar to the previous case, membranes were characterized by SEM to understand the inhibition mechanisms and crystal manipulation effect due to the different antiscalants. As seen in Figure 30, membrane with PAA antiscalant showed several calcite crystals on its surface that were bigger in size and appearing as deformed cuboids with disintegrated, pointed structures. Again, despite stable flux behaviour, PAA+DTPMP showed many small calcite crystals on the membrane surface suggesting high dispersion ability. SEM characterization of DTPMP operated membrane also revealed a surface covered with calcite crystals, albeit the structure modified into much larger calcite blocks compared to the small cubes typical formed in the

absence of any antiscalant. Both PBTC and ATMP showed almost no crystals on their surface, consistent with their stable flux behaviour in the pilot plant. Interestingly, XRD analysis by Ji et al. 2017 of ATMP on carbonate scaling, derived that ATMP with $-PO_3(OH)_2$ could modify $CaCO_3$ precipitation from the most stable calcite crystal to the most unstable vaterite crystal. Additionally, they hypothesized that ATMP inhibited the growth of calcite in landscape orientation but improved the growth longitudinally. Although these claims could not be verified in ths study due to higher temperature and saturation conditions used in the given study, ATMP was also demonstrated to possess excellent chelating properties which may be considered to be the primary mechanism towards superior calcite inhibition potential reported in this study.

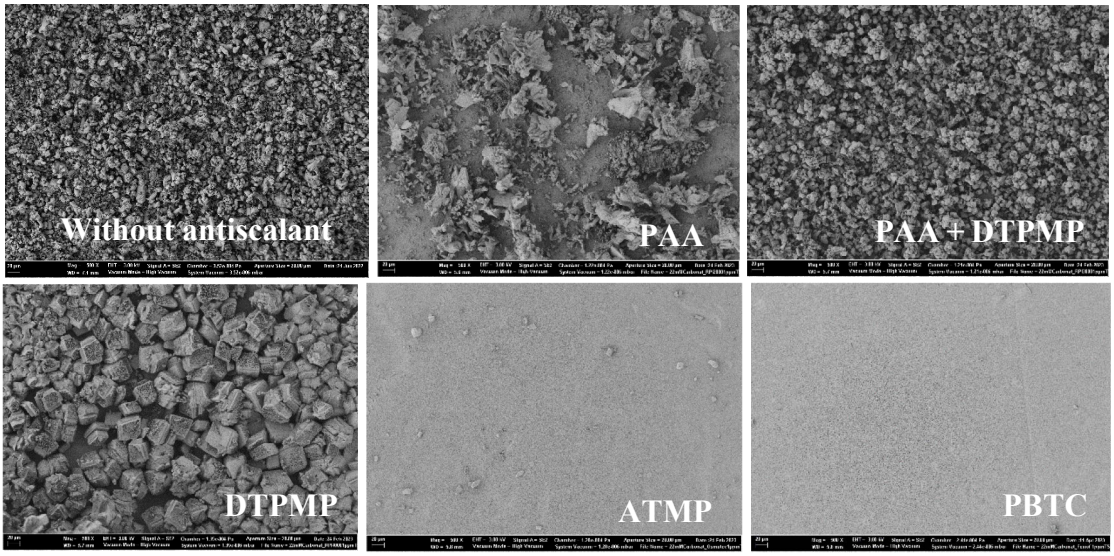

Figure 30: SEM pictures (Mag = 500 X, 20 µm) of RO membrane surface after crossflow filtration with 22 mM $NaHCO_3$ and $CaCl_2$ + 1 $mg \cdot L^{-1}$ TS of different commercial antiscalants

Induction times obtained in the stirred-beaker test were verified with the permeate flux behaviour in the crossflow filtration pilot plant at constant TMP. Although the induction time for PAA antiscalant in calcite solution in the stirred-beaker test increased to 96 min at a dosage of 1 $mg \cdot L^{-1}$ TS, it was evident from the flux behaviour in the pilot plant that the predominant inhibition mechanism of dispersion remained unchanged for the product despite higher dosage. Besides a slightly longer stable flux in the beginning (up to ~ 160 min), there was little difference to the overall PAA antiscalant effectiveness against calcite precipitation at higher dosage. Strangely, although the induction time for PAA+DTPMP increased to about 134 min at 1 $mg \cdot L^{-1}$ TS, indicating sufficiently good threshold inhibition against calcite and the fact that permeate flux in the pilot plant remained mostly constant throughout the experimental duration, prevalence of several calcite crystals on the membrane surface indicated that the primary inhibition mechanism at play for PAA+DTPMP is dispersion. A closer look at the turbidity behaviour in the stirred-beaker test shows that although induction time (nucleation inhibition) for the antiscalant is high, the crystallization time is relatively low (Annex II-8), suggesting that crystal growth inhibition ability of the antiscalant is poor. The induction time of DTPMP remained comparatively low and thus, also showed continuous flux decline after about 300 min,

with several calcite crystals forming on the membrane surface. At higher dosage of 1 $mg \cdot L^{-1}$ TS, the induction times for commercial PBTC and ATMP were highest at over 200 min in the stirred-beaker test, fitting well with stable permeate flux in the pilot plant and almost nil crystals on the membrane surface, suggesting strong threshold / calcite nucleation inhibition property of these phosphonate based antiscalants.

Al-Hamzah et al. 2014 found that PAA causes highest distortion amongst $CaCO_3$ polymorphs, similar to the SEM image observations in this study. Lee et al. 2020 compared the effectiveness of 2 $mg \cdot L^{-1}$ of DTPMP and PAA as suitable inhibitors against calcite scaling in a similar lab-scale crossflow filtration setup with RO membranes. They found that addition of both antiscalants could delay rate of gypsum crystallization in comparison to the scenario with no antiscalants. Interestingly, they found that DTPMP was able to maintain stable flux for slightly longer compared to PAA, although both inhibitors eventually led to flux loss. The slight differences in the results obtained in this study may be attributed to different operating conditions used in their study, including higher temperature, combination of permeate recirculation and collection modes, but more crucially, it was noted that the feed water consisted of some Fe ions. Several studies have reported that the performance of PAA antiscalant is significantly affected by the presence of iron (Yu et al. 2020). Li et al. 2022 evaluated in detail the behaviour of PAA, DTPMP and PBTC antiscalants against $CaCO_3$. Similar to the PAA effectiveness observed in this study, it was found that PAA was least likely to inhibit formation of $CaCO_3$. However, as demonstrated in this study, it must be noted that this does not directly translate to a poor performing antiscalant since PAA shows high dispersion capability in the membrane filtration test conducted in this study. They found that DTPMP and PBTC show similar effectiveness against $CaCO_3$; this result is somewhat contradictory to the findings in this study which shows that DTPMP has much lower calcite inhibition potential compared to PBTC. The differences may be attributed to different commercial antiscalants used in both studies, which reinstates the challenge that antiscalants from different manufacturers may potentially show different scale inhibition behavior at different dosages. Subsequently, this necessitates the use of antiscalant effectiveness tests as a means to pre-determine the efficacy of antiscalants against different salts.

4.4 Overview of test methods to determine antiscalant effectiveness against sulfate and carbonate scaling

The scale inhibition potential of antiscalants is varied depending on type of active ingredient(s) and often have one or more complex mechanisms responsible for the inhibition effect. While guidance from antiscalant manufacturers on antiscalant selection and experience-based application are useful to ensure smooth operation of membrane systems, there is growing need from water utilities and end-users to close the knowledge gap on suitable antiscalant application by less-laborious pre-determination techniques that may be carried out before it is applied in real membrane treatment applications. Methods are researched to evaluate the scale inhibition potential of antiscalants under different conditions are diverse in terms of the type(s) of scalant

and its underlying scaling mechanism, solution saturation conditions, measurable evaluation parameters, type(s) of antiscalant and its underlying inhibition mechanism, extent and expense of the nature of the setup and/or detection devices and the sensitivity and resulting reproducibility of the method (Amjad 2014). This section summarizes the various techniques used to evaluate the effectiveness of commercial antiscalants in this study, including the tests described in Sections 4.2 and 4.3, as well as additional results and examples that illustrate the nature of the findings and their associated limitations.

Stirred-beaker test vs. crossflow filtration test:

Evaluation of antiscalants using the stirred-beaker test is one of the most commonly used techniques to determine antiscalant effectiveness using a simple experimental setup. A supersaturated scaling solution with an antiscalant was continuously stirred in a beaker and evaluated for its induction time based on time required for turbidity increase by 1 NTU. Evaluating scale inhibition performance in dynamic systems using a laboratory NF/RO unit to simulate an actual high-pressure membrane filtration process has also been researched in literature (Li et al. 2018, Rahardianto et al. 2007, Shmulevsky et al. 2017). Scale inhibition performance can be determined by comparing the changes in permeate flux with and without antiscalant addition, and in some cases by direct visual membrane surface monitoring to evaluate scale surface coverage and surface number density that can reflect the effectiveness of antiscalants in the membrane treatment processes. In this study, a laboratory scale RO filtration setup was operated under constant, slightly supersaturated scaling conditions with an antiscalant and evaluated for the rate of flux decline and resulting SEM characterization of the scaled membrane surface. Experiments with RO membrane filtration were only carried out once but augmented with SEM analysis post filtration.

Both tests could be carried out for sulfate and carbonate scaling salts at typical groundwater temperature range of 11 °C (in Germany) and for a wide-variety of commercial antiscalants with different active ingredients. As seen in Figure 31(a), at antiscalant dosage of 0.5 $mg \cdot L^{-1}$ TS with gypsum solution ($SI_{gypsum} \approx 0.72$), PAA shows high induction time of 61 min in the stirred-beaker test and 100% permeate flux stabilization after 10 h of pilot plant operation (Figure 31(b)), indicating excellent nucleation and threshold inhibition property of the antiscalant against sulfate salts. In comparison, absence of an antiscalant resulted in 10 min induction time and 59% flux stabilization in 10 h in the pilot plant. Consequently, PBTC which had negligible inhibition against sulfate salt precipitation but good calcite binding potential, was associated with 13 min induction time in the gypsum stirred-beaker test and decreased flux stabilization of 60% after 10 h of operation of RO pilot plant.

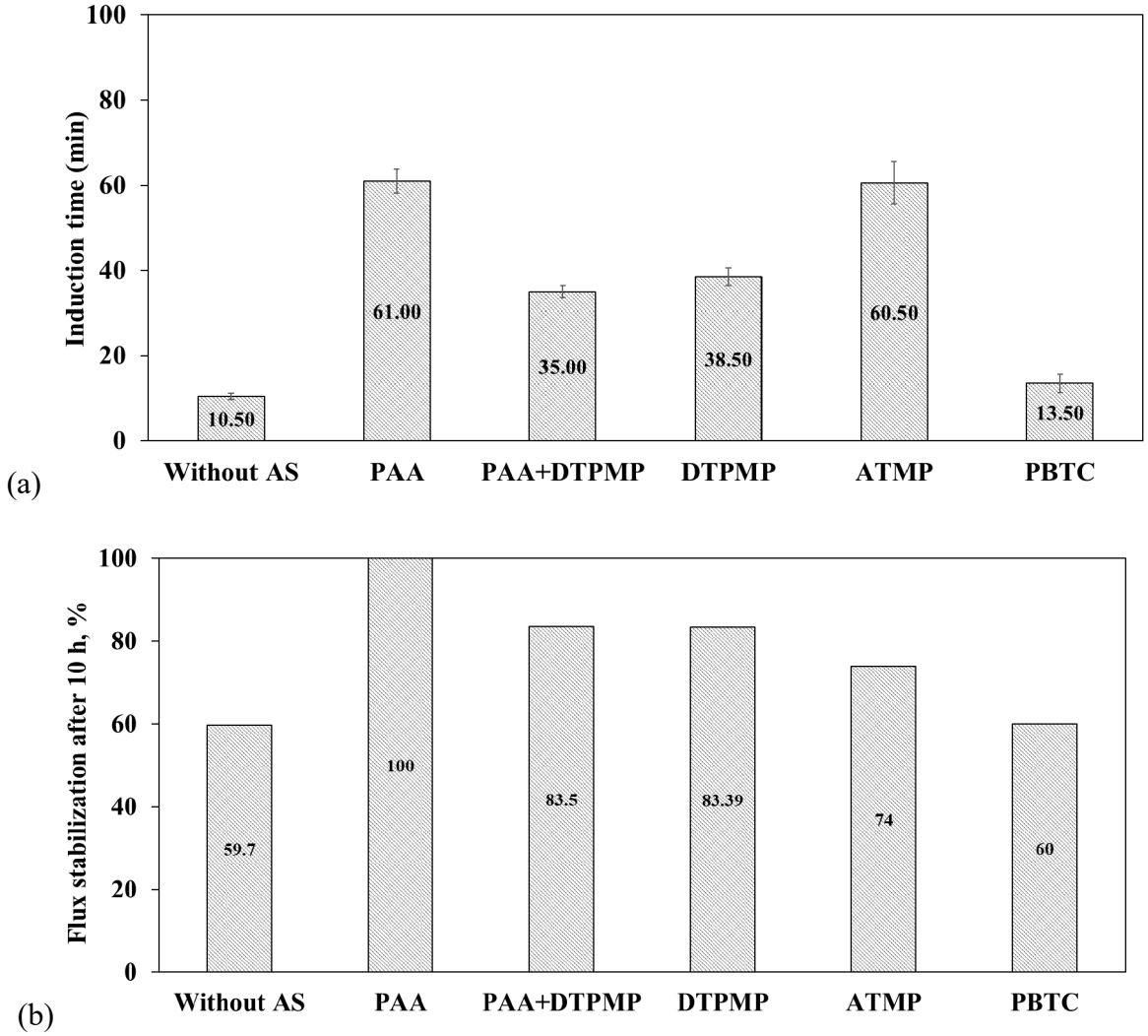

Figure 31: Comparison of antiscalant effectiveness at 0.5 mg·L^{-1} TS against gypsum scaling using (a) induction time determined via turbidity increase in the stirred-beaker test ($SI_{gypsum} \approx 0.72$) and (b) extent of permeate flux stabilization after 10 h operation in the crossflow filtration test carried out at constant TMP and temperature ($SI_{gypsum} \approx 0.2$)

While the two tests are able to produce corroborating results in case of gypsum scaling for antiscalants that have exceptionally good or exceptionally poor inhibiting performance based on inhibition potential of nucleation step (threshold inhibition mechanism), the analysis of the suitability of the test for antiscalant selection becomes more complex when the underlying inhibition mechanisms are dispersion or combined phenomena. For instance, in Figure 31(a) and (b), ATMP shows high induction time similar to PAA in the stirred-beaker setup but only 73 % flux stabilization in the RO pilot plant, suggesting that it is no better than the other phosphonates, PAA+DTPMP mixture and DTPMP antiscalant.

This characteristic is even more pronounced when comparing the two tests for their suitability to evaluate antiscalant effectiveness against calcite scaling. Figure 32(a) and (b) show that carbonate scaling in the pilot plant does not lead to drastic flux decline and maintains almost 80 % stabilization despite showing low induction time of 11 min in the stirred-beaker test in

the absence of any antiscalant, potentially due to the crystallizing nature and size of calcite crystals formed within the membrane system.

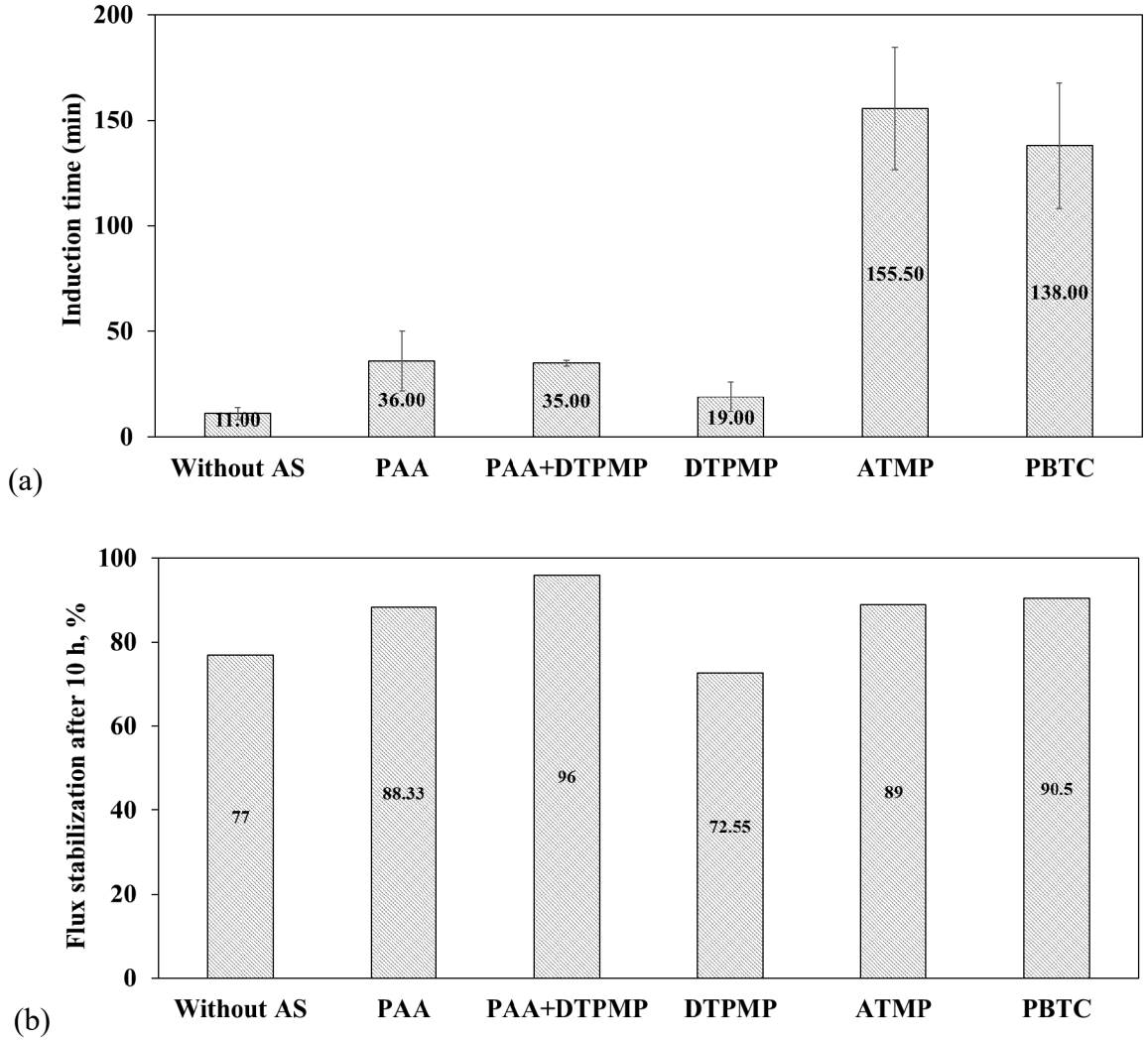

Figure 32: Comparison of antiscalant effectiveness at 0.5 mg·L^{-1} TS against calcite scaling using (a) induction time determined via turbidity increase in the stirred-beaker test ($SI_{calcite} \approx 2.06$) and (b) extent of permeate flux stabilization after 10 h operation in the crossflow filtration test carried out at constant TMP and temperature ($SI_{calcite} \approx 1.09$)

Addition of antiscalants leads to only slightly higher induction times in the beaker setup for 0.5 mg TS/L of PAA and PAA+DTPMP mixture, but more than 90 % flux stabilization in the pilot plant. This implies that exclusive stirred-beaker test results may be misleading regarding antiscalant effectiveness, since these two products incorporate dispersion as the predominant scale inhibition mechanism which is impossible to derive from induction time determination via turbidity measurement defined in this study. This hypothesis was additionally verified by SEM of scaled membrane after pilot plant experiment which showed several calcite crystals, despite high induction time and stable flux behaviour. Meanwhile, phosphonates PBTC and ATMP showed exceptionally high induction times in the stirred–beaker test and 90 % flux

stabilization in the pilot plant after 10 h of operation, indicating high threshold inhibition potential.

Yu et al. 2020 concluded that compared to static evaluation methods, the operational conditions of membrane filtration tests are more instructive due to their close resemblance to NF/RO in terms of presence of a membrane and operational parameters like transmembrane pressure, crossflow velocity, etc. This study showed that the stirred-beaker test is simple to set up and useful to determine the threshold inhibition potential of antiscalants against different scalants at different dosages. However, since threshold inhibition is not the only mechanism responsible for scale inhibition, a membrane filtration simulation test may be useful to gain additional information and further insights into antiscalant application. Thus, it may be stated that low induction times in the stirred-beaker test are not conclusive of low scale inhibition potential without additional filtration and visual investigation. Conversely, high flux stabilization indicates sufficiently good inhibition potential, but does not give full information on the nature of the antiscalant mechanism without subsequent visual investigation of the membrane for scaling crystals or lack of it. In most cases, this may be successfully verified by long induction time measurement but not conclusive. For instance, PAA has high threshold inhibition against sulfate solution with long induction time and high flux stabilization, but primarily disperses carbonate salts from the membrane surface and may still be a suitable antiscalant despite low induction times with carbonate salts. RO pilot plant experiments based on flux monitoring tend to provide more conclusive results on antiscalant effectiveness when optimised for the experimental time, operating parameters and supplemented with visual examination of the scale crystals or lack thereof.

Besides the complex underlying inhibition mechanisms governing suitability of a test for antiscalant selection, both tests to determine antiscalant effectiveness are additionally varied in the nature of the test setup and application. The stirred-beaker test though easy to set up, is highly dependent on the sensitivity of the evaluation parameter being measured, for instance, the precision of turbidity measurement used in this study. Changing hydrodynamic conditions also highly influence the end-result and are subsequently crucial to the reproducibility and reliability of the test method. It is therefore recommended to carry out stirred-beaker tests with multiple trials under identical conditions and compare with a blank (without antiscalant) in order to interpret antiscalant effectiveness by this method.
Crossflow filtration experiments may provide information about antiscalant effectiveness under realistic NF/RO filtration conditions and offer more scope to incorporate different solution and operating conditions. When these experiments are augmented with visual investigation of the membrane post filtration, it indeed has the potential to become a reliable, conclusive technique to determine antiscalant effectiveness. Additionally, online monitoring of physical parameters such as pH, turbidity or conductivity during the experiment in the different filtration streams may also enhance timely scaling detection or antiscalant effectiveness as shown by Futterlieb and Panglisch 2025. However, such a setup requires a full-fledged laboratory with extensive investment cost in terms of material needed, operating costs and skilled personnel to carry out such challenging experiments with complex operation.

The following sub-sections briefly discuss other static and dynamic methods that were explored in this study to evaluate scaling and antiscalants, but were limited in their approach or level of precision.

Dead-end filtration test:

In addition to the stirred-beaker test and crossflow pilot plant experiments, a high-pressure dead-end filtration method was also evaluated as a suitable test to determine antiscalant effectiveness. Details of the experimental setup have been described under Section 3.2.3. While the stirred-beaker test was a simple method to pre-determine the effectiveness of antiscalants at different dosages, it was sometimes associated with high standard deviations and did not reflect all underlying inhibition mechanisms in a membrane filtration system. The lab-scale crossflow filtration test together with SEM characterization was more informative on antiscalant efficacy at different conditions, but associated with long experimental times and elaborate preparation and cleaning steps, besides high material and investment cost. To overcome this, a lab-scale dead-end filtration cell operated with a flatsheet RO membrane at 25 bar with stirring on the membrane surface (quasi crossflow conditions) was tested to ascertain antiscalant effectiveness. The rate of flux decline was determined based on weight of permeate collected. Figure 33 shows the flux behaviour during dead-end filtration of sulfate feed (initial $SI_{gypsum} \approx 0.2$) without any antiscalant, at constant TMP 25 bar and at room temperature.

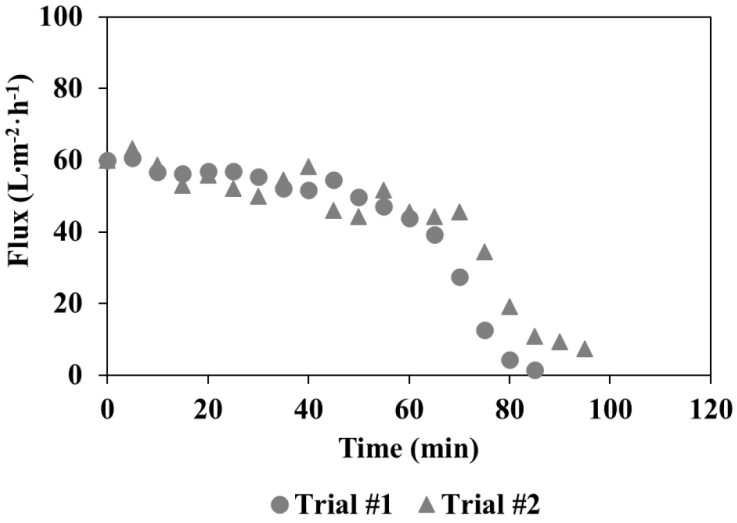

Figure 33: Rate of change of flux in dead-end filtration test with initial feed $SI_{gypsum} \approx 0.2$, without antiscalants, constant TMP 25 bar, room temperature 22 ± 1 ºC

The flux starts at about 60 $L \cdot m^{-2} \cdot h^{-1}$ and reduces to almost 0 in about 85 min, implying that the membrane is saturated with gypsum crystals by continuous concentration of feed. Reproducibility achieved using the dead-end filtration setup was satisfactory for gypsum salts. In the following step, the effectiveness of antiscalants PAA and PBTC at 0.5 $mg \cdot L^{-1}$ TS was tested against 25 mM Na_2SO_4 and $CaCl_2$. Since it was already pre-determined from the stirred-beaker test and crossflow pilot plant experiments that PAA has good inhibition against gypsum and PBTC is a poor gypsum inhibitor, similar conclusions were expected from the dead-end filtration test. As seen in Figure 34(c), the flux with PAA decreases to 0 after about 140 min, in

contrast to PBTC which decreases within 90 min, similar to the blank, confirming the antiscalant behaviour obtained by other methods (Figure 34(a) and (b)).

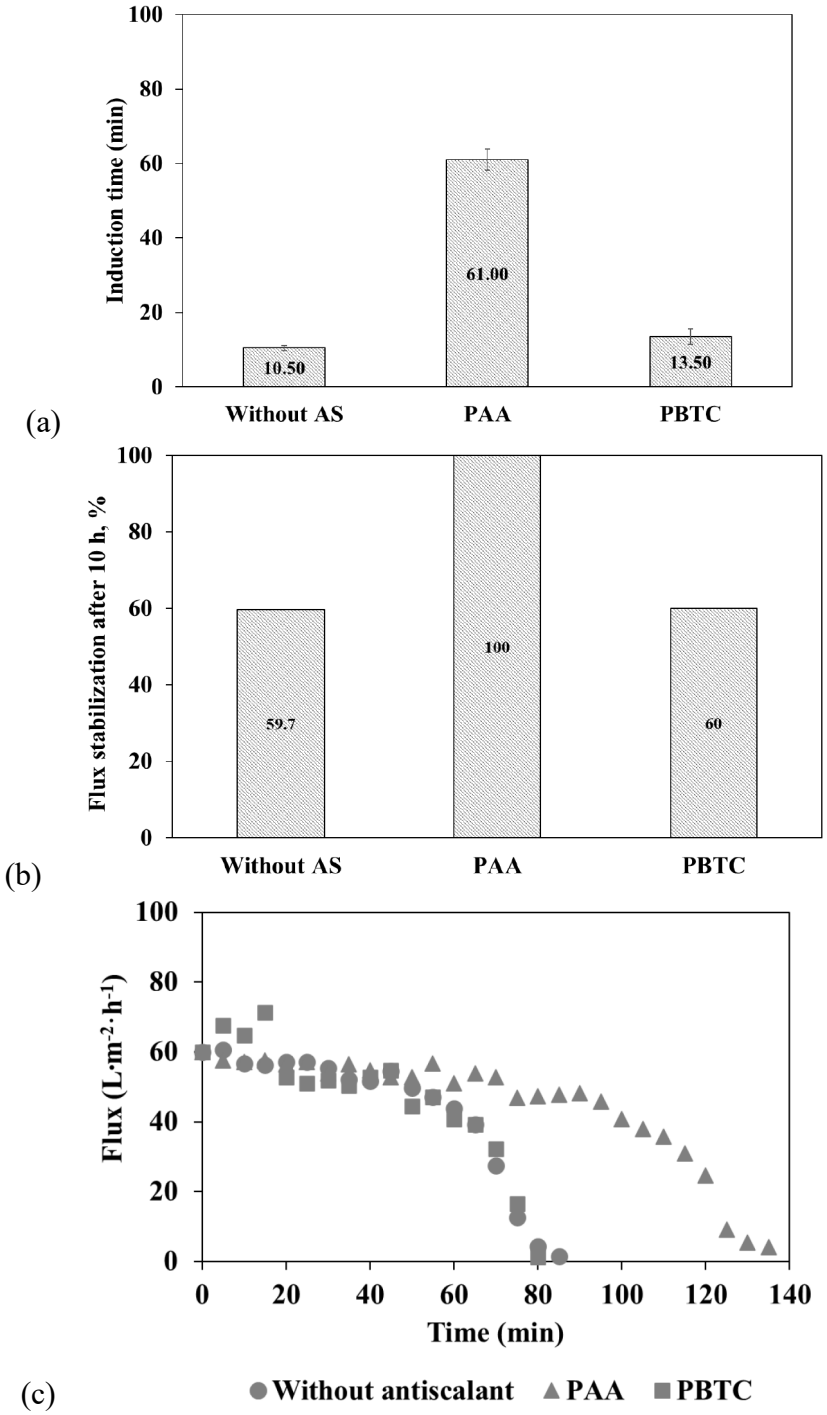

Figure 34: Comparison of antiscalant effectiveness at 0.5 mg·L^{-1} TS against gypsum scaling using (a) induction time determined via turbidity increase in the stirred-beaker test ($SI_{gypsum} \approx 0.72$), (b) extent of permeate flux stabilization after 10 h operation in the crossflow filtration test (TMP = 25 bar, T = 11 ºC, $SI_{gypsum} \approx 0.2$) and (c) rate of change of flux in dead-end filtration test at constant TMP 25 bar and room temperature 22 ± 1 ºC ($SI_{gypsum} \approx 0.2$)

When the dead-end filtration test was evaluated for other antiscalants (PAA+DTPMP, DTPMP and ATMP), the flux decline was in a similar range of about 90-120 min for all 3 products with more significant differences in reproducibility (Annex II-9). This suggested that for sulfate solutions the test was only capable of differentiating between antiscalants with underlying principle of threshold inhibition mechanism and antiscalants that were starkly different from each other in terms of their effectiveness.
When the dead-end filtration test was applied to determine antiscalant effectiveness against carbonate scaling, long flux decline times of 130 min was produced for blank (absence of antiscalant). Addition of antiscalants led to overlapping times with the blank for the antiscalants. Although optimization of the test setup with respect to the permeate weight collection led to some improvement in terms of slightly higher flux stabilization time for the PAA+DTPMP mixture (Annex II-10) which also showed good inhibition potential via dispersion in the crossflow filtration setup, this method was largely unsuccessful for antiscalant effectiveness determination for carbonate salts in the current form.
Despite its potential as a useful method for antiscalant selection, particularly for gypsum scaling, the dead-end filtration test presented several practical limitations that restricted its application for extensive investigations. Besides requiring a suitable filtration cell capable of withstanding high pressures, the cell consisted of small feed volume of 200 ml and with no access to influence the feed solution during the experiment, implying that the temperature of the experiment could not be controlled and had to be carried out at room temperature. The online tool supplied by the manufacturer to determine the weight of the permeate and used to determine flux was associated with several bugs that demanded frequent IT expert intervention. Nevertheless, based on previous experience, it is assumed that such a dead-end filtration test with larger feed capacity and reliable data measuring / monitoring system may be help overcome the tedious and long experimental requirements of the crossflow filtration setup. However, it remains questionable if the dead-end filtration test has some considerable advantages over the simple stirred-beaker test with a sufficiently sensitive turbidity detection.

Whispering gallery mode:

Whispering gallery mode (WGM) is a novel technique that monitors change in resonant frequency / wavelength on a single nanoparticle embedded in a microfluidic chip. WGM experiments were carried out by Surflay Nanotech GmbH, Berlin. Since WGM is typically used in protein or ligand analyses and this was the first time it was being tested for its suitability against scaling detection, WGM trials were only conducted with carbonate solutions to ensure reliable cleaning of the system after each experiment and without antiscalants. Detailed setup and pre-preparations for WGM carried out by Surflay Nanotech GmbH are described under Section 3.2.4. The output of WGM analysis is a plot of wavelength against time, with shift in wavelength associated with scaling.

The test chips were coated with 4 double layers of different polycations (PAH, PEI, PVBTMA and PDADMAC) and negatively charged WGM sensor particles (polystyrene) alternately and finally immobilized within the chip. First attempts were carried out to make the scaling visible

on the surface of the sensors by adding 10 µl of 50 mM $NaHCO_3$ and 5 mM solution of $CaCl_2$ to the chip. As seen in Figure 35, this resulted in rapid crystallization of several calcite crystals on the surface of the sensor particles and also outside it.

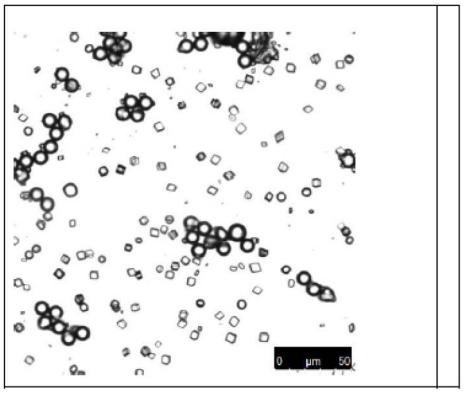

Figure 35: Formation of $CaCO_3$ precipitates (Vaterite and Calcite) in bulk and on the sensor surface

Successive additions of 1M bicarbonate produced distinct WGM signal shifts corresponding to crystal precipitation, followed by slight dissolution or detachment of crystals from the sensor surface, resulting in a peak in the wavelength (Figure 36).

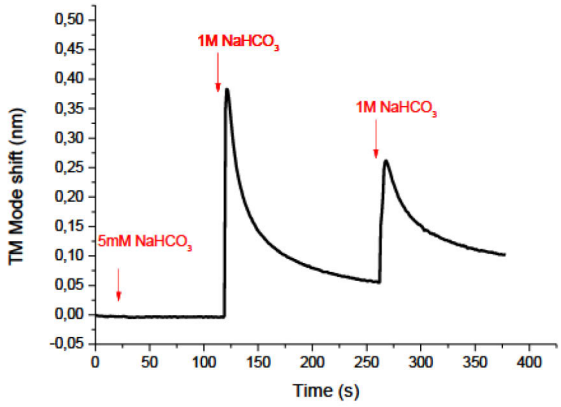

Figure 36: Shift of the WGM spectrum due to the successive addition of $NaHCO_3$ solution, (measuring interval 1 s)

In the second experiment, $NaHCO_3$ solution with a lower concentration of 5 mM was used (Figure 37). Time-dependent precipitation was quite successful with curve becoming increasingly noisy as the deposition progressed. On smoothing the curve, speed of scaling and shift in signal could be recorded quantitatively.

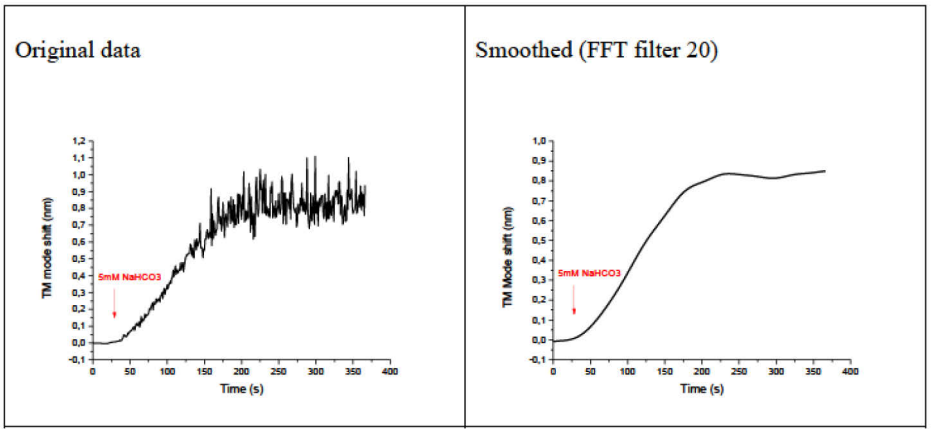

Figure 37: Kinetics of calcium carbonate deposition (scaling) on the surface of the WGM sensor particles

Initial experiments showed that Surflay's novel LowQ WGM technology could potentially be able to detect calcite scaling on surface (heterogeneous scaling) but needed to be optimized for more specific scaling characteristics like reactant concentrations, mixing ratios, pH and dosing protocols, to achieve reproducible scaling kinetics. Additionally, since the negatively charged sensors were only coated with polycations, it was suggested that the sensor surface should also be optimized with layer-by-layer (positive-negative) coating that is responsive to calcite detection. Functionalization of the sensor surface with membrane-relevant coatings was recommended to better mimic membrane properties and promote heterogeneous nucleation, for more uniform crystal deposition across the sensor particles. Hexametaphosphate-coated sensor particles coated with $(PSS/PAH)_2$ double layer showed selective and partial homogeneous precipitation of $CaCO_3$ crystals, but of low stability. Precipitation on the alkaline polystyrene (PS) beads resulted in non-uniform cover and low selectivity.

However, additional measurements of calcite growth detectable by WGM showed non-reproducible results in terms of shift in wavelength over time. Microscopic investigation of polystyrene (PS) WGM sensor particles suspended in saturated carbonate solutions were useful to obtain insights into affinity of crystals to the particle surface. As seen in Figure 38, calcite crystallization with the current functionalized polystyrene WGM sensor was minimal and arbitrary; crystallization was likely to occur within the solution rather than on the surface of the particle. This was confirmed by Surflay for different saturation concentrations of calcite and at different temperatures.

The microscopic analysis provided crucial information on the type of scaling mechanism taking place within the WGM system during the experiment. It could be confirmed that calcite crystals had the tendency to undergo rapid homogeneous nucleation compared to heterogeneous nucleation. Since it was established that the reliability and reproducibility of the shift in wavelength peak from WGM analysis is highly dependent on uniform crystallization around the particle embedded within the chip, the current modification of the chip size and sensor particle type was considered to have low affinity towards carbonate crystals and therefore unsuitable to reliably detect scaling and antiscalant effectiveness.

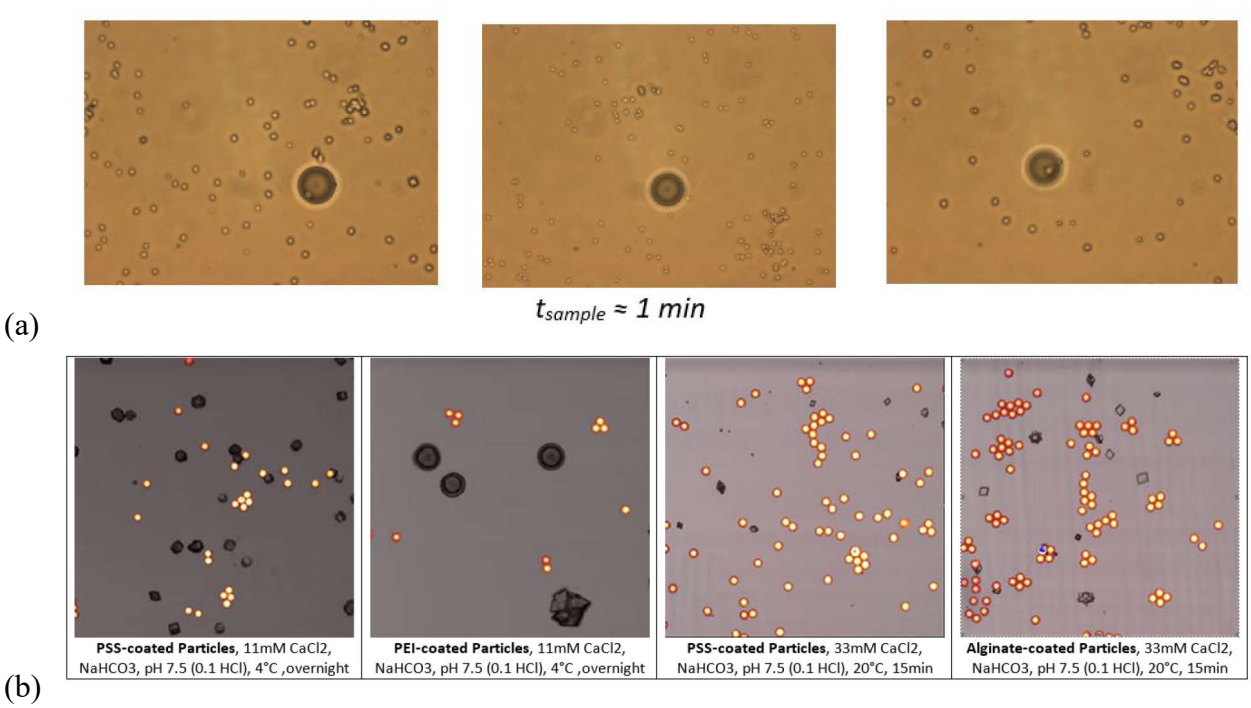

Figure 38: Light microscopic images of polystyrene (PS) WGM sensor particles suspended in carbonate scaling solutions of different saturation levels (a) 5 mM $NaHCO_3$ and $CaCl_2$ (light spheres with dark border) at pH 7.5 with 0.5 % PS solution (dark spheres) heated to 50 ºC, sample taken after 1 min reaction time (b) interaction of 11 mM and 33mM $NaHCO_3$ and $CaCl_2$ (dark forms) at pH 7.5 with PS WGM sensors (yellow sphere with red border) at 4 ºC and 20 ºC carried out by Surflay GmbH

While the working principle of WGM may potentially be utilized in the context of scaling detection and antiscalant selection, it was unsuccessful in the given conditions and significant time and material resources to be invested to optimize the suitable WGM sensor particle with the right chemistry and specific to each scalant type.

Heterogeneous scaling detection using Lagotec Deposens 3 sensor

A variation to the previously described stirred-beaker method was carried out by incorporating the Lagotec Deposens 3 sensor to setup. The sensor was recommended by the manufacturer to investigate carbonate scaling solutions. The aim of integrating the sensor to the stirred-beaker setup was to correlate homogeneous and heterogeneous scaling behaviour in the presence and absence of antiscalants. The Deposens 3 is typically successfully used to monitor and detect biofilm formation and inorganic deposition in pipes. The detection is based on the decrease of heat transfer due to the formation of a heat isolating layer via two positively integrated heat sensitive areas with different thermodynamic characteristics. Heat transfer is recorded in the bulk phase before the sensor and temperature within the sensor is heated to 60 ºC ± 0.2 ºC which triggers precipitation. Following first crystal precipitation within the sensor and based on the temperature difference of the two heat sensitive areas, the thickness of the layer of deposit on the inner side of the pipe is and displayed as the deposit thickness (µm).

The volume of the stirred-beaker setup was increased to 1 L to accommodate recirculation of the scaling solution through the Deposens 3 (Annex I-4). Besides heterogeneous scaling induced within the sensor, homogeneous scaling was monitored in the bulk solution within the beaker via the turbidity measurement. Since the sensor was only recommended for calcium carbonate scaling detection to avoid irreversible damage by the scaling crystals, it was also decided to record the pH of the solution during each experiment. Calibration of the sensor was carried out in the beginning of each experiment for 15-40 min to stabilize the baseline deposit thickness value. Voltage of the electric pump was adjusted so that the uniform flow conditions were established for recirculation from the beaker through the Deposens 3. After repeated trials, rotation speed in the beaker had to be optimized to 350 rpm to ensure uniform crystal formation in bulk solution and eliminate frequent noise in sensor baseline curve. The sensor was cleaned with citric acid after each trial based on manufacturer recommendations.

First experiments were carried out with 33 mM carbonate solution ($SI_{calcite} \approx 2.06$) in the beaker without an antiscalant. As seen in Figure 39, turbidity in the solution increased steadily with time for the double trials, reflecting homogeneous scaling detection which could be quantified via the induction time. Accordingly, a drop in pH was recorded in the solution as carbonate crystals continued to precipitate within the solution. The Deposens 3 sensor was unable to consistently maintain a stable baseline the beginning of the experiment. However, as more scaling crystals formed in the solution, deposit thickness increased continuously indicating that the crystals were also heterogeneously influenced.

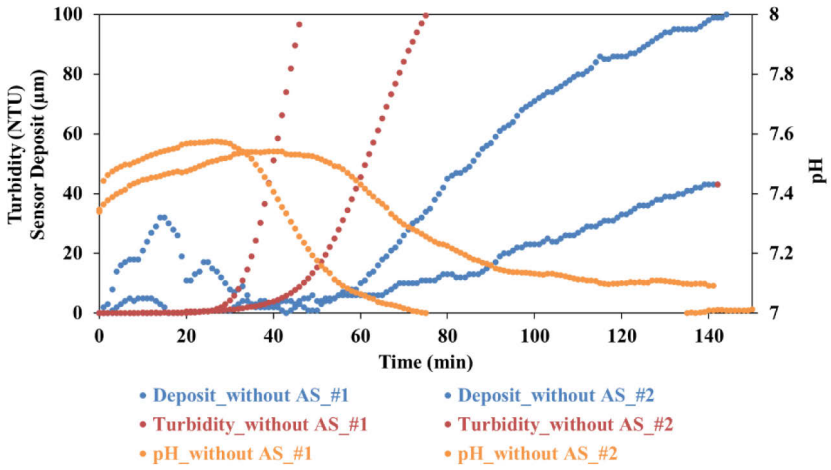

Figure 39: Behaviour of turbidity, pH and thickness of deposit on sensor in stirred-beaker setup with 33 mM $NaHCO_3$ and $CaCl_2$ ($SI_{calcite} \approx 2.06$) without antiscalants, integrated with Deposens 3 sensor (T = 11 ºC)

Contrary to expectations, the detection of heterogeneous scaling in the sensor was only accomplished after significant scaling the bulk solution had already taken place, which was given by increased turbidity values. Further experiments were carried out with calcite scaling solution and antiscalants PAA, PAA+DTPMP and DTPMP given in Figure 40.

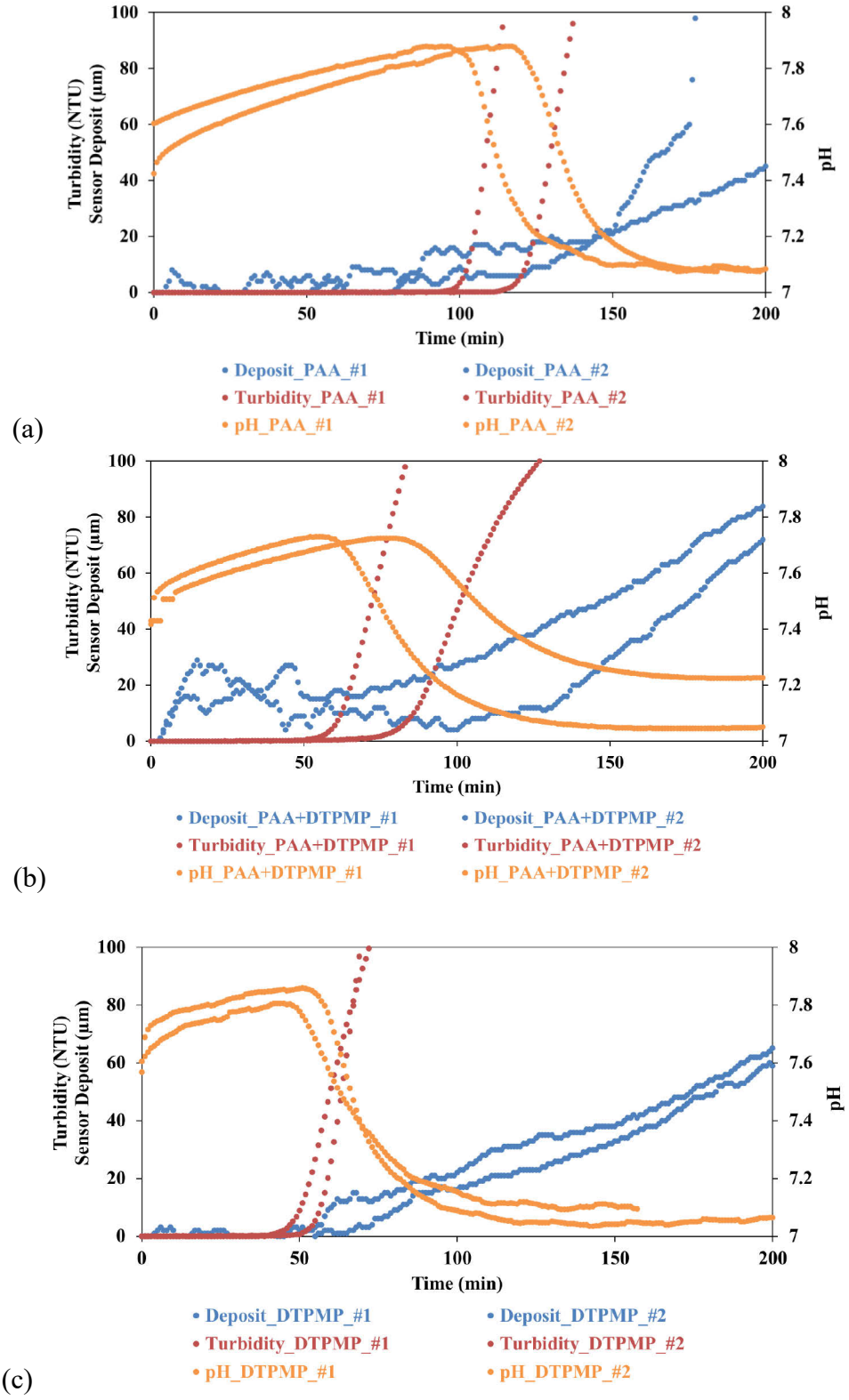

Figure 40: Behaviour of turbidity, pH and thickness of deposit on sensor in stirred-beaker setup integrated with Deposens 3 sensor (T = 11 ºC) using 33 mM $NaHCO_3$ and $CaCl_2$ ($SI_{calcite} \approx 2.06$) with (a) 1.84 mg·$L^{-1}$ of PAA (b) 1.54 mg·$L^{-1}$of PAA+DTPMP and (c) 1.51 mg·L^{-1} of DTPMP antiscalant

As seen in Figure 40(a), at 1.84 mg·L^{-1} of PAA dosage, the turbidity of solution remained stable for upto approximately 100 min, after which nucleation was triggered followed by continuous calcite crystal growth. Concordant decrease in pH was subsequently observed in the beaker solution. In this case too, inconsistent 0 baseline for the sensor was not obtained and a vague continuous increase in deposit thickness value was recorded through the experiment but reached a maximum of less than 20 µm. Similar observations were made for PAA+DTPMP antiscalant dosed at 1.54 mg·L^{-1}, although the baselines for both trials with this antiscalants resulted in similar non-uniform deposit thickness in the sensor from the beginning and the thickness curves reached upto 40 µm (Figure 40(b)). Experiments with DTPMP antiscalants at 1.51 mg·L^{-1} concentration resulted in most reproducible behaviour for the deposit thickness in the sensor with turbidity and pH values. As seen in Figure 40(c), turbidity in bulk solution is stable up to 40-50 min, following which it starts to increase, accompanied by continuous drop in pH and concordant increase in thickness of scale deposit within the sensor.

After several experiments, it was observed that although the Deposens 3 is able to detect scaling in the form of thickness of the salt deposit on the sensor, a continuous increase in the deposit was only detectable after the induction time (based on the increase in turbidity by 1 NTU) or after first observed decrease in pH of the bulk solution. Inconsistent baseline data for the sensor made it inconclusive to hypothesize if the sensor was able to detect heterogeneous scaling before onset of homogeneous scaling measured by turbidity value. While the nature of the beaker setup and recirculation pump may have played a part in non-uniform detection of scaling within the sensor, it nonetheless offers potential to be optimized further for more precise heterogeneous scaling crystal detection. The Deposens 3 may even be a prospective successful scaling detection method, and thereby ascertain effectiveness of antiscalants within membrane filtration plants which have a more uniform flow rate and rate of scale formation.

4.5 Overview of antiscalant effectiveness to inhibit CaSO4 and CaCO3 scaling

In this study, the effectiveness of different commercial antiscalants based on different phosphonates, namely DTPMP, PBTC and ATMP and P-free antiscalants comprised of PAA and later a CMI antiscalant were studied. While the previous section already established that different methods exist in the laboratory-scale to investigate antiscalant effectiveness that differ in their extent of application depending on the scaling salt, ease of implementation and preciseness of evaluation, insights into specific characteristics of different antiscalants were also obtained. The stirred-beaker experiments were a quick pre-determination method to compare different antiscalant products at different dosages, while the crossflow membrane filtration experiments along with SEM characterization were able to confirm and elucidate nature of inhibition mechanism by different ingredients. According to the results presented in Section 4.2 and Section 4.3, P-free antiscalant PAA was able to most successfully inhibit gypsum scaling via good threshold inhibition mechanism even at low antiscalant dosage of about 0.5 mg TS/L, whereas the same antiscalant was not so effective at preventing nucleation of calcite scaling crystals even if the dosing concentration was doubled. Membrane pilot plant

experiments showed that same antiscalant predominantly works on the principle of dispersion to inhibit calcite scaling on the membrane surface. Detailed discussion of PAA and CMI antiscalants is given below in Section 4.6.1.

Experimental investigation of phosphonate antiscalants showed varied behavior during scale inhibition depending type of phosphonate active ingredient. Phosphonates PBTC and ATMP showed exceptionally good threshold inhibition of calcite crystals even at low antiscalant dosages, compared to DTPMP and PAA+DTPMP product. However, gypsum scaling could only be controlled by ATMP when dosed at 1 mg TS/L, whereas PBTC product was rendered not suitable for gypsum scale inhibition. Other phosphonate products like DTPMP and mixed product of PAA+DTPMP were able to successfully inhibit gypsum scaling via threshold mechanism when dosed at sufficiently high dosage > 0.5 mg TS/L. In contrast, in the presence of calcite solution, PAA+DTPMP showed excellent dispersion property while DTPMP did not stand out in its carbonate scale inhibition. Lee et al. 2020 evaluated phosphonates and PAA as calcite scale inhibitors and found that phosphonate antiscalant with higher PBTC ingredient were superior in calcite inhibition compared to PAA, which fits with the results obtained in this study.

Besides the active ingredients of the antiscalants and the nature of the scaling salt, experimental results demonstrate how effectiveness of the antiscalant influences scaling inhibition potential. While certain phosphonates may work reasonably well even at low dosages against calcite scaling, better inhibition performance for gypsum inhibition is obtained by increasing the dosage. While there exists a regulatory requirement on the maximum allowed dosage of antiscalants in feed which is based on the total solids content as discussed in Section 2.5, there is usually no clear approach to choose the right antiscalant and dosage. Some antiscalant manufacturers offer softwares that are either free or partially or fully licensed which are used to aid in choice of antiscalants and their recommended dosage (Annex I-3). Most of these dosage recommendations are largely dependent on type of water matrix and the resulting saturation index. In some cases, special requirements such as changing raw water quality or shift to P-free ingredients may involve customized recommendation for antiscalant application in drinking water treatment. While these measures certainly aid the water suppliers to operate their plants without problems, elaborate research into wide variety of ingredients and their varied inhibition behavior are crucial for waterworks to cope with any short-term changes in raw water quality or sudden changes in the market with product availability. Additionally, environmental constraints such as eutrophication of receiving water bodies with phosphonates and regulatory requirements on antiscalant application serve as a pivot to understand antiscalant application and dosage in greater detail.

4.6 Investigation of commercial P-free antiscalants

The development of low-phosphorus or phosphorus-free scale inhibitors has become a major issue to reduce phosphorus emissions from the use of antiscalants. Increasingly strict regulations from the concerned authorities have additionally triggered growing interest towards the application of phosphorous-free antiscalants such as synthetic polymeric inhibitors and novel "green" antiscalants from plant-based sources. Typical synthetic P-free antiscalants are comprised of polycarboxylic groups synthesized through polymerization of monomers that have scale inhibition properties. Sometimes, the monomers could also be fortified with other functional groups for stronger antiscaling effect (Yu et al. 2020). More recently, use of antiscalants that are P-free and biodegradable has also gathered significant interest, by both water utilities and regulatory bodies (KonTriSol 2023, Royo et al. 2023, Warne et al. 2014).
PAA-based antiscalants are increasingly being recommended as a good alternative to the P-based products. However, due to proprietary reasons and the challenges of low concentration polymer analysis, there is still limited information on the different components of these products, their effectiveness and consequences.
Previous chapters have comprehensively evaluated PAA-based antiscalants and phosphonate products approved for drinking water treatment in Germany and from similar manufacturers regarding their scale inhibition performance. Therefore, PAA is not re-investigated as a novel antiscalant in this chapter but is used as an established reference material for comparison with a potential alternative. The following chapter focuses on assessing a plant-derived CMI-based antiscalant by directly comparing its scale inhibition efficiency and bioavailability with those of the commercial PAA-based antiscalant. Furthermore, the molecular weight fractions of PAA are examined specifically to understand their contribution to biological growth potential and to evaluate the implications of P-free antiscalants for drinking water treatment.

4.6.1 Comparison of commercial CMI and PAA antiscalant

Increasing environmental concerns have triggered a transition towards phosphorous-free antiscalants that are biodegradable or plant sourced and cost-effectiveness (Ganguly et al. 2024). While inhibitors like PASP and polyepoxysuccinic acid (PESA) have previously been suggested in the past as alternatives to P-based and non-biodegradable polymer antiscalants, the last decade has seen considerable research in the direction of natural polymers (Yu et al. 2020). Starch, cellulose, lignin, inulin, tannin, and collagen are considered to have good chelation and dispersion properties and are also considered sources of potential environment-friendly antiscalants due to their advantages of abundant source, low cost, and biodegradability (Boels and Witkamp 2011, Guo et al. 2021, Yu et al. 2020, Zhang et al. 2016b).

Chemical modifications of natural derived ingredients are reported to have scale inhibition property. Li et al. 2019 showed that soluble extracellular polymeric substances (s-EPS) comprising proteins, polysaccharides and humic-like substances extracted from Bacillus cereus (B. cereus), demonstrated good anti-scale and anti-corrosion performance due to good chelating, adsorption, and biomineralization abilities. It was reported that this natural ingredient

has advantages of biodegradability, strong biosorption affinity, and multiple fixation sites, thereby offering a green, sustainable, and economic strategy for developing environment-friendly antiscalants. More recently, carboxymethyl inulin (CMI) has gained a lot of popularity as an environmentally friendly "green" antiscalant. This inhibitor is produced from chemical reactions with plant-derived biopolymer, inulin, which is a polysaccharide consisting of many repeating fructose units in its molecule. It is extracted from the chicory plant roots which contains 14.9-18.3% inulin content and 20-25% dry matter content (Akın et al. 2008). According to Johannsen 2003 and Fiume et al. 2016, regulatory agencies like OECD, EEC and U.S. EPA reported that CMI is considered to be non-toxic as it contains the same level of impurities as other polysaccharides do in food sources. CMI consists of carboxymethyl groups which are introduced into the polysaccharide through carboxymethylation with sodium monochloroacetate in alkaline conditions. The amount of carboxyl groups present in the CMI fructose unit is known as the degree of substitution and this degree determines the effectiveness of inhibition of CMI, with higher substitution resulting in higher inhibition (Hasson et al. 2011).

Similar to synthetic polymeric products, the molecular structures of antiscalants, including the contents, types and distribution of functional groups functional groups and long-chain morphologies are crucial to the antiscalant efficacy against a particular scalant. More crucially, plant-based or "green" antiscalants may potentially cause biofouling on the NF/RO membrane due to the biomaterials present, reducing membrane flux and leading to other subsequent problems (Matin et al. 2011).
This section aims to directly compare the effectiveness of two P-free antiscalants that are increasingly popular in Europe - a commercial "green" antiscalant based on CMI and a commercial PAA antiscalant.

4.6.1.1 Characterization of CMI and PAA antiscalant using TOC and LC-OCD

The TOC of the commercial CMI and PAA antiscalant was determined using the Shimadzu TOC-V CSM total organic carbon analyzer with triplicate samples for each antiscalant and five measurements per sample. The antiscalants were analyzed at different concentrations from 1 to 15 $mg \cdot L^{-1}$ of the manufactured product. As the antiscalants were supplied in liquid phase, the total solids content of the commercial CMI antiscalant was measured to have about 33 % TS content and the commercial PAA antiscalant with about 30 % TS content.

As seen in Figure 41, both the P-free antiscalants showed linear correlation of increasing TOC content with increasing antiscalant concentration. Interestingly, at lower concentrations of antiscalant up to 2 $mg \cdot L^{-1}$, the CMI antiscalant shows slightly higher TOC content in comparison to PAA. Over 4 $mg \cdot L^{-1}$, both antiscalants show similar TOC with CMI being marginally higher over the entire range.

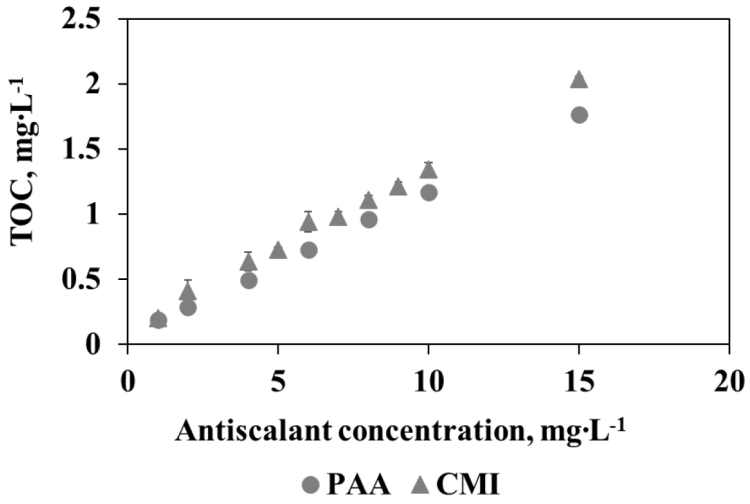

Figure 41: Total organic carbon (TOC) content of commercial PAA and CMI antiscalants at different concentrations

Following TOC characterization, the two antiscalants were characterized using LC-OCD at different concentrations up to 20 mg·L^{-1}. Figure 42 shows the OC-signals for the commercial CMI and PAA antiscalants from 1 to 20 mg·L^{-1}. Distinct TOC signals could not be reliably obtained for antiscalants < 0.3 mg·L^{-1} C and therefore not considered during data interpretation. Over 1 mg·L^{-1} antiscalant concentration, increasing OC-signal intensities could be obtained for both products with linearly increasing concentrations. Figure 42(a) shows that the CMI antiscalant displayed a distinct peak at about 34 min which remained consistent at all dosages, indicating that this was the primary OC-signal corresponding to the CMI active ingredient in the antiscalant. Increasing concentrations resulted in higher peaks, as expected. However, an additional small signal at about 47 min was detected for all concentrations, which could be attributed to impurities or unknown ingredients within the solution. Figure 42(b) shows the OC-signal for the commercial PAA antiscalant. Similar to the CMI antiscalant, the PAA product showed linear increase in OC-signal intensity with higher concentrations of the antiscalant. In case of PAA, distinct peaks corresponding to the PAA active ingredient were recognisable at higher retention times of about 43 min compared to the CMI product. Surprisingly, a second linearly increasingly OC-signal could be detected at about 58 min at all concentrations. Since the second signal was significant and appearing in all antiscalant concentrations from 1 to 20 mg·L^{-1}, it could be interpreted as an additional ingredient or a by-product of the polymerization process of the antiscalant during manufacture. Deeper investigations on the commercial PAA antiscalant are discussed under Section 4.6.2.

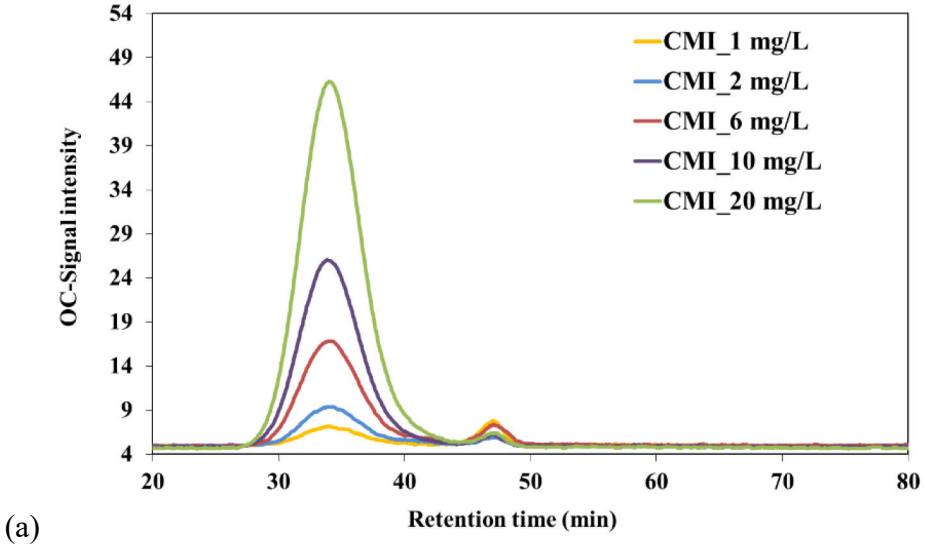

(a)

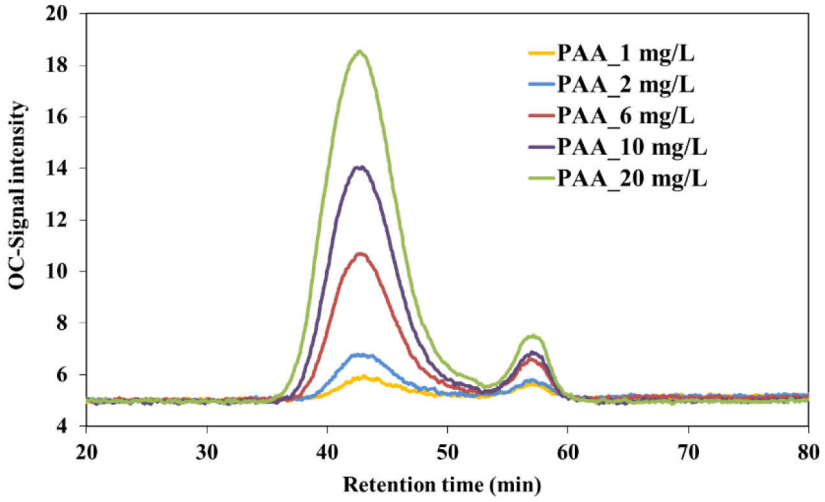

(b)

Figure 42: Liquid (size exclusion) chromatography – organic carbon detection (LC-OCD) chromatograms for (a) CMI antiscalants and (b) PAA antiscalants at different concentrations

The results above imply that antiscalants may be detected by organic substance characterization techniques when available in sufficient concentration. While TOC and LC-OCD are not always the ideal method for characterization of antiscalants in real water due to overlaps and indistinction from typical organic components occurring in the water matrix, it is evident that both these methods are useful to gain some background information on these commercial products protected by proprietary rights. In some cases, it also raises additional questions on the properties of the antiscalants.

Following this characterization, the commercial CMI and PAA antiscalants were directly compared for their scale inhibition effectiveness using the stirred-beaker and crossflow pilot plant tests, which are discussed in detail in the following two sections.

4.6.1.2 Effectiveness of CMI vs. PAA against CaSO4 scaling

This section dives into comparing the effectiveness of the commercial CMI and PAA antiscalant at different dosages based on TS using the already established stirred-beaker test and cross-flow filtration pilot plant test methods. Since the drinking water ordinance in Germany currently prescribes a feed dosage limit of 2.5 mg·L^{-1} based on dry substance and the increasing criticism of P-based antiscalant occurrence in brine, it was decided to compare the effectiveness of commercial CMI and PAA antiscalant at dosages of 0.5 mg·L^{-1} TS, 1 mg·L^{-1} TS and 2 mg·L^{-1} TS. Based on measurement results reported in previous section, this corresponded to the liquid product concentration range of about 1.5 mg·L^{-1} to 7 mg·L^{-1} and TOC range of 0.2 mg·L^{-1} to 1 mg·L^{-1} TOC.

Figure 43 compares CMI and PAA effectiveness against gypsum scale inhibition at different dosages using the stirred-beaker test. The induction time based on time taken for turbidity increase of 1 NTU was determined for both products in 68 mM Na_2SO_4 and $CaCl_2$ ($SI_{gypsum} \approx 0.72$) solution. Absence of an antiscalant leads to an induction time of only 10 min. Addition of antiscalant leads to longer induction time for both CMI and PAA, with the CMI resulting in higher induction times than PAA at all dosages. At 0.5 mg·L^{-1} TS, PAA has an induction time of 61 min, while CMI has an induction time of about 106 min. Similarly, at 1 mg·L^{-1} TS, PAA has induction time of about 115 min while CMI has slightly longer induction time of 141 min. When the dosage is increased to 2 mg·L^{-1} TS, the induction time of both CMI and PAA are significantly increased to above 400 min and 300 min, respectively. This indicates that both the P-free antiscalants have good scale inhibition potential towards gypsum precipitation, with higher dosages resulting in better threshold inhibition of the scaling salt.

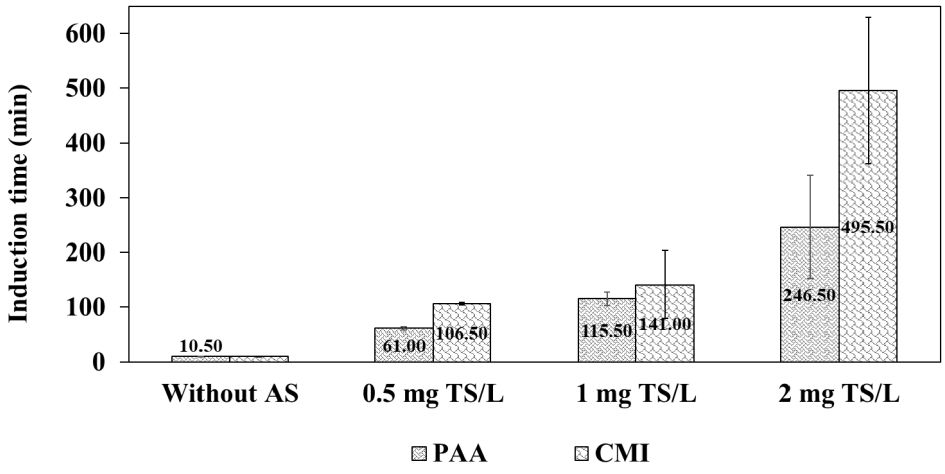

Figure 43: Induction time (based on 1 NTU turbidity increase) using the stirred beaker test with 68 mM Na2SO4 and CaCl2 and different concentrations of CMI and PAA antiscalants (T=11 °C, $SI_{CaSO4} \approx 0.72$, n=2)

The effectiveness of given P-free antiscalants were then verified for their scale inhibition potential against gypsum in the crossflow filtration pilot plant described in the Section 3.2.2. Slightly supersaturated gypsum solution ($SI_{gypsum} \approx 0.2$) with lower concentrations than the

batch test was chosen to enable steady precipitation of the scaling salts on the membrane and uniform detection via flux change in reasonable time interval. Gypsum feed containing the antiscalant was filtered through the lab-scale pilot plant at constant TMP of 25 bar, temperature 11 °C and with complete retentate and permeate circulation and monitored for the rate of change of flux over 10 h. (Figure 44).

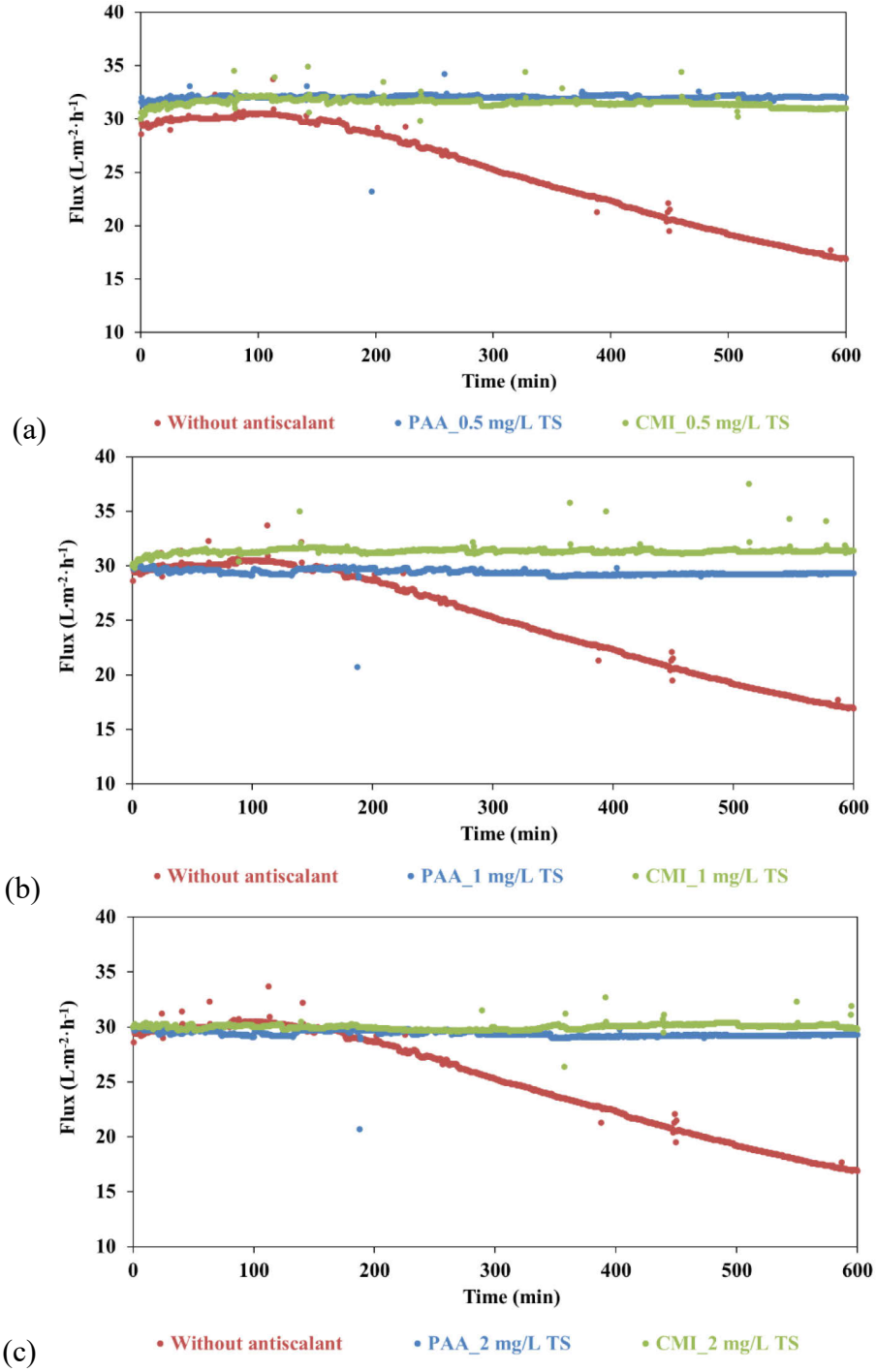

Figure 44: Comparison of flux behaviour in crossflow filtration setup using flat sheet RO membrane operated with 25 mM Na_2SO_4 and $CaCl_2$ ($SI_{gypsum} \approx 0.2$) feed in complete recirculation mode (crossflow velocity 0.1 $m \cdot s^{-1}$, TMP=25 bar, T=11 °C) using (a) 0.5 $mg \cdot L^{-1}$ TS, (b) 1 $mg \cdot L^{-1}$ TS and (c) 2 $mg \cdot L^{-1}$ TS CMI and PAA antiscalant

As seen in Figure 44(a), (b) and (c), while the blank sulfate solution with no antiscalant shows drastic flux decrease within 10 h, both PAA and CMI are able to maintain stable fluxes in the pilot plant over the entire time period at all three dosages of 0.5 mg·L^{-1} TS, 1 mg·L^{-1} TS and 2 mg·L^{-1} TS. This corroborates well with stirred-beaker results that both P-free antiscalants have sufficiently good inhibition against gypsum precipitation.

Though it is expected that both CMI and PAA have higher inhibition with increasing antiscalant dosage, the flux behaviour in the pilot plant experiment did not differ considerably from each other different dosages, since they remained almost constant even at the lower dosage of 0.5 mg·L^{-1} TS. The membranes were visually characterized using SEM after the crossflow filtration experiment, as shown in Figure 45.

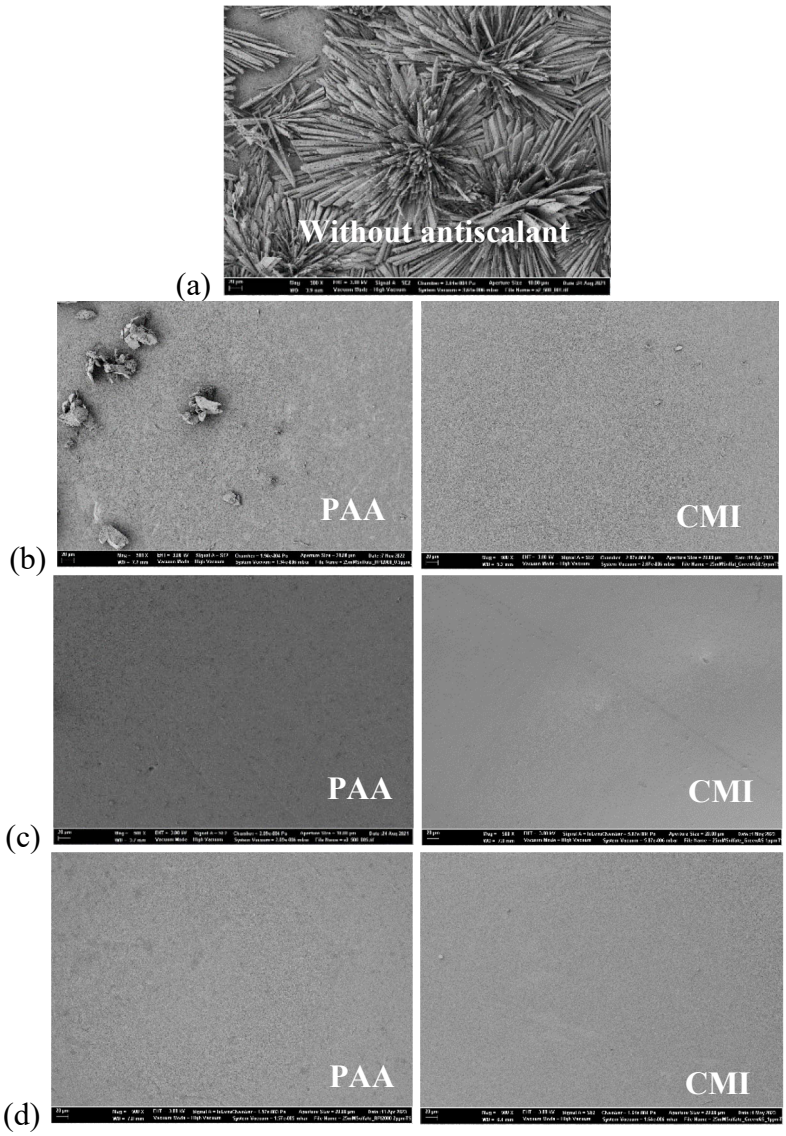

Figure 45: SEM pictures (Mag = 500 X, 20 µm) of RO membrane surface after crossflow filtration using 25 mM Na_2SO_4 and $CaCl_2$ (a) without antiscalant and with (b) 0.5 mg·L^{-1} TS (c) 1 mg·L^{-1} TS and (d) 2 mg·L^{-1} TS of CMI and PAA antiscalant

The membrane operated with no antiscalant had several gypsum rosettes on its surface, while addition of 0.5 mg·L^{-1} TS of PAA and CMI led to significantly fewer crystals in case of the former and negligible crystals in case of the latter antiscalant. This confirms that both P-free antiscalants have very good threshold inhibition effect against gypsum precipitation, with CMI having a higher inhibition potential compared to PAA. This observation fits well with the induction time results obtained in the stirred-beaker test where CMI has longer induction time compared to PAA, indicating that it has excellent ability to prevent nucleation of sulfate salts. Increasing CMI and PAA antiscalant dosage to 1 mg·L^{-1} TS and 2 mg·L^{-1} TS leads to smooth membrane surface or complete lack of gypsum crystals in both cases, corroborating with the long induction time results from the stirred-beaker test and nearly 100 % flux stabilization over 10 h in the crossflow pilot plant

4.6.1.3 Effectiveness of CMI vs. PAA against CaCO3 scaling

After establishing sufficiently good gypsum scale inhibition potential of PAA and CMI, the antiscalants were tested for their effectiveness against calcite inhibition using the two established test methods, stirred-beaker test and crossflow pilot plant experiment.

Figure 46 directly compares the induction time results of different concentrations of PAA and CMI, based on turbidity increase of 1 NTU, obtained from the stirred-beaker test in a supersaturated carbonate solution ($SI_{calcite} \approx 2.06$).

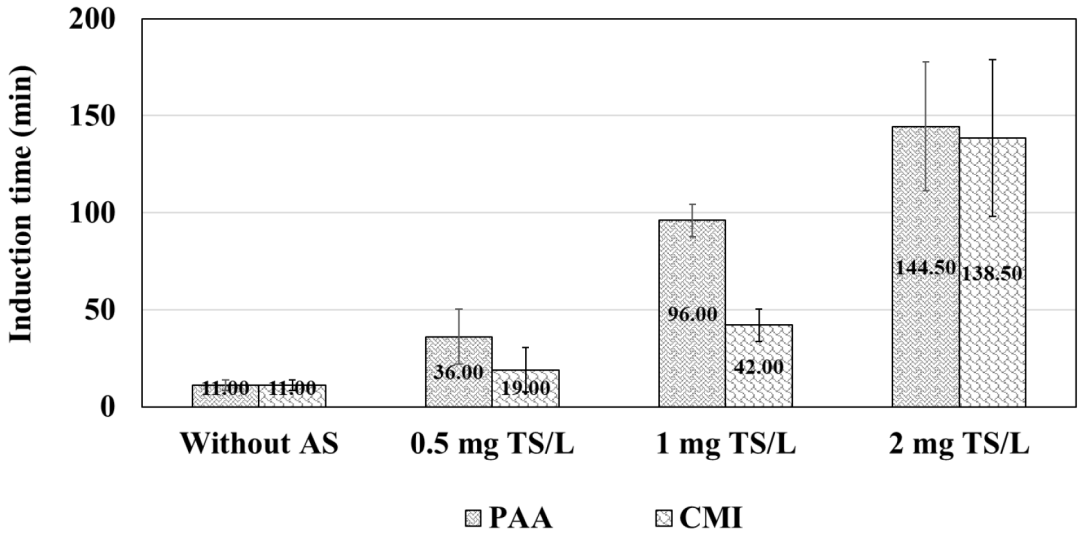

Figure 46: Induction time (based on 1 NTU turbidity increase) using the stirred beaker test with 33 mM $NaHCO_3$ and $CaCl_2$ and different concentrations of CMI and PAA antiscalants (T=11 °C, $SI_{CaCO3} \approx 2.06$, n=2)

Supersaturated carbonate solution without any antiscalant (blank) has an induction time of only 11 min. Addition of different amounts of the commercial P-free antiscalants increases the induction of the solution by different amounts. At lower dosages, PAA shows slightly higher induction time compared to CMI; for instance, at 0.5 mg·L^{-1} TS, PAA has an induction time of about 36 min while CMI shows 19 min and at 1 mg·L^{-1} TS, PAA has longer induction time of 96 min and CMI slightly longer at 42 min. High antiscalant dosage of 2 mg TS/L improves the induction time of both antiscalants to over 100 min indicating much better calcite inhibition at higher dosages for the given P-free products.

The effectiveness of PAA and CMI antiscalants was then verified in the lab-scale crossflow filtration RO pilot plant at constant TMP 25 bar and monitoring rate of change of flux by complete recirculation of saturated carbonate solution through the membrane, at constant temperature. Figure 47 shows the flux behaviour in the pilot plant with calcite scaling solution, where the blank carbonate solution without antiscalant has continuous flux decline from the beginning of the experiment and decreases by maximum of about 27 % in 10 h. In the presence of 0.5 mg·L^{-1} TS of CMI, the flux is slightly unstable but surprisingly does not decrease as rapidly as the blank as expected from the similar induction times in the stirred-beaker test. PAA demonstrated more rapid flux decrease in the beginning followed by an increase to the original value after about 400 min, indicating dispersion effect. While higher antiscalant concentration of 1 mg·L^{-1} TS did not significantly alter the flux behaviour of PAA, the increased dosage resulted in a much stable flux for CMI antiscalant over 10 h, which was also unexpected considering that CMI had a considerably lower induction time compared to PAA. At antiscalant concentration of 2 mg·L^{-1} TS, both P-free antiscalants were able to maintain stable permeate flux through the membrane, when compared to the absence of an antiscalant.

The scaled membranes were characterized using SEM after the pilot plant experiments for a better understanding into the antiscalant mechanisms. As seen in Figure 48, typical calcite crystals have a small, cuboid /rhomboid structure, which is altered in the presence of both P-free antiscalants. Interestingly, at 0.5 mg·L^{-1} TS, PAA shows several dense crystals on its surface which corresponds to the faster decline in flux in the pilot plant compared to CMI which also has deformed calcite crystals on its surface that are longer, smaller and thread-like clots. At 1 mg·L^{-1} TS, the number of calcite crystals in presence of PAA is reduced, leading to bigger crystals with flatter deformed shape and some sharp edges, though the flux behaviour remains unchanged. In contrast, CMI at the same dosage shows very few calcite crystals on the membrane surface that are small and flat, which corroborates with the stable flux observed with CMI in the pilot plant.

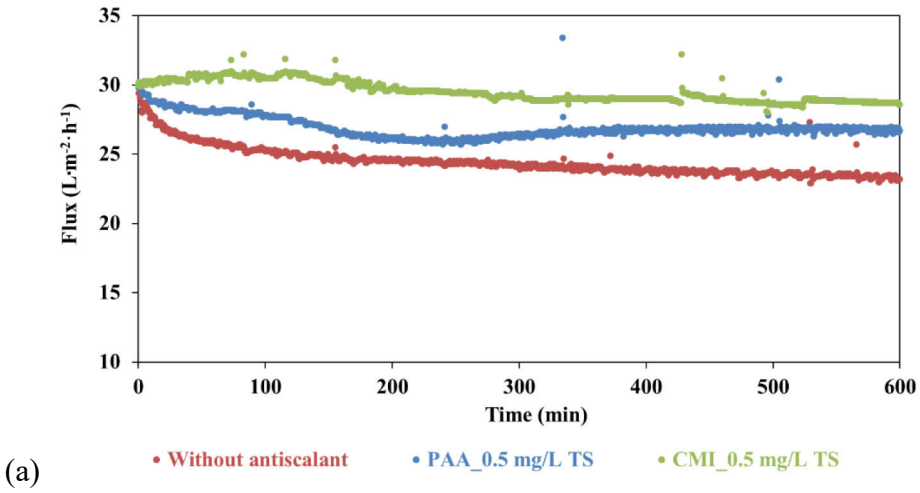

(a)

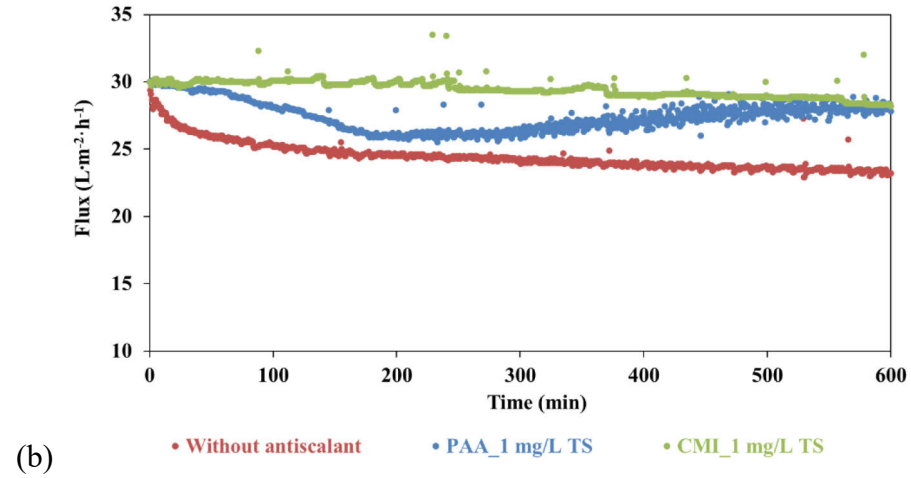

(b)

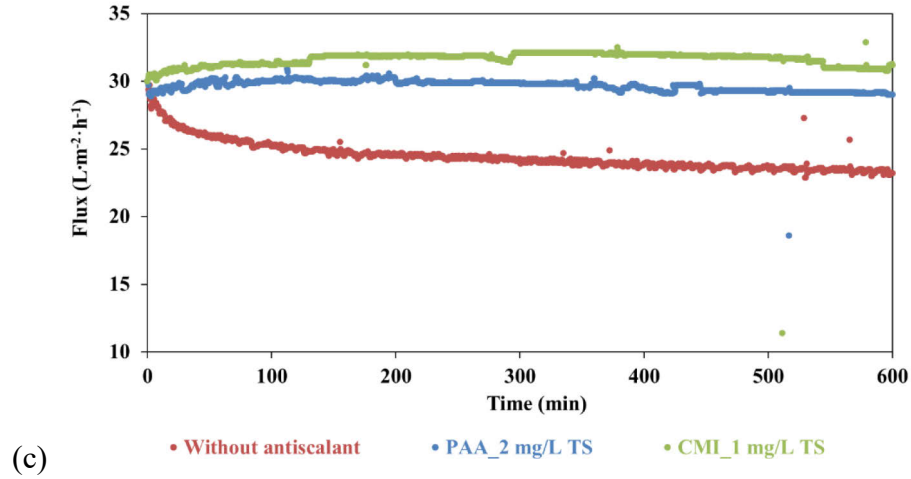

(c)

Figure 47: Comparison of flux behaviour in crossflow filtration setup using flat sheet RO membrane operated with 22 mM $NaHCO_3$ and $CaCl_2$ ($SI_{calcite} \approx 1.09$) feed in complete recirculation mode (crossflow velocity 0.1 ms^{-1}, TMP=25 bar, T=11 °C) using (a) 0. $mg \cdot L^{-1}$ TS, (b) 1 $mg \cdot L^{-1}$ TS and (c) 2 $mg \cdot L^{-1}$ TS CMI and PAA antiscalant

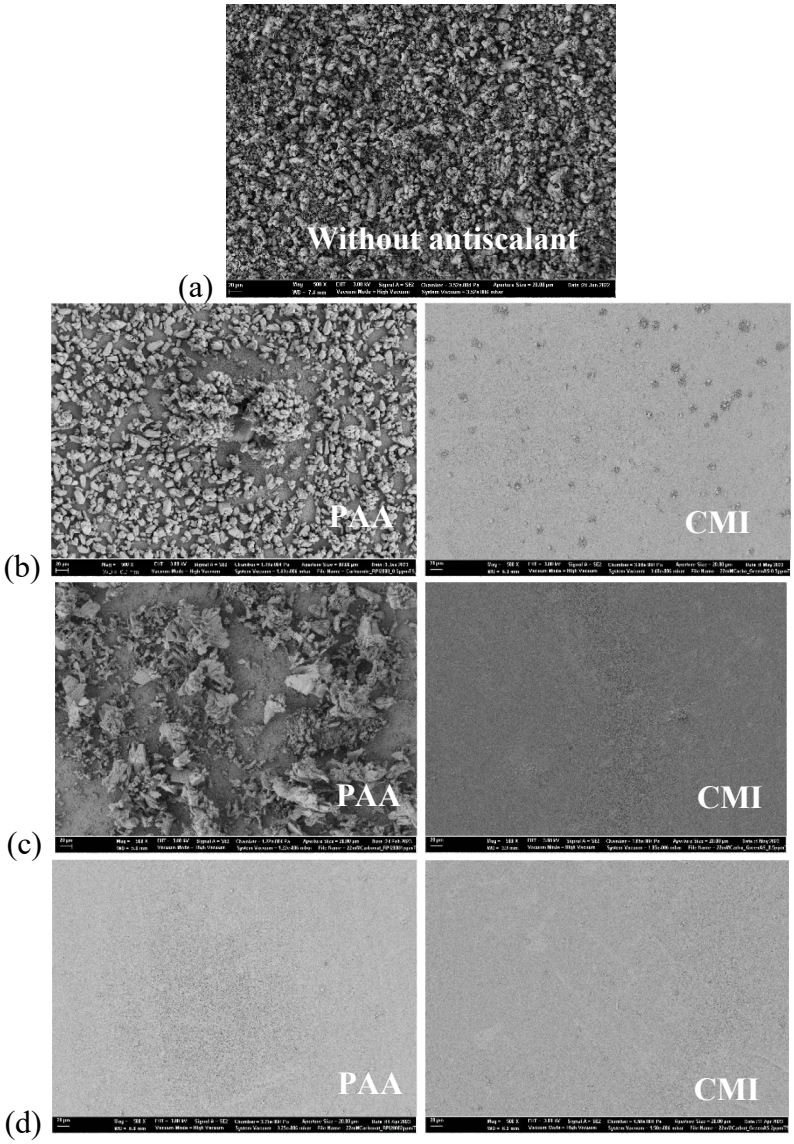

Figure 48: SEM pictures (Mag = 500 X, 20 µm) of RO membrane surface after crossflow filtration using 22 mM $NaHCO_3$ and $CaCl_2$ (a) without antiscalant and with (b) 0.5 mg·L^{-1} TS (c) 1 mg·L^{-1} TS and (d) 2 mg·L^{-1} TS of CMI and PAA antiscalant

While there is a general agreement with the flux behaviour observed for PAA and CMI in the pilot plant and their respective SEM characterized membranes, there seem to be inconsistencies between the antiscalant effectiveness against calcite scaling given by the stirred-beaker test and in the pilot plant for the P-free antiscalants at lower dosages, despite similar, constant temperature (11 ºC) and pH (7.5) conditions for both antiscalants. Although the stirred-beaker test suggests that PAA has better threshold inhibition ability compared to CMI up to 1 mg·L^{-1} TS concentration, based on flux stabilization and crystal morphology, it may be derived that PAA could possibly prevent calcite nucleation better but form crystals rapidly after nucleation (low crystallization time) and its main antiscaling property against carbonate salts is dispersion. Intriguingly, according to the stirred-beaker test, CMI is supposed to have low ability to prevent calcite nucleation due to low induction time in the stirred-beaker test. However, the pilot plant

experiments showed that CMI is able to maintain more stable flux than PAA over long periods of time and additionally do not show as many crystals on its surface, which seems contradictory to the stirred-beaker predictions. While clear reasons for low induction time for CMI could not be verified, some explanations could lie in the effect of scaling mechanisms. It is possible that at homogeneous scaling conditions prevalent due to high turbulence in the stirred beaker setup, CMI is unable to overcome the free energy barrier of calcite crystal and therefore not as successful in preventing its crystallization, whereas at low crossflow velocity conditions of the pilot plant, CMI is successfully able to interact with the calcite nuclei and prevent its precipitation by attaching onto its active sites and ultimately change its morphology and preventing growth of $CaCO_3$ crystals. Additionally, since CMI leads to several small, thin and wire-like calcite formations combined with oval geometric crystals, in contrast to more large rhomboid shapes caused by PAA, it may also be possible that the former leads to higher turbidity measurement compared to the latter. Such indiscrepancies highlight the importance of being cautious while exclusively using the stirred-beaker test for antiscalant selection, as they may not take into account all possible antiscalant mechanisms underway during membrane treatment application.

4.6.1.4 Bioavailability of CMI vs. PAA

Addition of antiscalants to the feed water during membrane filtration remains the most cost-effective and convenient method to control scaling during NF/RO filtration, especially at high water recoveries which is usually desired in drinking water treatment. While phosphonates continue to remain popular active ingredients used in antiscalants, P-free antiscalants like polymer based PAA and natural derivatives like chicory-based inulin referred to as “green” antiscalants is rapidly gaining attention as a promising alternative to conventional phosphorous-based antiscalants, offering the potential to mitigate the environmental impacts associated with phosphorus discharge into water bodies (Hasanin et al. 2023). Flemming 2020, Sweity et al. 2013 and Sweity et al. 2015 have previously warned about biofouling caused on the membrane during application of P-based and polymer-based P-free antiscalants. Besides polymer based antiscalants, emerging green antiscalants contain biodegradable derivatives, which causes a real concern about the biofouling potential of these products within the membrane system. With increasing interest from regulatory bodies to apply P-free antiscalants, biofouling potential is an additional crucial parameter during antiscalant selection. While unequivocal information on biofouling is most effectively derived by long-term monitoring of membrane filtration systems, this is often tedious and time-consuming to carry out.

This section aims to gain insights into the biological growth ability in the presence of commercial P-free antiscalants based on PAA and CMI. This was carried out by determining the total cell count (TCC) using a flow cytometer over a 28-day period. Since both the antiscalants contain slightly varying amounts of organic content, tap water solutions of PAA and CMI were prepared containing same amount of TOC concentration. Figure 49 compares the 28-day TCC behaviour of 0.5 $mg \cdot L^{-1}$ TOC of PAA and CMI prepared in Hamburg University of Technology tap water which provides the initial bacterial community.

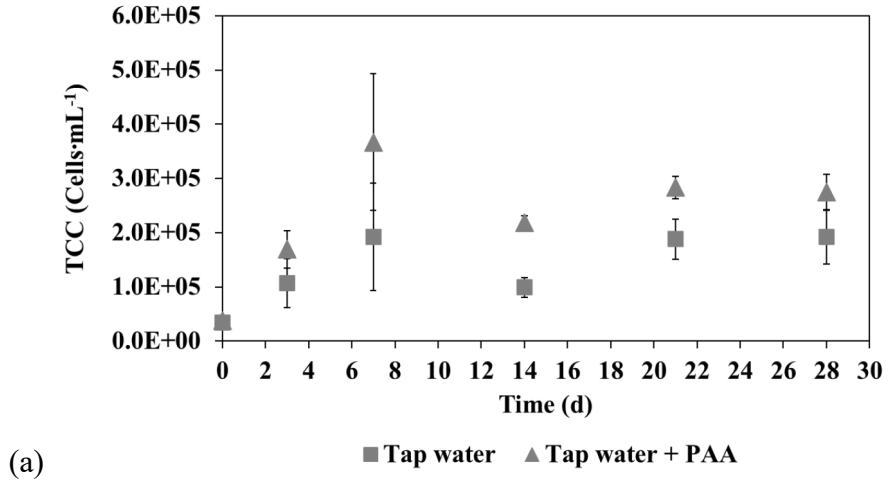

(a)

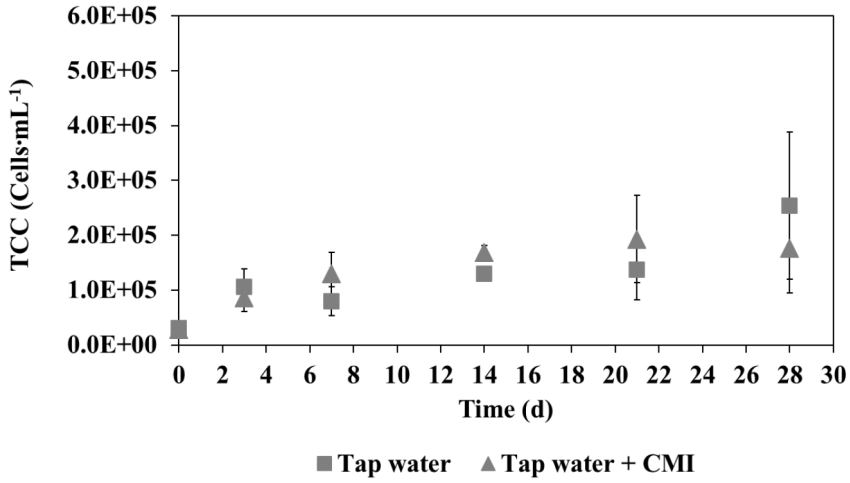

(b)

Figure 49: Total cell count (TCC) values of commercial (a) PAA antiscalant and (b) CMI antiscalant at 0.5 mg·L^{-1} TOC dosage measured in Hamburg tap water using flow cytometer

Since the two antiscalant samples were prepared on different days, the resulting TCC is compared with the tap water corresponding to that day. It evident from Figure 49(a) that CMI has a very similar bioavailability to that observed in tap water, suggesting that it does not pose immediate biofouling danger despite its biodegradable nature of carboxymethyl inulin. Since CMI is a relatively new antiscalant that is commercially available, there have been almost no reference yet to any evidence suggesting that it might cause biofouling. Surprisingly, the PAA based antiscalant showed slightly higher TCC compared to tap water at the same antiscalant concentration of 0.5 mg·L^{-1} TOC (Figure 49(b)). Although the increase is only marginally higher than that of tap water, a non-trivial spike in TCC is observed on day 7. Previously, PAA application has been reported to biofouling in several instances, but the cause of biofouling has been attributed to varied factors. For instance, Sweity et al. 2013 reported that commonly used polymer antiscalant based on acrylic acid caused higher probability of biofilm formation by making the polyamide membrane surface more hydrophobic.

The PAA and CMI antiscalants were also filtered through a NF270 (nanofiltration) membrane at 8 bars, at a dosage of 1 mg·L^{-1} TOC prepared in Hamburg tap water with a background TOC of approximately 0.5 mg·L^{-1}. For practical reasons and due to time constraints, each filtration cycle with the antiscalants was limited to 40 min at the end of which permeate samples were collected. Figure 50 shows the TCC behaviour of PAA and CMI antiscalant over 28-day period in correlation to the respective background tap water that they were prepared in.

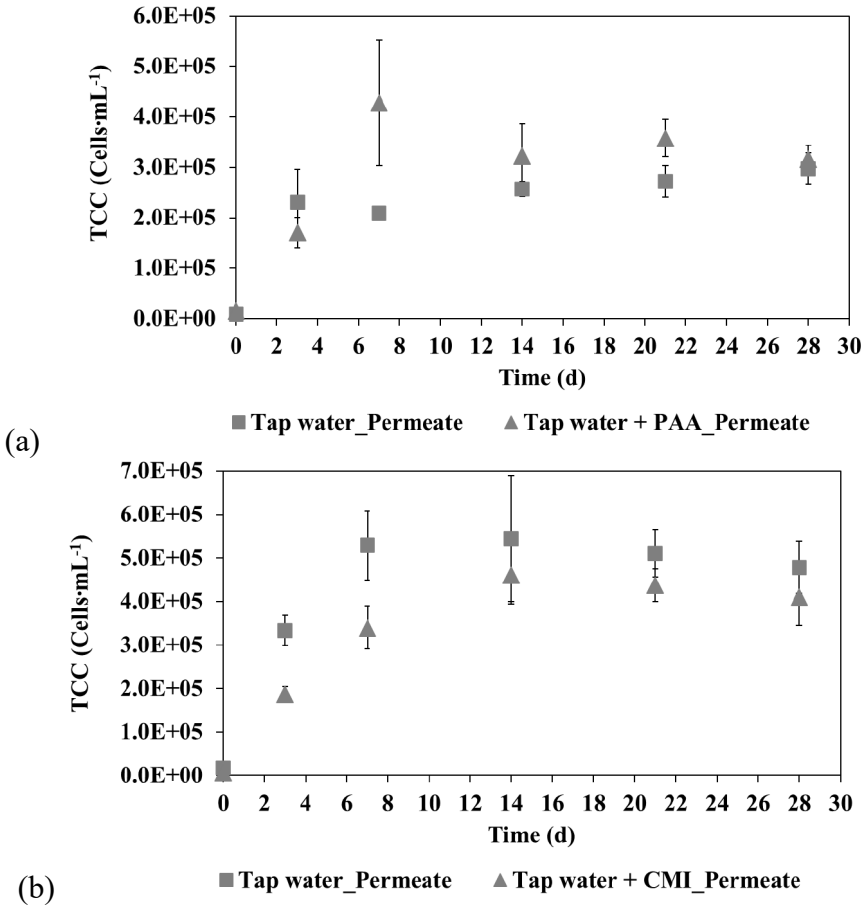

Figure 50: Total cell count (TCC) determined via flow cytometer over 28-days of permeate samples obtained by filtration of NF270 membranes with Hamburg tap water containing 1 mg·L^{-1} TOC of commercial (a) PAA antiscalant and (b) CMI antiscalant

Interestingly, commercial PAA antiscalant showed slightly enhanced TCC after 7 days when compared to tap water, whereas CMI antiscalant showed overall TCC behavior like tap water.

Although the CMI product is derived from plant-based derivatives, first results show that the permeates resulting from antiscalant application may be more biologically stable than PAA antiscalants. Longer filtration times and varying concentrations must be tested to confirm this behavior. The following sections present a more thorough investigation of the commercial PAA antiscalant and its MW fractions.

4.6.2 Insights into commercial PAA antiscalant and its fractions

Commercial PAA antiscalants contain varying molecular weights distributions based on the production process and/or the manufacturer, which remain unknown to users. This section delved into the characterization and scale inhibition effectiveness of a commonly used commercial PAA antiscalant and its molecular weight fractions ≤ and ≥ 500 Da that were derived by TZW, Karlsruhe. The experiments conducted and results generated were supported by analytical efforts from Dominic Armbruster from DVGW- TZW Karlsruhe, Germany.

Contents of this chapter have been published in collaboration with Armbruster D., Dittmer J., Bruniecka-Sulewski D., Wendler B., and Ernst M. (2024). Investigation of scaling inhibition and biofouling potential of different molecular weight fractions of a PAA antiscalant. npj Clean Water, 7(1), 36.

Characterization of the PAA antiscalant fractions via IC-ESI-QTOF

The PAA-based antiscalant and its subsequently derived low and high molecular weight fractions were analyzed via anion chromatography coupled to electrospray ionization and quadrupole-time-of-flight mass spectrometry (IC-ESI-QTOF) adapted according to the method given by Armbruster et al. 2024. Polyacrylates were identified as a series of homologous signals with retention times increasing in accordance to their molecular weight (MW) and confirmed by comparison with a commercial standard (Sigma-Aldrich, CAS 9003-04-7). The mass difference between consecutive homologue signals was 72.0211 Da, which correlates with the acrylic acid units ($C_3H_4O_2$). Molecules with chain lengths of one to ten acrylic acid units were considered for the characterization of the PAA antiscalant as well as the derived fractions. As polymer molecules of increasing chain length possess similar chemical and physical properties, a sharp separation was not achieved. In the resulting fractions, either the smallest or the largest of the observed polymer molecules were significantly reduced (by 97% and 82%, respectively) in comparison to the initial antiscalant (Figure 51). The PAA molecule #6 with a chain length of six acrylic acid units (m/z 509.1334) was present in both fractions at approximately equal proportions. Thus, the fractions were denominated as ≤ 500 Da (low MW fraction) and ≥ 500 Da (high MW fraction).

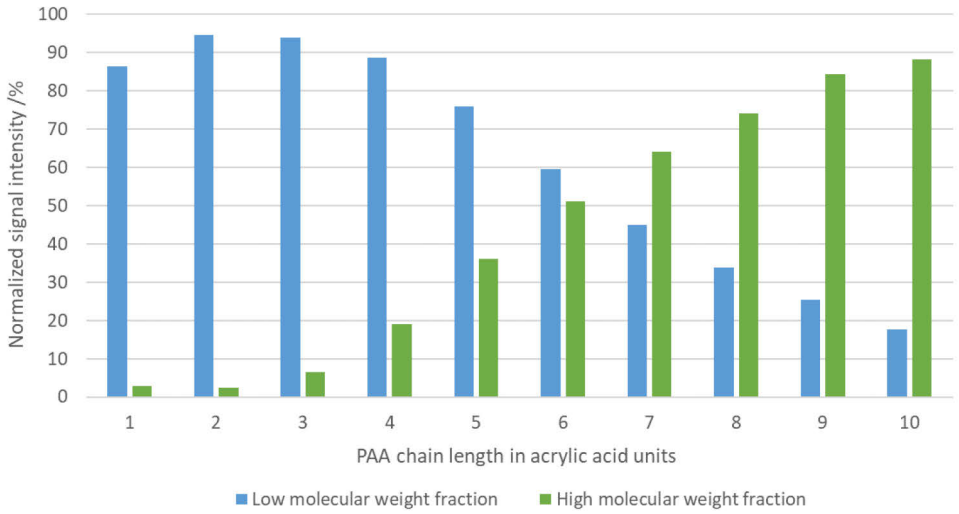

Figure 51: Composition of the low and high MW fractions according to PAA chain length expressed as the number of acrylic acid units within the molecule determined by DVGW-TZW. The signals determined in the fractions were related to the signal intensities of the native PAA antiscalant.

The PAA antiscalant its two molecular weight fractions were then sent to TUHH where they were subsequently characterized and tested further for their effectiveness, as part of this study.

4.6.2.1 Characterization of PAA fractions using TOC and LC-OCD

The TOC/DOC of the commercial PAA antiscalant and its fractions were determined using the Shimadzu TOC-V CSM total organic carbon analyzer. Triplicate samples were used for the analysis, with the device performing 5 measurements per sample. The commercial antiscalant is comprised of a mixture of PAA molecules with varying chain lengths, i.e. molecular weights, which were fractionated into two molecular weight fractions of $\leq$ 500 Da and $\geq$ 500 Da. However, the fractions still represent non-uniform mixtures of PAA molecules with their molecular weight distribution shifted to either the high or the low end of the initial distribution within the commercial product. While the low molecular fraction contains a large number of smaller molecules, the large molecular fraction contains a comparatively small number of larger molecules. The determination of the molar concentration of a polymeric mixture is nontrivial. Concurrently, the comparison according to substance concentration, e.g. via dry weight, would not reflect the molar constitution. In order to experimentally compare the three PAA solutions, standardization according to TOC measurements was performed. As the PAA molecules primarily consist of polyacrylic acid chains with repeating [-CH_2-CH(COOH)-]-units, the TOC may be regarded as a function of the carboxyl group concentration. Carboxyl groups are the primary functional groups of PAAs and contribute to the antiscaling properties. Thus, it was decided to evaluate the effectiveness of the antiscalant and the derived fractions based on the TOC. Different concentrations between 1 and 20 $mg \cdot L^{-1}$ of the commercial PAA antiscalant and its two molecular weight fractions were prepared using the 0.1% stock solution (for ex. 1

mL·L^{-1} for the former concentration and 20 mL·L^{-1} for the latter dosage). Molecular weights of the commercial PAA product and its two fractions were characterized by size-exclusion chromatography coupled to organic carbon detection (LC-OCD) and UV-detection (UVD; 254 nm) (DOC-Labor Dr. Huber). This setup was also used to identify qualitative changes in TOC within the samples. ChromeRES and ChromeCALC by DOC-Labor Dr. Huber were used for data analyses and correction measures.

Antiscalant characterization using TOC

The TOC/DOC of the commercial PAA antiscalant and its fractions between concentrations between 1 to 20 mg·L^{-1}, were determined using the Shimadzu TOC-V CSM total organic carbon analyzer. As seen in Figure 52(a), (b) and (c), the low molecular weight fraction is associated with a lower TOC concentration compared to the high MW fraction as well as the commercial PAA product.

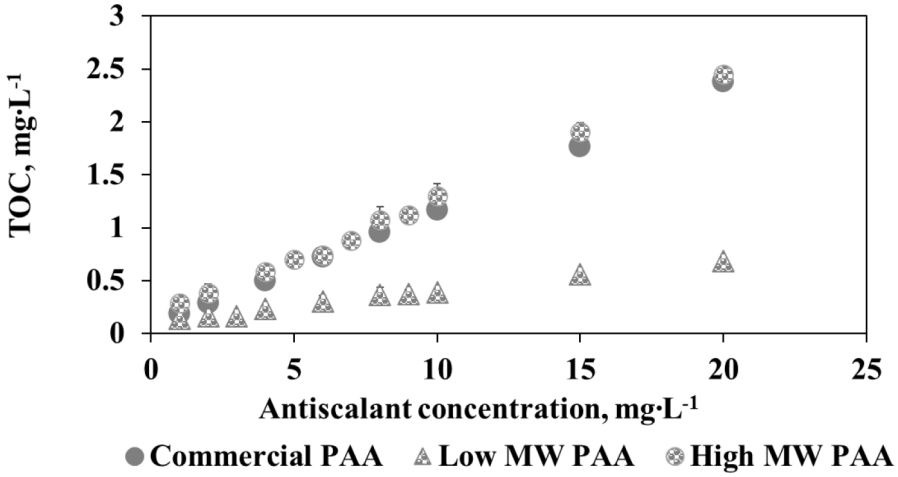

Figure 52: TOC linearization of (a) commercial PAA antiscalant, (b) low molecular weight PAA fraction and (c) high molecular weight PAA fraction between concentrations 1 to 20 mg·L^{-1}

The antiscalants as well as the fractions were compared at the same dosage based on TOC, to ensure comparable concentrations of carboxyl groups that are responsible for the scale inhibition effect.

Antiscalant characterization using LC-OCD

The antiscalant fractions were also characterized using the LC(SEC)-OCD. As seen in Figure 53, at a dosage of 0.5 mg·L^{-1} TOC, the commercial PAA antiscalant shows two distinct peaks between 30-40 min and between 45-50 min. At the same TOC concentration, the high MW PAA shows a vertex between 30-40 min, coinciding with the commercial product and thereby indicating that this range corresponds to the large MW of the commercial PAA. The low MW PAA shows an apex that is slightly shifted to the right of the high MW fraction (35-40 min),

which probably correspond to the PAA molecules that are overlapping in the fractions and commercial PAA (which also tails slightly towards the right at 40 min). Based on the OC-signal intensities given in Figure 53 and TOC measurements from the previous section, it may be approximated that 27 % of the TOC of the commercial PAA corresponds to the low MW PAA, which indicates non-trivial amounts in the overall PAA product.

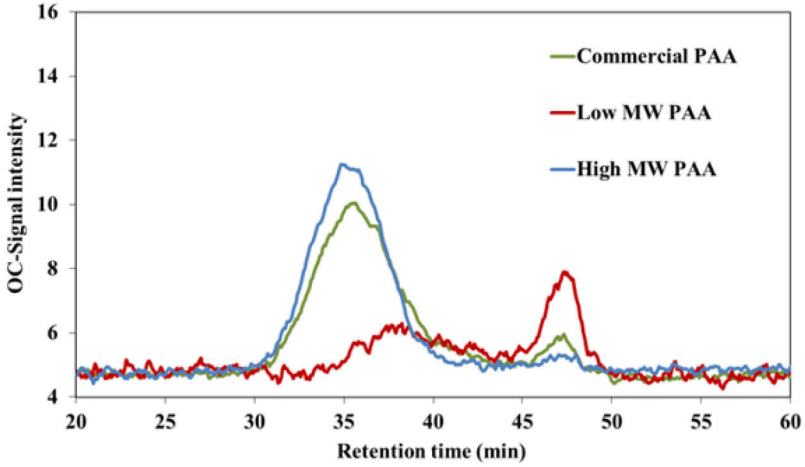

Figure 53: LC(SEC)-OCD characterization of commercial PAA, its low and high MW fraction normalized to similar TOC concentration of 0.5 mg·L^{-1}

Although it appears that the peak between 45 – 50 min in the commercial product could correspond to the low MW fraction, there is still the possibility that the antiscalants contain other small organic acids or residual monomers that have not yet been characterized by the analytical method but detected through the LC(SEC)-OCD. The retention time for the primary peak of the commercial PAA antiscalant differs from the 40-50 min measured in Figure 42(b), due to exchange of the LC-OCD columns for both measurements.

The effectiveness of the commercial PAA-based antiscalant and its molecular weight fractions were thereafter tested for their scale inhibition effectiveness based on the stirred-beaker test and in the lab-scale crossflow filtration pilot plant.

4.6.2.2 Effectiveness of PAA fractions in stirred-beaker test

To compare the performance of the commercial PAA antiscalant as well as the two fractions, an identical TOC concentration of 0.5 mg·L^{-1} each was dosed. The antiscalants were first evaluated for their inhibition potential against $CaSO_4$ and $CaCO_3$ scaling via the induction time using the batch stirred beaker test, with three experimental replicates. As seen in Figure 54, in the absence of an antiscalant, supersaturated sulfate and carbonate solutions have an induction time of only about 10 min. Adding 0.5 mg·L^{-1} TOC of the commercial PAA antiscalant caused a significant increase in the induction time for both salts (130 min to 155 min). Interestingly, the investigation of the fractions clearly showed that the low MW fraction (≤ 500 Da) led to a very low induction time for sulfate and carbonate scalants (35 min and 14 min, respectively).

In contrast, the high MW fraction led to high induction times for both scaling salts, comparable to the commercial PAA product.

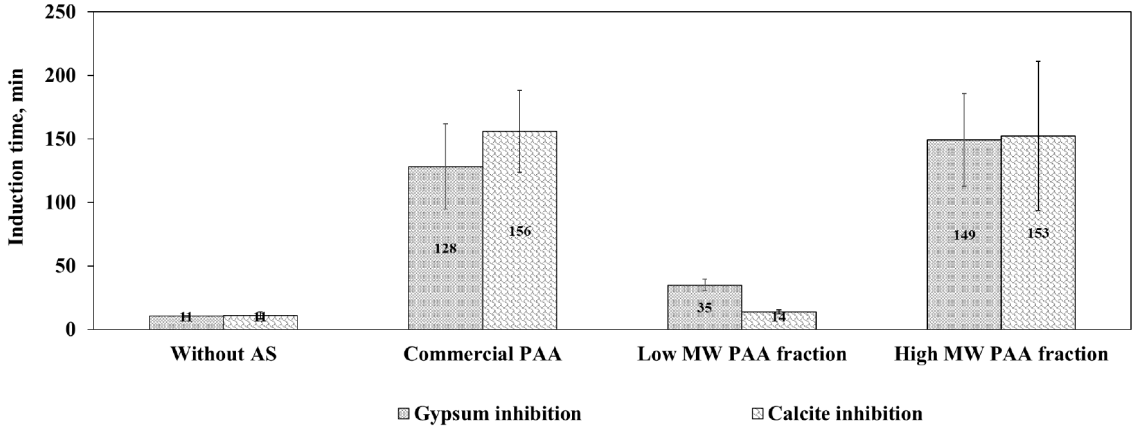

Figure 54: Induction time (1 NTU turbidity increase) using the stirred beaker test with 0.5 mg·L^{-1} TOC commercial PAA and its low and high MW fractions, against 68 mM sulfate solution and 33 mM carbonate solution (T=11 °C, SI_{CaSO4} = 0.72, SI_{CaCO3} = 2.06, n=3)

Since it can be expected that higher induction times correlate to a better performing antiscalant, these results imply that the performance of the commercial PAA is mainly controlled by the large MW fraction (≥ 500 Da). This information is largely in agreement to several earlier studies reporting effective scale inhibition performance by PAAs in the range of 2,000 Da to 7,000 Da and 100,000 Da against calcium sulfate and calcium carbonate, as summarized in Table 5.

Table 5: Comparison of different molecular weights of PAA antiscalants and their corresponding scale inhibition effectiveness according to cited studies and the present study

Parameter to evaluate antiscalant effectiveness	**Molecular weight of PAA reported**	**Effectiveness of respective PAA against $CaSO_4$ / $CaCO_3$ scaling**	**Study**
Induction time based on turbidity increase of 1 NTU	≤ 500 Da	Low / nil inhibition of both $CaSO_4$ and $CaCO_3$ scaling	Current study
	≥ 500 Da	High $CaSO_4$ and $CaCO_3$ inhibition	
Inhibition efficiency via residual Ca^{2+} concentration (EDTA titration)	2,500 Da – 7,000 Da	Effective $CaCO_3$ inhibition by PAA with MW 2,500 Da; no enhanced inhibition by PAA with higher MW	Shen et al. 2018
Induction time via slope of turbidity (0-100 %) vs. time (0-300 min) plots	2,000 Da	10 % turbidity increase in ~ 200 min against $CaSO_4$	Rabizadeh et al. 2019
	100,000 Da	10 % turbidity increase in ~ 50 min against $CaSO_4$	
Inhibition efficiency via residual Ca^{2+} concentration (EDTA titration)	6,043 Da	Good $CaCO_3$ inhibition reported for given PAA compared to other antiscalants	Zuo et al. 2020

The induction times derived from stirred-beaker tests at elevated concentrations of sparingly soluble salts are often associated with high standard deviations. Lab-scale RO pilot plant experiments were performed to cross-verify the outcomes of the inhibition performance.

4.6.2.3 Effectiveness of PAA fractions in crossflow filtration test

To verify the inhibition effectiveness observed during the batch setup, an identical antiscalant dosage of 0.5 mg·L^{-1} TOC was used. As seen in Figure 55, when tested at constant TMP of 25 bar against 25mM sulfate feed, application of the low MW PAA fraction led to a continuous decrease in flux. Almost 15% decline was recorded after 200 min, comparable to the blank experiment without any antiscalant, indicating low gypsum scale inhibition potential. After 200 min, the blank flux further decreased at a linear rate whereas the flux of the experiment with the low MW fraction decreased at an attenuated rate. In contrast, application of the commercial product as well as its high MW fraction was able to maintain a relatively constant and comparable flux throughout the experiment (500 min), thus confirming effective scale inhibition against gypsum. Comparable inhibition performance results were observed with 22mM carbonate solutions (Figure 56), with the low MW fraction showing poor calcite inhibition when compared to the high MW fraction and the commercial product.

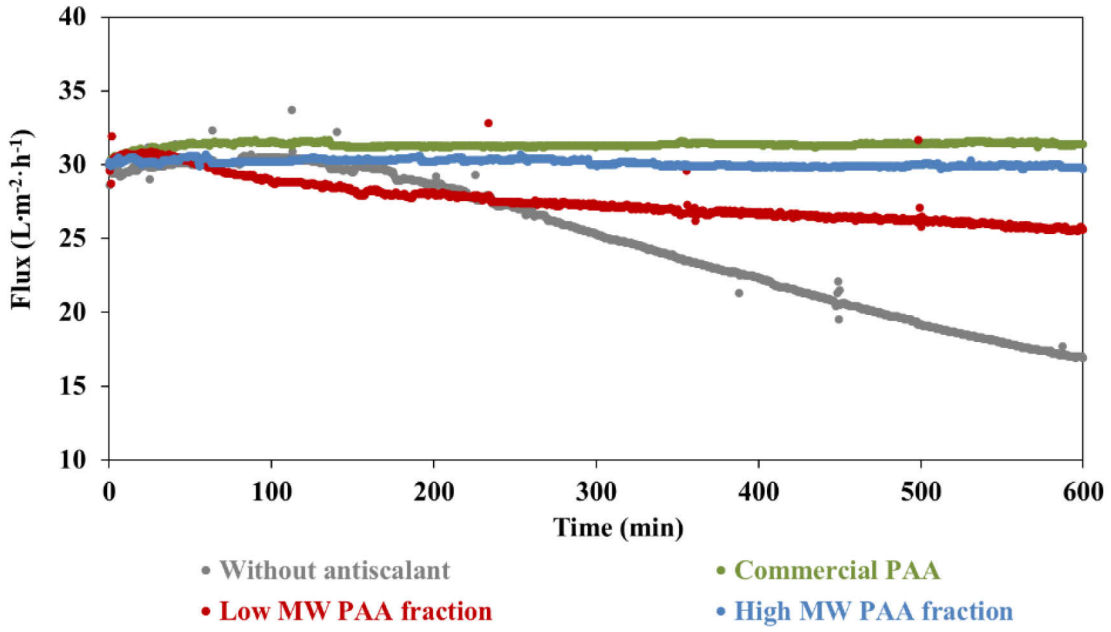

Figure 55: Flux behaviour in lab plant using flat sheet RO membrane operated with 25 mM Na_2SO_4 and $CaCl_2$ feed and commercial PAA and its low and high MW fractions (Antiscalant dosing as 0.5 mg·L^{-1} TOC in each experiment); TMP=25 bar, complete recirculation mode, T=11 °C, $SI_{gypsum} \approx 0.2$

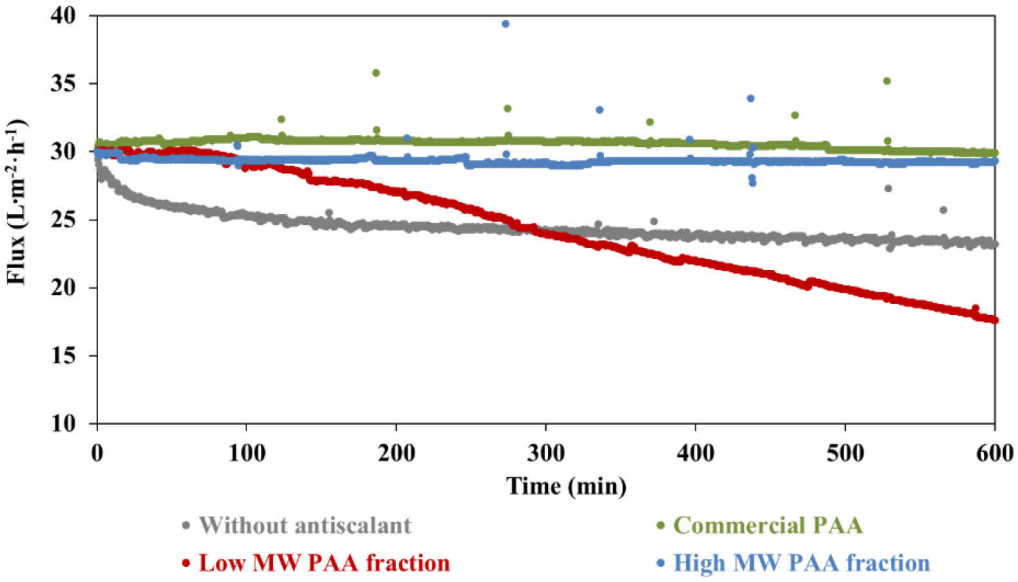

Figure 56: Flux behaviour in lab plant using flat sheet RO membrane operated with 22 mM $NaHCO_3$ and $CaCl_2$ feed and commercial PAA and its low and high MW fractions (Antiscalant dosing as 0.5 mg·L^{-1} TOC in each experiment); TMP=25 bar, complete recirculation mode, T=11 °C, $SI_{calcite} \approx 1.09$

Al-Hamzah et al. 2014 studied the calcium carbonate scale inhibition efficiency of PAAs with different average molar masses (determined using ^{1}H-NMR spectroscopy and Gel Permeation Chromatography), synthesized by Atomic Transfer Radical Polymerization (ATRP) and containing different end groups. They report that, at room temperature, PAA polymers with average molar masses between 1,000-3,000 Da, containing short (carboxymethyl-1,1-dimethyl-PAA & ethyl-isobutyrate-PAA) to moderately sized (cyclohexyl-isobutyrate-PAA & N-hexyl-isobutyrate-PAA) end groups, provide good inhibition against carbonate scaling. In comparison to that, dosing of larger PAA polymers (approx. > 9000 Da) failed in being effective against scale prevention. The molecular weight distributions of the commercial PAA as well as its large MW fraction (≥ 500 Da) have not yet been conclusively investigated. It is likely that the high molecular weight fraction of the commercial PAA (≥ 500 Da) used in this study lies in a similar range as the molecular weight range determined as suitable for effective scaling inhibition by. However, the low MW fraction investigated in the present study (≤ 500 Da) clearly falls below it. Additionally, the pilot plant tests using the crossflow cell confirmed the inhibition and performance results obtained from the batch stirred beaker test for both gypsum and calcium carbonate.

SEM characterization of the membranes

The membranes tested in the lab-scale plant were then characterized by SEM analysis to identify the crystal behaviour and formation of gypsum and carbonate salts. Similar to the scale inhibition trends observed in the pilot plant, it was seen that the membranes operated with the low MW fraction of the antiscalant showed several gypsum and calcite crystals on their surfaces (Figure 55 and Figure 56), similar to the membranes that were scaled without antiscalants, although of a slightly different size and morphology.

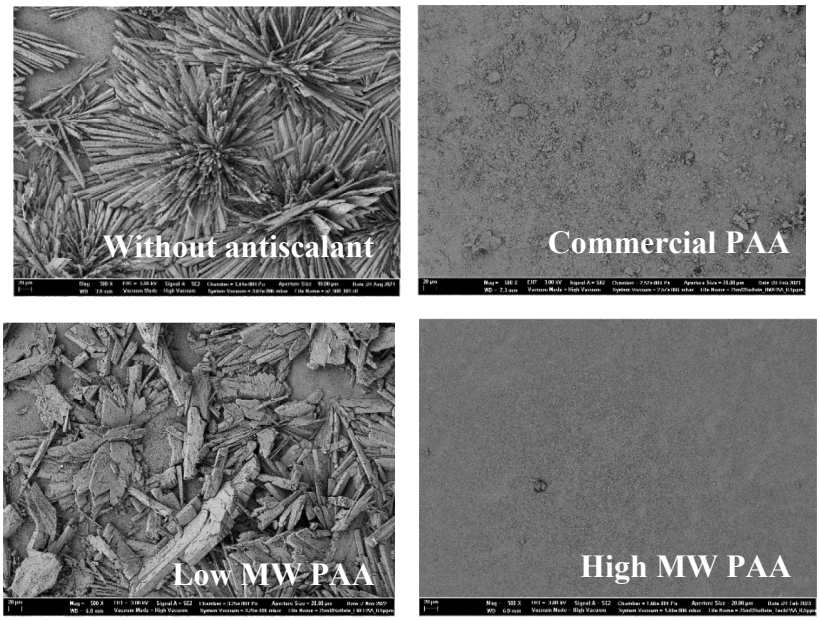

Figure 57: SEM pictures (Mag = 500 X, 20 µm) of RO membrane surface after operation with 25 mM Na_2SO_4 and $CaCl_2$ + 0.5 mg·L^{-1} TOC of PAA antiscalant and its low and high MW fractions

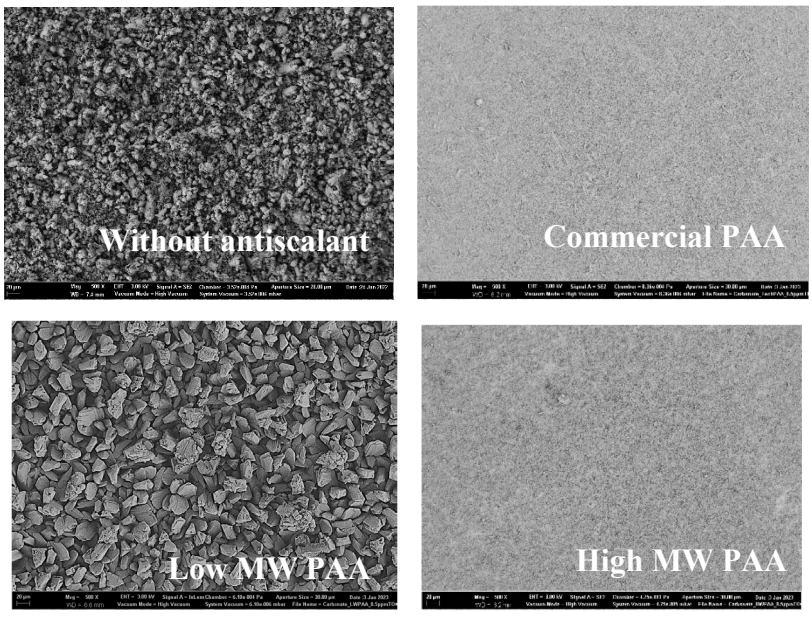

Figure 58: SEM pictures (Mag = 500 X, 20 µm) of RO membrane surface after operation with 22 mM $NaHCO_3$ and $CaCl_2$ + 0.5 mg·L^{-1} TOC of PAA antiscalant and its low and high MW fractions

Differences in the size and morphology of the crystals are believed to be responsible for the respective flux decline for the two scalants. Deformed gypsum crystals in the presence of low

MW PAA fraction leads to faster flux decline compared to blank in the beginning, but at an attenuated rate after 200 min (Figure 55). Blank calcite crystals being smaller and denser lead to faster initial flux decline, while the low MW PAA which forms larger calcite crystals, leads to slower flux decline in the beginning, but becomes more rapid after 300 min (Figure 56). As seen in Figure 57 and Figure 58, the membranes operated with the high MW fraction of the PAA were the cleanest of all experiments, closely followed by the membrane operated with the commercial PAA product, thus proving again that the lower MW fractions of the commercial PAA product have little to no contribution on the overall scale inhibition potential of the antiscalant.

4.6.2.4 Bioavailability of PAA antiscalant and its fractions

Biofouling in NF/RO systems is a relevant topic investigated in numerous studies (Chong et al. 2008; Sweity et al. 2013). The primary focus of the cited studies was on (i) biofouling caused by water constituents, (ii) the applied antiscalants, (iii) methods for detection and (iv) strategies to mitigate scaling. Sweity et al. 2013 revealed that biofouling within the RO system can also be initiated or promoted by antiscalants dosed during treatment, with a particular biofouling potential pointed out for PAA based agents. Vrouwenvelder et al. 2008 recommended AOC measurements for the rapid screening of biofouling potential.

In order to verify this accordingly, tests on the biological stability of the two molecular weight fractions and the commercial PAA product itself were conducted, based on likewise TOC dosage of 1 $mg \cdot L^{-1}$. The antiscalant samples were prepared in Hamburg tap water (TOC ≈ 0.5 $mg \cdot L^{-1}$), providing an initial bacterial concentration of about 34,700 $Cells \cdot mL^{-1}$. The total cell count measurements were performed over a 28-day duration at regular measuring intervals. The flow cytometry data shown in Figure 59 was converted to AOC values as shown in

Table 6. Tap water maintained most stable AOC and was the lowest over the entire 28-day range and the high MW fraction led to comparable results. The commercial product showed a similar trend as tap water but with a slightly enhanced AOC value. The low MW fraction, in contrast, led to a significantly increased AOC over the entire 28-day range, implying that the PAA constituents of low MW are readily bioavailable to bacteria and susceptible to enhance the biofouling potential.

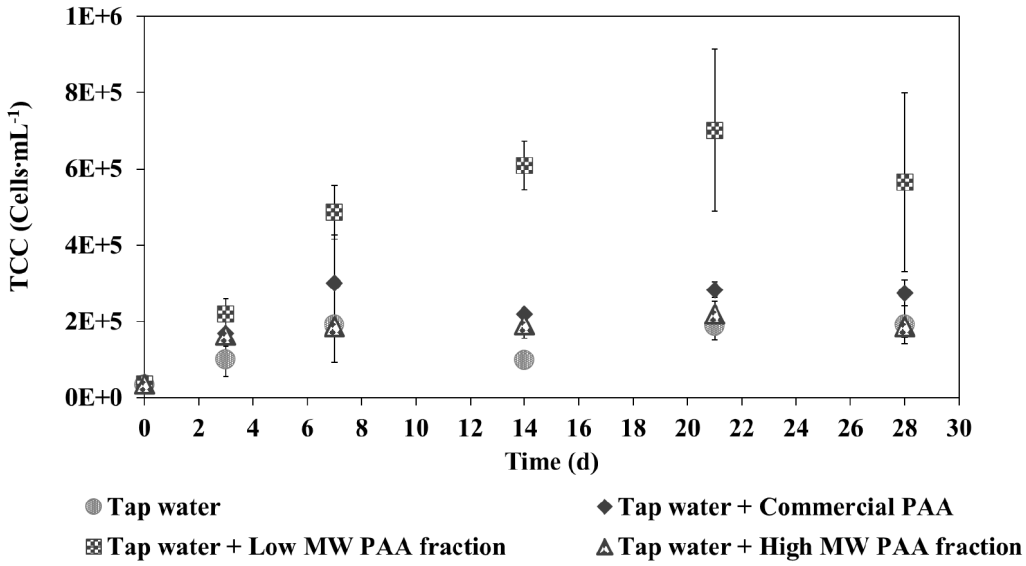

Figure 59: Total cell count (TCC) values of commercial PAA and its low and high MW fractions (1 mg·L^{-1} TOC) conducted in Hamburg tap water using flow cytometer

Table 6: Assimilable organic carbon (AOC) values of commercial PAA, its low and high MW fractions (each 1 mg·L^{-1} TOC) conducted in Hamburg tap water, determined by flow cytometer via total cell counts

Sample Label	AOC, µgC_{eq}·L^{-1}
Tapwater	15.7 ± 9.9
Tapwater + Commercial PAA (1 mg·L^{-1} TOC)	26.2 ± 12.6
Tapwater + Low MW Fraction (1 mg·L^{-1} TOC)	66.6 ± 21.3
Tapwater + High MW Fraction (1 mg·L^{-1} TOC)	18.2 ± 3.5

These results are in agreement with previous observations of increased biofouling and degradation of RO membranes operated with PAA-based antiscalants (Ashfaq et al. 2019; Sweity et al. 2015). Sweity et al. 2015 found that PAA-based antiscalants alter the physico-chemical properties of thin film composite RO membranes, e.g. increased hydrophobicity and surface charge, rendering them more susceptible for the deposition and attachment of bacterial cells. also suggested that PAA-based antiscalants contribute to biofouling on membranes and focused on devising a biofouling screening method for antiscalants using FTIR multivariate analysis and principle component analysis (PCA) with colony forming unit (CFU) counts.

The results from this study supports these earlier findings in regard to enhanced biofouling potential on membranes operated with PAA-based antiscalants.

Bioavailability of NF permeate

The biological stability of the PAA's organic carbon is of particular concern regarding the possibility of transfer of the small PAA molecules into the permeate. Therefore, AOC measurements of the permeate arising from a NF membrane (NF270) filtration with tap water feed and dosage of 1 mg·L^{-1} TOC commercial PAA (equivalent to approx. 10 mg·L^{-1} of liquid AS product) and its low and high MW fractions were performed in Hamburg tap water matrix (TOC ≈ 0.5 mg·L^{-1}). For practical reasons involving membrane preparation and timely measurement of samples in the flow cytometer, each filtration cycle was limited to 40 min at the end of which permeate samples were collected.

The TOC of tap water permeate was about 0.1 mg·L^{-1}, whereas commercial PAA permeate led to 0.1 mg·L^{-1}, high weight PAA to 0.1 mg·L^{-1} and low weight PAA to 0.2 mg·L^{-1}. Corresponding TCC values over 28 day and AOC values are given under Figure 60 and Table 7, respectively. As seen in Figure 60, NF permeates obtained with the commercial PAA product and its low MW fraction showed slightly enhanced biological growth (> 25% more) as compared to the permeate derived from application of the high molecular weight fraction. Comparatively low AOC values are attributed to low TOC values in the feed water and zero recovery rate. Due to the stabilization of the NF process during prolonged running times, this trend became more obvious after 14 days.

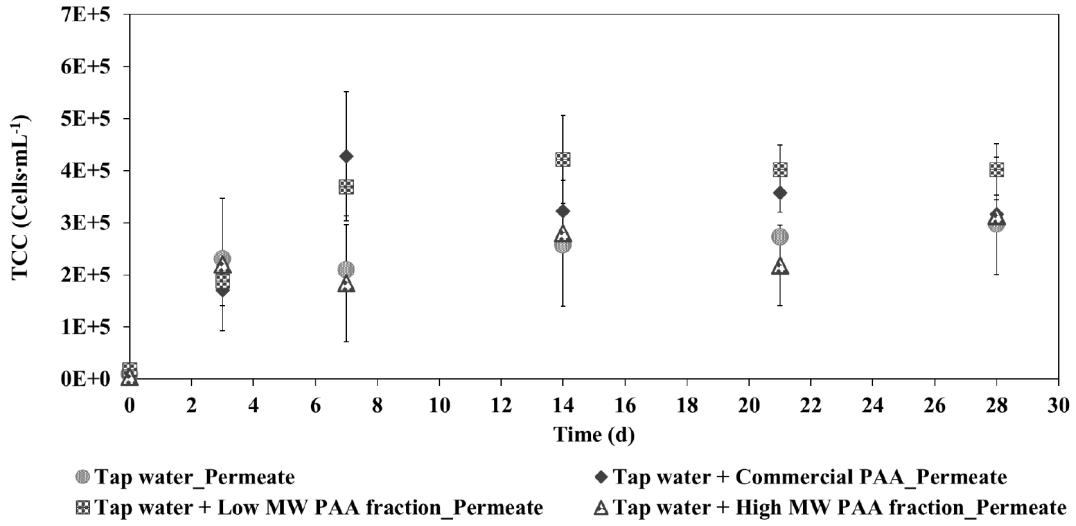

Figure 60: Total cell count (TCC) values of nanofiltration (NF270) permeate when operated with tap water feed containing commercial PAA or its low and high MW fractions (each adjusted to 1 mg·L^{-1} TOC), determined by flow cytometer via total cell count

Table 7: Assimilable organic carbon (AOC) values of nanofiltration (NF270) permeate when operated with tap water feed containing commercial PAA or its low and high MW fractions (each adjusted to 1 mg·L^{-1} TOC), determined by flow cytometer via total cell count

Sample Label	**AOC, µg C_{eq}·L^{-1}**
Tapwater permeate	28.8 ± 3.2
Tapwater + Commercial PAA permeate (1 mg TOC/L)	41.3 ± 12.4
Tapwater + Low weight PAA permeate (1 mg TOC/L)	40.4 ± 4.8
Tapwater + High weight PAA permeate(1 mg TOC/L)	30.7 ± 7.8

Nonetheless, they are indicative that prolonged operation with the PAA antiscalant could lead to biofouling on the membrane surface due to the low MW fraction and possible enhanced bioavailability of the resulting membrane permeate.

5 Conclusions and Outlook

This chapter summarizes the main findings of this study from different chapters, highlights practical implications and offers direction of future research.

5.1 Conclusions and outcomes

5.1.1 Experimental methods to evaluate effectiveness of antiscalants

Scaling is typically comprised of heterogeneous crystallization on the membrane surface and homogeneous crystallization occurring in the bulk solution. During NF/RO operation, depending on the mode of operation and saturation conditions, either or both of these crystallization phenomena may occur in varying degrees of severity. Section 4.2 to 4.4 described the various methods used to determine antiscalant effectiveness in this study:

- The stirred-beaker test with induction time determination offered an easy way to test different antiscalants against both sulfate and carbonate scaling salts in a relatively short amount of time, with a simple, straight-forward setup. Supersaturated solutions of gypsum ($SI_{gypsum} \approx 0.72$) and calcite ($SI_{calcite} \approx 2.06$) were stirred continuously at 11 °C. Induction time measurement based on rate of turbidity increase of 1 NTU was considered for the comparison of different products. Longer induction time implied that the antiscalants had good threshold inhibition property which indicates ability to inhibit nucleation stage of scaling.

  Although the stirred-beaker test could easily determine antiscalant effectiveness in homogeneous scaling condition, it was often found to be highly sensitive to changes in hydrodynamic conditions and sometimes associated with low reproducibility, especially at longer experimental times. Although it is able to distinguish between an exceptionally well performing inhibitor and exceptionally poor performing antiscalant, it is unable to discern antiscalants with similar induction times. For instance, in Section 4.2.1, according to the stirred-beaker test, at 0.5 $mg \cdot L^{-1}$ TS concentration, PAA antiscalant resulted in induction time of 61 min against gypsum scaling, while ATMP resulted in 60 min implying that they have similar performance, in contrast to PBTC which showed an induction time of only 13.5 min. Membrane filtration test proved that PAA and ATMP performed better than PBTC, but ATMP showed poor inhibition potential against nucleation and more flux decline in comparison to PAA. Additionally, in Section 4.6.1.3, although CMI antiscalant showed lower induction time than PAA to inhibit calcite scaling (Figure 46), crossflow filtration test and SEM characterization proved that CMI antiscalants have a better threshold inhibition effect than PAA antiscalants (Figure 47 and Figure 48).

  Due to its distant dissociation from real membrane filtration condition where several complex mechanisms are underway, the stirred-beaker test requires a additional precise measuring parameters system to be able to independently and precisely predict antiscalant effectiveness for real membrane applications.

- Using alternative variations to the stirred-beaker setup using the Deposens 3 or the application of novel WGM tests showed some potential to be used a scaling detection system, but was imprecise in the given arrangement, possibly due to high salt concentrations and low flow rate. Additionally, these alternatives were not suitable to test gypsum scaling due to potential difficulties with the cleaning step. Dead-end filtration experiments were comparatively faster than crossflow filtration experiments, but were not reproducible in all cases and could not provide any insights into scale inhibition mechanisms.
- Section 4.3 evaluated a membrane crossflow filtration setup to test effectiveness of different antiscalants using slightly supersaturated gypsum ($SI_{gypsum} \approx 0.2$) and calcite ($SI_{calcite} \approx 1.09$) solution as feed, filtered through CR100 RO membrane at constant TMP = 25 bar and T = 11 °C, with permeate and retentate recirculation. Rate of change of permeate flux was monitored for different antiscalant products – rapidly declining flux indicated poor scale inhibition performance whereas stable flux implied a better inhibition potential. Experimental investigation in this study showed inferences based on solely on flux behaviour in the crossflow membrane test may be misleading with respect to scaling nucleation inhibition. For instance, similar to PBTC and ATMP, PAA+DTPMP antiscalant shows stable flux for 10 h in the crossflow filtration test at concentrations of 0.5 $mg \cdot L^{-1}$ TS and 1 $mg \cdot L^{-1}$ TS (Figure 27 and Figure 29), indicating they have excellent scale inhibition potential. However, this cannot be interpreted as lack of crystals on the membrane surface. SEM characterization of membranes shows abundance of calcite crystals on the PAA+DTPMP operated membranes at both concentrations, while PBTC and ATMP membranes are mostly free of any carbonate crystals (Figure 28 and Figure 30), implying that the former antiscalant product is has excellent dispersion properties resulting in stable permeate flux, while the latter antiscalants have excellent threshold inhibition potential and prevent nucleation.
  Although crossflow filtration tests require an elaborate setup, more materials and are associated with a tedious membrane pre-preparation and post-cleaning steps, when combined with visual characterization of scaling crystals, they serve as an informative and reliable method in order to evaluate different antiscalants and different concentrations with different water matrices. Additionally, they have the advantage that the different filtration streams may be further analysed for antiscalant behaviour, side-products and aid in decision-making regarding concentrate disposal.

  A summary comparing scaling and antiscalant effectiveness methods is given in Table 8.

Table 8: Comparison of methods evaluated to determine scaling and antiscalant effectiveness

Experimental methods	**Stirred-beaker test**	**Membrane crossflow filtration test**	**Membrane dead-end filtration test**	**Stirred-beaker test integrated with Lagotec sensor**	**Whispering gallery mode**
Evaluating parameter	Induction time (turbidity increase of 1 NTU)	Rate of change in permeate flux	Rate of change in permeate flux	Rate of increase in scaling deposit thickness	Wavelength shift on WGM sensor
Suitability for gypsum	✓	✓	✓	×	×
Suitability for calcite	✓	✓	(✓)	✓	(✓)
Scaling solution matrix	Highly supersaturated	Slightly supersaturated	Slightly supersaturated	Highly supersaturated	Slightly supersaturated
Material requirements, ease of setup and operation	●●● (Easy)	● (Tedious)	●● (Moderate)	●●● (Easy)	● (Moderate)
Major scale inhibition mechanisms identified	Threshold inhibition	Threshold inhibition, dispersion and change in crystal morphology (with imaging)	Threshold inhibition	Threshold inhibition	-
Additional requirements	-	Microscopy (Ex. SEM)	-	-	Microscopy (Ex. light microscope)
Remarks	-	-	Optimization of saturation conditions and precise flux measurement necessary	Deposens sensor able to detect carbonate scaling, but requires more uniform flow conditions, for ex. in membrane filtration plants	Additional optimization & modification of suitable WGM sensors necessary

5.1.2 Antiscalant effectiveness to inhibit gypsum scaling

Section 4.3.1 and 4.6.1.2 describe detailed results on the comparison of PAA, CMI, PAA+DTPMP, DTPMP, ATMP and PBTC antiscalants to inhibit gypsum scaling using the stirred-beaker test ($SI_{gypsum} \approx 0.72$) and crossflow filtration test ($SI_{gypsum} \approx 0.2$).

- At a dosage of 0.5 $mg \cdot L^{-1}$ TS, P-free antiscalant based on CMI has a higher induction time of 106 min in the stirred-beaker test ($SI_{gypsum} \approx 0.72$), compared to PAA with 61 min. This result is corroborated by the stable flux behaviour in the crossflow filtration test ($SI_{gypsum} \approx 0.2$, RO membrane, TMP = 25 bar, T = 11°C, complete recirculation mode). SEM characterization shows minimal crystals on PAA membrane compared to CMI membrane. Increasing concentration to 1 $mg \cdot L^{-1}$ TS and 2 $mg \cdot L^{-1}$ TS increases the induction times of both CMI and PAA, while flux behavior remains stable and no gypsum crystals are formed on the membrane surface, suggesting complete threshold inhibition at higher antiscalant dosages.
- Among the phosphonates, the induction time of ATMP is highest at 60 min at a concentration of 0.5 $mg \cdot L^{-1}$ TS while PBTC is lowest at 13 min. At lower concentration, P-free PAA and CMI show better inhibition against gypsum scaling compared to the tested P-based products. Concordant flux behaviour and crystal characterization was obtained during crossflow filtration tests.
- Increasing antiscalant dosage to 1 $mg \cdot L^{-1}$ TS resulted in enhanced gypsum scale inhibition for PAA+DTPMP, DTPMP and ATMP products. Induction times in the stirred-beaker test were increased to approximately more than 100 min for these antiscalants and constant flux with no crystallization on membrane surface. The PBTC antiscalant, however, did not show much improvement in its inhibition effect and remained unsuitable for gypsum scale inhibition.

The following table (Table 9) summarizes effectiveness of the antiscalants tested in this study for their gypsum scale inhibition potential.

Table 9: Effectiveness of different antiscalant against gypsum scale inhibition at 0.5 mg/L TS and 1 mg/L TS

Antiscalants used in the study	**Efficacy against gypsum scaling at 0.5 mg·L^{-1} TS**	**Efficacy against gypsum scaling at 1 mg·L^{-1} TS**
PAA	●●●	●●●
CMI	●●●	●●●
PAA+DTPMP	●●	●●●
DTPMP	●●	●●●
ATMP	●●	●●●
PBTC	●	●

5.1.3 Antiscalant effectiveness to inhibit calcite scaling

Section 4.2.2, Section 4.3.2 and Section 4.6.1.3 describe detailed results on the comparison of PAA, CMI, PAA+DTPMP, DTPMP, ATMP and PBTC antiscalants to inhibit calcite scaling using the stirred-beaker test ($SI_{calcite} \approx 1.09$) and crossflow filtration test ($SI_{calcite} \approx 2.06$).

- P-based antiscalants PBTC and ATMP show high inhibition potential against calcite scaling with long induction times over 100 min at a concentration of 0.5 mg·L^{-1} TS in the stirred-beaker test, which increases to over 200 min at 1 mg·L^{-1} TS concentration. This inhibition potential is confirmed by the stable flux behaviour in the crossflow filtration test and lack on crystals on the membrane surface characterized by SEM.
- DTPMP based product resulted in lowest calcite inhibition with 19 min induction time at 0.5 mg·L^{-1} TS, which increases to 60 min at 1 mg/L TS. However, in both cases there was a considerable decline in flux with time and SEM confirmed prevalence of several crystals on the surface of the membrane.
- PAA+DTPMP antiscalant mixture, although manifested as stable flux in the crossflow filtration test at 0.5 mg·L^{-1} TS and 1 mg·L^{-1} TS, was characterized by several crystals on the membrane in both cases. Comparatively lower induction times in the stirred-beaker test suggested that this antiscalant is unable to inhibit calcite scale nucleation, but presents excellent dispersion ability even at low dosages.

- Among the P-free antiscalants tested in this study, CMI antiscalant shows excellent threshold property for calcite salts even at low dosage, whereas PAA antiscalants show enhanced calcite inhibition only at higher dosages.

The following table (Table 10) summarizes effectiveness of the antiscalants tested in this study for their gypsum scale inhibition potential:

Table 10: Effectiveness of different antiscalant against gypsum scale inhibition at 0.5 mg·L^{-1} TS and 1 mg·L^{-1} TS

Antiscalants used in the study	**Efficacy against calcite scaling at 0.5 mg·L^{-1} TS**	**Efficacy against calcite scaling at 1 mg·L^{-1} TS**
PAA	●●	●●
CMI	●●	●●●
PAA+DTPMP	●●	●●
DTPMP	●	●
ATMP	●●●	●●●
PBTC	●●●	●●●

5.1.4 Effect of PAA antiscalant and its fractions

This study evaluated the behaviour of different antiscalant ingredients for their effectiveness against gypsum and calcite scaling. Different P-based antiscalants showed reasonable efficacy against scaling salts, especially when dosed at higher dosages. Literature has pointed out that P-based antiscalant application in NF/RO for drinking water production may be associated with concentrate streams with problematic concentrations of phosphonates and their side-products, risking safe concentrate disposal and their side-products and may additionally trigger AMPA formation when the water is disinfected. Therefore, focus on suitability and application of P-free antiscalants has increased. Section 4.6 compared CMI and PAA antiscalants and showed that both products showed excellent threshold inhibition against sulfate scaling, but PAA product mainly dispersed carbonate crystals into the bulk solution, but are good threshold inhibitors at higher dosages of 2 mg/L TS.

Section 4.6.2 delved into the effectiveness of PAA antiscalant, its fractions ≤ 500 Da (low MW PAA) and ≥ 500 Da (high MW PAA) and biological stability. The commercial PAA antiscalant and its given fractions were compared at same TOC concentration to ensure that similar number of C-chains were accounted for in the evaluation. The following conclusions were derived from the experimental results:

- The commercial PAA antiscalant showed very good gypsum and calcite scale inhibition at 0.5 mg/L TOC with over 100 min induction time in the stirred beaker tests (SI_{gypsum} ≈ 0.72, $SI_{calcite}$ ≈ 2.06) for both the scalants. The fractions of PAA antiscalant ≥ 500 Da showed also resulted in over 100 min induction time for gypsum and calcite salts, whereas the PAA fraction ≤ 500 Da resulted in very low induction time below 40 min for the given salts at same TOC dosage. This implied that the scale inhibition characteristics of the commercial PAA antiscalant was mainly governed by the high MW PAA fractions ≥ 500 Da.
- Section 4.6.2.3 described the results of crossflow filtration experiments with the CR100 (RO) membrane with SI_{gypsum} ≈ 0.2 / $SI_{calcite}$ ≈ 1.09, TMP = 25 bar, T = 11°C, complete recirculation mode) for the PAA antiscalants and its low MW and high MW fractions. The high MW PAA fraction (≥ 500 Da) did not show any change in permeate flux over 5 h filtration for gypsum and calcite salts, which was similar to the flux behavior of the commercial PAA antiscalant. In contrast to the high MW PAA fraction, the low MW PAA fraction (≤ 500 Da) showed continuous flux decline from the beginning of the filtration with gypsum scale, while flux decline with calcite salt was relatively gradual but nonetheless continuous and similar to permeate flux behavior in absence of an antiscalant, implying lack of scale inhibition ability. SEM images of the membrane verified that low MW PAA fraction was unsuccessful in preventing crystal deposition on the membrane and also accounted for some changes to gypsum and calcite crystal morphology.
- Section 4.6.2.4 determined the biological availability of the commercial PAA antiscalant and its low and high MW fractions in tap water matrix. Figure 58 and Table 5 experimentally showed that the low MW PAA fraction (≤ 500 Da) has a higher biological growth potential when compared to the high MW fraction and the commercial antiscalant. Since NF/RO membranes differ widely in their pore size, the likelihood of the low MW PAA antiscalant fractions which are more bioavailable, passing through the membrane is not trivial, which may be determined by analysing the permeate samples after sufficient filtration time.

5.2 Future implications

This work presented a comprehensive evaluation of the nature scaling in NF/RO filtration systems and its control using antiscalants. While chemical-free operation of NF/RO systems by process changes are alternatives to ensure smooth operation, it remains that the use of antiscalants is the easiest way to avoid long-term problems with the expensive NF/RO treatment step. Due to the varied number of antiscalant products and lack of a standardized test to select the suitable antiscalant and dosing concentration, a variety of tests differing in their ease of application and limited by the extent of their detection were compared for their suitability to compare and determine the effectiveness of different antiscalants. While the tests described in this study may not always replicate real drinking water treatment conditions, it was possible to arrive at worthwhile test conditions that may be applied by water suppliers or regulatory bodies to determine antiscalant effectiveness before applying it directly in the NF/RO filtration system which may involve high practical and economic risks.

Since the application of NF/RO filtration for drinking water production is a popular solution to ensure reliable and safe water supply, this study aims to fill certain knowledge gaps relating to the effectiveness of different antiscalant ingredients and their concentrations. While antiscalants containing phosphonic acids generally show sufficient scale inhibition potential at higher dosages, it is not always desirable to dose high concentrations of these products due to risk of eutrophication from the resulting concentrate stream in natural water bodies. Currently, only few P-free antiscalants are available on the market and while they may show similar inhibition potential as P-based products, they may sometimes specifically be the preferred choice due to lower risk with NF/RO concentrate stream management and disposal. This study sheds light on the effectiveness of different P-free antiscalants and some initial insights on the possibility of the antiscalants to pass through the membrane and pose risk of enhanced biological growth potential or biofouling.

Although several commercial antiscalant formulations were used in this study, it is expected that the inhibition effectiveness determined for gypsum and calcite inhibition are not universally conclusive for all antiscalants containing the given active ingredients. Therefore, the difficulty remains that different commercial formulations with same active ingredient may vary significantly from one another. Additionally, complicated analytical techniques or lack of it present difficulties to understand antiscalant working mechanism, and are therefore an impediment during decision making to use NF/RO safely for drinking water production. Accordingly, future work on scale inhibition using antiscalant should focus on more sensitive detection methods for scaling so that antiscalant effectiveness may also be determined in a timely manner, testing several commercial antiscalant formulations, especially P-free products since they are attributed with safer concentrate disposal, deeper investigation of ability of antiscalants to pass through the membrane and other potential side-effects including biofouling.

References

Akın, B., Öner, M., Bayram, Y., & Demadis, K. D. (2008). Effects of carboxylate-modified,“green” inulin biopolymers on the crystal growth of calcium oxalate. *Crystal Growth and Design, 8(6),* (1997–2005).

Akyol, E., Oner, M., Barouda, E., & Demadis, K. D. (2009). Systematic structural determinants of the effects of tetraphosphonates on gypsum crystallization. *Crystal Growth & Design, 9(12),* (5145–5154).

Al-Hamzah, A. A., East, C. P., Doherty, W. O.S., & Fellows, C. M. (2014). Inhibition of homogenous formation of calcium carbonate by poly (acrylic acid). The effect of molar mass and end-group functionality. *Desalination, 338,* (93–105). doi:10.1016/j.desal.2014.01.020

Al-Roomi, Y. M., & Hussain, K. F. (2016). Potential kinetic model for scaling and scale inhibition mechanism. *Desalination, 393,* (*4*, 186–195). doi:10.1016/j.desal.2015.07.025

Alzahrani, S., Mohammad, A. W., Abdullah, P., & Jaafar, O. (2013). Potential tertiary treatment of produced water using highly hydrophilic nanofiltration and reverse osmosis membranes. *Journal of Environmental Chemical Engineering, 1,* (*4*, 1341–1349). doi:10.1016/j.jece.2013.10.002

Amjad, Z. (2014). *Mineral scales in biological and industrial systems:* CRC Press Taylor & Francis Group.

Ang, W. L., Mohammad, A. W., Hilal, N., & Leo, C. P. (2015). A review on the applicability of integrated/hybrid membrane processes in water treatment and desalination plants. *Desalination, 363,* (2–18). doi:10.1016/j.desal.2014.03.008

Ansari, S. Z., & Pandit, A. B. (2020). Evaluation of gypsum (CaSO 4 ·2H 2 O) scale formation and its inhibition by different antiscalants by static and dynamic test. *Indian Chemical Engineer, 62,* (*3*, 251–262). doi:10.1080/00194506.2019.1658547

Antony, A., Low, J. H., Gray, S., Childress, A. E., Le-Clech, P., & Leslie, G. (2011). Scale formation and control in high pressure membrane water treatment systems: A review. *Journal of Membrane Science, 383,* (*1-2*, 1–16). doi:10.1016/j.memsci.2011.08.054

Aptel, P., & Buckley, C. A. (1996). *Categories of membrane operations.* (2-1) (Water treatment membrane processes).

Armbruster, D., Müller, U., & Happel, O. (2019). Characterization of phosphonate-based antiscalants used in drinking water treatment plants by anion-exchange chromatography coupled to electrospray ionization time-of-flight mass spectrometry and inductively coupled plasma mass spectrometry. *Journal of chromatography. A, 1601,* (189–204). doi:10.1016/j.chroma.2019.05.014

Armbruster, D., Happel, O. and Egner, S. (2024), Charakterisierung und Spurenanalytik technischer Polyacrylate als Antiscalants in der Trinkwasseraufbereitung. Vom Wasser, 122: 15-18. https://doi.org/10.1002/vomw.202400004

Ashfaq, M. Y., Al-Ghouti, M. A., Qiblawey, H., & Zouari, N. (2019). Evaluating the effect of antiscalants on membrane biofouling using FTIR and multivariate analysis. *Biofouling, 35,* (*1*, 1–14). doi:10.1080/08927014.2018.1557637

Baggio, G., Qadir, M., & Smakhtin, V. (2021). Freshwater availability status across countries for human and ecosystem needs. *The Science of the total environment, 792,* (148230). doi:10.1016/j.scitotenv.2021.148230

Basheer, C., Shaikh, A. A., Al-Mutairi, E. M., Noor El Deen, M., & Qureshi, K. K. (2021). Calcium Carbonate Scale Inhibition with Ultrasonication and a Commercial Antiscalant. *Water, 13,* (*23*, 3428). doi:10.3390/w13233428

Beckmann, W. (Ed.). (2013). *Crystallization: basic concepts and industrial applications:* John Wiley & Sons.

Benecke, J. (2018). *Gypsum scaling during reverse osmosis desalination − characterization and effects of natural organic matter*. (TUHH Universitätsbibliothek).

Bergdolt, U., Müller, U., Sacher, F., Maier, U., Ungermann, A., Lehmann, M., et al. (2019). Beurteilung von Konzentrateinleitungen aus Membrananlagen für die zentrale Trinkwasserenthärtung: Fachinformationen für die Wasserbehörden. *Landesanstalt für Umwelt Baden-Württemberg (LUBW), Karlsruhe.*

Boels, L., & Witkamp, G.-J. (2011). Carboxymethyl Inulin Biopolymers: A Green Alternative for Phosphonate Calcium Carbonate Growth Inhibitors. *Crystal Growth & Design, 11,* (*9*, 4155–4165). doi:10.1021/cg2007183

Chen, J. C., Li, Q., & Elimelech, M. (2004). In situ monitoring techniques for concentration polarization and fouling phenomena in membrane filtration. *Advances in colloid and interface science, 107,* (*2-3*, 83–108). doi:10.1016/j.cis.2003.10.018

Chong, T., Wong, F., & Fane, A. (2008). The effect of imposed flux on biofouling in reverse osmosis: Role of concentration polarisation and biofilm enhanced osmotic pressure phenomena. *Journal of Membrane Science, 325,* (*2*, 840–850). doi:10.1016/j.memsci.2008.09.011

Crittenden, J. C., Trussell, R. R., Hand, D. W., Howe, K. J., & Tchobanoglous, G. (2012). *MWH's water treatment: principles and design:* John Wiley & Sons.

Darton, E. G. (2000). Membrane chemical research: centuries apart. *Desalination, 132,* (121–131).

Dobberschütz, S., Nielsen, M. R., Sand, K. K., Civioc, R., Bovet, N., Stipp, S. L. S., et al. (2018). The mechanisms of crystal growth inhibition by organic and inorganic inhibitors. *Nature communications, 9,* (*1*, 1578). doi:10.1038/s41467-018-04022-0

Du Plessis, A. (2022). Persistent degradation: Global water quality challenges and required actions. *One Earth, 5,* (*2*, 129–131). doi:10.1016/j.oneear.2022.01.005

Engelbart, L., Bieger, S., Thompson, K., Fischer, L., Bader, T., Kramer, M., et al. (2025). In-situ formation of glyphosate and AMPA in activated sludge from phosphonates used as antiscalants and bleach stabilizers in households and industry. *Water research, 280,* (123464). doi:10.1016/j.watres.2025.123464

Falkenberg, L. J., & Styan, C. A. (2015). The use of simulated whole effluents in toxicity assessments: A review of case studies from reverse osmosis desalination plants. *Desalination, 368,* (3–9). doi:10.1016/j.desal.2015.01.014

Feiner, M., Beggel, S., Jaeger, N., & Geist, J. (2015). Increased RO concentrate toxicity following application of antiscalants - acute toxicity tests with the amphipods Gammarus pulex and Gammarus roeseli. *Environmental pollution (Barking, Essex : 1987), 197,* (309–312). doi:10.1016/j.envpol.2014.11.021

Fiume, M. M., Heldreth, B., Bergfeld, W. F., Belsito, D. V., Hill, R. A., Klaassen, C. D., Liebler, D. C., Marks, J. G., Jr, Shank, R. C., Slaga, T. J., Snyder, P. W., & Andersen, F. A. (2016). Safety Assessment of Microbial Polysaccharide Gums as Used in Cosmetics. International journal of toxicology, 35(1 Suppl), 5S–49S. https://doi.org/10.1177/1091581816651606

Flemming, H.-C. (2020). Biofouling and me: My Stockholm syndrome with biofilms. *Water research, 173,* (115576). doi:10.1016/j.watres.2020.115576

Fritzmann, C., Löwenberg, J., Wintgens, T., & Melin, T. (2007). State-of-the-art of reverse osmosis desalination. *Desalination, 216,* (*1-3*, 1–76). doi:10.1016/j.desal.2006.12.009

Futterlieb, M., & Panglisch, S. (2025). Incipient CaCO3-scaling detection for scaling mitigation. *Desalination, 613,* (*1*, 119023). doi:10.1016/j.desal.2025.119023

Ganguly, S., Kelland, M. A., Ellis, R. J., Andresen, M., Subramanian, S., & Theodossiou, A. (2024). Sustainable Calcite Scale Inhibitors via Oxidation of Lignosulfonates. *ACS omega, 9,* (*23*, 25162–25171). doi:10.1021/acsomega.4c02716

Ganie, S. A., Baig, M. T., & Mady, M. F. (2025). Innovative dual-functional, green and biodegradable dicarboxylated inulin as scale and corrosion inhibitors for sustainable oil and gas operations. *Carbohydrate polymers, 367,* (124022). doi:10.1016/j.carbpol.2025.124022

Grossmann, T. (2012). *Whispering-Gallery-Mode Lasing in Polymeric Microcavities*. (Doctoral dissertation, Karlsruher Instituts f□ur Technologie).

Guo, X., Joy, J. S. C., Cheng, Y., Zhao, X., Liu, Z., & Xu, Y. (2021). Scale Inhibitors for Industrial Circulating Water Systems: A Review. *Journal of Water Chemistry and Technology, 43,* (*6*, 517–525). doi:10.3103/S1063455X21060102

Hammes, F. A., & Egli, T. (2005). New method for assimilable organic carbon determination using flow-cytometric enumeration and a natural microbial consortium as inoculum. *Environmental science & technology, 39,* (*9*, 3289–3294). doi:10.1021/es048277c

Hasanin, G., Mosquera, A. M., Emwas, A.-H., Altmann, T., Das, R., Buijs, P. J., et al. (2023). The microbial growth potential of antiscalants used in seawater desalination. *Water research, 233,* (119802). doi:10.1016/j.watres.2023.119802

Hasson, D., & Semiat, R. (2006). Scale Control in Saline and Wastewater Desalination. *Israel Journal of Chemistry, 46,* (97–104).

Hasson, D., Shemer, H., & Sher, A. (2011). State of the art of friendly "green" scale control inhibitors: a review article. *Industrial & Engineering Chemistry Research, 50(12),* (7601–7607).

Howe, K. J., Hand, D. W., Crittenden, J. C., Trussell, R. R., & Tchobanoglous, G. (2012). *Principles of water treatment:* John Wiley & Sons.

Hu, B., Huang, L., Chang, H., Ji, Z., Yan, Z., Qu, D., et al. (2025). A review of key parameters affecting inorganic scaling in thermal, pressure, and osmosis-driven membranes for produced water desalination. *Separation and Purification Technology, 354,* (129023). doi:10.1016/j.seppur.2024.129023

Ismail, F., Khulbe, K. C., & Matsuura, T. (2019). *Reverse osmosis:* Elsevier.

Jain, T., Sanchez, E., Owens-Bennett, E., Trussell, R., Walker, S., & Liu, H. (2019). Impacts of antiscalants on the formation of calcium solids: implication on scaling potential of desalination concentrate. *Environmental Science: Water Research & Technology, 5,* (*7*, 1285–1294). doi:10.1039/C9EW00351G

Ji, Y., Chen, Y., Le, J., Qian, M., Huan, Y., Yang, W., et al. (2017). Highly effective scale inhibition performance of amino trimethylenephosphonic acid on calcium carbonate. *Desalination, 422,* (165–173). doi:10.1016/j.desal.2017.08.027

Johannsen, F. R. (2003). Toxicological profile of carboxymethyl inulin. *Food and Chemical Toxicology, 41,* (49–59).

Joo, S. H., & Tansel, B. (2015). Novel technologies for reverse osmosis concentrate treatment: a review. *Journal of environmental management, 150,* (322–335). doi:10.1016/j.jenvman.2014.10.027

Karthika, S., Radhakrishnan, T. K., & Kalaichelvi, P. (2016). A review of classical and nonclassical nucleation theories. *Crystal Growth & Design, 16(11),* (6663–6681).

Kelle Zeiher, E. H., Ho, B., & Williams, K. D. (2003). Novel antiscalant dosing control. *Desalination, 157,* (209–216).

Ketrane, R., Saidani, B., Gil, O., Leleyter, L., & Baraud, F. (2009). Efficiency of five scale inhibitors on calcium carbonate precipitation from hard water: Effect of temperature and concentration. *Desalination, 249,* (*3*, 1397–1404). doi:10.1016/j.desal.2009.06.013

Khormali, A., Petrakov, D. G., & Afshari Moein, M. J. (2016). Experimental analysis of calcium carbonate scale formation and inhibition in waterflooding of carbonate reservoirs. *Journal of Petroleum Science and Engineering, 147,* (*1–2*, 843–850). doi:10.1016/j.petrol.2016.09.048

KonTriSol. (2023). Konzentrate aus der Trinkwasseraufbereitung – Lösungsansätze für die technischen, rechtlichen und wirtschaftlichen Hemmnisse beim Einsatz von NF/UO-Prozessen in der Trinkwasseraufbereitung. *BMBF (02WAV1530B) and DVGW(W 201807)*. Gemeinsamer Abschlussbericht aller Verbundpartner.

Kucera, J. (2023). *Reverse osmosis:* John Wiley & Sons.

Lee, H.-J., Halali, M. A., Baker, T., Sarathy, S., & Lannoy, C.-F. de. (2020). A comparative study of RO membrane scale inhibitors in wastewater reclamation: Antiscalants versus pH adjustment. *Separation and Purification Technology, 240,* (116549). doi:10.1016/j.seppur.2020.116549

Li, W., Su, X., Palazzolo, A., Ahmed, S., & Thomas, E. (2017). Reverse osmosis membrane, seawater desalination with vibration assisted reduced inorganic fouling. *Desalination, 417,* (102–114). doi:10.1016/j.desal.2017.05.016

Li, X., Hasson, D., & Shemer, H. (2018). Flow conditions affecting the induction period of CaSO4 scaling on RO membranes. *Desalination, 431,* (119–125). doi:10.1016/j.desal.2017.08.014

Li, S., Qu, Q., Li, L., Xia, K., Li, Y., & Zhu, T. (2019). Bacillus cereus s-EPS as a dual bio-functional corrosion and scale inhibitor in artificial seawater. *Water research, 166,* (115094). doi:10.1016/j.watres.2019.115094

Li, A., Zhang, H., Liu, Q., & Zeng, H. (2022). Effects of chemical inhibitors on the scaling behaviors of calcite and the associated surface interaction mechanisms. *Journal of Colloid and Interface Science, 618,* (507–517). doi:10.1016/j.jcis.2022.03.105

Liu, Y., & Zhang, P. (2022). Review of Phosphorus-Based Polymers for Mineral Scale and Corrosion Control in Oilfield. *Polymers, 14,* (*13*). doi:10.3390/polym14132673

Liwarska-Bizukojc, E. (2022). Evaluation of Ecotoxicity of Wastewater from the Full-Scale Treatment Plants. *Water, 14,* (*20*, 3345). doi:10.3390/w14203345

MacAdam, J., & Parsons, S. A. (2004). Calcium carbonate scale formation and control. *Reviews in Environmental Science and Bio/Technology, 3,* (159–169).

Matin, A., Khan, Z., Zaidi, S.M.J., & Boyce, M. C. (2011). Biofouling in reverse osmosis membranes for seawater desalination: Phenomena and prevention. *Desalination, 281,* (*3*, 1–16). doi:10.1016/j.desal.2011.06.063

Matin, A., Rahman, F., Shafi, H. Z., & Zubair, S. M. (2019). Scaling of reverse osmosis membranes used in water desalination: Phenomena, impact, and control; future directions. *Desalination, 455,* (*1–2*, 135–157). doi:10.1016/j.desal.2018.12.009

McGovern, R. K., Zubair, S. M., & Lienhard V, J. H. (2014). The benefits of hybridising electrodialysis with reverse osmosis. *Journal of Membrane Science, 469,* (*7*, 326–335). doi:10.1016/j.memsci.2014.06.040

Melnik, L. A., Kucheruk, D. D., & Pshinko, G. N. (2020). Antiscalants in the Process of Reverse Osmosis: Antiscaling Mechanism and Modern Problems of Application. *Journal of Water Chemistry and Technology, 42,* (*6*, 450–464). doi:10.3103/S1063455X20060077

Mi, B., & Elimelech, M. (2010). Gypsum scaling and cleaning in forward osmosis: measurements and mechanisms. *Environmental science & technology, 44,* (*6*, 2022–2028). doi:10.1021/es903623r

Milne, N. A., O'Reilly, T., Sanciolo, P., Ostarcevic, E., Beighton, M., Taylor, K., et al. (2014). Chemistry of silica scale mitigation for RO desalination with particular reference to remote operations. *Water research, 65,* (107–133). doi:10.1016/j.watres.2014.07.010

Mpelwa, M., & Tang, S.-F. (2019). State of the art of synthetic threshold scale inhibitors for mineral scaling in the petroleum industry: a review. *Petroleum Science, 16,* (*4*, 830–849). doi:10.1007/s12182-019-0299-5

Mulay, A. R. (2022). *Investigation of Scaling and Scale Inhibition Potential by Antiscalants in Reverse Osmosis Treatment*. (Master thesis, Hamburg University of Technology (TUHH)).

Müller, U. (2010). Einsatz von Nanofiltration und Niederdruckumkehrosmose zur Einsatz von Nanofiltration und Niederdruckumkehrosmose zur Trinkwasseraufbereitung in Deutschland. *bbr – Fachmagazin für Leitungs- und Brunnenbau, 06,* (54–60).

Mullin, J. W. (2001). *Crystallization:* Elsevier.

Ojelade, B. S., Durowoju, O. S., Adesoye, P. O., Gibb, S. W., & Ekosse, G.-I. (2022). Review of Glyphosate-Based Herbicide and Aminomethylphosphonic Acid (AMPA): Environmental and Health Impacts. *Applied Sciences, 12,* (*17*, 8789). doi:10.3390/app12178789

Oshchepkov, M. S., Rudakova, G. Y., Tkachenko, S. V., Larchenko, V. E., Popov, K. I., & Tusheva, M. A. (2021). Recent State-of-the-Art of Antiscalant-Driven Scale Inhibition Theory (Review). *Thermal Engineering, 68,* (*5*, 370–380). doi:10.1134/S0040601521040054

Park, Y.-M., Yeon, K.-M., & Park, C.-h. (2020). Silica treatment technologies in reverse osmosis for industrial desalination: A review. *Environmental Engineering Research, 25,* (*6*, 819–829). doi:10.4491/eer.2019.353

Popov, K., Oshchepkov, M., Afanas'eva, E., Koltinova, E., Dikareva, Y., & Rönkkömäki, H. (2019). A new insight into the mechanism of the scale inhibition: DLS study of gypsum nucleation in presence of phosphonates using nanosilver dispersion as an internal light scattering intensity reference. *Colloids and Surfaces A: Physicochemical and Engineering Aspects, 560,* (*2016*, 122–129). doi:10.1016/j.colsurfa.2018.10.015

Prien, R. (2021). *Evaluation of effectiveness of scale inhibition capacity of different antiscalants against carbonate scaling*. (Master thesis, Hamburg University of Technology).

Prisciandaro, M., Olivieri, E., Lancia, A., & Musmarra, D. (2012). PBTC as an Antiscalant for Gypsum Precipitation: Interfacial Tension and Activation Energy Estimation. *Industrial & Engineering Chemistry Research, 51,* (*39*, 12844–12851). doi:10.1021/ie302060t

Rabizadeh, T., Morgan, D. J., Peacock, C. L., & Benning, L. G. (2019). Effectiveness of Green Additives vs Poly(acrylic acid) in Inhibiting Calcium Sulfate Dihydrate Crystallization. *Industrial & Engineering Chemistry Research, 58,* (*4*, 1561–1569). doi:10.1021/acs.iecr.8b02904

Rahardianto, A., Gao, J., Gabelich, C. J., Williams, M. D., & Cohen, Y. (2007). High recovery membrane desalting of low-salinity brackish water: Integration of accelerated precipitation softening with membrane RO. *Journal of Membrane Science, 289,* (*1-2*, 123–137). doi:10.1016/j.memsci.2006.11.043

Reiss, A. G., Gavrieli, I., & Ganor, J. (2020). The effect of phosphonate-based antiscalant on gypsum precipitation kinetics and habit in hyper-saline solutions: An experimental and modeling approach to the planned Red Sea – Dead Sea Project. *Desalination, 496,* (*7*, 114638). doi:10.1016/j.desal.2020.114638

Reznik, I. J., Gavrieli, I., Antler, G., & Ganor, J. (2011). Kinetics of gypsum crystal growth from high ionic strength solutions: A case study of Dead Sea – seawater mixtures. *Geochimica et Cosmochimica Acta, 75,* (*8*, 2187–2199). doi:10.1016/j.gca.2011.01.034

Roberts, D. A., Johnston, E. L., & Knott, N. A. (2010). Impacts of desalination plant discharges on the marine environment: A critical review of published studies. *Water research, 44,* (*18*, 5117–5128). doi:10.1016/j.watres.2010.04.036

Rolf, J., Cao, T., Huang, X., Boo, C., Li, Q., & Elimelech, M. (2022). Inorganic Scaling in Membrane Desalination: Models, Mechanisms, and Characterization Methods. *Environmental science & technology, 56,* (*12*, 7484–7511). doi:10.1021/acs.est.2c01858

Rosenberg, Y. O., Reznik, I. J., Zmora-Nahum, S., & Ganor, J. (2012). The effect of pH on the formation of a gypsum scale in the presence of a phosphonate antiscalant. *Desalination, 284,* (207–220). doi:10.1016/j.desal.2011.08.061

Royo, M. C., Adroer, N., Aumatell, J., Cortada, E., Vega, A., Villanueva, O., et al. (2023). Sustainable antiscalant for municipal reverse osmosis plants. *Desalination and Water Treatment, 309,* (*02*, 58–65). doi:10.5004/dwt.2023.29880

Rozova, J. (2014). *Incipient Crystallization of Gypsum in Aqueous Solutions and Reverse Osmosis Desalination – Reproducibility and Effects of Antiscalants and Natural Organic Matter*. (Master thesis, Hamburg University of Technology). Hamburg.

Sablani, S. S., Goosena, M. F. A., Al-Belushi, R., & Wilf, M. (2001). Concentration polarization in ultrafiltration and reverse osmosis: a critical review. *Desalination, 141,* (269–289).

Sagiv, A., Avraham, N., Dosoretz, C. G., & Semiat, R. (2008). Osmotic backwash mechanism of reverse osmosis membranes. *Journal of Membrane Science, 322,* (*1*, 225–233). doi:10.1016/j.memsci.2008.05.055

Saji, V. S., Meroufel, A. A., & Sorour, A. A. (Eds.). (2020). *Corrosion and Fouling Control in Desalination Industry*. Cham: Springer International Publishing.

Shaffer, D. L., Tousley, M. E., & Elimelech, M. (2017). Influence of polyamide membrane surface chemistry on gypsum scaling behavior. *Journal of Membrane Science, 525,* (249–256). doi:10.1016/j.memsci.2016.11.003

Shen, C., Xu, X., Hou, X.-Y., Wu, D.-X., & Yin, J.-H. (2018). Molecular weight effect on PAA antiscale performance in LT-MED desalination system: Static experiment and MD simulation. *Desalination, 445,* (*7*, 1–5). doi:10.1016/j.desal.2018.07.021

Shirazi, S., Lin, C.-J., & Chen, D. (2010). Inorganic fouling of pressure-driven membrane processes — A critical review. *Desalination, 250,* (*1*, 236–248). doi:10.1016/j.desal.2009.02.056

Shmulevsky, M., Li, X., Shemer, H., Hasson, D., & Semiat, R. (2017). Analysis of the onset of calcium sulfate scaling on RO membranes. *Journal of Membrane Science, 524,* (299–304). doi:10.1016/j.memsci.2016.11.055

Söhnel, O., & Mullin, J. W. (1988). Interpretation of Crystallization Induction Periods. *Journal of Colloid and Interface Science, 123 (1)*.

Spinthaki, A., & Demadis, K. D. (2020). Chemical Methods for Scaling Control. In V. S. Saji, A. A. Meroufel, & A. A. Sorour (Eds.), *Corrosion and Fouling Control in Desalination Industry* (pp. 307–342). Cham: Springer International Publishing.

Sweity, A., Oren, Y., Ronen, Z., & Herzberg, M. (2013). The influence of antiscalants on biofouling of RO membranes in seawater desalination. *Water research, 47,* (*10*, 3389–3398). doi:10.1016/j.watres.2013.03.042

Sweity, A., Zere, T. R., David, I., Bason, S., Oren, Y., Ronen, Z., et al. (2015). Side effects of antiscalants on biofouling of reverse osmosis membranes in brackish water desalination. *Journal of Membrane Science, 481,* (172–187). doi:10.1016/j.memsci.2015.02.003

Tang, Y., Yang, W., Yin, X., Liu, Y., Yin, P., & Wang, J. (2008). Investigation of CaCO3 scale inhibition by PAA, ATMP and PAPEMP. *Desalination, 228,* (*1-3*, 55–60). doi:10.1016/j.desal.2007.08.006

Tong, T., Wallace, A. F., Zhao, S., & Wang, Z. (2019). Mineral scaling in membrane desalination: Mechanisms, mitigation strategies, and feasibility of scaling-resistant membranes. *Journal of Membrane Science, 579,* (52–69). doi:10.1016/j.memsci.2019.02.049

Tresnakova, N., Stara, A., & Velisek, J. (2021). Effects of Glyphosate and Its Metabolite AMPA on Aquatic Organisms. *Applied Sciences, 11,* (*19*, 9004). doi:10.3390/app11199004

van der Bruggen, B., Lejon, L., & Vandecasteele, C. (2003). Reuse, treatment, and discharge of the concentrate of pressure-driven membrane processes. *Environmental science & technology, 37,* (*17*, 3733–3738). doi:10.1021/es0201754

van Driessche, A.E.S., Stawski, T. M., & Kellermeier, M. (2019). Calcium sulfate precipitation pathways in natural and engineered environments. *Chemical Geology, 530,* (*6*, 119274). doi:10.1016/j.chemgeo.2019.119274

Vanoppen, M., Stoffels, G., Demuytere, C., Bleyaert, W., & Verliefde, A. R. D. (2015). Increasing RO efficiency by chemical-free ion-exchange and Donnan dialysis: Principles and practical implications. *Water research, 80,* (59–70). doi:10.1016/j.watres.2015.04.030

Verma, C., Ebenso, E. E., Quraishi, M. A., & Hussain, C. M. (2021). Recent developments in sustainable corrosion inhibitors: design, performance and industrial scale applications. *Materials Advances, 2,* (*12*, 3806–3850). doi:10.1039/D0MA00681E

Vital, M., Füchslin, H. P., Hammes, F., & Egli, T. (2007). Growth of Vibrio cholerae O1 Ogawa Eltor in freshwater. *Microbiology (Reading, England), 153,* (*Pt 7*, 1993–2001). doi:10.1099/mic.0.2006/005173-0

Vrouwenvelder, J. S., Manolarakis, S. A., van der Hoek, J. P., van Paassen, J. A. M., van der Meer, W. G. J., van Agtmaal, J. M. C., et al. (2008). Quantitative biofouling diagnosis in full scale nanofiltration and reverse osmosis installations. *Water research, 42,* (*19*, 4856–4868). doi:10.1016/j.watres.2008.09.002

Waly, T., Kennedy, M. D., Witkamp, G.-J., Amy, G., & Schippers, J. C. (2012). On the induction time of CaCO3: effect of ionic strength. *Desalination and Water Treatment, 39,* (*1-3*, 55–69). doi:10.5004/dwt.2012.2561

Wang, F., & Tarabara, V. (2007). Coupled effects of colloidal deposition and salt concentration polarization on reverse osmosis membrane performance. *Journal of Membrane Science, 293,* (*1-2*, 111–123). doi:10.1016/j.memsci.2007.02.003

Warne, M. S. J., Batley, G. E., Braga, O., Chapman, J. C., Fox, D. R., Hickey, C. W., et al. (2014). Revisions to the derivation of the Australian and New Zealand guidelines for toxicants in fresh and marine waters. *Environmental science and pollution research international, 21,* (*1*, 51–60). doi:10.1007/s11356-013-1779-6

Weijnen, M.P.C., & Van Rosmalen, G. M. (1986). Adsorption of phosphonates on gypsum crystals. *Journal of Crystal Growth, 79,* (157–168).

Yang, L., Yang, W., Xu, B., Yin, X., Chen, Y., Liu, Y., et al. (2017). Synthesis and scale inhibition performance of a novel environmental friendly and hydrophilic terpolymer inhibitor. *Desalination, 416,* (*2*, 166–174). doi:10.1016/j.desal.2017.05.010

Yin, Y., Kalam, S., Livingston, J. L., Minjarez, R., Lee, J., Lin, S., et al. (2022). The use of anti-scalants in gypsum scaling mitigation: Comparison with membrane surface modification and efficiency in combined reverse osmosis and membrane distillation. *Journal of Membrane Science, 643,* (120077). doi:10.1016/j.memsci.2021.120077

Yu, W., Di Song, Chen, W., & Yang, H. (2020). Antiscalants in RO membrane scaling control. *Water research, 183,* (115985). doi:10.1016/j.watres.2020.115985

Zeino, A., Albakri, M., Khaled, M., & Zarzour, M. (2018). Comparative study of the synergistic effect of ATMP and DTPMPA on CaSO 4 scale inhibition and evaluation of induction time effect. *Journal of Water Process Engineering, 21,* (1–8). doi:10.1016/j.jwpe.2017.11.013

Zhai, Y., Liu, G., & van der Meer, W. G.J. (2022). One-Step Reverse Osmosis Based on Riverbank Filtration for Future Drinking Water Purification. *Engineering, 9,* (*5*, 27–34). doi:10.1016/j.eng.2021.02.015

Zhang, R., Liu, Y., He, M., Su, Y., Zhao, X., Elimelech, M., et al. (2016a). Antifouling membranes for sustainable water purification: strategies and mechanisms. *Chemical Society reviews, 45,* (*21*, 5888–5924). doi:10.1039/c5cs00579e

Zhang, H.-p., Luo, X.-g., Lin, X.-y., Tang, P.-p., Lu, X., Yang, M.-j., et al. (2016b). Biodegradable carboxymethyl inulin as a scale inhibitor for calcite crystal growth: Molecular level understanding. *Desalination, 381,* (1–7). doi:10.1016/j.desal.2015.11.029

Zhang, P., Zhang, N., Liu, Y., Lu, Y.-T., Kan, A. T., & Tomson, M. B. (2018). Application of a novel tube reactor for investigation of calcium carbonate mineral scale deposition kinetics. *Chemical Engineering Research and Design, 137,* (113–124). doi:10.1016/j.cherd.2018.07.001

Zuo, Y., Yang, W., Zhang, K., Chen, Y., Yin, X., & Liu, Y. (2020). Experimental and Theoretical Studies of Carboxylic Polymers with Low Molecular Weight as Inhibitors for Calcium Carbonate Scale. *Crystals, 10,* (*5*, 406). doi:10.3390/cryst10050406

Annex I. Supplemental Materials and Methods

Table I-1: Membrane details for crossflow filtration experiments and dead-end filtration experiments

Membrane name	Filmtec™ CR100
Manufacturer	Dow / DuPont
Type	Polyamide Thin-Film Composite
Maximum operating pressure	41 bar
pH range	2 - 11
NaCl rejection	99.5 %

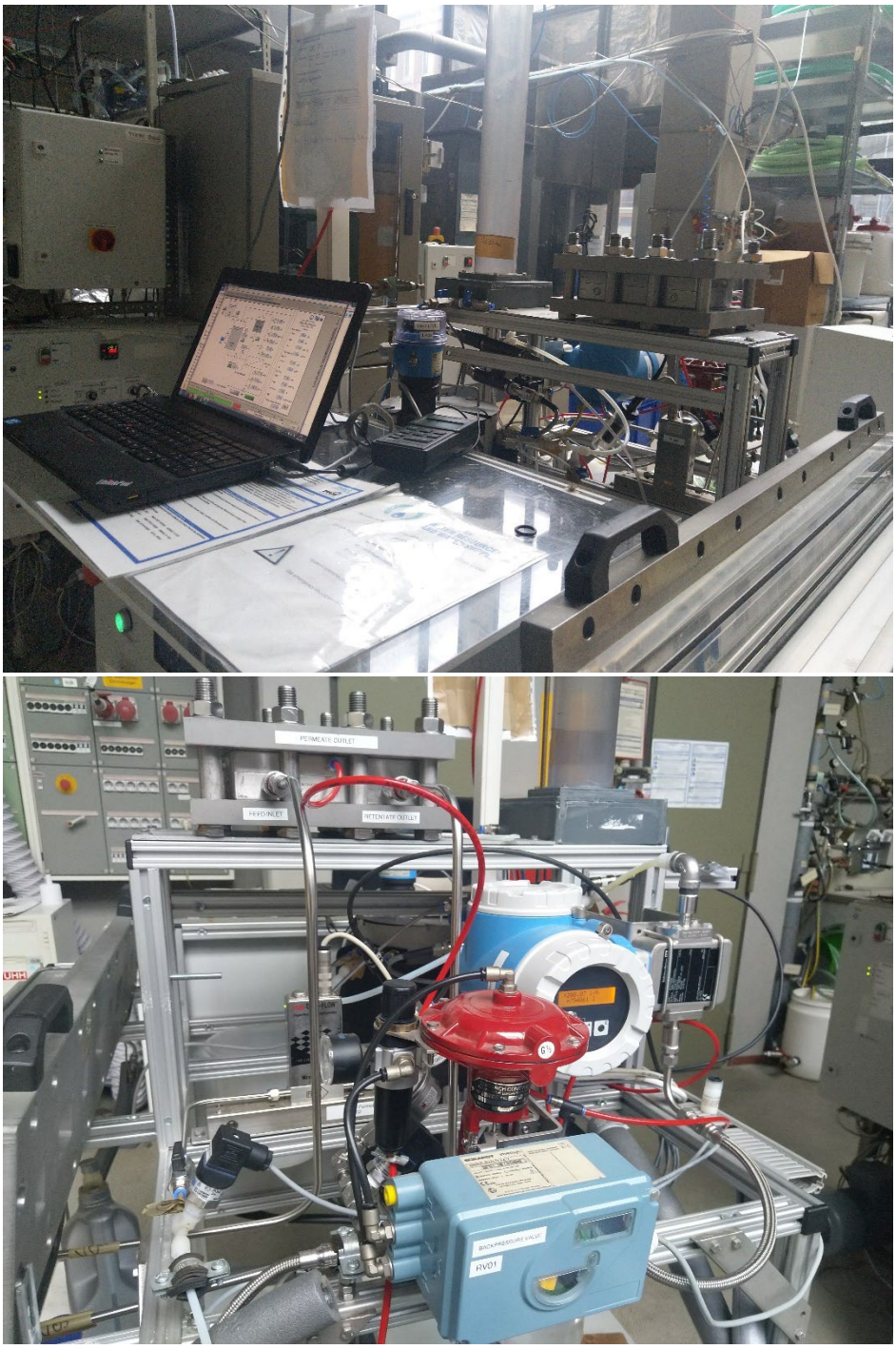

Figure I-1: Sterlitech membrane cell setup used for crossflow filtration experiments at Institute for Water Resources and Water Supply, TUHH

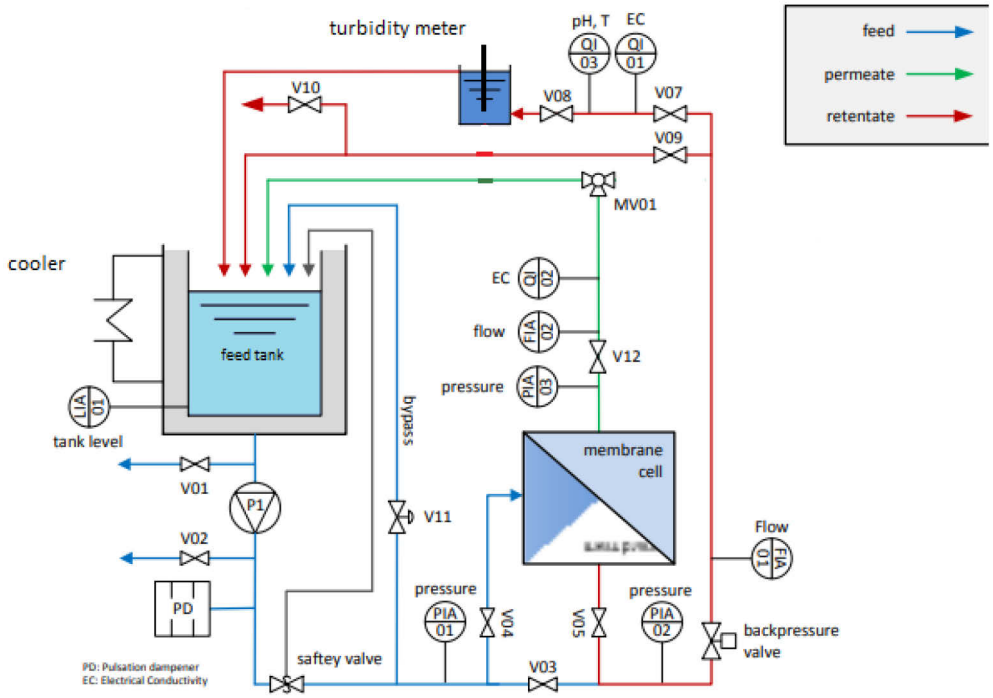

Figure I-2: Schematic of the Sterlitech membrane cell setup used for crossflow filtration experiments at Institute for Water Resources and Water Supply, TUHH (Mulay 2022)

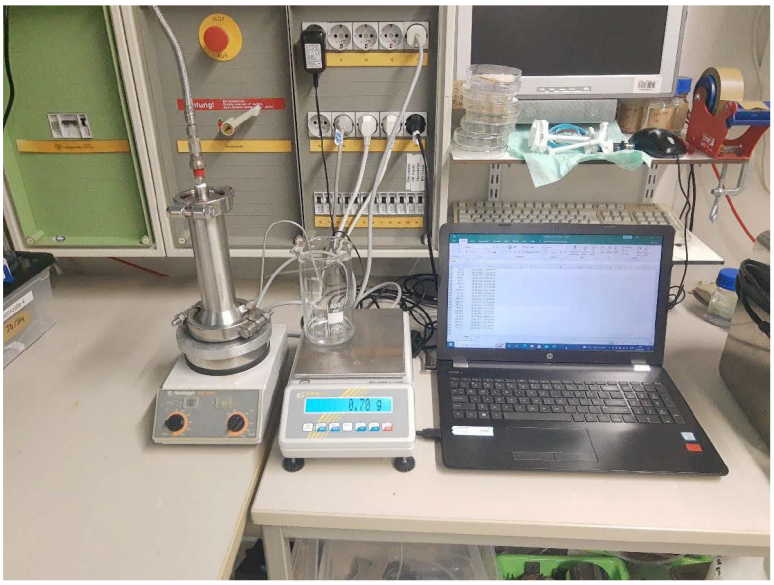

Figure I-3: Sterlitech high pressure membrane cell setup used for deadend filtration experiments at Institute for Water Resources and Water Supply, TUHH (Mulay 2022)

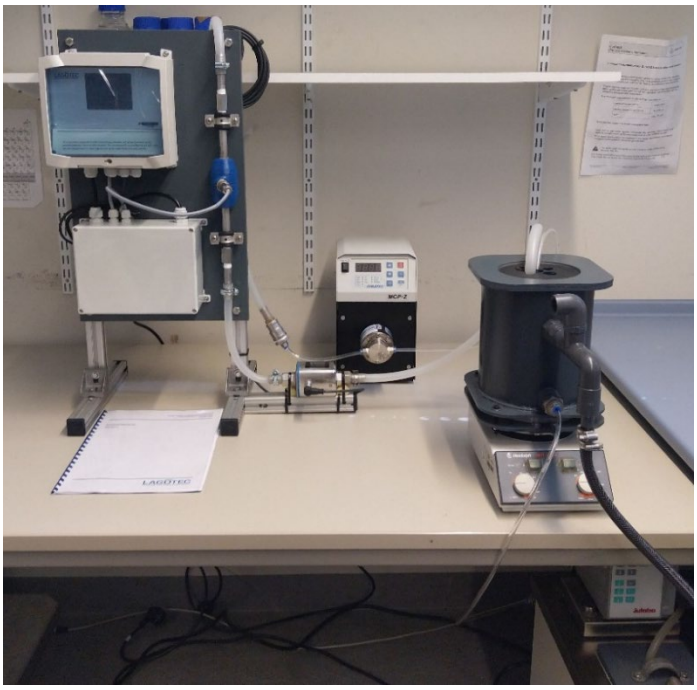

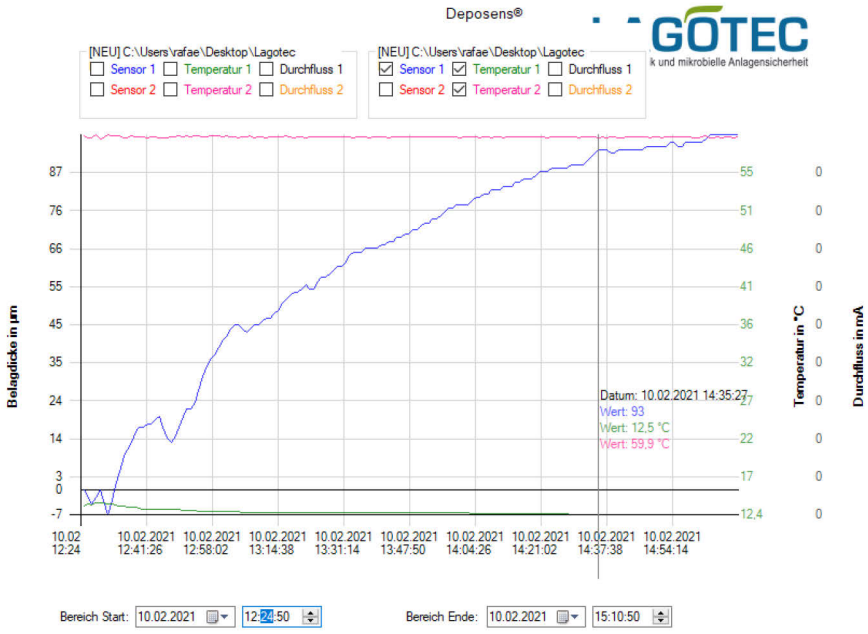

Figure I-4: Stirred-beaker setup integrated with the Lagotec Deposen3 sensor for scaling detection and evaluation of antiscalant effectiveness and data visualisation

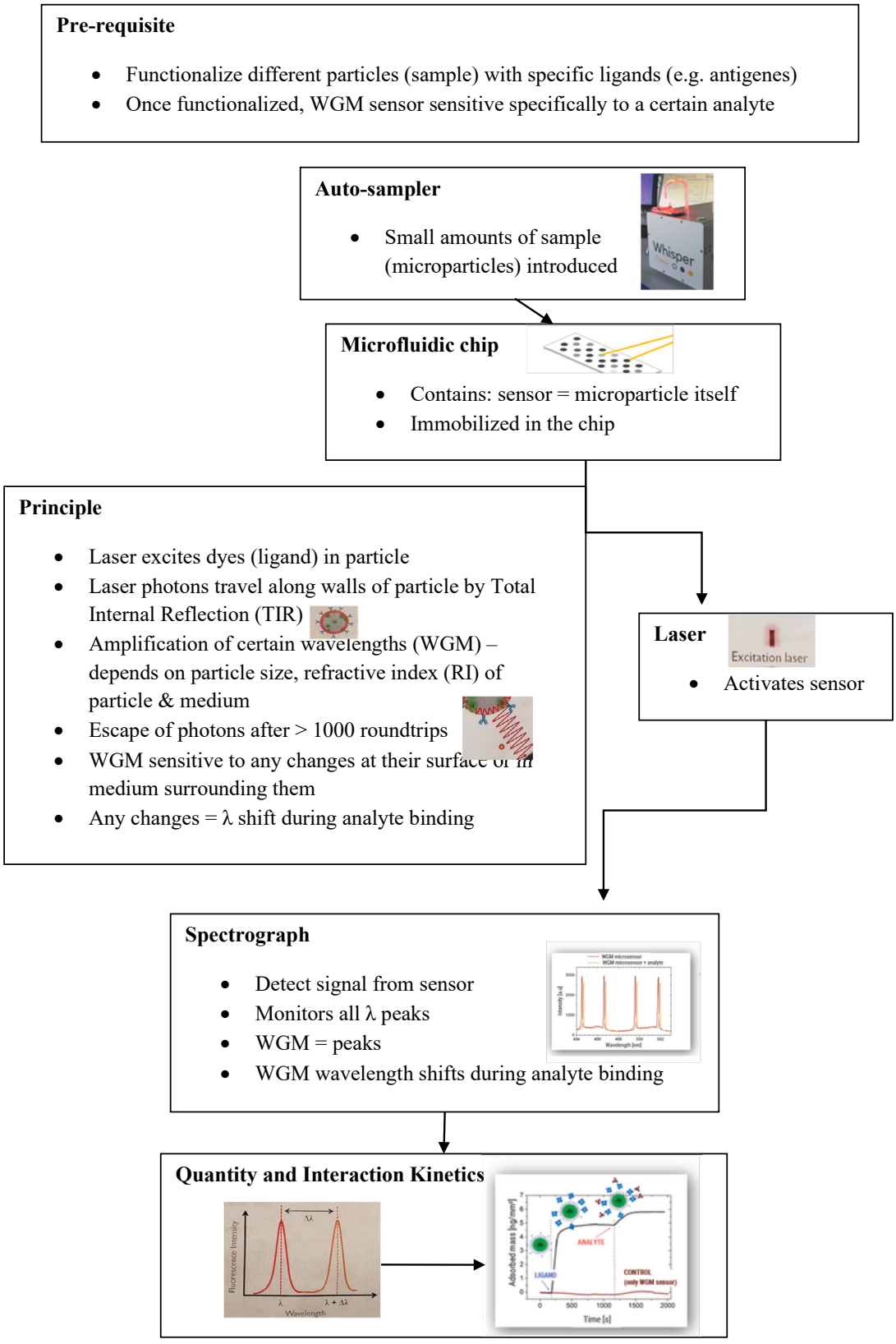

Figure I-5: Working principle of the Whispering Gallery Mode (WGM) according to Surflay GmbH

Table I-3: Overview of softwares reviewed for determining scaling potential and antiscalant dosage (in collaboration with KonTriSol project partners) (KonTriSol 2023)

Software	*Plant design*	*Scaling potential*	*Cost calculation*	*Life cycle analysis (LCA)*	*Antiscalant seleletion / dosage*
RPI Calculator		✓			✓
Membrane Master		✓			✓
Flodose		✓			✓
RO Xpert		✓			✓
IMS Design	✓	(✓)	✓		
WAVE (formerly ROSA)	✓	✓	✓		
LewaPlus	✓	✓	✓		
hyd-RO-dose	(✓)	✓			✓
SIMBA	✓			(✓)	
GaBi				✓	
SimaPro				✓	
Aquolizer		✓			✓
AQION		✓			

Annex II. Supplemental Results

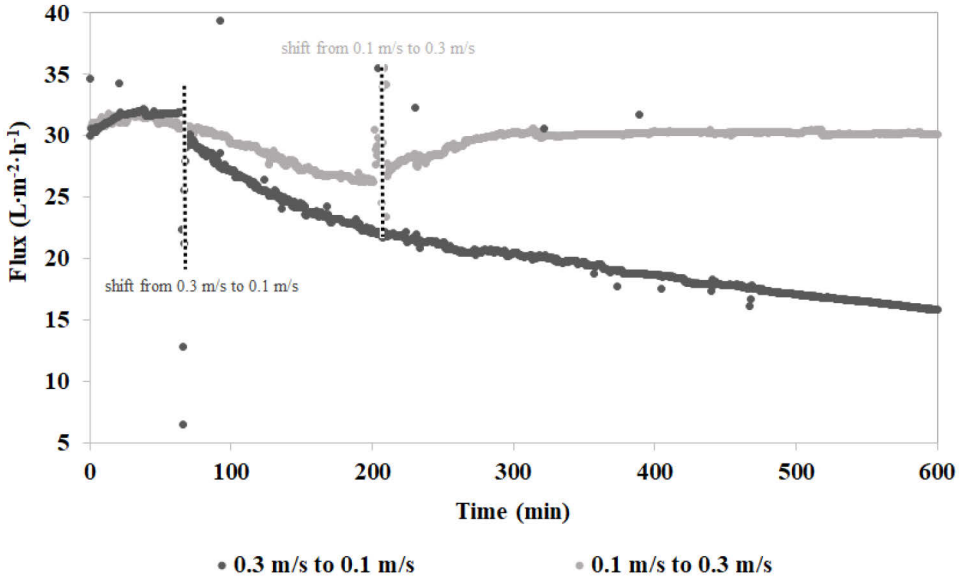

Figure II-1: Flux behaviour in crossflow filtration setup using flat sheet RO membrane operated with gypsum ($SI_{gypsum} \approx 0.1$) feed and without antiscalant, in complete recirculation mode, at crossflow velocities 0.1 ms^{-1} and 0.3 ms^{-1} (TMP=25 bar, T=11 °C)

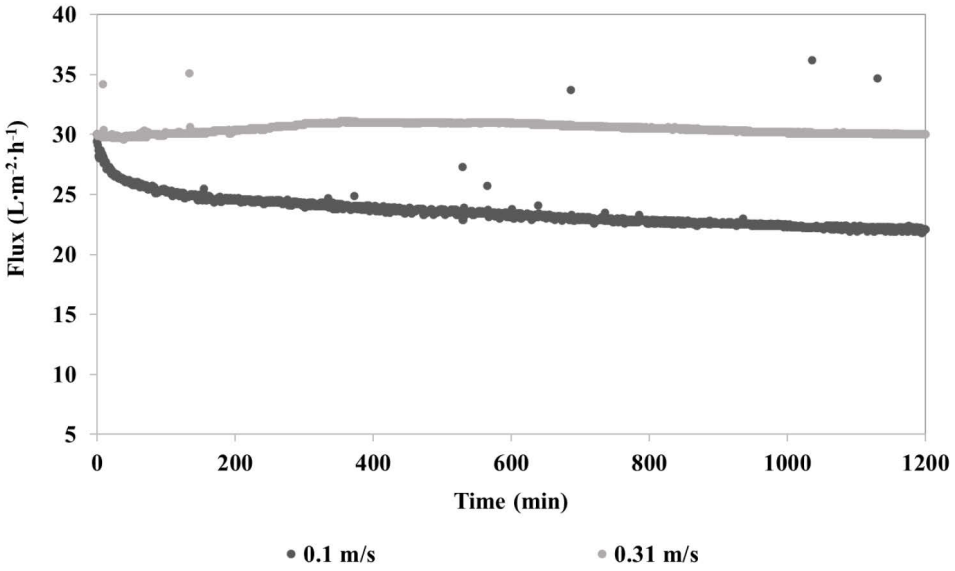

Figure II-2: Flux behaviour in crossflow filtration setup using flat sheet RO membrane operated with calcite ($SI_{calcite} \approx 1.09$) feed and without antiscalant, in complete recirculation mode, at crossflow velocities 0.1 ms^{-1} and 0.3 ms^{-1} (TMP=25 bar, T=11 °C)

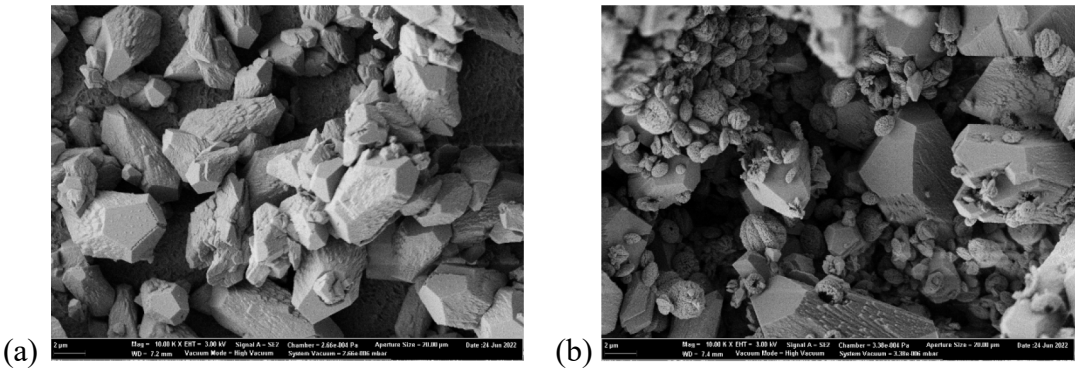

Figure II-3: SEM pictures (Mag = 5 X, 2 µm) of RO membrane surface after crossflow filtration with calcite feed ($SI_{calcite} \approx 1.09$) and without antiscalant, in complete recirculation mode, at crossflow velocities (a) 0.3 ms^{-1} and (b) 0.1 ms^{-1}

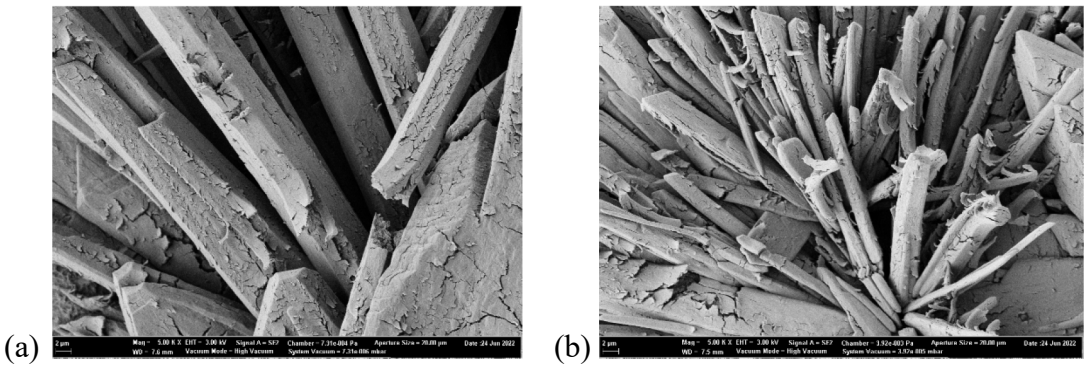

Figure II-4: SEM pictures (Mag = 5 X, 2 µm) of RO membrane surface after crossflow filtration with gypsum feed ($SI_{gypsum} \approx 0.1$) and without antiscalant, in complete recirculation mode, at crossflow velocities (a) 0.3 ms^{-1} and (b) 0.1 ms^{-1}

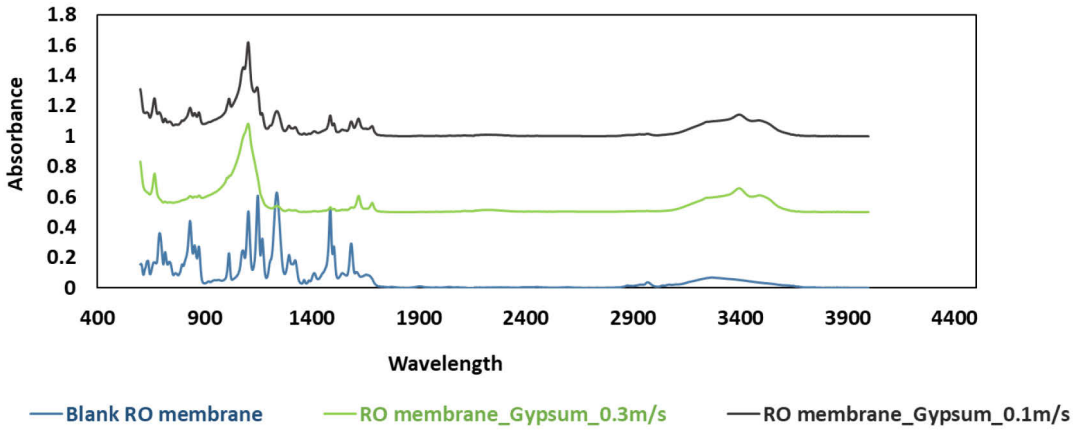

Figure II-5: FTIR analysis of RO membrane operated with gypsum feed ($SI_{gypsum} \approx 0.1$) and without antiscalant, in complete recirculation mode, at crossflow velocities 0.1 ms^{-1} and 0.3 ms^{-1} (TMP=25 bar, T=11 °C)

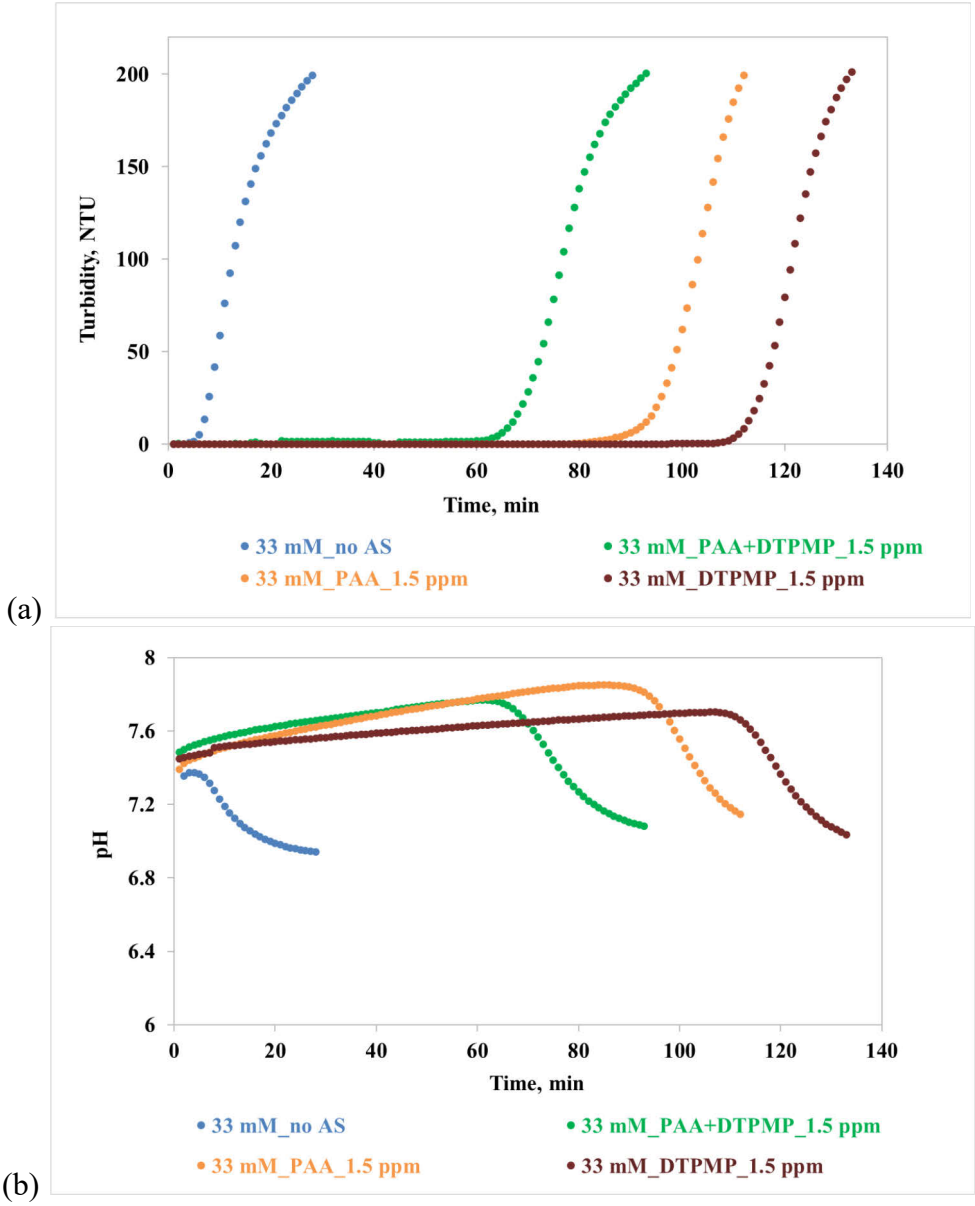

Figure II-6: Comparison of (a) turbidity and (b) pH behavior of 33 mM $NaHCO_3$ and $CaCl_2$ without antiscalants and with 1.5 mg·L^{-1} of PAA+DTPMP, PAA and DTPMP based antiscalants in the stirred-beaker test for induction time determination

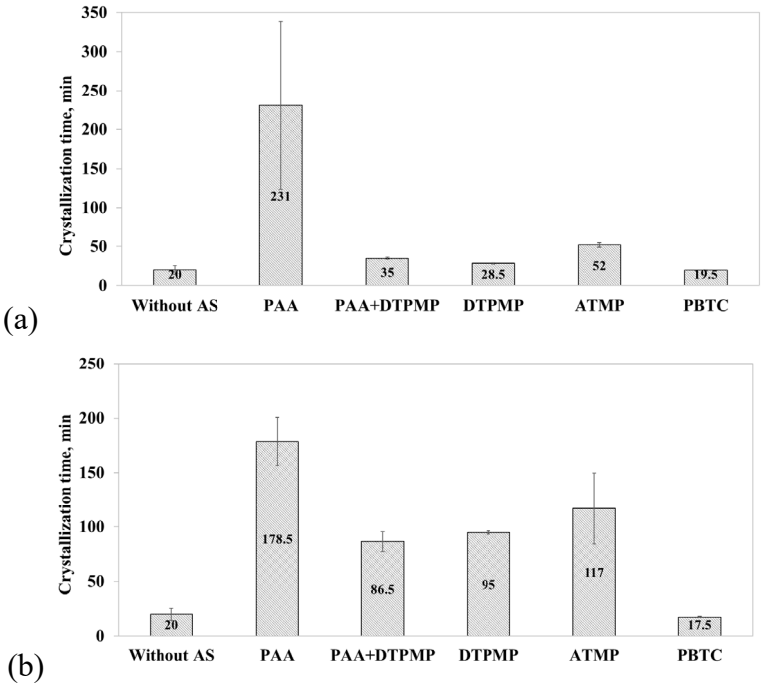

Figure II-7: Crystallization time (based on turbidity increase from 1 NTU to 200 NTU) using the stirred beaker test with $SI_{CaSO4} \approx 0.72$ and (a) 0.5 mg/L TS and (b) 1 mg/L TS of commercial antiscalants based on different active ingredients (T=11 °C, n=2)

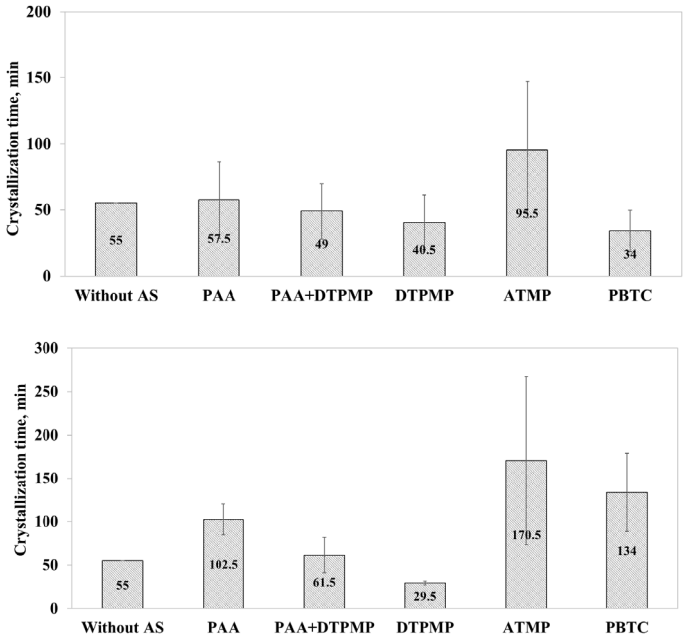

Figure II-8: Crystallization time (based on turbidity increase from 1 NTU to 200 NTU) using the stirred beaker test with $SI_{CaCO3} \approx 2.06$ and (a) 0.5 mg/L TS and (b) 1 mg/L TS of commercial antiscalants based on different active ingredients (T=11 °C, n=2)

Table II-1: Characterization of gypsum scaling crystals in stirred beaker setup using light microscope; T=11 °C, $SI_{CaSO4} \approx 0.72$ and 1.5 $mg \cdot L^{-1}$ of antiscalant, pH =7.5

	Turbidity			
	0 NTU	**5 NTU**	**100 NTU**	**1000 NTU**
Without AS	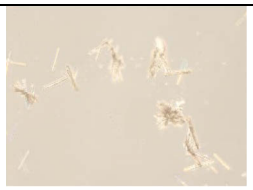 t_{sample} = 1 min	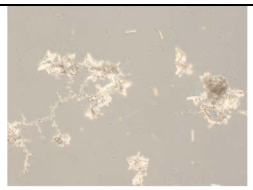 t_{sample} = 16 min	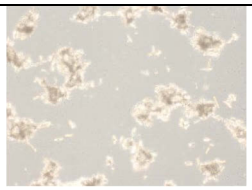 t_{sample} = 30 min	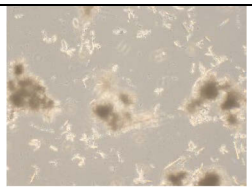 t_{sample} = 76 min
PAA	 t_{sample} = 1 min	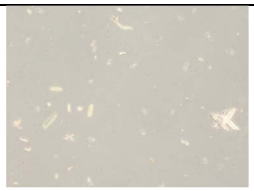 t_{sample} = 110 min	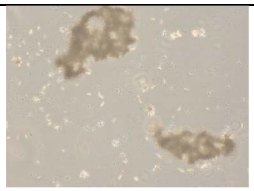 t_{sample} = 163 min	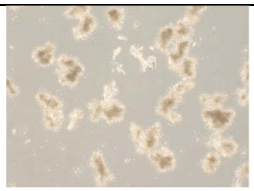 t_{sample} = 194 min
PAA + DTPMP	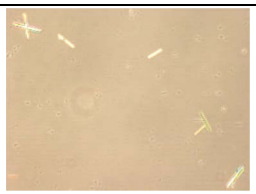 t_{sample} = 1 min	 t_{sample} = 19 min	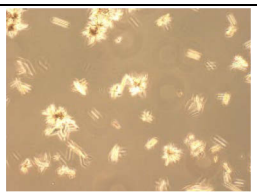 t_{sample} = 32 min	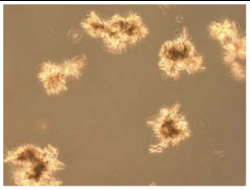 t_{sample} = 97 min
DTPMP	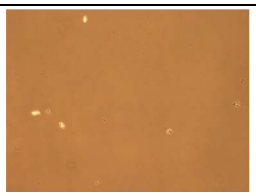 t_{sample} = 1 min	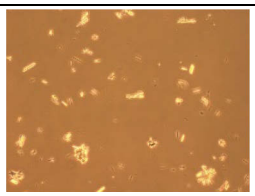 t_{sample} = 32 min	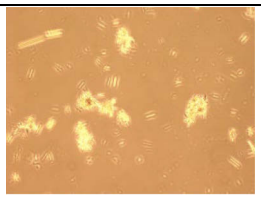 t_{sample} = 45 min	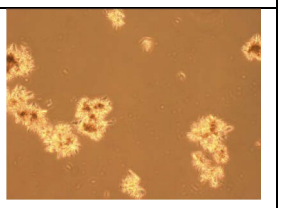 t_{sample} = 71 min

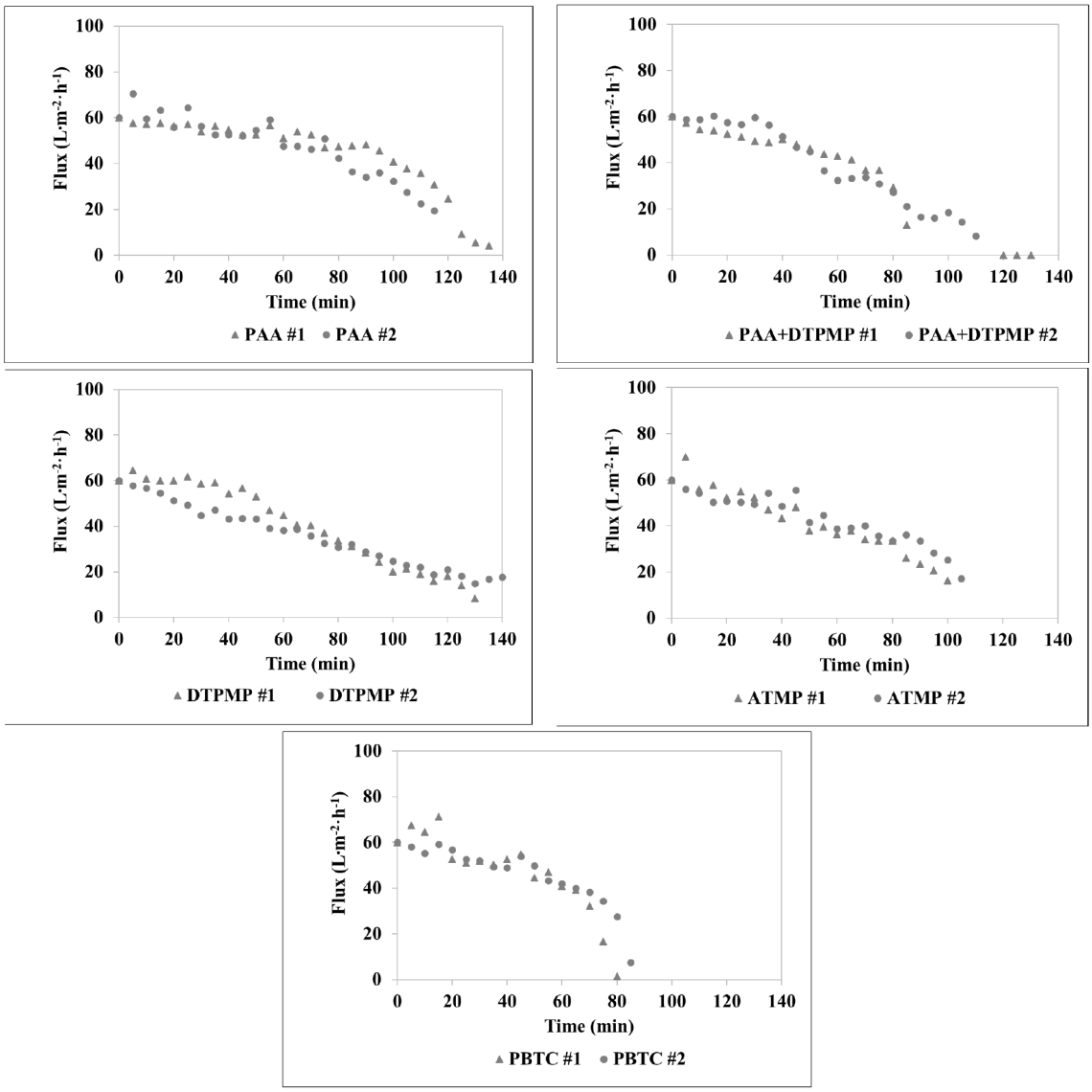

Figure II-9: Comparison of antiscalant effectiveness against gypsum scaling ($SI_{gypsum} \approx 0.2$) via rate of change of flux in dead-end filtration test at room temperature 22 ± 1ºC, constant TMP 25 bar and two experimental trials

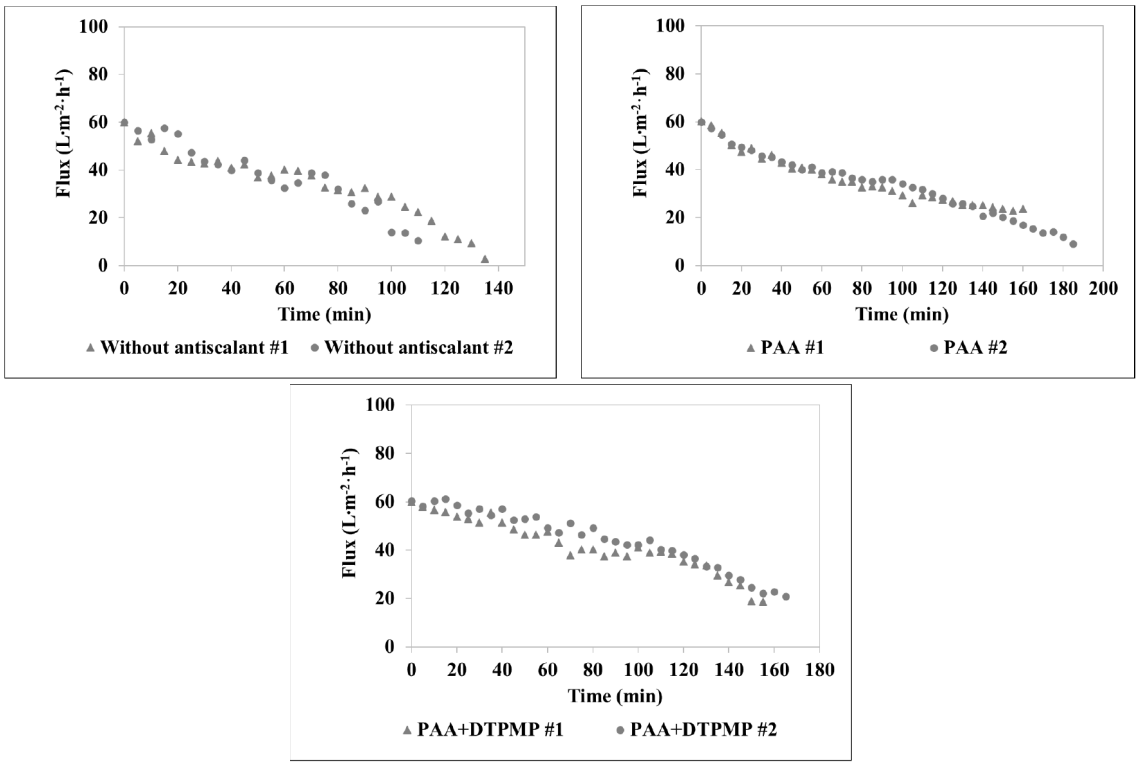

Figure II-10: Comparison of antiscalant effectiveness against calcite scaling ($SI_{calcite} \approx 1.09$) via rate of change of flux in dead-end filtration test at room temperature 22 ± 1ºC, constant TMP 25 bar and two experimental trials

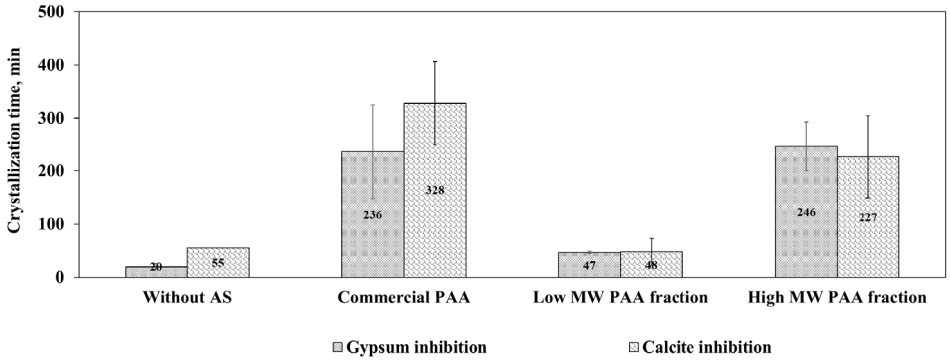

Figure II-11: Crystallization time (1 NTU to 200 NTU turbidity increase) using the stirred beaker test with 0.5 mg TOC/L commercial PAA and its low and high MW fractions, against 68 mM sulfate solution and 33 mM carbonate solution (T=11 °C, $SI_{CaSO4} = 0.72$, $SI_{CaCO3} = 2.06$, n=3)

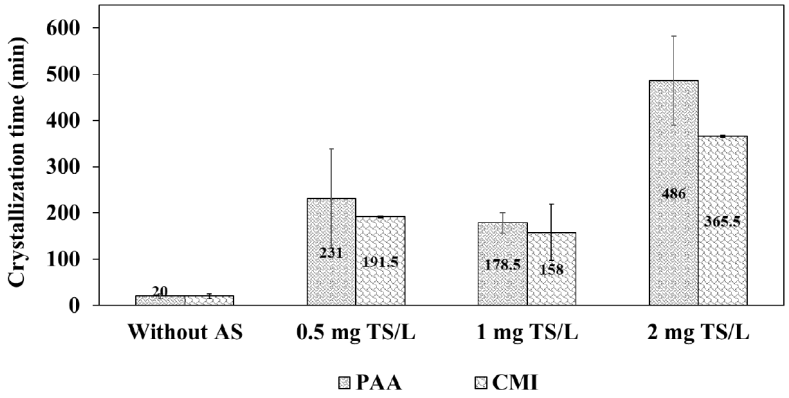

Figure II-12: Crystallization time (based on 1 NTU to 200 NTU turbidity increase) using the stirred beaker test with 68 mM Na2SO4 and CaCl2 and different concentrations of CMI and PAA antiscalants (T=11 °C, $SI_{CaSO4} \approx 0.72$, n=2)

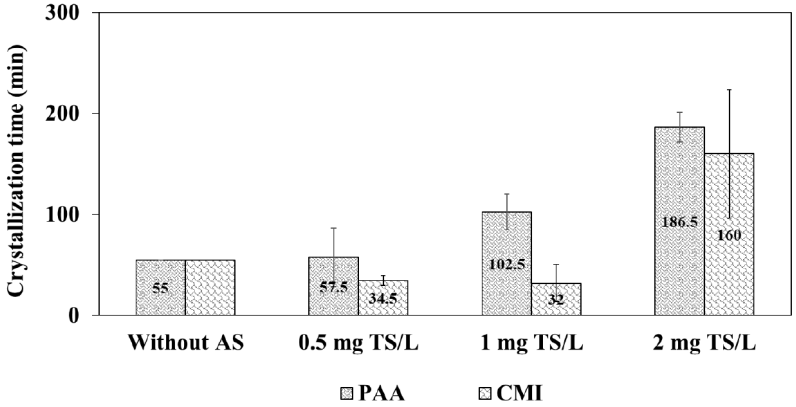

Figure II-13: Crystallization time (based on 1 NTU to 200 NTU turbidity increase) using the stirred beaker test with 33 mM $NaHCO_3$ and $CaCl_2$ and different concentrations of CMI and PAA antiscalants (T=11 °C, $SI_{CaCO3} \approx 2.06$, n=2)

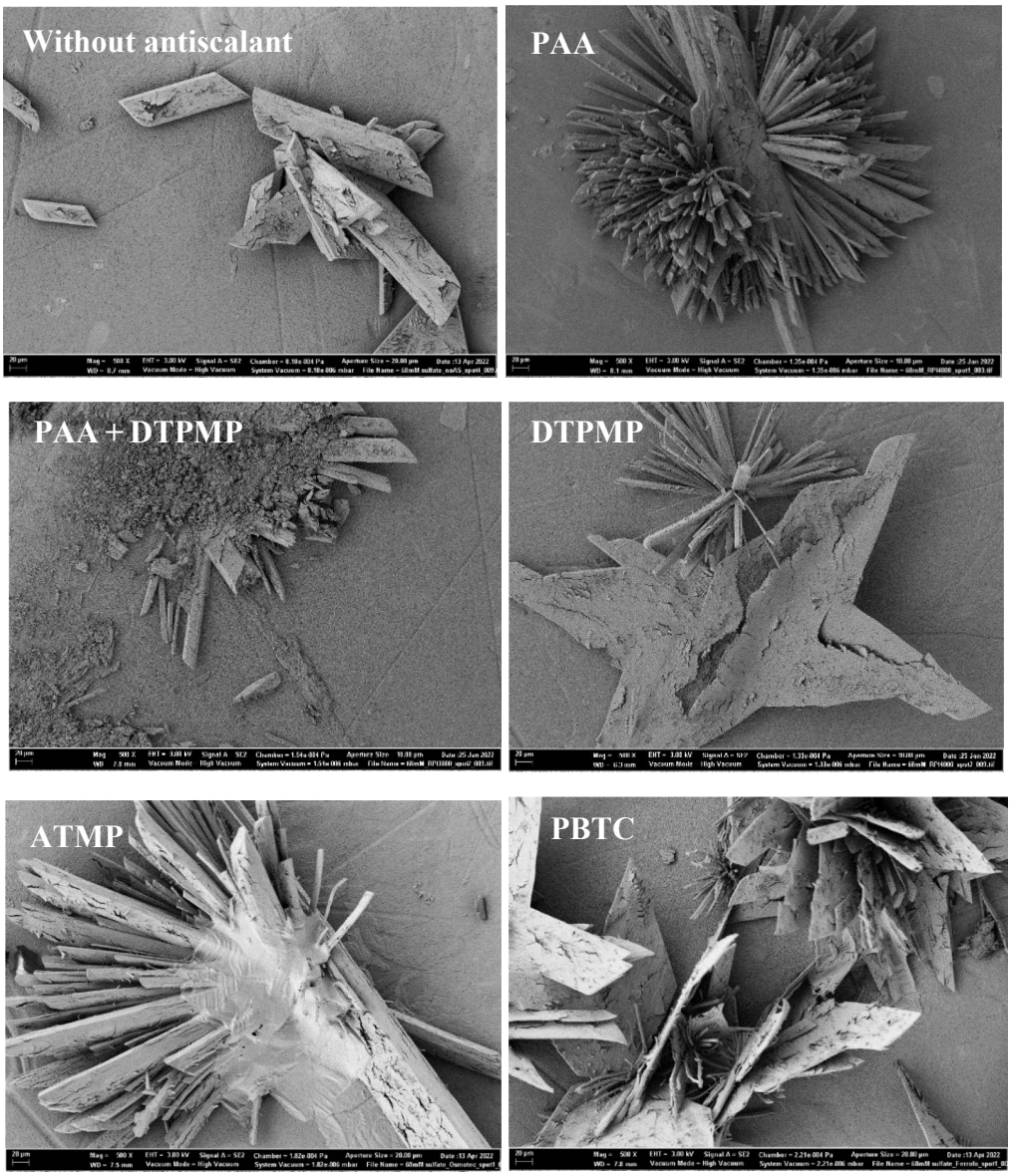

Figure II-14: SEM images (Mag: 500 X, 20 µm) of antiscalant influence on gypsum crystal morphology with gypsum, $SI_{CaSO4} \approx 0.72$ and 1 mg/L TS of antiscalants based on different active ingredients

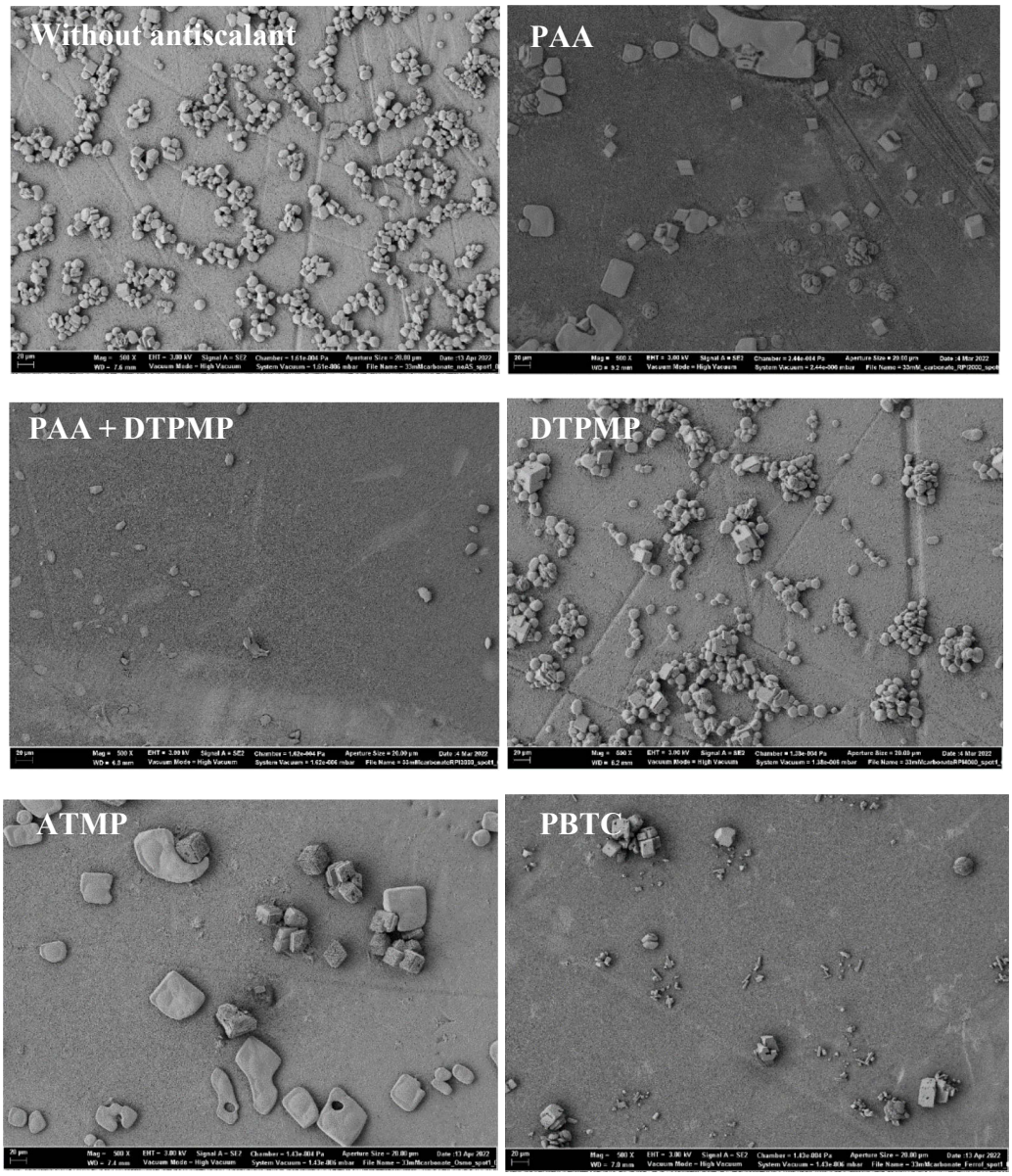

Figure II-15: SEM images (Mag: 500 X, 20 µm) of antiscalant influence on gypsum crystal morphology with calcite, $SI_{CaCO3} \approx 2.06$ and 1 mg/L TS of antiscalants based on different active ingredients

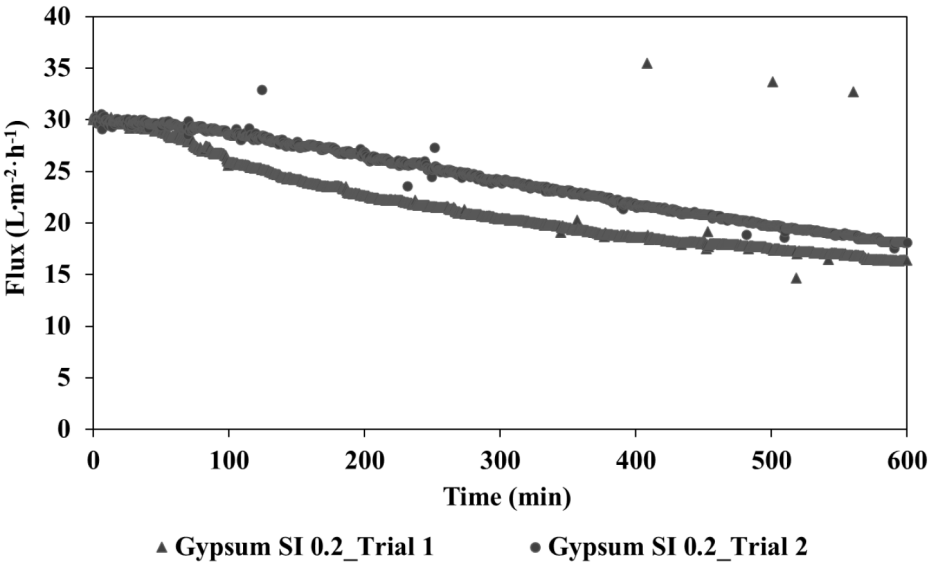

Figure II-16: Flux behaviour in crossflow filtration setup using flat sheet RO membrane operated with gypsum, $SI_{gypsum} \approx 0.2$ feed in complete recirculation mode, at crossflow velocity 0.1 ms^{-1} (TMP=25 bar, T=11 °C)

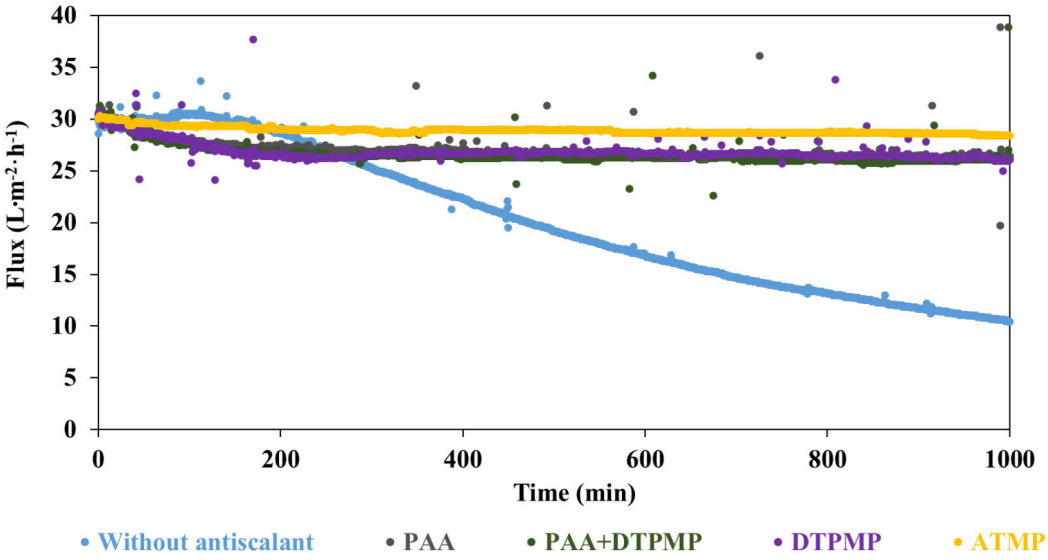

Figure II-17: Flux behaviour in crossflow filtration setup using flat sheet RO membrane operated with gypsum, $SI_{gypsum} \approx 0.2$ feed and 1 mg/L TS of commercial antiscalants in complete recirculation mode, at crossflow velocity 0.1 ms^{-1} (TMP=25 bar, T=11 °C)

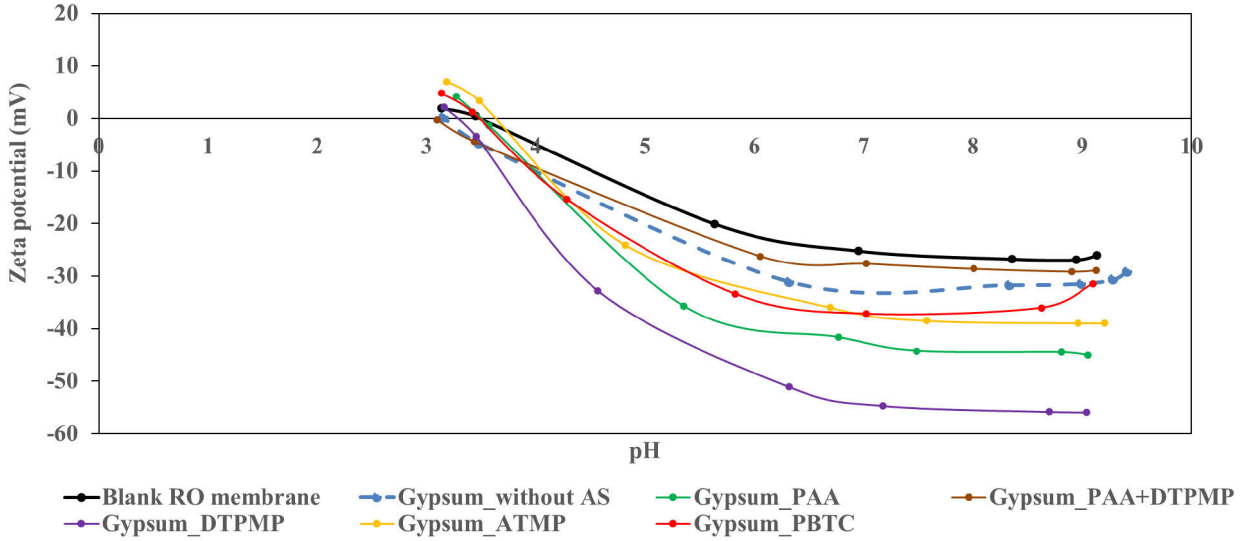

Figure II-18: Zeta potential of RO membrane filtered with gypsum, $SI_{gypsum} \approx 0.2$ and 1 mg/L TS of different commercial antiscalants in complete recirculation mode, at crossflow velocity 0.1 ms^{-1} (TMP=25 bar, T=11 °C)

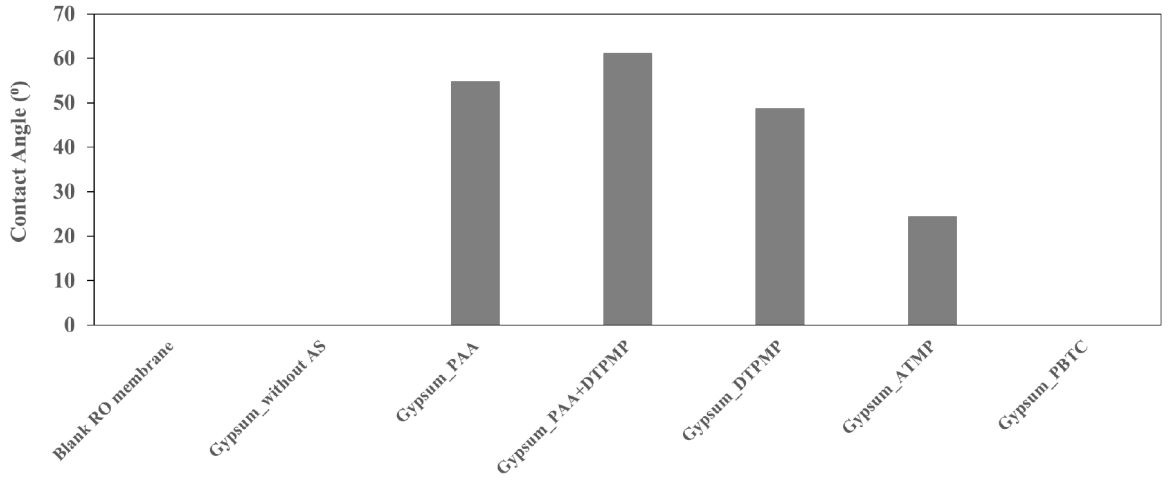

Figure II-19: Contact angle of RO membrane filtered with gypsum, $SI_{gypsum} \approx 0.2$ and 1 mg/L TS of different commercial antiscalants in complete recirculation mode, at crossflow velocity 0.1 ms^{-1} (TMP=25 bar, T=11 °C)